

**ANKARA UNIVERSITY
INSTITUTE OF NUCLEAR SCIENCES**

MASTER'S THESIS

**GAMMA DOSE RATE EFFECTS IN TL AND OSL OF
VARIOUS LUMINESCENCE DOSIMETRIC MATERIALS**

MİRAY BAŞDOĞAN

**DEPARTMENT OF MEDICAL PHYSICS
HEALTH PHYSICS MASTER'S PROGRAM**

ANKARA

2019

All Rights Reserved

THESIS APPROVAL

The thesis entitled “Gamma Dose Rate Effects in TL and OSL of Various Luminescence Dosimetric Materials” prepared by Miray BAŞDOĞAN in partial fulfillment of the requirements for the degree of Master of Science in Health Physics Program of the Medical Physics Department of Institute of Nuclear Sciences in Ankara University has been examined and approved by the undersigned jury members.

Supervisor: Assoc. Prof. Dr. Gaye Özgür ÇAKAL

Co- Supervisor: Dr. George S. POLYMERIS

Jury Members:

Assoc. Prof. Dr. Gaye Özgür ÇAKAL
Ankara University Institute of Nuclear Sciences

Dr. George S. POLYMERIS
Ankara University Institute of Nuclear Sciences

Prof. Dr. Ali Ulvi YILMAZER
Ankara University Faculty of Engineering Physics Engineering Department

Prof. Dr. Ayşen YILMAZ
Middle East Technical University Faculty of Arts and Sciences Department of Chemistry

Assoc. Prof. Dr. TURAN OLĞAR
Ankara University Faculty of Engineering Physics Engineering Department

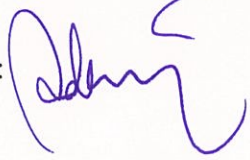
Approved

Prof. Dr. Niyazi MERİÇ
Head of the Institute of Nuclear Sciences

I hereby declare that all information in this thesis has been obtained and presented in accordance with academic rules and ethical conduct. I also declare that, as required by these rules and conduct, I have fully cited and referenced all material and results that are not original to this work.

Name, Last Name : Miray BAŞDOĞAN

Signature

: 

ABSTRACT

Master's Thesis

GAMMA DOSE RATE EFFECTS IN TL AND OSL OF VARIOUS LUMINESCENCE DOSIMETRIC MATERIALS

Miray BAŞDOĞAN

Ankara University Institute of Nuclear Sciences
Department of Medical Physics
Health Physics Master's Degree Program

Supervisor: Assoc. Prof. Dr. Gaye Özgür ÇAKAL
Co-Supervisor: Dr. George S. POLYMERIS

Thermoluminescence (TL) and Optically stimulated luminescence (OSL) are the measuring methods used to determine previously absorbed energy because of irradiation. TL and OSL methods are widely used in retrospective dosimetry studies to calculate the dose absorbed by inorganic materials exposed to ionizing radiation and to determine the age. The present study, luminescence dosimetric materials which have good response in TL and OSL measurements were examined. BeO and quartz were used in OSL measurements. In TL measurements, LiB₄O₇: Cu, In, MgB₄O₇: Dy, Na, CaF₂:Dy (TLD 200), LiF: Mg, Ti (TLD100) and BeO which were known as artificial materials were used at different dose rates and dose steps. Dose rates for TL measurements were 2 Gy/h and 30 Gy/h., dose steps were 52, 104, 199.33, 303.33, 502.66, 797.33, 996.66, 1499.33, 2002, 2496, 2998.66 and 3501.33 mGy. Quartz which is one of the natural luminescence dosimetric materials and BeO used in OSL measurements. While BeO was irradiated at 2 Gy/h and 30 Gy/h, quartz was irradiated at 27 Gy/h, 311 Gy/h and 1305 Gy/h, respectively. Dose steps for quartz were, 2000, 1500, 1000, 750, 500, 250, 150, 100, 75, 54, 25, 13 Gy,

The main aim of the present study was studying the possible dose rate effects of the TL signal on various materials by checking the dose response curves and after deconvolution analyses signal deconvolution parameters were determined. OSL signals were examined in dose response behavior and after deconvolution analyses OSL decay curve's components were determined. The construction of the dose response curve, the dose rate applied is quite faster so the dose rate effect is important. Characteristic properties of the all artificial luminescence materials such as TL activation energy and internal fitting parameters were calculated following a deconvolution analysis for all different dose rates and dose steps. Kinetic parameters of each material, at 2 Gy/h and 30 Gy/h dose rates, show differences, mostly in terms of activation energy values. Internal fitting parameters were calculated following a deconvolution analysis at the OSL decay curves and the components of OSL decay curves' were find and evaluated. The dose response features for all materials of the present study both in TL and OSL, namely the linearity index k and also the lowest detectable dose limit (LDDL) for each peak/component of each signal of TL/OSL were calculated and compared to the literature. Some parameters were independent on the dose rate supporting the results of previous studies.

2019, 127 pages

Keywords : TL, OSL, gamma dose rate, luminescence dosimeters, deconvolution, deconvolution parameters.

ÖZET

Yüksek Lisans Tezi

TL VE OSL İLE ÇEŞİTLİ LUMİNESANS DOZİMETRİK MALZEMELERDE GAMA DOZ HIZI ETKİLERİNİN BELİRLENMESİ

Miray BAŞDOĞAN

Ankara Üniversitesi Nükleer Bilimler Enstitüsü
Medikal Fizik Anabilim Dalı
Sağlık Fiziği Yüksek Lisans Programı

Danışmanı: Doç. Dr. Gaye Özgür ÇAKAL
Eş-Danışmanı: Dr. George S. POLYMERIS

Termoluminesans (TL) ve Optik uyarılmış luminesans (OSL), radyasyona maruziyetten dolayı absorbe edilen enerjinin belirlenmesi için kullanılan ölçüm yöntemleridir. TL ve OSL yöntemleri, iyonlaştırıcı radyasyona maruz kalan inorganik maddeler tarafından soğurulan dozu hesaplamak ve yaş tayini yapmak amacıyla retrospektif dozimetri çalışmalarında yaygın olarak kullanılmaktadır. Bu çalışmada, TL ve OSL ölçüm yöntemlerinde doğru cevap verebilen luminesans özellikli dozimetrik malzemeler incelenmiştir. BeO ve kuvars OSL ölçümlerinde kullanılmış olup TL ölçümlerinde ise yapay luminesans malzeme olan LiB_4O_7 : Cu, In, MgB_4O_7 : Dy, Na, CaF_2 :Dy (TLD 200), LiF: Mg, Ti (TLD100) ve BeO kullanılmıştır. TL ölçümlerindeki doz hızları 2 Gy/h ve 30 Gy/h iken doz değerleri ise sırasıyla 52, 104, 199.33, 303.33, 502.66, 797.33, 996.66, 1499.33, 2002, 2496, 2998.66 and 3501.33 mGy dir. OSL ölçümlerinde BeO için kullanılan doz hızları ve doz değerleri TL ölçümleriyle aynı iken kuvars için kullanılan doz hızları sırasıyla 27 Gy/saat, 311 Gy/saat and 1305 Gy/saat, doz değerleri ise 2000, 1500, 1000, 750, 500, 250, 150, 100, 75, 54, 25, 13 Gy dir.

Bu çalışmanın temel amacı, TL sinyalinin çeşitli malzemeler üzerindeki olası doz hızı etkilerini, TL ışınma eğrilerinin doz cevaplarını, dekonvolüsyon analizi yaparak kinetik parametreleri incelemektir. OSL sinyallerinin hem doz cevap davranışını hem de dekonvolüsyon analizlerinden sonra OSL bozunma eğrisinin bileşenlerini tespit ederek değerlendirmektir. Doz cevap eğrisi oluşturmak için uygulanan doz hızı oranı oldukça hızlıdır bu nedenle doz hızı etkisinin incelenmesi önemlidir. Çalışmada kullanılan yapay luminesans malzemelerin tüm doz hızlarında ve doz değerlerinde incelemeleri yapılarak TL ve OSL karakteristik özellikleri incelenmiştir. Dekonvolüsyon analizi sonrasında bu malzemelerin TL kinetik parametreleri farklı iki doz hızında özellikle aktivasyon enerjileri farklılık göstermiştir. OSL ölçümlerinde kullanılan BeO yukarıda belirtildiği gibi iki farklı doz hızında, doğal luminesans özelliği olan kuvars malzemesi ise üç farklı doz hızında incelenmiştir.

Doğrusallık indeksi k ve ayrıca her bir TL/OSL sinyalinin her tepe noktası / bileşeni için saptanabilir en düşük doz limiti (LDDL) hesaplandı. Bazı parametrelerin daha önceki çalışmaları destekler nitelikte doz hızından bağımsız olduğu görülmüştür.

2019, 127 sayfa

Anahtar Kelimeler: TL, OSL, gama doz hızı, luminesans dozimetre, dekonvolüsyon, dekonvolüsyon parametreleri

ACKNOWLEDGMENTS

Firstly, I would like to thank my supervisor Dear Assoc. Prof. Dr. Gaye Özgür ÇAKAL for her sincere suggestions for preparing this thesis. I feel comfortable to have her as a mentor who guided me with her knowledge and experiences. I appreciate her kindness and support. I would like to thank my co-supervisor, Dear Dr. George S. POLYMERIS, who gave me the honour to be his student in the Ankara University Institute of Nuclear Sciences. I offer my sincerest gratitude to him for his continuous support, patience and motivation during my master's thesis. I would like to thank Dear Prof. Dr. Niyazi MERİÇ, who provided me with the technical infrastructure at the Ankara University Institute of Nuclear Sciences during my studies. I would like to thank Dear Dr. Çiğdem YILDIZ who has made a great contribution in the Department of Radiation Accelerator Technologies during my studies. I would like to thank Secondary Standard Dosimetry Laboratory staff and Experimental Irradiation Laboratory staff for all their help and guidance. I would like to thank my dear friends and Research Assistants Dear Engin AŞLAR, Dear İbrahim DEMİREL and Lecturer Dear Şule KAYA KELEŞ for the share of their knowledge, experience and recommendation.

Above all, I am very grateful for the endless love and support of my dear parents, my husband Emir BAŞDOĞAN and my children Naz and Çağın. I feel stronger and happier with their love and support.

TABLE OF CONTENTS

ABSTRACT	i
ÖZET	ii
ACKNOWLEDGMENTS	iii
TABLE OF CONTENTS	iv
LIST OF SYMBOLS AND ABBREVIATIONS	vii
LIST OF FIGURES	ix
LIST OF TABLES	xxi
1. INTRODUCTION	1
2. THEORY	2
2.1 Gamma Rays and the Interaction of Gamma Rays with Matter	3
2.1.1 Photoelectric event	4
2.1.2 Compton scattering	4
2.1.3 Pair production	5
2.2 Dosimetry System	6
2.3 Luminescence	6
2.4 Thermoluminescence	10
2.4.1 Thermoluminescence kinetics	11
2.4.1.1 First order kinetics	11
2.4.1.2 Second order kinetics	13
2.5 OSL Theory	14
2.6 OSL Mechanism	14
2.7 Determination of Kinetic Parameters	17
2.7.1 Deconvolution	17
3. MATERIALS AND METHODS	23
3.1 Dosimetric Materials	23

3.1.1 MgB ₄ O ₇ : Dy.....	23
3.1.2 Thermo Scientific LiF: Mg, Ti (TLD 100)	24
3.1.3 Li ₂ B ₄ O ₇ :Cu:In	25
3.1.4 CaF ₂ Dy TLD 200.....	26
3.1.5 BeO	27
3.1.6 Quartz	28
3.2 Artificial Materials Preparation.....	29
3.3 Quartz Preparation.....	30
3.3.1 Equipments for quartz preparation	31
3.3.1.1 Jaw crusher.....	31
3.3.1.2 Sieves	31
3.3.1.3 Magnetic stirrer.....	32
3.3.1.4 Analytical balance	32
3.4 Calculation of Calibration Factors.....	33
3.5. Irradiation Facilities	34
3.5.1 First facility (Co-60 source).....	34
3.5.2 Second facility (Co-60 source).....	37
3.6 Riso TL / OSL reader	39
3.6.1 Reader unit	40
3.6.2 Control unit	40
3.6.3 Sample preparation	41
3.6.4 Optical stimulation system	42
3.6.5 Heating system	43
3.6.6 Reference light source.....	43
3.6.7 Photo-multiplier tube (PMT)	44
3.6.8 Detection filters	44
3.6.9 Beta irradiator.....	44

3.7 TLD Harshaw 3500.....	44
3.8 Elsec 9010 OSL system	46
3.9 Freiburg Type 1321 Oven	47
3.10 Protherm Furnace.....	48
4. RESULTS	49
4.1 TL Glow Curves and OSL Decay Curves.....	49
4.2 TL and OSL Deconvolution	59
4.3 Dose Response Curves For TL Peaks Following Deconvolution Of TL Glow Curves	67
4.4 Kinetic Parameters For TL Peaks Following Deconvolution Of TL Glow Curves	73
4.5 Dose Response Curves for OSL Components Following Deconvolution of OSL Decay Curves	82
4.6 Kinetic Parameters of OSL Components Following Deconvolution of OSL Decay Curves	85
5. DISCUSSION	90
5.1 Case of LiF:Mg,Ti.....	114
5.2 Case of Li₂B₄O₇:Cu:In.....	114
5.3 Case of MgB₄O₇:Dy	116
5.4 Case of CaF₂:Dy	116
5.5 Case of BeO TL	116
5.6 Case of BeO OSL	118
5.7 Case of Quartz OSL.....	118
6. CONCLUSION	120
REFERENCES.....	122
CURRICULUM VITAE.....	128

LIST OF SYMBOLS AND ABBREVIATIONS

b	Order of Kinetic
BeO	Beryllium Oxide
C	Coulomb
°C	Celsius Degree
CaF₂:Dy	Calcium Floride Dysprosium dopped
E	Activation energy
e⁻	Electron
e⁺	Positron
eV	Elektronvolt
FWHM	Full Width Half Maximum
GBq	Giga Bequerel
GLSL	Green Light Stimulated Luminescence
Gy	Gray
h	Planck's constant
h	hour
IRSL	Infrared Stimulated Luminescence
K	Boltzmann's constant
K	Kelvin
keV	Kiloelectronvolt
kg	Kilogram
LiF: Mg,Ti	Lithium Floride Mg and Ti dopped
LiB₄O₇:Cu:In	Lithium Borate Copper and Indium dopped
m	Meter
mCi	Milicurie
mm	Milimeter
MeV	Million Electron Volt
mGy	MiliGray
MgB₄O₇:Dy:Na	Magnesium Borate Dysprosium and Sodium dopped
n	Neutron
nm	Nanometer

OSL	Optically Stimulated Luminescence
PMT	Photomultiplier tube
R	Roentgen
Rpm	Revolutions per minute
s	Frequency factor
s	Second
T	Absolute Temperature
TBq	Tera Bequerel
TL	Thermoluminescence
TLD	Thermoluminescence Dosimeter
Γ	Gamma ray
α	Alpha particles
β	Beta particles
λ	Wavelength
ν	Frequency of radiation
ν_0	Threshold frequency
σ	Standard Deviation
μg	Microgram
μm	Micrometer
τ	Life time

LIST OF FIGURES

Figure 2.1 Illustration of Photoelectric effect	4
Figure 2.2 Schematic diagram of Compton scattering.....	5
Figure 2.3 Illustration of Pair Production	5
Figure 2.4 Mechanism of fluorescence and phosphorescence.....	7
Figure 2.5 Energy-band model	8
Figure 2.6 Crystal defects and electron transitions	10
Figure 2.7 Peak 5 and peak 4 are an example of the description of the kinetic parameters after deconvolution.	20
Figure 2.8 TL glow curves of CaF ₂ : Dy TLD 200.....	20
Figure 2.9 TL glow curves of Li ₂ B ₄ O ₇ :Cu:In	21
Figure 2.10 TL glow curves of Li ₂ B ₄ O ₇ :Cu:In	22
Figure 3.1 MgB ₄ O ₇ :Dy chips	23
Figure 3.2 LiF: Mg,Ti TLD 100 chip	24
Figure 3.3 Li ₂ B ₄ O ₇ :Cu:In chips	25
Figure 3.4 CaF ₂ :Dy TLD 200 chips	26
Figure 3.5 Thermalox TM 995 BeO chips.....	27
Figure 3.6 Quartz	28
Figure 3.7 Preparation of quartz	30
Figure 3.8 Jaw crusher	30
Figure 3.9 Sieves.....	31
Figure 3.10 Heidolph MR Hei-Tec magnetic stirrer.....	31
Figure 3.11 Analytical balance	32
Figure 3.12 Linear positioning bench	35
Figure 3.13 Platform on the bench.....	35
Figure 3.14 Sample holder on the bench	36
Figure 3.15 PTW 0.6cc farmer ionisation chamber	36
Figure 3.16 Gamma source irradiator	37
Figure 3.17 Gamma source irradiator	37
Figure 3.18 Gamma source irradiator	37
Figure 3.19 Sample located in the box.....	37
Figure 3.20 Riso TL / OSL reader	38

Figure 3.21 Schematic Diagram of the RisØ TL / OSL luminescence reader (RisØ DTU Guide to the RisØ TL / OSL, 2008).....	39
Figure 3.22 Sample discs and cups (planchettes) are shown on the left. On the right a sample carrousel (sometimes referred to as “turntable”) is shown	40
Figure 3.23 TLD Harshaw 3500	43
Figure 3.24 Schematic Diagram of a TLD Harshaw 3500	43
Figure 3.25 Elsec 9010 system (PM tube were placed).....	44
Figure 3.26 ELSEC 9010 OSL system (β source were placed)	44
Figure 3.27 PTW Freiburg Typ 1321 Oven.....	46
Figure 3.28 Stainless steel Annealing Tray	46
Figure 3.29 Protherm Furnace PLF 120/12	46
Figure 4.1 TL glow curves of $\text{Li}_2\text{B}_4\text{O}_7:\text{Cu}:\text{In}$ obtained after various doses within the range 50 mGy – 3500 mGy at a dose rate of 2Gy/h. Each TL glow curve is the average of two individual measurements. Reheats (background) has been subtracted.....	49
Figure 4.2 TL glow curves of $\text{Li}_2\text{B}_4\text{O}_7:\text{Cu}:\text{In}$ obtained after various doses within the range 50 mGy – 3500 mGy at a dose rate of 30Gy/h. Each TL glow curve is the average of two individual measurements. Reheats (background) has been subtracted	50
Figure 4.3 TL glow curves of $\text{LiF}:\text{Mg},\text{Ti}$ -TLD 100 obtained after various doses within the range 50 mGy – 3500 mGy at a dose rate of 2Gy/h. Each TL glow curve is the average of two individual measurements. Reheats (background) has been subtracted	51
Figure 4.4 TL glow curves of $\text{LiF}:\text{Mg},\text{Ti}$ -TLD 100 obtained after various doses within the range 50 mGy – 3500 mGy at a dose rate of 30Gy/h. Each TL glow curve is the average of two individual measurements. Reheats (background) has been subtracted	52
Figure 4.5 TL glow curves of $\text{MgB}_4\text{O}_7:\text{Dy}:\text{Na}$ obtained after various doses within the range 50 mGy – 3500 mGy at a dose rate of 2Gy/h. Each TL glow curve is the average of two individual measurements. Reheats (background) has been subtracted	53
Figure 4.6 TL glow curves of $\text{MgB}_4\text{O}_7:\text{Dy}:\text{Na}$ obtained after various doses within the range 50 mGy – 3500 mGy at a dose rate of 30Gy/h. Each TL glow curve is the average of two individual measurements. Reheats (background) has been subtracted	54
Figure 4.7 TL glow curves of $\text{CaF}_2:\text{Dy}$ TLD 200 obtained after various doses within the range 50 mGy – 3500 mGy at a dose rate of 2Gy/h. Each TL glow curve is the average of two measurements. Reheats (individual background) has been subtracted.....	54
Figure 4.8 TL glow curves of $\text{CaF}_2:\text{Dy}$ TLD 200 obtained after various doses within the range 50 mGy – 3500 mGy at a dose rate of 30Gy/h. Each	

	TL glow curve is the average of two individual measurements. Reheats (background) has been subtracted	55
Figure 4.9	TL glow curves of BeO obtained after various doses within the range 50 mGy – 3500 mGy at a dose rate of 2Gy/h. Each TL glow curve is the average of two individual measurements. Reheats (background) has been subtracted	55
Figure 4.10	TL glow curves of BeO obtained after various doses within the range 50 mGy – 3500 mGy at a dose rate of 30Gy/h. Each TL glow curve is the average of two individual measurements. Reheats (background) has been subtracted	56
Figure 4.11	OSL decay curves of BeO obtained after various doses within the range 50 mGy – 3500 mGy at a dose rate of 2Gy/h. Each OSL curve is the average of two individual measurements (OSL axis is logarithmic)	57
Figure 4.12	OSL decay curves of BeO obtained after various doses within the range 50 mGy – 3500 mGy at a dose rate of 30Gy/h. Each OSL curve is the average of two individual measurements (OSL axis is logarithmic)	57
Figure 4.13	OSL decay curves of Quartz obtained after various doses within the range 50 mGy – 3500 mGy at a dose rate of 27Gy/h. Each OSL curve is the average of two individual measurements (OSL axis is logarithmic)	58
Figure 4.14	OSL decay curves of Quartz obtained after various doses within the range 50 mGy – 3500 mGy at a dose rate of 311Gy/h. Each OSL curve is the average of two individual measurements (OSL axis is logarithmic)	58
Figure 4.15	OSL decay curves of Quartz obtained after various doses within the range 50 mGy – 3500 mGy at a dose rate of 1305Gy/h. Each OSL curve is the average of two individual measurements (OSL axis is logarithmic)	59
Figure 4.16	Deconvolution example for the TL glow curve of $\text{Li}_2\text{B}_4\text{O}_7:\text{Cu}:\text{In}$. The curve corresponds to a dose of 2002mGy at a dose rate of 2Gy/h. Open dots correspond to experimentally obtained data points, while lines correspond to the individual TL peaks as well as the theoretical (fitted) line. Two TL peaks were used for fitting of high quality. FOM value was 1.990	60
Figure 4.17	Deconvolution example for the TL glow curve of $\text{Li}_2\text{B}_4\text{O}_7:\text{Cu}:\text{In}$. The curve corresponds to a dose of 2496mGy at a dose rate of 30Gy/h. Open dots correspond to experimentally obtained data points, while lines correspond to the individual TL peaks as well as the theoretical (fitted) line. Two TL peaks were used for fitting of high quality. FOM value was 2.622	61
Figure 4.18	Deconvolution example for the TL glow curve of $\text{CaF}:\text{Dy}$ TLD 200. The curve corresponds to a dose of 2998mGy at a dose rate of 2Gy/h.	

Open dots correspond to experimentally obtained data points, while lines correspond to the individual TL peaks as well as the theoretical (fitted) line. Two TL peaks were used for fitting of high quality. FOM value was 2.74	61
Figure 4.19 Deconvolution example for the TL glow curve of CaF:Dy TLD 200. The curve corresponds to a dose of 2998mGy at a dose rate of 30Gy/h. Open dots correspond to experimentally obtained data points, while lines correspond to the individual TL peaks as well as the theoretical (fitted) line. Two TL peaks were used for fitting of high quality. FOM value was 1.085	62
Figure 4.20 Deconvolution example for the TL glow curve of LiF: Mg,Ti TLD 100. The curve corresponds to a dose of 2496mGy at a dose rate of 2Gy/h. Open dots correspond to experimentally obtained data points, while lines correspond to the individual TL peaks as well as the theoretical (fitted) line. Two TL peaks were used for fitting of high quality. FOM value was 3.117	62
Figure 4.21 Deconvolution example for the TL glow curve of LiF TLD 100. The curve corresponds to a dose of 2998mGy at a dose rate of 30Gy/h. Open dots correspond to experimentally obtained data points, while lines correspond to the individual TL peaks as well as the theoretical (fitted) line. Two TL peaks were used for fitting of high quality. FOM value was 5.147	63
Figure 4.22 Deconvolution example for the TL glow curve of BeO. The curve corresponds to a dose of 2496mGy at a dose rate of 2Gy/h. Open dots correspond to experimentally obtained data points, while lines correspond to the individual TL peaks as well as the theoretical (fitted) line. Two TL peaks were used for fitting of high quality. FOM value was 0.580	63
Figure 4.23 Deconvolution example for the TL glow curve of BeO. The curve corresponds to a dose of 2496mGy at a dose rate of 30Gy/h. Open dots correspond to experimentally obtained data points, while lines correspond to the individual TL peaks as well as the theoretical (fitted) line. Two TL peaks were used for fitting of high quality. FOM value was 0.762	64
Figure 4.24 Deconvolution example for the OSL decay curve of BeO. The curve corresponds to a dose of 2496mGy at a dose rate of 2Gy/h. Open dots correspond to experimentally obtained data points, while lines correspond to the individual OSL components as well as the theoretical (fitted) line. Two OSL components were used for fitting of high quality. FOM value was 0.39	65
Figure 4.25 Deconvolution example for the OSL decay curve of BeO. The curve corresponds to a dose of 2496mGy at a dose rate of 30Gy/h. Open dots correspond to experimentally obtained data points, while lines correspond to the individual OSL components as well as the	

theoretical (fitted) line. Two OSL components were used for fitting of high quality. FOM value was 0.80	65
Figure 4.26 Deconvolution example for the OSL decay curve of Quartz. The curve corresponds to a dose of 75Gy at a dose rate of 27Gy/h. Open dots correspond to experimentally obtained data points, while lines correspond to the individual OSL components as well as the theoretical (fitted) line. Three OSL components were used for fitting of high quality. FOM value was 5.15.....	66
Figure 4.27 Deconvolution example for the OSL decay curve of Quartz. The curve corresponds to a dose of 1500Gy at a dose rate of 311Gy/h. Open dots correspond to experimentally obtained data points, while lines correspond to the individual OSL components as well as the theoretical (fitted) line. Three OSL components were used for fitting of high quality. FOM value was 5.78.....	66
Figure 4.28 Deconvolution example for the OSL decay curve of Quartz. The curve corresponds to a dose of 1500Gy at a dose rate of 311Gy/h. Open dots correspond to experimentally obtained data points, while lines correspond to the individual OSL components as well as the theoretical (fitted) line. Three OSL components were used for fitting of high quality. FOM value was 4.15.....	67
Figure 4.29 Component resolved TL dose response curves obtained for TL single peak of MgB ₄ O ₇ :Dy:Na. Dots correspond to 2 Gy/h and squares correspond to 30 Gy/h. Each data point corresponds to an average of two individually measured values. Error bars correspond to 1σ (Errors are very small).....	68
Figure 4.30 Component resolved TL dose response curves obtained for TL peak 4 of Li ₂ B ₄ O ₇ :Cu:In. Dots correspond to 2 Gy/h and squares correspond to 30 Gy/h. Each data point corresponds to an average of two individually measured values. Error bars correspond to 1σ (Errors are very small).....	69
Figure 4.31 Component resolved TL dose response curves obtained for TL peak 5 of Li ₂ B ₄ O ₇ :Cu:In. Dots correspond to 2 Gy/h and squares correspond to 30 Gy/h. Each data point corresponds to an average of two individually measured values. Error bars correspond to 1σ (Errors are very small).....	69
Figure 4.32 Component resolved TL dose response curves obtained for TL peak 4 of CaF ₂ : Dy TLD 200. Dots correspond to 2 Gy/h and squares correspond to 30 Gy/h. Each data point corresponds to an average of two individually measured values. Error bars correspond to 1σ (Errors are very small) (TL&dose axis are logarithmic)	70
Figure 4.33 Component resolved TL dose response curves obtained for TL peak 5 of CaF ₂ : Dy TLD 200. Dots correspond to 2 Gy/h and squares correspond to 30 Gy/h. Each data point corresponds to an average of two individually measured values. Error bars correspond to 1σ (Errors are very small).....	70

Figure 4.34 Component resolved TL dose response curves obtained for TL peak 4 of LiF TLD 100. Dots correspond to 2 Gy/h and squares correspond to 30 Gy/h. Each data point corresponds to an average of two individually measured values. Error bars correspond to 1σ (Errors are very small).....	71
Figure 4. 35 Component resolved TL dose response curves obtained for TL peak 5 of LiF TLD 100. Dots correspond to 2 Gy/h and squares correspond to 30 Gy/h. Each data point corresponds to an average of two individually measured values. Error bars correspond to 1σ (Errors are very small).....	71
Figure 4.36 Component resolved TL dose response curves obtained for TL peak 1 of BeO. Dots correspond to 2 Gy/h and squares correspond to 30 Gy/h. Each data point corresponds to an average of two individually measured values. Error bars correspond to 1σ (Errors are very small).....	72
Figure 4.37 Component resolved TL dose response curves obtained for TL peak 2 of BeO. Dots correspond to 2 Gy/h and squares correspond to 30 Gy/h. Each data point corresponds to an average of two individually measured values. Error bars correspond to 1σ (Errors are very small).....	72
Figure 4.38 Order of kinetic, b, versus dose curves obtained for TL peak 4 of $\text{Li}_2\text{B}_4\text{O}_7$: Cu: In; the values were yielded after deconvolution analysis. Dots correspond to 2 Gy/h and squares correspond to 30 Gy/h. Each data point corresponds to an average of two individually measured values. Error bars correspond to 1σ	74
Figure 4.39 Order of kinetic, b, versus dose curves obtained for TL peak 5 of $\text{Li}_2\text{B}_4\text{O}_7$: Cu: In; the values were yielded after deconvolution analysis. Dots correspond to 2 Gy/h and squares correspond to 30 Gy/h. Each data point corresponds to an average of two individually measured values. Error bars correspond to 1σ	74
Figure 4.40 Order of kinetic, b, versus dose curves obtained for TL peak 4 of CaF_2 : Dy TLD 200; the values were yielded after deconvolution analysis. Dots correspond to 2 Gy/h and squares correspond to 30 Gy/h. Each data point corresponds to an average of two individually measured values. Error bars correspond to 1σ (Errors are very small).....	75
Figure 4.41 Order of kinetic, b, versus dose curves obtained for TL peak 5 of CaF_2 : Dy TLD 200; the values were yielded after deconvolution analysis. Dots correspond to 2 Gy/h and squares correspond to 30 Gy/h. Each data point corresponds to an average of two individually measured values. Error bars correspond to 1σ	75
Figure 4.42 Order of kinetic, b, versus dose curves obtained for TL peak 4 of LiF: Mg,Ti TLD 100; the values were yielded after deconvolution analysis. Dots correspond to 2 Gy/h and squares correspond to 30 Gy/h. Each data point corresponds to an average of two individually measured values. Error bars correspond to 1σ	76

Figure 4.43 Order of kinetic, b , versus dose curves obtained for TL peak 5 of LiF : Mg,Ti TLD 100; the values were yielded after deconvolution analysis. Dots correspond to 2 Gy/h and squares correspond to 30 Gy/h. Each data point corresponds to an average of two individually measured values. Error bars correspond to 1σ	76
Figure 4.44 Order of kinetic, b , versus dose curves obtained for TL peak 1 of BeO; the values were yielded after deconvolution analysis. Dots correspond to 2 Gy/h and squares correspond to 30 Gy/h. Each data point corresponds to an average of two individually measured values. Error bars correspond to 1σ	77
Figure 4.45 Order of kinetic, b , versus dose curves obtained for TL peak 2 of BeO; the values were yielded after deconvolution analysis. Dots correspond to 2 Gy/h and squares correspond to 30 Gy/h. Each data point corresponds to an average of two individually measured values. Error bars correspond to 1σ	77
Figure 4.46 Activation energy, E , versus dose curves obtained for TL peak 4 of $\text{Li}_2\text{B}_4\text{O}_7$:Cu:In; the E values were yielded after deconvolution analysis. Dots correspond to 2 Gy/h and squares correspond to 30 Gy/h. Each data point corresponds to an average of two individually measured values. Error bars correspond to 1σ	78
Figure 4.47 Activation energy, E , versus dose curves obtained for TL peak 5 of $\text{Li}_2\text{B}_4\text{O}_7$:Cu:In; the E values were yielded after deconvolution analysis. Dots correspond to 2 Gy/h and squares correspond to 30 Gy/h. Each data point corresponds to an average of two individually measured values. Error bars correspond to 1σ	78
Figure 4.48 Activation energy, E , versus dose curves obtained for TL peak 4 of CaF_2 : Dy TLD 200; the E values were yielded after deconvolution analysis. Dots correspond to 2 Gy/h and squares correspond to 30 Gy/h. Each data point corresponds to an average of two individually measured values. Error bars correspond to 1σ (Errors are very small).....	79
Figure 4.49 Activation energy, E , versus dose curves obtained for TL peak 5 of CaF_2 : Dy TLD 200; the E values were yielded after deconvolution analysis. Dots correspond to 2 Gy/h and squares correspond to 30 Gy/h. Each data point corresponds to an average of two individually measured values. Error bars correspond to 1σ (Errors are very small).....	79
Figure 4.50 Activation energy, E , versus dose curves obtained for TL peak 4 of LiF: Mg,Ti TLD 100; the E values were yielded after deconvolution analysis. Dots correspond to 2 Gy/h and squares correspond to 30 Gy/h. Each data point corresponds to an average of two individually measured values. Error bars correspond to 1σ	80
Figure 4.51 Activation energy, E , versus dose curves obtained for TL peak 5 of LiF: Mg,Ti TLD 100; the E values were yielded after deconvolution analysis. Dots correspond to 2 Gy/h and squares correspond to 30 Gy/h. Each data point corresponds to an average of two individually measured values. Error bars correspond to 1σ	80

Figure 4.52	Activation energy, E , versus dose curves obtained for TL peak 1 of BeO; the E values were yielded after deconvolution analysis. Dots correspond to 2 Gy/h and squares correspond to 30 Gy/h. Each data point corresponds to an average of two individually measured values. Error bars correspond to 1σ	81
Figure 4.53	Activation energy, E , versus dose curves obtained for TL peak 2 of BeO; the E values were yielded after deconvolution analysis. Dots correspond to 2 Gy/h and squares correspond to 30 Gy/h. Each data point corresponds to an average of two individually measured values. Error bars correspond to 1σ	81
Figure 4.54	Component resolved OSL dose response curves obtained for OSL component c_1 of BeO. Dots correspond to 2 Gy/h and squares correspond to 30 Gy/h. Each data point corresponds to an average of two individually measured values. Error bars correspond to 1σ . (Errors are very small)(axis are logarithmic).....	83
Figure 4.55	Component resolved OSL dose response curves obtained for OSL component c_2 of BeO. Dots correspond to 2 Gy/h and squares correspond to 30 Gy/h. Each data point corresponds to an average of two individually measured values. Error bars correspond to 1σ . (Errors are very small)(axis are logarithmic).....	83
Figure 4.56	Component resolved OSL dose response curves obtained for OSL component c_1 of Quartz. Dots correspond to 27 Gy/h, squares correspond to 311 Gy/h and triangles correspond to 1305Gy/h. Each data point corresponds to an average of two individually measured values. Error bars correspond to 1σ . (Errors are very small)(axis are logarithmic).....	84
Figure 4.57	Component resolved OSL dose response curves obtained for OSL component c_2 of Quartz. Dots correspond to 27 Gy/h, squares correspond to 311 Gy/h and triangles correspond to 1305Gy/h. Each data point corresponds to an average of two individually measured values. Error bars correspond to 1σ . (Errors are very small)(axis are logarithmic).....	84
Figure 4.58	Component resolved OSL dose response curves obtained for OSL component c_3 of Quartz. Dots correspond to 27 Gy/h, squares correspond to 311 Gy/h and triangles correspond to 1305Gy/h. Each data point corresponds to an average of two individually measured values. Error bars correspond to 1σ . (Errors are very small)(axis are logarithmic).....	85
Figure 4.59	OSL component lifetime, τ , versus dose curves obtained for OSL component τ_1 of BeO; these τ values were yielded after deconvolution analysis. Dots correspond to 2 Gy/h and squares correspond to 30 Gy/h. Each data point corresponds to an average of two individually measured values. Error bars correspond to 1σ	86
Figure 4. 60	OSL component lifetime, τ , versus dose curves obtained for OSL component τ_2 of BeO; these τ values were yielded after deconvolution	

analysis. Dots correspond to 2 Gy/h and squares correspond to 30 Gy/h. Each data point corresponds to an average of two individually measured values. Error bars correspond to 1σ .	86
Figure 4.61 OSL component lifetime, τ , versus dose curves obtained for OSL component τ_1 of Quartz; these τ values were yielded after deconvolution analysis. Dots correspond to 27 Gy/h, squares correspond to 311 Gy/h and triangles correspond to 1305Gy/h. Each data point corresponds to an average of two individually measured values. Error bars correspond to 1σ	87
Figure 4.62 OSL component lifetime, τ , versus dose curves obtained for OSL component τ_2 of Quartz; these τ values were yielded after deconvolution analysis. Dots correspond to 27 Gy/h, squares correspond to 311 Gy/h and triangles correspond to 1305Gy/h. Each data point corresponds to an average of two individually measured values. Error bars correspond to 1σ	88
Figure 4.63 OSL component lifetime, τ , versus dose curves obtained for OSL component τ_3 of Quartz; these τ values were yielded after deconvolution analysis. Dots correspond to 27 Gy/h, squares correspond to 311 Gy/h and triangles correspond to 1305Gy/h. Each data point corresponds to an average of two individually measured values. Error bars correspond to 1σ .	89
Figure 5.1 OSL component lifetime differences, $\Delta\tau$, versus dose curves obtained for OSL component τ_1 of Quartz. The differences were calculated for the dose rates 1305 Gy/h and 311 Gy/h Error bars correspond to 1σ . (Errors are small)	93
Figure 5.2 OSL component lifetime differences, $\Delta\tau$, versus dose curves obtained for OSL component τ_2 of Quartz. The differences were calculated for the dose rates 1305Gy/h and 311 Gy/h. Error bars correspond to 1σ .	93
Figure 5.3 OSL component lifetime differences, $\Delta\tau$, versus dose curves obtained for OSL component τ_3 of Quartz. The differences were calculated for the dose rates 1305Gy/h and 311 Gy/h. Error bars correspond to 1σ .	94
Figure 5.4 OSL component lifetime differences, $\Delta\tau$, versus dose curves obtained for OSL component τ_1 of Quartz. The differences were calculated for the dose rates 1305Gy/h and 27 Gy/h. Error bars correspond to 1σ . (Errors are small)	94
Figure 5.5 OSL component lifetime differences, $\Delta\tau$, versus dose curves obtained for OSL component τ_2 of Quartz. The differences were calculated for the dose rates 1305Gy/h and 27 Gy/h. Error bars correspond to 1σ .	95
Figure 5.6 OSL component lifetime differences, $\Delta\tau$, versus dose curves obtained for OSL component τ_3 of Quartz. The differences were calculated for the dose rates 1305Gy/h and 27 Gy/h. Error bars correspond to 1σ . (Errors are small)	95

Figure 5.7 OSL component lifetime differences, $\Delta\tau$, versus dose curves obtained for OSL component τ_1 of Quartz. The differences were calculated for the dose rates 311Gy/h and 27 Gy/h. Error bars correspond to 1σ	96
Figure 5.8 OSL component lifetime differences, $\Delta\tau$, versus dose curves obtained for OSL component τ_2 of Quartz. The differences were calculated for the dose rates 311Gy/h and 27 Gy/h. Error bars correspond to 1σ	96
Figure 5.9 OSL component lifetime differences, $\Delta\tau$, versus dose curves obtained for OSL component τ_3 of Quartz. The differences were calculated for the dose rates 311Gy/h and 27 Gy/h. Error bars correspond to 1σ	97
Figure 5.10 OSL component lifetime differences, $\Delta\tau$, versus dose curves obtained for OSL component τ_1 of BeO. The differences were calculated for the dose rates 30Gy/h and 2Gy/h. Error bars correspond to 1σ	97
Figure 5.11 OSL component lifetime differences, $\Delta\tau$, versus dose curves obtained for OSL component τ_2 of BeO. The differences were calculated for the dose rates 30Gy/h and 2Gy/h. Error bars correspond to 1σ	98
Figure 5.12 OSL component integrated intensity differences, ΔI_{ci} , versus dose curves obtained for OSL component c_1 of Quartz. The differences were calculated for the dose rates 1305 Gy/h and 311 Gy/h. Error bars correspond to 1σ .(Errors are very small)	99
Figure 5.13 OSL component integrated intensity differences, ΔI_{ci} , versus dose curves obtained for OSL component c_2 of Quartz. The differences were calculated for the dose rates 1305 Gy/h and 311 Gy/h. Error bars correspond to 1σ .(Errors are very small)	99
Figure 5.14 OSL component integrated intensity differences, ΔI_{ci} , versus dose curves obtained for OSL component c_3 of Quartz. The differences were calculated for the dose rates 1305 Gy/h and 311 Gy/h. Error bars correspond to 1σ .(Errors are very small)	100
Figure 5.15 OSL component integrated intensity differences, ΔI_{ci} , versus dose curves obtained for OSL component c_1 of Quartz. The differences were calculated for the dose rates 1305 Gy/h and 27 Gy/h. Error bars correspond to 1σ (Errors are very small)	100
Figure 5.16 OSL component integrated intensity differences, ΔI_{ci} , versus dose curves obtained for OSL component c_2 of Quartz. The differences were calculated for the dose rates 1305 Gy/h and 27 Gy/h. Error bars correspond to 1σ	101
Figure 5.17 OSL component integrated intensity differences, ΔI_{ci} , versus dose curves obtained for OSL component c_3 of Quartz. The differences were calculated for the dose rates 1305 Gy/h and 27 Gy/h. Error bars correspond to 1σ (Errors are very small)	101
Figure 5.18 OSL component integrated intensity differences, ΔI_{ci} , versus dose curves obtained for OSL component c_1 of Quartz. The differences were calculated for the dose rates 311 Gy/h and 27 Gy/h. Error bars correspond to 1σ (Errors are very small)	102

Figure 5.19 OSL component integrated intensity differences, ΔI_{ci} , versus dose curves obtained for OSL component c_2 of Quartz. The differences were calculated for the dose rates 311 Gy/h and 27 Gy/h. Error bars correspond to 1σ (Errors are very small)	102
Figure 5.20 OSL component integrated intensity differences, ΔI_{ci} , versus dose curves obtained for OSL component c_3 of Quartz. The differences were calculated for the dose rates 311 Gy/h and 27 Gy/h. Error bars correspond to 1σ (Errors are very small)	103
Figure 5.21 OSL component integrated intensity differences, ΔI_{ci} , versus dose curves obtained for OSL component c_1 of BeO. The differences were calculated for the dose rates 30 Gy/h and 2 Gy/h. Error bars correspond to 1σ (Errors are very small)	103
Figure 5.22 OSL component integrated intensity differences, ΔI_{ci} , versus dose curves obtained for OSL component c_2 of BeO. The differences were calculated for the dose rates 30 Gy/h and 2 Gy/h. Error bars correspond to 1σ (Errors are very small)	104
Figure 5.23 TL peak integrated intensity differences, ΔI_{pi} , versus dose curves obtained for TL peak 4 of $\text{Li}_2\text{B}_4\text{O}_7:\text{Cu:In}$. The differences were calculated for the dose rates 30 Gy/h and 2 Gy/h. Error bars correspond to 1σ (Errors are very small)	105
Figure 5.24 TL peak integrated intensity differences, ΔI_{pi} , versus dose curves obtained for TL peak 5 of $\text{Li}_2\text{B}_4\text{O}_7:\text{Cu:In}$. The differences were calculated for the dose rates 30 Gy/h and 2 Gy/h. Error bars correspond to 1σ (Errors are very small)	105
Figure 5.25 TL peak integrated intensity differences, ΔI_{pi} , versus dose curves obtained for TL peak 4 of $\text{CaF}_2:\text{Dy}$ TLD 200. The differences were calculated for the dose rates 30 Gy/h and 2 Gy/h. Error bars correspond to 1σ (Errors are very small)	106
Figure 5.26 TL peak integrated intensity differences, ΔI_{pi} , versus dose curves obtained for TL peak 5 of $\text{CaF}_2:\text{Dy}$ TLD 200. The differences were calculated for the dose rates 30 Gy/h and 2 Gy/h. Error bars correspond to 1σ (Errors are very small)	106
Figure 5.27 TL peak integrated intensity differences, ΔI_{pi} , versus dose curves obtained for TL peak 4 of LiF: Mg,Ti TLD 100. The differences were calculated for the dose rates 30 Gy/h and 2 Gy/h. Error bars correspond to 1σ (Errors are very small)	107
Figure 5.28 TL peak integrated intensity differences, ΔI_{pi} , versus dose curves obtained for TL peak 5 of LiF: Mg,Ti TLD 100. The differences were calculated for the dose rates 30 Gy/h and 2 Gy/h. Error bars correspond to 1σ (Errors are very small)	107
Figure 5.29 TL peak integrated intensity differences, ΔI_{pi} , versus dose curves obtained for TL single peak of $\text{MgB}_4\text{O}_7:\text{Dy:Na}$. The differences were calculated for the dose rates 30 Gy/h and 2 Gy/h. Error bars correspond to 1σ (Errors are very small)	108

Figure 5.30 TL peak integrated intensity differences, ΔI_{pi} , versus dose curves obtained for TL peak 1 of BeO. The differences were calculated for the dose rates 30 Gy/h and 2 Gy/h. Error bars correspond to 1σ (Errors are very small).....	108
Figure 5.31 TL peak integrated intensity differences, ΔI_{pi} , versus dose curves obtained for TL peak 2 of BeO. The differences were calculated for the dose rates 30 Gy/h and 2 Gy/h. Error bars correspond to 1σ (Errors are very small).....	109
Figure 5.32 Activation energy differences, ΔE , versus dose curves obtained for TL peak 4 of $Li_2B_4O_7 :Cu:In$. The differences were calculated for the dose rates 30 Gy/h and 2 Gy/h. Error bars correspond to 1σ	110
Figure 5.33 Activation energy differences, ΔE , versus dose curves obtained for TL peak 5 of $Li_2B_4O_7 :Cu:In$. The differences were calculated for the dose rates 30 Gy/h and 2 Gy/h. Error bars correspond to 1σ	110
Figure 5.34 Activation energy differences, ΔE , versus dose curves obtained for TL peak 4 of $CaF_2:Dy$ TLD 200.The differences were calculated for the dose rates 30 Gy/h and 2 Gy/h. Error bars correspond to 1σ	111
Figure 5.35 Activation energy differences, ΔE , versus dose curves obtained for TL peak 5 of $CaF_2:Dy$ TLD 200.The differences were calculated for the dose rates 30 Gy/h and 2 Gy/h. Error bars correspond to 1σ	111
Figure 5.36 Activation energy differences, ΔE , versus dose curves obtained for TL peak 4 of LiF TLD 100.The differences were calculated for the dose rates 30 Gy/h and 2 Gy/h. Error bars correspond to 1σ	112
Figure 5.37 Activation energy differences, ΔE , versus dose curves obtained for TL peak 5 of LiF TLD 100.The differences were calculated for the dose rates 30 Gy/h and 2 Gy/h. Error bars correspond to 1σ	112
Figure 5.38 Activation energy differences, ΔE , versus dose curves obtained for TL peak 1 of BeO.The differences were calculated for the dose rates 30 Gy/h and 2 Gy/h. Error bars correspond to 1σ	113
Figure 5.39 Activation energy differences, ΔE , versus dose curves obtained for TL peak 2 of BeO.The differences were calculated for the dose rates 30 Gy/h and 2 Gy/h. Error bars correspond to 1σ	113
Figure 5.40 Component resolved TL dose response curves obtained for TL peak 1 of BeO. Dots correspond to 2 Gy/h and squares correspond to 30 Gy/h. Each data point corresponds to an average of two individually measured values. Error bars correspond to 1σ (Errors are very small)(Axis are logarithmic)	117
Figure 5.41 An example of dose response fitting using equation 5.1 for the fast (c_1) component of quartz. The fitting parameters are presented in Table 5.1.	119

LIST OF TABLES

Table 3.1 All procedures applied to the dosimetric materials.....	29
Table 5.1 Dose response curve behaviours of the de-convolved TL peaks and OSL components	91



1. INTRODUCTION

The mechanism of luminescence and all studies related to this mechanism carry information about the radiation dose in a given period of time from the past to the present. The materials with the luminescence mechanism can maintain the radiation dose on it for many years. For this reason, to reach some information about the past or recent past, luminescence method can be used. After exposed to radioactive rays in the environment dosimeters are used to determine the radiation doses. Dosimeters are used for determining the dose and dose rate in all radiation application processes. In the literature gamma dose response and analysing of kinetic parameters were studied but the originality of this thesis is to determine the kinetic parameters and dose response curves at different gama dose rates. Especially for quartz materials, only one study was done about the gamma dose rate effects on quartz (Chen et al 1981).

The luminescence response of all materials was calibrated using 0.5 Gy irradiation. All artificial materials were irradiated using a 130 TeraBq Co-60 source in two different dose rates, 2 Gy/h and 30 Gy/h respectively and the only natural material quartz was irradiated using a 140 TeraBq Co-60 source in three different dose rates, 27 Gy/h, 311 Gy/h and 1305 Gy/h respectively. For each artificial material, 12 dose steps were included, while for every dose step, 2 chips were used. The dose steps were 52, 104, 199.33, 303.33, 502.66, 797.33, 996.66, 1499.33, 2002, 2496, 2998.66 and 3501.33 mGy. For quartz at 27 G/h dose rate, dose steps were, 500, 250, 150, 75, 54, 25, 13 Gy and for both 311 Gy/h and 1305 Gy/h, dose steps were 2000, 1500, 1000, 750, 500, 250, 150, 100, 75, 54, 25, 13 Gy. All luminescence measurements were carried out using Harshaw 3500 TLD reader and Riso within 3 days after irradiation.

2. THEORY

The environment which we live in, has a natural radiation effect so we are exposed to radioactive rays in our environment continuously. Any substance in this environment is affected by the radiation. Thus, radiation applications and radiation measurements are becoming increasingly important due to the use of radiation with advancement of technology. Measurement of the amount of radiation is very important in both health and other sciences such as physics. To measure the radiation doses such as exposure, kerma, absorbed dose, equivalent dose or other related quantities, a dosimeter is used; which is a device, that measures doses directly or indirectly. Dosimeters are used to determine the dose and dose rate in all radiation applications. The luminescence process is used in the radiation dosimeter to detect radiation to which humans are exposed to and to date archaeological artifacts.

Radioactive rays, in particular as a result of their interaction with semiconductor materials, can produce permanent effects on the structure of the substance. The luminescence method is one of the nuclear techniques used to determine these effects that occur in semiconductor materials. The observed luminescence is referred to the source used to trap electrons or the source used to remove electrons from the traps. The luminescence resulting from the use of heat or light to remove electrons from traps is termed thermoluminescence (TL) and optically stimulated luminescence (OSL), respectively.

TL has been widely used since the early 1950s to measure radiation doses (Bøtter-Jensen et al. 2003). The method began to be used in dating in the 1960s with a rapid development and was first used in 1985 by Huntley et al. OSL was also introduced for the purpose of dating by Huntley et al. in 1985.

Many natural materials, such as quartz and feldspar minerals, have been studied as thermoluminescence dosimeters. Quartz yields good luminescence signals and is frequently used in dating studies using luminescence method. Various applications of quartz include thermoluminescence (TL) dosimeter (de Lima et al. 2002, Hashimoto et al. 1998), dating (Huntley et al. 1988, McKeever 1991) and electronic instrumentation.

Natural quartz is one of the most studied materials among dosimetric materials due to its abundance in the world. Quartz composes nearly 11 percent of the Earth's crust. Because of its internal structures, dosimetric properties of quartz have been examined in a wide area (Preusser et al 2009, Topaksu et al 2013 and Martini et al 2014). For example; The TL radiation curve of natural quartz consists of several peaks observed between 100°C and 450°C (de Lima et al. 2002, Santos et al. 2001). The great diversity of its dosimetric properties has led to so many studies on luminescence properties of quartz (Preusser et al 2009, Wintle and Murray 1997, Tsukamoto et al 2007 and Wintle and Adamiec 2017). In addition, $\text{Al}_2\text{O}_3\text{:C}$; fiber, LiF, Mg, Ti; CaF_2 ; BeO; and various artificial dosimeters such as MgO are produced. These dosimeters are used as environmental dosimeters or personal dosimeters according to their effective atomic number.

In this study specific luminescence materials have been used. In the literature lots of luminescence material have been used for dosimetric properties at different doses but the originality is this study lies behind using different gamma dose rates. There is lack of studies in the literature with different gamma dose rate especially with different materials. The luminescence dosimeter measures dose response of the luminescence material. Response of the material depends on the absorption of radiation in the material. Thermoluminescence method is widely used in diagnosis and treatment in medical field together with investigations of dosimetric materials and determination of trap parameters. In the thermoluminescence technique; heating is used for the stimulation. Thermoluminescence process has various uses in archeology, geology, solid state physics, biology and organic chemistry. In the optically stimulated luminescence technique light is used for the stimulation.

2.1 Gamma Rays and the Interaction of Gamma Rays with Matter

Radiation is the energy emitted by energy packages called waves, particles or photons. According to quantum theory, this form of energy, which makes a wave motion, is spread and swallowed into very small packets of energy called quantum or photon. Radioactivity can be in the form of alpha (α) particles, beta (β) particles, X rays, gamma (γ) rays, and neutrons (n). Substances are influenced by either X and γ rays which have

penetration properties in the electromagnetic spectrum or α and β particles, which have particle characteristics. The radiation source used in this study is gamma rays. The interaction of gamma rays with matter occurs in three ways except the resonance event.

2.1.1 Photoelectric event

Whole energy of the beam, $h\nu$, is transferred to the electron at the quantized energy level of the atom. Therefore, this electron comes out of its orbit with kinetic energy $\Delta E = h\nu - h\nu_0$ (Güneşdoğdu, 1998). The ionization energy of the electron in that orbit is $h\nu_0$ energy. This is because the electron in the orbit swallows all of the incoming energy. This electron is removed from the atom and by gaining speed and is called “photoelectron”(Figure 2.1).

h : Planck's constant : $6,62 \times 10^{-34}$ Js

ν : frequency of radiation s^{-1}

ν_0 : threshold frequency s^{-1}

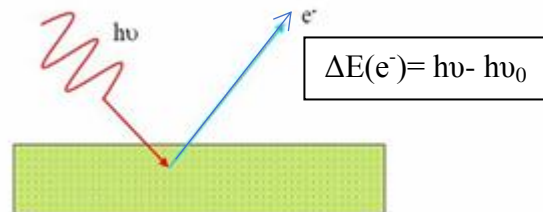


Figure 2.1 Illustration of Photoelectric effect

2.1.2 Compton scattering

Gamma rays have elastic collisions with the free electrons of the atom. Therefore, by giving some part of its energy to this electron, it enables this electron to gain speed. Therefore, energy of gamma rays decreases and electrons are scattered in different directions.

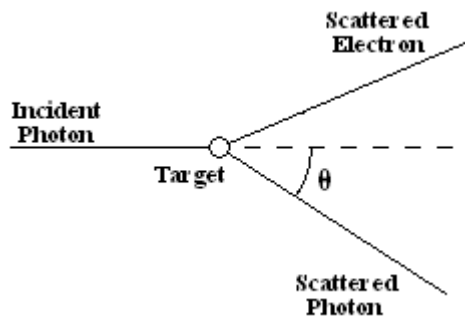


Figure 2.2 Schematic diagram of Compton scattering

2.1.3 Pair production

A gamma ray disappears near an atomic nucleus due to its strong magnetic field. This results in two electrons, one negative and one positively charged. The mass energy of an electron or positron is 0.51 MeV, so the pair production requires a photon energy of at least 1.02 MeV. The increasing part of the photon energy is the kinetic energy of the electron (e^-) and positron (e^+). The largest photon wavelength corresponding to this energy ($h\nu$) is 1.2×10^{-12} m. Electromagnetic radiation in this wavelength is called gamma rays. They are emitted by radioactive nuclei in nature, are located between cosmic rays and are represented by the symbol γ .

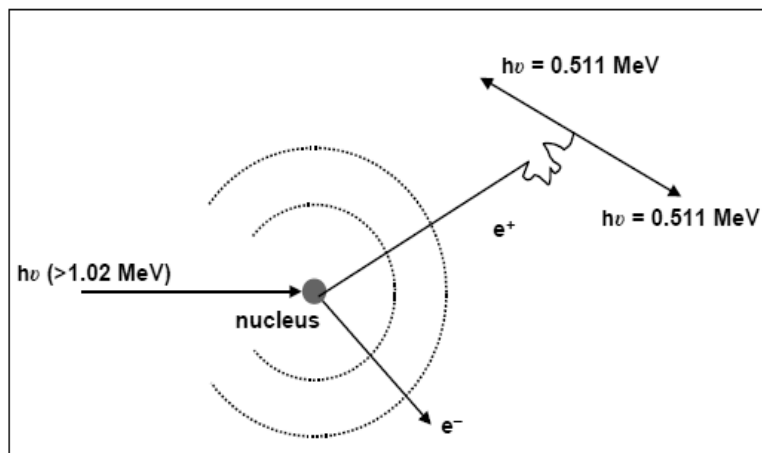


Figure 2.3 Illustration of Pair Production (Khairi A. 2014)

2.2 Dosimetry System

The system in which the processes for determining the exposed ionizing radiation dose are executed is called the dosimetry system. The devices used to determine the dose of ionizing radiation exposed are called dosimeters (<http://www.taek.gov.tr>, 2019). Individual dosimeters are divided into active and passive. Dosimeters that measure instant dose, ion chambers, electronic personnel dosimeters and so on is called active dosimeter. The dosimeters in which the radiation dose is determined after by a certain process are passive dosimeters. Examples include personel dosimeters which are made of thermoluminescence and optically stimulated dosimeters.

Retrospective dosimeters are dosimeters that are used to determine the radiation dose exposed retrospectively, especially used in either age determination or accident dosimeter. Luminescent substances are used as a retrospective dosimeters. Some materials like in this study have good luminescence properties and they can be used in dosimetric studies to determine the radiation dose.

2.3 Luminescence

Luminescence is a light in the visible region and is a general term for electromagnetic radiation that is generated by the excitation of an atom or molecule by external energy. The main difference of luminescence from other electromagnetic radiation is that it can be released without a change in the temperature of the atom or molecule. This feature is also called cold light (Thomsen 2004). Luminescent materials can absorb energy, store some of it, and convert it into light. These materials have crystalline structure.

Photoluminescence, one of the types of luminescence is caused by moving electrons to energetically higher levels through the absorption of photons and classified as fluorescence and phosphorescence.

Fluorescence: Light emission from an electron's transition from an excited state to a ground state. The excited electron state caused by energy absorption and light photon oscillation goes into the ground state. This interval is known as the lifetime of the

excitation state. Trap life is less than 10^{-8} seconds. The time spent by the electron in the trap is called the "life time". The equation 2.1 explain the life time.

$$\tau = \frac{1}{s} e^{E/kT} \quad (\text{Fleming 1979, Aitken 1985}) \quad (2.1)$$

where, τ is the life time, s is the frequency factor, E is the energy depth of trap, k is Boltzman's constant, T is absolute temperature.

Phosphorescence: The transition to the ground state is delayed by the transition from the stimulated state to a meta-stable state; there is no direct transition to the ground state. These meta-stable states function as electron traps. Excitation occurs for periods greater than 10^{-8} s (Chen and McKeever 1997). During phosphorescence, the difference between the stable state and the meta-stable state is very small, and with lattice vibrations at ambient temperature, electrons can escape from traps, and also no external energy is required. Mechanism of fluorescence and phosphorescence is given below in Figure 2.4 (McKeever 1985).

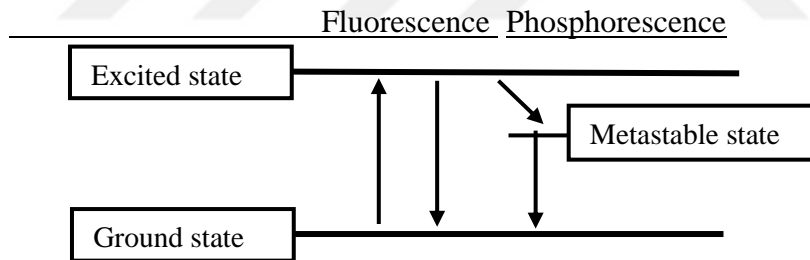


Figure 2.4 Mechanism of fluorescence and phosphorescence

An electron in the orbit of an atom is only allowed to exist at a certain energy level. Energy band model is shown in Figure 2.5 and electrons are allowed at the two outermost bands. The lowest energy band is called the valence band, the highest energy band is the conduction band. Metals have no gap between the valence and the conduction band. As for semiconductors the band gap's energy called ΔE has a value ≤ 3.2 eV. Insulators have the largest gap between valence and the conduction band (~ 3.2 to 10 eV) which is called the forbidden band and this band's energy is called Fermi energy.

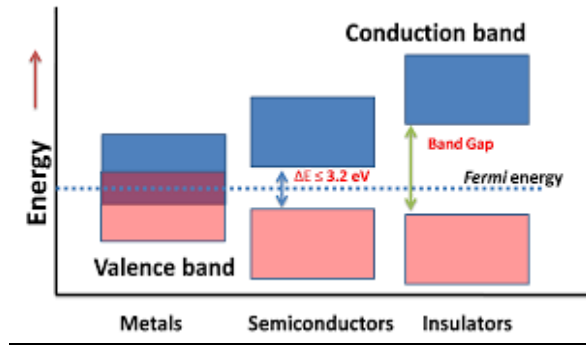


Figure 2.5 Energy-band model

Metals, semiconductors and insulators are crystalline materials. These materials are solid and classified according to the width of band gap as described in the above section. In a perfect crystal there is no electron in this forbidden band however in the real case the crystal structure is not perfect. Some crystals in nature (such as quartz and feldspar) do not always provide this ideal state and may contain a number of imperfections within their crystal structure (Vandenberghe 2004). The most common observed defects are point defects which are either intrinsic or extrinsic. The existence of the defects provide the creation of different energy states in the forbidden band. These energy states are described as trap centers and recombination centers. The state is defined as a trap center if the defect is able to catch an electron or hole and re-emit it back to the band where it come from, provided that it will get the required amount of energy. The state is defined as a recombination center if the defect is able to catch opposite sign charge carriers (electron and hole) (Larsen 1999). Structural defects in the crystal lattice create a localized charge gap that can temporarily catch a conduction band electron trying to return to the valence band. Until thermal excitation occurs, the captured electron stays in the trap at the defect E_t . After thermal excitation, captured electron goes back to the conduction band. The electron leave its trapping state according to an equation, given in Equation 2.2. The probability p is per unit time is expressed as follows:

$$p = s \exp\left(-\frac{\Delta E}{kT}\right) \quad (2.2)$$

where $\Delta E = E_c - E_t$ is the energy depth of the trap compared to the conduction band, k is the Boltzmann's constant, T is the absolute temperature and s is the frequency factor, which is the product of the electron's oscillation frequency and the coefficient of reflection (Becker, 1973). The lifetime of trap (time which the electron resides in trap) depends on ΔE , the temperature T and the frequency factor s . To evaluate the trap as a dosimetric study, the trapped electrons must have a sufficient depth (ΔE) to prevent shaking by lattice vibrations; that is, the half-life of the captured electrons in the trap must be at least in the order of weeks (Thomsen 2004).

In Figure 2.6, crystal defects and transitions are explained (Thomsen 2004). E_V is the maximum energy level of the valance band. Since the electrons tend to complete the lowest available energy states, the valance band is almost completely filled with electrons. E_C is the minimum energy level of the conduction band. Electrons which are in the conduction band are not bound to any other single atom so they are free to move in the crystal with any external electrical field. Required energy to break the bond in the crystal is $E_g(\text{gap}) = E_C - E_V$. If the electron has gain $\geq E_g$, using this energy, electrons transferred are from the valance band to the conduction band where the electrons are separated and electron-hole pairs are created.

Ionisation results in the formation of electron-hole pairs. These electrons and holes are retained in the T and H defects. Trap T_s represents an unstable trap with a high probability of thermal evacuation. T_t trap refers to the storage of electrons. In this case, without external stimulation the possibility of thermal evacuation can be neglected. This trapping level is related to dosimetry. After applying the stimulation (by heating or light) to the electron, electron gains energy. Using this energy, electron escaped from the trap and goes to the conduction band. Some electrons which escape from the traps goes to the recombination centers (R). In the recombination center, released electrons recombine with the trapped holes after then luminescence is emitted ($h\nu_{lum}$).

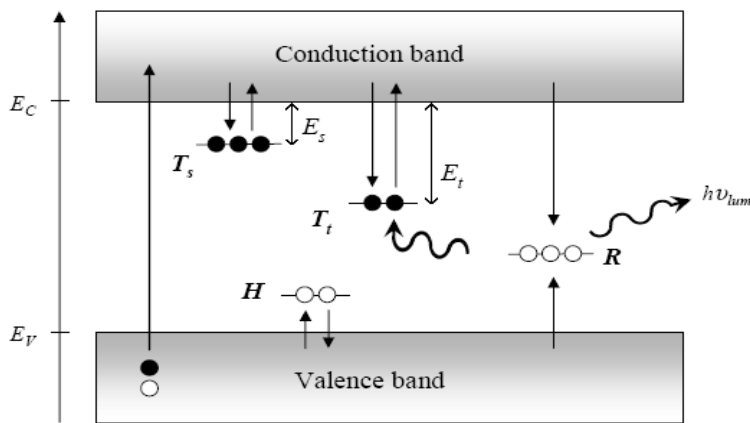


Figure 2.6 Crystal defects and electron transitions (Thomsen 2004).

2.4 Thermoluminescence

Although phosphorescence can be classified as a form of photoluminescence, it can also be classified as a special type of luminescence called thermoluminescence. When the previously irradiated insulator or semiconductor materials are heated, the radiation of energy absorbed these materials are given as light. In briefly, TL is a form of light emission that occurs when the temperature of the object is increased after exposure to some form of energy but it is not a black body radiation.

In the material, the number of electrons which reside in the trap proportional to the absorbed dose at low dose levels. The higher the temperature of the crystal, the greater the likelihood of eviction. At a given temperature range, electrons held in a particular trap type gain enough energy to overcome the potential barrier of the trap and the electrons are released into the conduction band. These electrons are called detrapped electrons and they spread in the crystal. A fraction of the detrapped electrons goes to the recombination center to recombine with a hole (Figure 2.6). The size of this fraction can change between 0 and 1, depending on crystal's properties such as crystal temperature and type of impurity (Horowitz, 1984). In the TL measurement, intensity of the emitted light (recombination light) is determined and plotted against to the temperature. This plot is called the glow-curve of the crystal.

Each of the material contains lots of trap types at different energy levels so the glow curve may contains a number of glow peaks, each of the peaks corresponds to different trapping levels. The life time of electrons in deep traps (ΔE large) is longer than the lifetime of electrons in shallow traps (ΔE small). For a trap to be considered useful in dosimetry applications its glow-peak is usually situated at $200 \pm ^\circ\text{C}$ or higher (Thomsen 2004).

2.4.1 Thermoluminescence kinetics

Two different calculations can be made to explain the thermoluminescence theory. These are “First Order Kinetics” and “Second Order Kinetics” theories. These two theories were established to calculate the probability that the electron in the crystal could escape from the traps. In both theories, it is assumed that phosphorus is irradiated at a sufficiently low temperature and that the heating rate is at a certain temperature, so that electrons are not released. The only different approach to the formation of two different theories is related to electron re-trapped. “First Order Kinetics” theory is based on the approach that “the electrons that have escaped from the trap recombine without catching the same traps”.

The “Second Order Kinetics” theory is used to describe a situation where re-trapped is assumed to be lack of the “First Order Kinetics” theory.

2.4.1.1 First order kinetics

Many researchers have worked to explain the thermoluminescence theory. The most important progress was made by the researches conducted by Randall and Wilkins. According to Randall and Wilkins, the probability of electrons escaping from traps in a crystal can be expressed by correlations in mathematical probability theories (Randall and Wilkins 1945). They took the assumptions which are given below:

-Phosphorus is exposed to radiation at a sufficiently low temperature to avoid the release of electrons.

-Rise the heating at a constant temperature rate

-The electrons that have escaped the trap recombine without being caught in the same traps again.

Randall and Wilkins established the TL theory, which considers first-order radiation (single molecular model), in which electrons released from the traps are not trapped again.

TL intensity, I , is directly proportional to the number of electrons released from the trap at any temperature.

$$I = -c \left(\frac{dn}{dt} \right) = pn(t) \quad (2.3)$$

$c = 1$ constant value, n is the concentration of trapped electrons at time t . After some derivative and integral solutions, the intensity equation is given below;

$$I(T) = n_0 s \exp\left(-\frac{E}{kT}\right) \exp\left[-\left(\frac{s}{b}\right) \int_{T_0}^T \exp\left(-\frac{E}{kT'}\right) dT'\right] \quad (2.4)$$

This correlation is the first-order TL radiation intensity of Randall and Wilkins, which correlates the shape and size of the thermoluminescence radiation curve to the trap parameters such as E (activation energy) and s (preexponential frequency factor), to the number of trapped electrons, to the test parameters such as T temperature and heating rate b . This equation is also called Randall and Wilkins formula. E is related to depth of the trap. s is a constant which is related to the vibration of the electrons in the traps. Electrons collide with the lattice phonons and its frequency is proportional to the s factor. s value is lies between 10^{-12} and 10^{-14} s^{-1} .

$$T = T_M \frac{dI}{dT} = 0 \quad (2.5)$$

Logarithmic derivative of this equation is used and following equation is obtained.

$$\frac{bE}{kT_M^2} = s \exp\left(-\frac{E}{kT_M}\right) \quad (2.6)$$

According to equation 2.6, T_M is the temperature corresponding to the maximum value of the radiation curve. When the heating rate of the crystal is increased, it is found that T_M shifted to high temperatures (Mc Keever 1985). If E , increases, or s , decreases, T_M shifts to higher temperatures. For the constant values of E , s and b , the maximum point of the peak can be used as a measure of the amount of radiation dose received; s and E values can be calculated by measuring T_M and b values.

2.4.1.2 Second order kinetics

The possibility of recombination of electrons escape from of traps, Garlick and Gibson (1948), starting from the assumption that it is equal to the probability of re-trapping, made calculations by following different methods in the energy and frequency factor determination method in Randall and Wilkins model.

The second order kinetic expression is used to describe a situation in which re-trapping is dominant. In this case the following mathematical expression, Equation 2.7, is used.

$$\frac{dn}{dt} = -n^2 s' e^{\left(\frac{E}{kT}\right)} \quad (2.7)$$

This expression differs from the result obtained in the case of the first order in which the probability of recombination is equal to 1. Because re-trapping is not possible. This quantity is represented by $s' = s / N$ called the effective pre-exponential factor. The unit of s' is $\text{cm}^{-3}\text{s}^{-1}$, N (cm^{-3}) is the trap density, n_0 is the total number of electrons trapped at time zero (initial time) (m^{-3}).

Equation 2.7 is detailed with derivative and integrated formulas, the final equation for second order kinetics is Equation 2.8.

$$\frac{1}{2} \left[1 + \left(\frac{s' n_0}{b} \right) \int_{T_0}^{T_M} \exp \left(- \frac{E}{kT'} \right) dT' \right] = \frac{s' n_0}{s} \quad (2.8)$$

T_M increases as b increases or s decreases for a constant E Amirouche Bouremani value. For a constant b value, T_M gives a direct proportional to E . In the case of second degree kinetics, T_M shows a 1% increase.

2.5 OSL Theory

In the optical stimulated luminescence method, the temperature in the reading process is constant. The luminescence mechanism is the same as TL and the only difference is that the excitation of the irradiated material is carried out with light at different wavelengths from different sources. In OSL studies, instead of temperature, light can be used at steady wavelengths and different intensities to create luminescence. The emitted luminescence is measured in a spectral region different from the excitation light. Otherwise, the excitation light may also be detected as a luminescence signal.

For luminescence depending on the wavelength of light used in OSL studies, different names may be used instead of OSL nomenclature, indicating the color (wavelength) of the light used. The terms IRSL (InfraRed Stimulated Luminescence) are used if the infrared light is used for excitation, BLSL (Blue Light Stimulated Luminescence) if the blue light is used, and GLSL (Green Light Stimulated Luminescence) if the green light is used (Watanuki and Tsukamoto 2001, Watanuki et al. 2005).

In the OSL equipments usually LED or laser source is used. During the excitation process, the light source is such that the luminous intensity called linear mode (LM-OSL) increases gradually, the luminous intensity called continuous wave mode (CW-OSL) is kept constant at a certain value, or the luminous intensity called pulse mode (P-OSL) It is used intermittently, as it is sent at regular intervals (Preusser et al. 2008).

2.6 OSL Mechanism

When one sample is stimulated with constant light intensity (CW mode), it is expected that the trapped electrons will be liberated from the trap and then reduced by the

stimulation time of the luminescence signal resulting from the radiated transitions by combining with the holes in the recombination centers. With using this idea OSL model has been developed (Levy 1985, Thomson 2004). The probability of the electron separated from the trapped state per unit time is proportional to the photon flux of the excitation light intensity (assumed to be constant) (Equation 2.9)

$$p = \sigma(\lambda)Z \quad (2.9)$$

where, σ is the cross section of the photo-ionization effect for charge release from the trap. σ strongly depends on the wavelength of the excitation light, but for simplicity it is assumed that the excitation light is monochromatic.

Release rate of electrons from the trap during the external excitation is given below according to equation 2.10.

$$\frac{dn_u}{dt} = -pn \quad (2.10)$$

where, n is the concentration of the trapped electrons. The speed of trapped or re-trapped electrons is proportional to the concentration of electrons in the conduction band and the concentration of their current state in the traps (Equation 2.11).

$$\frac{dn_d}{dt} = p_t n_c (N - n) \quad (2.11)$$

p_t is the trapping probability, n_c is the concentration of the electrons which are in the conduction band, N is the concentration of the electron traps.

Recombination rate (namely the rate of electrons from the conduction band to the recombination center-R) is proportional to the concentration of electrons in the conduction band and the holes in the re-combination center-R (Equation 2.12).

$$\frac{dh}{dt} = n_c P_r h \quad (2.12)$$

where, P_r is the possibility of recombination. The following equation 2.13, 2.14, 2.15 are used to define the flow of electrons between the conduction band and centers are given below.

$$\frac{dn_c}{dt} = -\frac{dn_u}{dt} - \frac{dn_d}{dt} - \frac{dn_h}{dt} = pn - p_t n_c (N - n) - p_r n_c h \quad (2.13)$$

$$\frac{dn}{dt} = \frac{dn_u}{dt} + \frac{dn_d}{dt} = -np + p_t n_c (N - n) \quad (2.14)$$

$$\frac{dh}{dt} = -n_c P_r h \quad (2.15)$$

If it is assumed that when the first ionization occurred, all holes, trapped in the re-combination center equation 2.16 is obtained, this equation is known as the equilibrium of charge.

$$n_c + n = h \quad \left| \frac{dn_c}{dt} \right| = - \left| \frac{dn}{dt} \right| + \left| \frac{dh}{dt} \right| \quad (2.16)$$

I_{OSL} intensity of the OSL signal is equal to the rate of the re-combination occurred (Equation 2.17).

$$I_{OSL} = -\frac{dh}{dt} = -\frac{dn_c}{dt} - \frac{dn}{dt} \approx -\frac{dn}{dt} \quad (2.17)$$

$n_c \ll n$ concentration of the electrons which are located in the conduction band are lower than the concentration of the trapped state and $\left| \frac{dn_c}{dt} \right| \ll \left| \frac{dn}{dt} \right|$ the changing rate of the concentration of electrons which are in the conduction band is lower than the trapped state this is called semi equilibrium.

$\frac{dn_c}{dt} \approx 0$ assumption is used in Equation 2.17 and Equation 2.18 is obtained.

$$I_{OSL}(t) \approx pn \left(1 - \frac{P_t(N-n)}{(P_r)(h) + (P_t)(N-n)} \right) \quad (2.18)$$

For OSL, this equation is called General One Trap (GOT).

2.7 Determination of Kinetic Parameters

The parameters that provide understanding of the thermoluminescence and optically stimulated mechanism are called kinetic parameters. For TL, these parameters include activation energy, kinetic order, maximum and absolute temperature of peak, frequency factor, maximum intensity. As for OSL these parameters include, intensity components (ci), kinetic order, τ decay lifetime. Kinetic parameters are obtained by analyzing different methods. These analysis methods are, heating rates method, deconvolution method, initial increase method, isothermal reduction method, discrete radiation curve method, peak shape method and T_m - T_{stop} method. In this study to determine and analyse the kinetic parameters for both TL and OSL, deconvolution method was used.

2.7.1 Deconvolution

Deconvolution is the process of the separation of each TL peaks. The result of this process, experimental peaks are fitted. The difference between the experimental datas and the fitted datas are called Figure of Merit (FOM) values. All glow curves were deconvolved using with first order kinetics expression given by Chen and Kirsh in 1981 and modified by Kitis et al in 1998, which is performed according to the following equation 2.19.

$$I(t) = I(m) \exp \left[\left(\frac{E}{kT} \frac{T - T_m}{T_m} \right) - \frac{T^2}{T_m^2} \exp \left(\frac{E}{kT} \frac{T - T_m}{T_m} \right) (1 - \Delta) - \Delta_m \right] \quad (2.19)$$

where, $\Delta = \frac{2kT}{E}$ and $\Delta_m = \frac{2kT_m}{E}$ is used in the expression,

$I(m)$: the intensity at the peak maximum,

T_m (K): maximum peak temperature,

T (K): the absolute temperature

E (eV): the activation energy

k (eV·K⁻¹) : the Boltzmann constant

First order of kinetics correctness are tested and verified at 110°C TL peak in the previous studies (Wintle 1975, Petrov 1995 and Bailey 2001), also for High Temperature Thermoluminescent Peaks (HTTL peaks) (Subedi et al 2002 and Bailey 2001).

Deconvolution of Continuous Wave OSL (CW-OSL) decay curves were done using the following general order kinetics equation 2.20 recommended by Bøtter-Jensen et al 2003.

$$I(t) = I_0 \left[1 + (b - 1) \frac{t}{\tau} \right]^{-b/b-1} \quad (2.20)$$

b: kinetic parameter, b values are changes between 1 and 2.

τ : decay lifetime of each OSL component

I_0 : maximum intensity of the OSL component.

The expressions given describe one single signal component only for the equation 2.19 and 2.20, the sum of many components was used for the deconvolution.

Software package Microsoft Excel with the Solver utility were used to fit all curves. To understand the goodness of fitting, there is a parameter, the figure of merit (FOM) of Balian and Eddy given by: FOM values was checked in the given below Equation 2.21 (Balian ve Eddy 1977).

$$FOM = \sum_i \frac{Y_{experimental} - Y_{fit}}{A} \quad (2.21)$$

where, Y_{exp} shows the counting values in the experimental TL radiation curve, Y_{fit} shows the counting values in the fit curve; fitted glow curve and A is the area of the fitted glow curve. The obtained FOM values in all cases of TL and CW-OSL were

below 6 %. In Figure 2.7 the behavior of the kinetic parameter T_m , E and b are shown and explained. When T_m gets higher values, as a result of this higher E values are obtained. E means the depth of the trap so deeper traps needs more energy to set free charge carriers (Bos 2007). More energy means higher T maximum values. Kinetic order b related to probability of capture cross section for traps and the recombination center and the concentration of the traps and the recombination center (Pagonis et al 2006). When b values gets higher, peak gets larger and the transitions (radiative or non radiative) are higher. In Figure 2.8 refer to the meaning of dose versus TL intensity. At the same dose rate, three different dose responses is shown. When the dose gets higher the peak is goes to up. Figure 2.7, 2.8, 2.9 and 2.10 were obtained after deconvolution analyses in the present study. These figures show the kinetic parameters of each peak of the related materials.

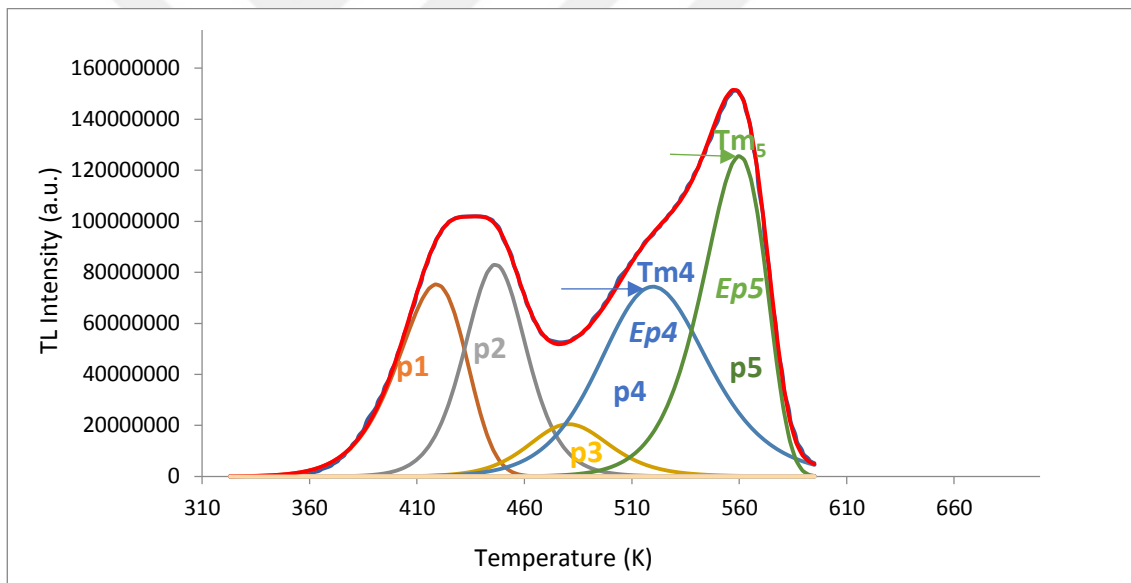


Figure 2.7 Peak 5 and peak 4 are an example of the description of the kinetic parameters after deconvolution.

In this figure, T_{m4} is the maximum temperature of the peak 4, T_{m5} is the maximum temperature of the peak 5. Ep_5 value is 1,805, Ep_4 value is 1,25. When excitation temperature T_m increases, E value gets increase and the peak width gets decreases. Kinetic order bp_4 is 1.90, bp_5 is 1,10. Lower b values caused narrow peak.

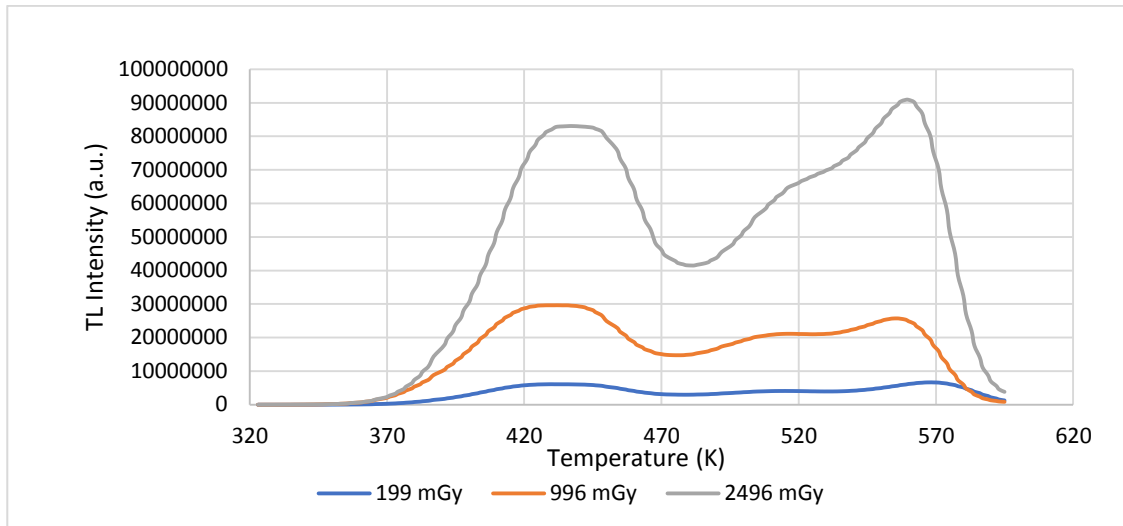


Figure 2.8 TL glow curves of CaF₂: Dy (TLD 200)

These curves are obtained after irradiation at three doses, 199 mGy, 996 mGy and 2496 mGy, respectively, at a dose rate of 30 Gy/h. Each TL glow curve is the average of two individual measurements. Reheats (background) has been subtracted

While the maximum intensity I_m , b kinetic order and T_m values are constant, the E value has changed. Higher E values caused narrow peak. Figure 2.9 is, deconvolution example of Li₂B₄O₇:Cu, In TL glow curve at 2 Gy/h, obtained from the deconvolution analyses in the present study. According to this deconvolution analyse, the life time of electrons in the trap is longer when E gets higher $E_1 > E_2 > E_3$.

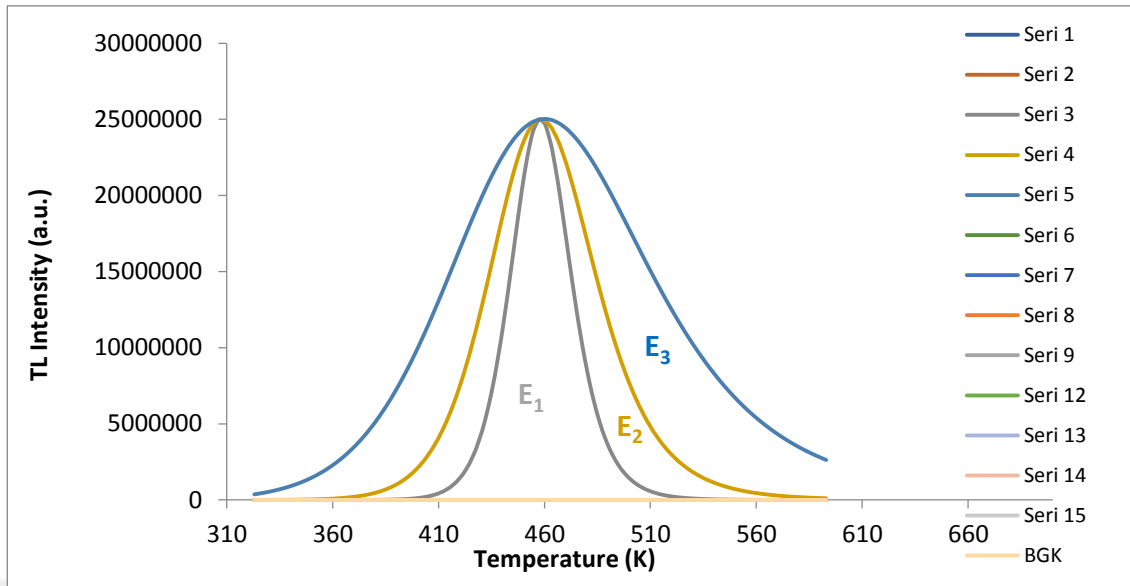


Figure 2.9 TL glow curves of $\text{Li}_2\text{B}_4\text{O}_7: \text{Cu, In}$

These curves are obtained irradiation at 2002 mGy at a dose rate 2 Gy/h after deconvolution analyses. Reheats (background) has been subtracted. Kinetic parameters except E value, are constant. The changes at different E values are examined.

Figure 2.10 is deconvolution example $\text{Li}_2\text{B}_4\text{O}_7: \text{Cu, In}$ TL glow curve at 2 Gy/h, where maximum intensity I_m , E activation energy and T_m values are constant and the b value has changed. While the other parameters are constant, higher b values caused larger peak. The probability of the transitions radiative or non radiative gets higher when b values higher. $b_1 > b_2 > b_3$.

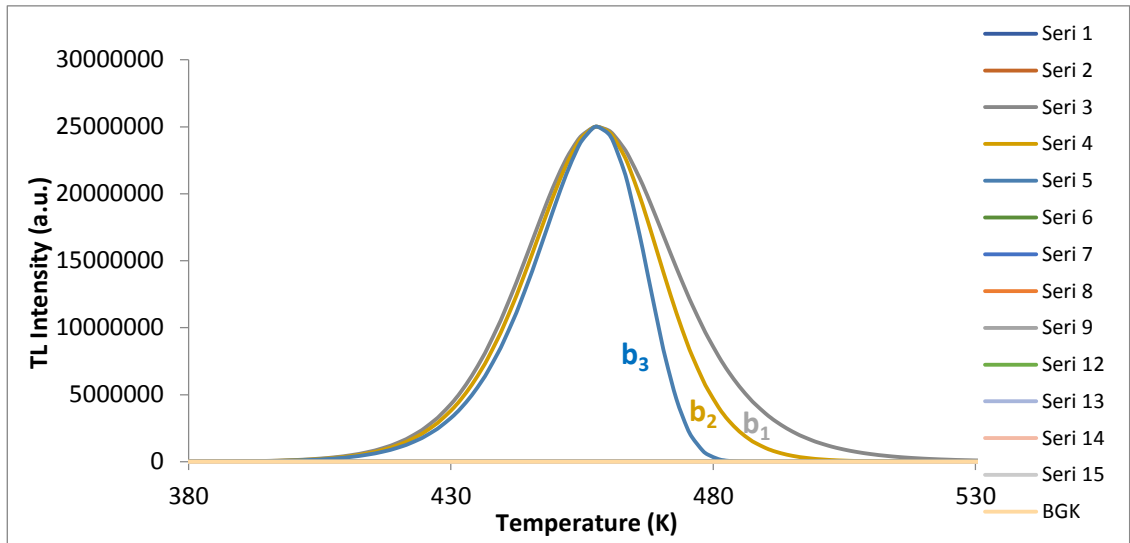


Figure 2.10 TL glow curves of $\text{Li}_2\text{B}_4\text{O}_7: \text{Cu, In}$

These curves are obtained irradiation at 2002 mGy at a dose rate 2 Gy/h after deconvolution analyses. Reheats (background) has been subtracted. Kinetic parameters except b value, are constant. The changes at different b values are examined.

This study aims to examine the possible effects of the different dose rates in dose response features and also signal deconvolution parameters, which are explained in the below part, of all the materials. There is a lack of literature focus on the dose rate effects. Only one study were done in the literature related to dose rate effects just in TL measurements (Chen et al. 1981).

3. MATERIALS AND METHODS

3.1 Dosimetric Materials

The dosimeters which are used in this study are LiB_4O_7 : Cu, In, MgB_4O_7 : Dy, Na, CaF_2 : Dy (TLD 200), LiF: Mg, Ti (TLD100), BeO and quartz. Except quartz, the other materials are artificial. Quartz is the natural luminescent material. Annealing procedure was applied for all artificial materials to evacuate the whole traps of the materials before the main irradiation because if the traps are empty before irradiation, the information from the trap is just related to main irradiation. All materials in the present study is explained in the below parts.

3.1.1 MgB_4O_7 : Dy

MgB_4O_7 :Dy dosimeter is based on a mixture of TL material and Polytetrafluoroethylene (PTFE) powder, in a weight ratio of 1:2 (McKeever et al 1995). The TL as a function of exposure for this dosimeter is linear up to $1.25 \times 10^{-2} \text{ C.kg}^{-1} (5 \times 10^3 \text{ R})$. Then after this point it becomes supralinear. Improved preparation of this material appears to have solved fading problems while maintaining a favourable sensitivity of 15 times higher than TLD 100. The linear dose response at the lower dose levels is consistent with earlier reports on the linearity of MgB_4O_7 :Dy in the dose range from 0.1 mGy to 100 Gy. Up to 350 Gy saturation occurs. The effective atomic number of this material is 8.4. Rods, chips and sintered powder format are used in general. The synthesis method is found in Kitis et al (2016). MgB_4O_7 :Dy chips which were produced by Vinca Institute of Nuclear Sciences are used in this study. These chips shown in Figure 3.1. The recommended annealing procedure for MgB_4O_7 :Dy is 500°C for 45 min (McKeever et al 1995).



Figure 3.1 MgB₄O₇:Dy chips

3.1.2 LiF: Mg, Ti (TLD 100)

LiF in the form of LiF:Mg,Ti has been the mainstay of the TLD industry for two decades and is most widely used TLD material on the market more than 50 years especially for personnel dosimetry. This dosimeter materials come in a variety of physical forms, including single crystal, extruded rods, hot pressed chips or powder. The most popular TLD has 3.2x3.2x0.9 mm dimension, hot pressed chip. The synthesis method is found in Kitis et al.(2015) and the rectangular prism TLD chips which was manufactured by Harshaw used in this study. These chips was shown in Figure 3.2. The dose response of LiF:Mg, Ti (TLD-100) is linear up to 1 Gy then it becomes supralinear up to 10³ Gy where supralinearity starts. These dosimeters, thanks to their high light intensity, have linear atomic response range over a wide range (from 10 μGy to 1 Gy) and good repeatability since their effective atomic number (8.2) is close to that of tissue (7.4) (Khan 2014). It is widely used to determine the body and skin dose in individual dosimeters and to determine the doses exposed in vivo measurements in the medical field (radiotherapy,radiology) (<https://www.thermofisher.com/order/catalog/product/SNO10106>, 2017). For TLD 100, recommended annealing procedure is pre-irradiation annealing 1 hour at 400°C followed by 2 hours at 200°C (McKeever et al 1995).



Figure 3.2 LiF: Mg,Ti TLD 100 chip

3.1.3 $\text{Li}_2\text{B}_4\text{O}_7$: Cu, In

The effective atomic number of $\text{Li}_2\text{B}_4\text{O}_7$: Cu, In is 7.3. The corresponding energy response is independent of photon energy within %10, in the energy range from 40 keV to 7 MeV. The hygroscopic nature of $\text{Li}_2\text{B}_4\text{O}_7$: Cu, In makes it sensitive to humidity. The integrity of the dosimeter and its fading characteristics may both be affected by the presence of water vapour (McKeever et al. 1995). Crystal, chips and powder format is used. The response of $\text{Li}_2\text{B}_4\text{O}_7$: Cu, In is linear up to exposure levels of approximately 10^5 R where it becomes sublinear. The lack of supralinearity is a significant advantage in accident dosimetry situations. The sensitivity of this material is approximately twice that of TLD 100. This material should be kept in low humidity environments. Linear dose range is 0.5 mGy to 1000 Gy for TL measurements and up to 1000 Gy saturation occurs. The synthesis method is found in Kitis et al (2016). $\text{Li}_2\text{B}_4\text{O}_7$: Cu, In chips which were produced by Vinca Institute of Nuclear Sciences. Annealing procedure is 1 hour at 300°C (McKeever et al 1995). TLD 100 which was used in this study is shown in Figure 3.3.



Figure 3.3 $\text{Li}_2\text{B}_4\text{O}_7$: Cu, In chips

3.1.4 CaF_2 : Dy (TLD 200)

The response of CaF_2 : Dy (TLD 200) is reported to be linear up to 600 R where it becomes supralinear, and finally saturates at approximately 5×10^4 R. Linear dose response range is 0.1 μGy to 10 Gy. The considerable structure of dose response curve is a result of the differences between the dose response curves of the various glow peaks. A pre-irradiation annealing at 600°C for at least 1 hour (McKeever et al 1995). This annealing procedure was applied in this study. Sensitivity of TLD 200 is more than an order of magnitude higher than that of TLD 100 (McKeever et al 1995). The photon energy dependence of TLD 200 in the energy range of 20 keV to 1.25 MeV. In this study rectangular prism in form of chips ($3.2 \text{ mm} \times 3.2 \text{ mm} \times 0.89 \text{ mm}$) which were purchased from the Harshaw Chemical Company were used (Karsu Asal et al. 2018). These chips was shown in Figure 3.4. In general, increasing the time and temperature of the post-irradiation thermal treatments (anneal or pre-heat) results in improved fading characteristics and reduced sensitivity.



Figure 3.4 CaF_2 : Dy TLD 200 chips

3.1.5 BeO

Beryllium oxide is one of the dosimeters used in personal dosimeter with an effective atomic number of 7.13. When added with suitable additives, it shows excellent TL property. This phosphor is obtained by mixing purified BeO powder and an alkalisulphate, pressing the resulting mixture, sintering at high temperature ($\sim 1500^\circ\text{C}$) and then slowly cooling to room temperature (Yamashita et al. 1974). Powdered BeO is highly toxic and leads to a condition known as berylliosis. Therefore, without strict security measures, the production of BeO TLD chips is not possible and is only produced in commercial laboratories. Secure BeO TLD chips are available in three similar versions, in particular from Brush Wellman (Brush Beryllium), ThermaloxTM 995, 998 and 999, and from Matsushita Electric Industrial Company (Japan), Consolidated Beryllium (UK), American Lava (USA). Crase and Gammage, defined as ThermaloxTM 995, are the most suitable for dosimetry and the most popular form of TLD in BeO form (McKeeever 1995). ThermaloxTM 995 has a diameter of 6-9 mm and a thickness of 0.9-1.5 mm. It is recommended that the BeO dosimeter be annealed at 400°C for 15 minutes before each use (Busuoli et al. 1984). The TL response of BeO as a function of dose is linear up to 1 Gy (Azorin 2014), in OSL $10\mu\text{Gy}$ to 100 Gy. It has high melting point and it is sensitive to light. In this study, square disc form with dimensions of 4 mm and thickness of 1mm ThermaloxTM 995 BeO chips which were taken from USA were used (Aşlar et al. 2000). These chips are shown in Figure 3.5 and their annealing procedure was 1 hour at 900°C .



Figure 3. 5 ThermaloxTM 995 BeO chips

3.1.6 Quartz

Quartz is one of the most common rock-forming mineral and it composes silicon and oxygen. Its chemical formula is SiO_2 . Quartz is the most abundant mineral found almost anywhere in the world and highly resistant to mechanical and chemical deterioration. 7 Mohs is the value of hardness of quartz in the Mohs scale which shows the measure of the resistance of the mineral to the applied pressure and force. According to this scale, the value of diamond, which is the hardest mineral, is 10. It is also highly resistant to quartz chemicals and heat. It has a higher melting temperature than most metals (<https://geology.com/minerals/quartz.shtml>, 2019). Quartz does not contain any radionuclide in its structure because of this reason. It is especially preferred in retrospective dosimeter applications. Quartz is one of the natural dosimeters. Due to its good luminescence signal, it is widely used in dating studies and dosimetric applications (Poolton et al 2000, Oniya et al 2012 and Li et al 2001). Natural quartz materials used in this study were Nigerian hydrothermal quartz samples (Figure 3.6).



Figure 3.6 Quartz

The brief summary of the procedures which are applied to every dosimetric material is shown in Table 3.1. Table 3.1 includes methods, annealing procedures and

measurement procedures after annealing for each material. Some materials have deconvolution analyses and their FOM values are also included in Table 3.1.

Table 3.1 Procedures applied to the dosimetric materials

Material	TL	OSL	Annealing procedure	Dose rate (Gy/h)	Heating rate (°C/s)	Calibration Factor (constant)	FOM value (TL)	FOM value (OSL)
Li ₂ B ₄ O ₇ : Cu, In	X		1 hour at 300°C	2, 30	2	0.9-1.1	1.990-2.622	-
CaF ₂ : Dy (TLD 200)	X		1 hour at 600°C	2, 30	2	0.9-1.1	1.085-2.74	-
MgB ₄ O ₇ : Dy (single peak, without deconvolution)	X		45 min at 500°C	2, 30	2	0.9-1.1	-	-
LiF: Mg, Ti (TLD 100)	X		pre-irradiation annealing 1 hour at 400°C followed by 2 hours at 200 °C.	2, 30	2	0.9-1.1	3.17-5.147	-
BeO	X	X	1 hour at 900 °C	2, 30	1	0.9-1.1	0.580-0.762	0.39-0.80
Quartz		X	without annealing	27, 311, 1305	1	9 – 11*	-	4.15-5.78

*the mass of the quartz materials in each carousel, miligram(mg)

3.2 Artificial Materials Preparation

BeO, CaF₂: Dy , MgB₄O₇:Dy, Li₂B₄O₇: Cu, In, LiF: Ti, Mg were the artificial materials and used in chip format in this study. There were no process to obtain the chips. For annealing, chips were located on the stainless steel tables and put into the furnace directly. For irradiation two chips of the same material were located directly on the band. Some materials are sensitive (especially BeO) to the light so during the irradiation and annealing , materials were covered with black bags and there were no

light in the irradiation room except red light. In the irradiation room the materials were located at the same position to obtain minimum uncertainty due to the different position of the chips.

3.3 Quartz Preparation

The natural quartz materials were big blocks and they need crushing. To get the crushed quartz material, some steps were added to preparation procedures (Figure 3.7). The quartz was first passed through the jaw crusher and brought to small particle sizes. Crushed quartz samples were prepared between the 90 μm and 140 μm dimensions using different sized sieves. It was observed that iron particles remained in the samples with a size of $90 \ll \mu\text{m} < 140$. The iron particles in the quartz were removed by magnetic stirrer which is used for mixing the solution in the laboratory. The quartz, whose iron pieces were cleaned, was dried and made ready. Samples were placed in a quartz tube. Quartz is sensitive to light so like the other materials, irradiation and measurements were performed in a dark room conditions and sample tubes were covered with black bags. Before the measurement using with Riso, quartz samples were scaled with the analytical balance. Each sample were weighed between the 9-11 mg then they were put on the discs which were located on the carousel for the measurement.



Figure 3.7 Preparation of quartz sample

3.3.1 Equipments for quartz preparation

3.3.1.1 Jaw crusher

The natural quartz having quite large dimensions were crushed and to obtain small sizes, with GS machine brand jaw (Figure 3.8).



Figure 3.8 Jaw crusher

3.3.1.2 Sieves

After natural quartz samples were cleaned, Retsch brand test sieves (Figure 3.9) were used to separate them into different particle sizes. The sizes of the sieves in the laboratory vary between 45 μm and 250 μm . In the thesis study, 90 μm and 140 μm sieves were used to measure the remaining samples between the 90 μm and 140 μm dimensions.



Figure 3.9 Sieves

3.3.1.3 Magnetic stirrer

The quartz samples, which are cleaned using different chemical substances, contain the latest amount of iron particles. Heidolph MR Hei-Tec brand magnetic stirrer is used to remove these iron particles (Figure 3.10). The agitator has the ability to heat the sample to 300°C and to stir the sample to 500 rpm.



Figure 3.10 Heidolph MR Hei-Tec magnetic stirrer

3.3.1.4 Analytical balance

To arrange the weight of the quartz, analytical balance was used (Figure 3.11). Quartz materials were weighed between 9 mg and 11 mg . Firstly, empty cup were weighed, tare was determined and subtracted from the final weight. The scaled screen arranged to zero. After then the sample were put into the cup and only weight of quartz sample were determined.



Figure 3.11 Analytical balance

3.4 Calculation of Calibration Factors

To obtain the best response from the dosimeters, it is very important to determine the best material which has good reproducibility. Calibration factors were obtained to choose the best dosimetric materials. Firstly all artificial materials were annealed according to their annealing procedures. After each annealing, the materials were irradiated with a beta source with 0,5 Gy. After the first irradiation the doses of the materials were read three times consecutively in the TLD Harshaw 3500. The important thing was that all traps should be empty. For this reason, readings were repeated three times. Following the reading, a second irradiation was done at the same source and the same dose value and they were also read three times after the second irradiation. The measurements were analyzed and each chip's total integral was calculated. For one material, all chips' total integral values were calculated and the values were averaged. Each chip's total integral was divided by the average of all chips' total integral. The chips which result between 0.9 and 1.10 were chosen and used in the thesis.

For quartz the samples were prepared between 9-11 mg for each disc on the carousel. Each sample's data was divided by its own weight so it was normalized. The luminescence signal was measured per unit of mass. This was the calibration factor for the quartz. This process allowed us to evaluate the measurement results regardless of the weight of the material.

3.5 Irradiation Facilities

In this study three irradiation equipments and two measurement devices were used. TL / OSL measurements and irradiation procedures were performed by Risø TL / OSL (model DA-20) device and only TL measurements were performed by Thermo Scientific Harshaw TLD 3500. Elsec 9010 OSL was used for irradiation to determine the calibration factor. Main irradiation facilities was Co-60 sources in Department of Radiation and Accelerator Technologies in Turkish Atomic Energy Authority. First facility is in the Secondary Standard Dosimetry Laboratory, second is in the Experimental Irradiation Laboratory. All artificial materials were irradiated in the first irradiation facility at two different dose rates, which are 2 Gy/h and 30 Gy/h. Only quartz was irradiated in the second facility at three different dose rates which are 27 Gy/h, 311 Gy/h and 1305 Gy/h.

3.5.1 First irradiation facility (Co-60 source)

Co-60 source with an activity of 130 TBq was used for 2 Gy/h and 30 Gy/h dose rates. In the irradiation system there is a linear positioning bench (Figure 3.12) and above the linear positioning system, there is a platform which can move in three dimensions as shown in Figure 3.13 and the material to be irradiated is placed on the bench with the sample holder (Figure 3.14). The linear positioning system and the platform ensure the proper positioning of the material to be irradiated (PTW manual). There were laser and it was used to adjust the homogeneous irradiation area, $10 \times 10 \text{ cm}^2$, having the same dose distribution. Before irradiation PTW 0.6 cc primary calibrated ionization chamber, PTB primary calibrated farmer ionisation chamber (Figure 3.15) was used to determine the exact dose rate at the reference distance, 1 meter. Gamma source was primary calibrated and the activity was known in order to get the exact dose rates decay formula and distance factor for calculations. There were 12 dose steps in two dose rates. Two chips for the same material were used at each dose step's irradiation. The dose steps were 52, 104, 199.33, 303.33, 502.66, 797.33, 996.66, 1499.33, 2002, 2496, 2998.66 and 3501.33 mGy, respectively. Primary standard Co-60 source activity was known. Thus before each irradiation dose values were calculated using with activity decay formula. To obtain the same doses both, irradiation time and irradiation distance was

changed day by day. At the first irradiation for 30 Gy/h and 2 Gy/h for each dose step, two dosimetric materials were located 950 mm, for 2 Gy/h 3752 mm far from the source at the linear bench, respectively. And for every irradiation day&time, decay formula was calculated again and to get the same dose values for every irradiation, bench distance and time was adjusted again.



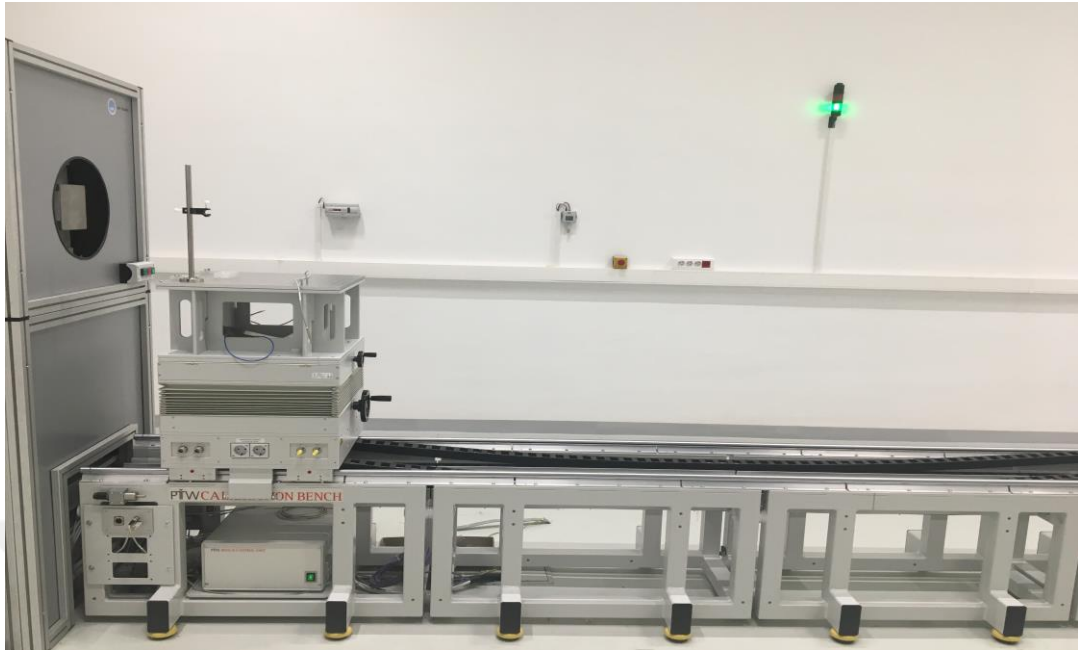


Figure 3. 12 Linear positioning bench

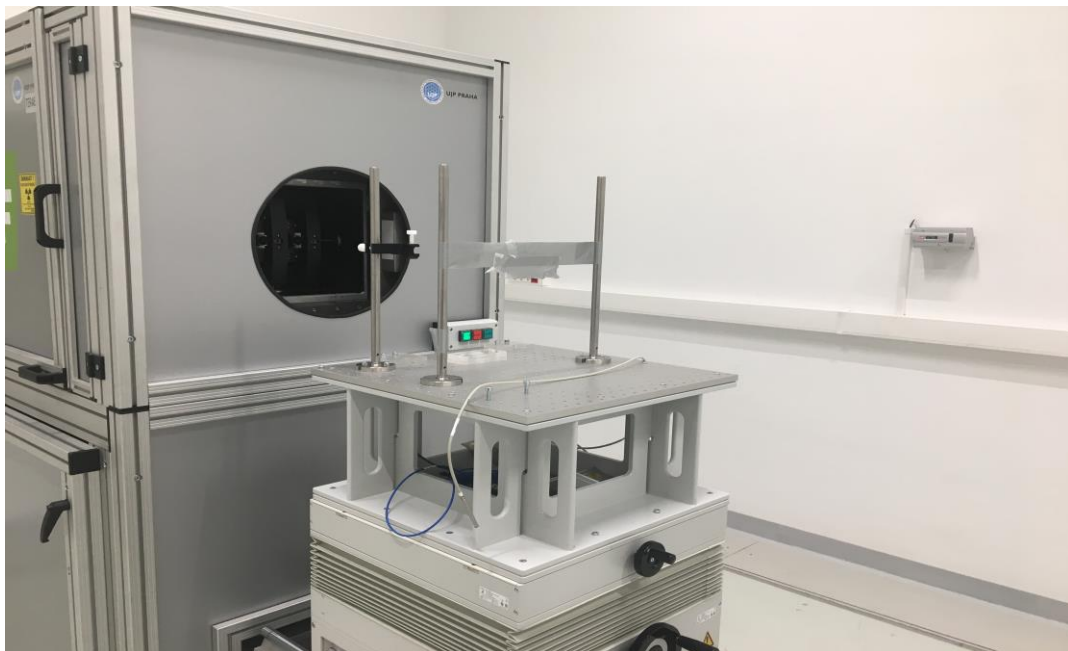


Figure 3.13 Platform on the bench

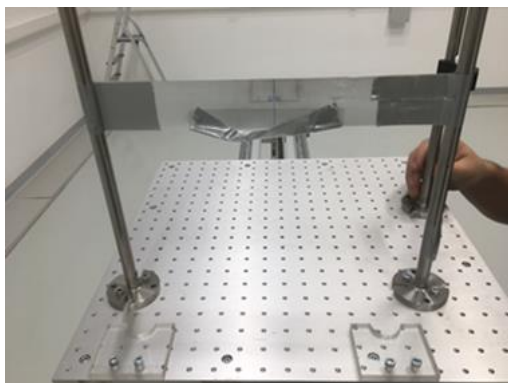


Figure 3.14 Sample holder on the bench



Figure 3.15 PTW 0.6cc farmer ionisation chamber

3.5.2 Second irradiation facility (Co-60 source)

Co-60 source with an activity of 140 TBq, was used for quartz irradiation and it is shown in Figures 3.16, 3.17, 3.18. The source has 3 dose rates, 27 Gy/h, 311 Gy/h and 1305 Gy/h, respectively. There were the decay formula so the dose rates changed day by day automatically. In the equipment there is a cylindrical box and quartz materials which are in the tubes were located in the box (Figure 3.19). Source rotated 360° around the box so the irradiation reached and homogenous radiation dose distribution whole material in the tube. In this equipment distance was constant, each dose rate to obtain each dose steps irradiation time was changed and adjusted.



Figure 3.16 Gamma source irradiator



Figure 3.17 Gamma source irradiator



Figure 3.18 Gamma source irradiator



Figure 3.19 Sample located in the box

3.6 Riso TL / OSL reader

Riso TL / OSL reader is a commercial device that makes automatic thermoluminescence (TL) and optically stimulated luminescence (OSL) measurements of signal and it is shown in Figure 3.20. It is in the Ankara University Institute Of Nuclear Sciences It has 48 sample capacity to heat individual samples from room temperature up to 700 °C and in continuous mode (CW), linear mode (LM) and pulse mode (PW) with various light sources stimulation. The measuring system is very sensitive and the reference internal radiation $^{90}\text{Sr} / ^{90}\text{Y}$ beta source is available in the device which was used in this thesis to determine the calibration factor.

The device is usually being used for geological and archaeological dating, forensic and accident dosimetry and radiation. It is widely used to determine radiation doses in natural and artificial materials with applications such as protection.

The main components of the system are light detection system, luminescence stimulated system (optical and thermal) and irradiation source. Riso TL/OSL automatic measurement system allows both TL and OSL measurements. Light detection system, photomultiplier tube and convenient optical detection filter are important parts of the system. TL measurements can be made in pure nitrogen flow or in a vacuum media but in generally nitrogen gas is used for measurements above 200 °C because nitrogen flow protects the heating system from oxidation at high temperatures and also provides process faster. The components of the Riso TL/OSL reader is shown in Figure 3.21.

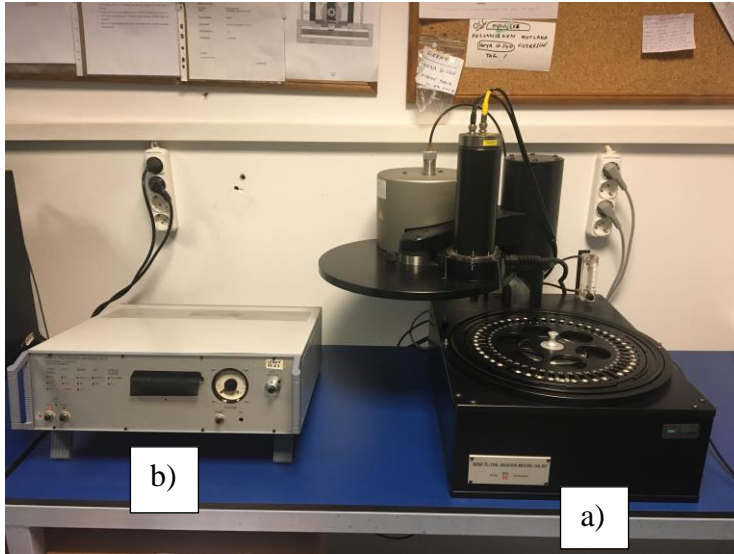


Figure 3.20 a) Riso TL/OSL reader unit b) control unit

Riso TL / OSL reader composes of two units.

3.6.1 Reader unit

Samples are placed in and optically or thermally stimulated, detected and irradiated with radiation source (Figure 3.20 a).

3.6.2 Control unit

This is the electronic control part of the system. It links between programs and the reader. It provides the parameters to be applied for the samples during the measurements. The application of the high voltage, the provision of the vacuum medium, the opening and closing of the sample carrier are carried out by the control unit (Figure 3.20 b).

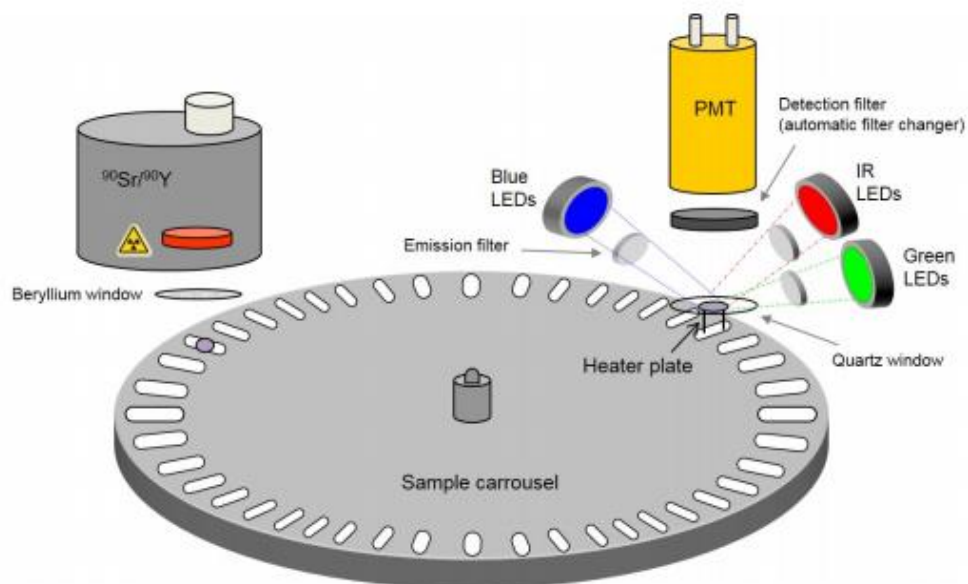


Figure 3.21 Schematic Diagram of the RisØ TL / OSL luminescence reader (RisØ DTU Guide to the RisØ TL / OSL, 2008)

The system is run using one of two programmes - the Sequence Editor (used to write elaborate measurements sequences) and the Control Program (used to carry out simple tests on the equipment) - installed on standard PC.

3.6.3 Sample preparation

Samples are loaded onto an exchangeable sample carousel that can accommodate up to 48 samples. The sample carousel is placed in the sample chamber which can be programmed to be evacuated or have a nitrogen atmosphere maintained by a e.g. nitrogen flow. The sample is lifted through slots in the sample carousel into the measurement position by a lift, which also functions as heating element. During the measurement position the sample can be stimulated thermally and/or optically. Thermal stimulation is obtained by linearly increasing the temperature of the heating element and optical stimulation is provided by different light sources focused onto the sample position. The emitted luminescence is measured by the light detection system.

The sample carousel rests on a motor driven turntable, which enables rotation of the sample carousel. Rotation is computer controlled and position holes drilled though the

carousel in close proximity to the sample positions enable the system to keep track of the position of the carousel using optoelectronics. An infrared light emitting diode (LED) is positioned underneath the turntable, which is switched on during rotation. The measurement is initiated by moving a given sample to the measurement position located directly underneath the light detection system. The sample carousel rotates at two different speeds (two-speed turntable) to reduce processing time. If a sample is moved to the next position then the turntable turns at the normal speed. However, the turntable must advance several positions, it is accelerated to a high speed for most of the move and decelerated to slow speed before stopping. Carrousel and the sample cups are shown in Figure 3.22.



Figure 3.22 Sample discs and cups (planchettes) are shown on the left. On the right a sample carrousel (sometimes referred to as “turntable”) is shown

The Risø TL/OSL reader has three luminescence stimulation systems: 1) a light stimulation system that can be used for OSL measurements. 2) a heating system that can be used for TL measurements. The two stimulation systems can be used in combination, e.g. OSL at elevated temperature is possible. 3) reference light source.

3.6.4 Optical stimulation system

The intensity of the emitted luminescence is many orders of magnitude smaller than the intensity of the stimulation light, so in order to effectively prevent stimulation light from reaching the PMT, the wavelengths of the stimulation light and the luminescence must be well separated. In general, samples are stimulated with constant light intensity in the OSL system. Electrons are evacuated from the traps in this manner, exponentially decreasing signal is generated. In the standard Risø TL/OSL

luminescence reader, two stimulation sources exist. Stimulated in two ways; IR LED and Blue LED. In the IR LED max power 145 mW/cm^2 wavelength 870 nm , in the Blue LED power 50 mW/cm^2 , wavelength 470 nm .

Two modes are used while in the OSL measurement, one is the continuous wave (CW-mode), which produces an exponentially decaying signal as the electron traps are being depleted. In linearly modulated OSL (LM-OSL) the stimulation light intensity is varied linearly (usually from zero to a predefined value). Electrons in traps most sensitive to light will be evicted at low intensities, whereas the less light sensitive traps will empty at higher intensities.

In this study, continuous wave (CW-mode) mode was used.

3.6.5 Heating system

The heating element and lift mechanism is located directly underneath the photomultiplier tube. Heating system has two functions:

- 1) it heats the sample
- 2) it lifts the sample into the measurement position. The heating system is able to heat samples to 700°C at constant heating rates from 0.1 to 10 K/s .

3.6.6 Reference light source

A blue light-emitting LED at 470 nm is mounted inside the reader as a reference source. It is used in routine checks of the detection system. The reference LED source has two important purposes: 1. To check the accuracy of optical filters placed in front of the PM tube before running the program. 2. to check the long-term stability of the detection system in the use of blue permeable filters.

The other components of the reader unit which is shown in figure 3.21 is explained in the below part. Photomultiplier tube and the detection filters are related to light detection system.

3.6.7 Photo-multiplier tube (PMT)

The standard photon detector in the Risø TL/OSL Reader is a blue/UV sensitive photomultiplier tube (PMT). The emitted luminescence is detected by a photomultiplier tube (PMT). The standard PMT in the Risø TL/OSL reader is an Electron Tube PDM. 9107-CP-TTL (160-630 nm) PMT, has maximum detection efficiency between 200 and 400 nm and it makes suitable for detection of luminescence from quartz.

3.6.8 Detection filters

The intensity of the stimulation light is $\sim 10^{18}$ orders of magnitude larger than the emitted luminescence. In order to be able to measure the emitted luminescence, detection filters must be used to prevent scattered stimulation light from reaching the PMT, and the spectral stimulation and detection windows must be well separated.

The Risø TL/OSL reader comes with the following three detection filters:

1. Hoya U-340 (5 and 2.5 mm thick, $\varnothing = 25$ mm)
2. Schott BG39 (2 mm thick, $\varnothing = 25$ mm)
3. BG3 (3 mm thick, $\varnothing = 25$ mm)

In this study Hoya U-340 filter were used in the measurements.

3.6.9 Beta irradiator

A detachable beta irradiator is located above the sample carousel. This irradiator includes a $^{90}\text{Sr}/^{90}\text{Y}$ beta source, which emits beta particles with a maximum energy of 2.27 MeV. The half life is 30 years. The source strength is usually about 1.48 GBq, which gives a dose rate in quartz at the sample position of approximately 0.1 Gy/s.

3.7 TLD Harshaw 3500

The Harshaw 3500 (Figure 3.23) includes a sample drawer for a single element TLD dosimeter, a linear, programmable and precisely controlled heating system and a cooled photomultiplier tube to measure the TL light output. The samples are heated by means

of the heating strip in the chamber where the samples are placed. Because of the heating the light emitted and a PMT detects the thermoluminescence light emission and convert it into an electrical signal linearly proportional to the detected photon fluence and an electrometer for recording the PMT signal as a charge or current. Planchet has one chip capacity, it is made of stainless steel and it uses the linear heating rate principle. Maximum operating temperature is 400° C and heating rate is between 1° C/s and 50°C/s (<https://assets.thermofisher.com/Catalogs/Harshaw-3500>). Schematic diagram of TLD 3500 Harshaw is located in Ankara University Institute of Nuclear Sciences, Figure 3.24.



Figure 3.23 TLD Harshaw 3500

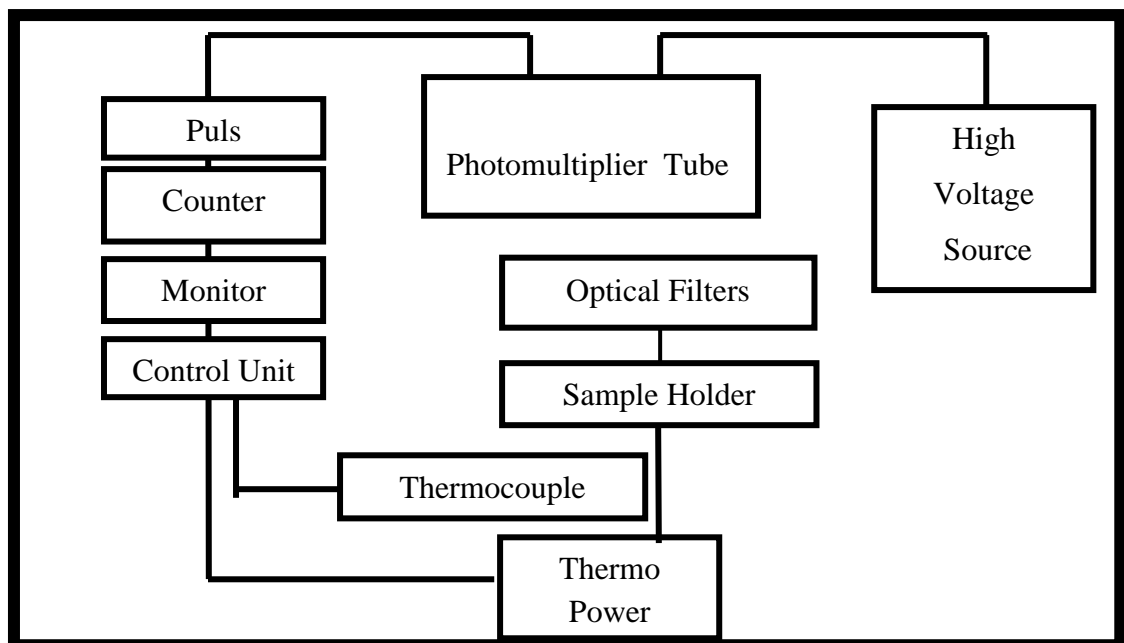


Figure 3.24 Schematic Diagram of a TLD Harshaw 3500

3.8 Elsec 9010 OSL system

Elsec 9010 OSL system has a OSL reader and the Sr/Y beta irradiator. It is controlled by the computer. If the device will be irradiated, the $^{90}\text{Sr}/^{90}\text{Y}$ beta source must be installed and the photomultiplier (PM) tube must be installed if it is to be read. PM tube and β source were placed in the system as shown in Figure 3.25 and 3.26, respectively. The system is located in Ankara University Institute of Nuclear Sciences. $^{90}\text{Sr}/^{90}\text{Y}$ beta source was used for the irradiation of the samples. Half life of the source is 28 years. The source's initial activity was 100 mCi and the dose rate on aluminum is 0.027 ± 0.003 Gy/s. A computer controls the switching on&off of the source automatically.



Figure 3.25 Elsec 9010 system (PM tube were placed) (Karagöz 2011)

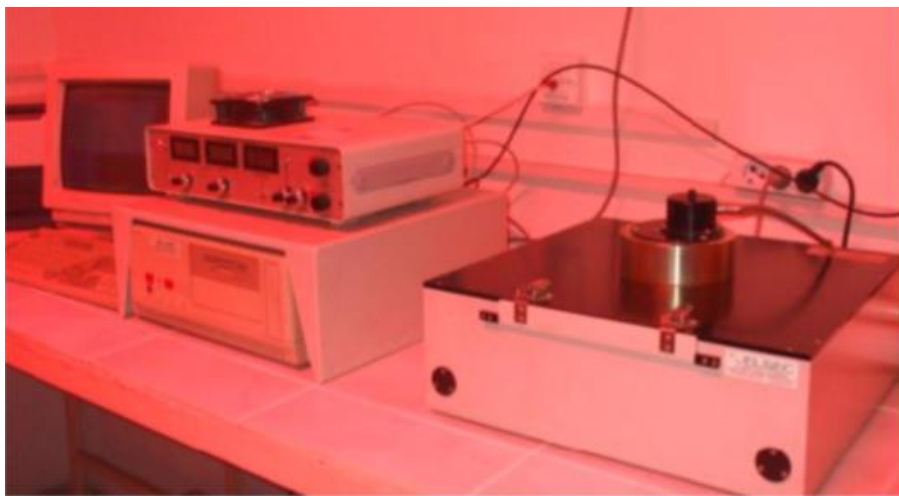


Figure 3.26 ELSEC 9010 OSL system (β source were placed) (Karagöz 2011)

With the sample stimulator (LEDs) of the OSL system, the cylindrical part of the photomultiplier (PM) tube is removed and replaced with a beta source so the source is transformed into a irradiator computer-controlled system.

The sample tray has cavities for receiving 10 mm diameter, 0.5 mm thick aluminum discs on which samples can be placed. This tray is also suitable for TLDs etc. The sample tray is capable of carrying 64 discs (samples) on it. The tray is placed on the tray carrier. The carrier is moved in the x-y plane under computer control and it moves the disc to be measured under the photomultiplier tube or Sr90-Y90 beta source. The system included Thorn EMI 9235 QA Photomultiplier tube which has quantum efficiency nearly 200 nm -400nm and the PMT transmits light photons from the sample to the system by converting them into electrical pulses. Hoya U-340 filter (λ : 270-380 nm, FWHM 80 nm) is included in the device. This is an optical filter and it is placed in front of the PMT to prevent the counting of the light which is only used for stimulation.

3.9 Freiburg Type 1321 Oven

PTW Freiburg type oven is used for annealing and preheating of the dosimeters. It is shown in Figure 3.27. It has two programmes for annealing and preheating .The first is a preheating mode that allows to clean signals by draining unstable traps with heating the TLD before reading. The preheat mode takes approximately 30 minutes. The second programme is for annealing procedures. During annealing; the oven heats the dosimeters up to maximum 400°C and maintains for one hour at that temperature after then it goes to cooling mode. Theldo software is used for adjustment of the temperature. The shelves inside the oven are made of stainless steel and contains ceramic fiber material as insulation material. Thanks to the stainless steel containers; annealing peocedures is applied to 360 dosimeters at the same time. (PTW manuel). This oven was used for the annealing of the TLD 100 and $\text{Li}_2\text{B}_4\text{O}_7\text{:Cu:In}$ dosimeters. The oven can heat 360 TLD in its drawers. Used stainless steel annealing tray is shown in Figure 3.28 (<https://www.radat.com.tr/documents/tld-oven.pdf> 2018).

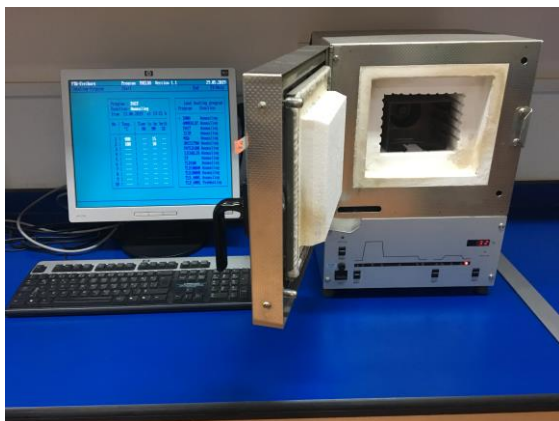


Figure 3. 27 PTW Freiburg Type 1321 Oven Figure 3. 28 Stainless Steel Annealing Tray

3.10 Protherm Furnace

The heating process during the preparation of the materials MgB_4O_7 : Dy, Na, CaF_2 :Dy (TLD 200), BeO was done with Protherm brand PLF 120/12 model electric oven (Figure 3.29). The furnace comprises nickel-chrome alloy heating elements. During the heating process, the temperature of the furnace can be continuously read digitally, heating is performed to a maximum of 1200°C and the temperature sensitivity is $\pm 2^\circ\text{C}$ (<http://www.prothermfurnaces.com/chamber-furnaces/plf-series110-130>).



Figure 3. 29 Protherm Furnace PLF 120/12

4. RESULTS

4.1 TL Glow Curves and OSL Decay Curves

For artificial materials $\text{Li}_2\text{B}_4\text{O}_7:\text{Cu}$, In , $\text{LiF}:\text{Mg,Ti}$ or alternative TLD 100, $\text{MgB}_4\text{O}_7:\text{Dy}$, Na , $\text{CaF}_2:\text{Dy}$ or alternatively TLD 200 besides BeO , TL measurements were done using the TLD Harshaw 3500. BeO TL measurements were done with Riso TL/OSL reader. Between Figure 4.1 and 4.10, TL glow curves (intensity versus dose) are shown for all applied doses at both irradiation rates, namely 2 Gy/h and 30 Gy/h dose rates. Each one of the TL glow curves at each dose step, is expressed as the mean value of the two TL glow curves obtained. Background measurements has been subtracted from every measurement.

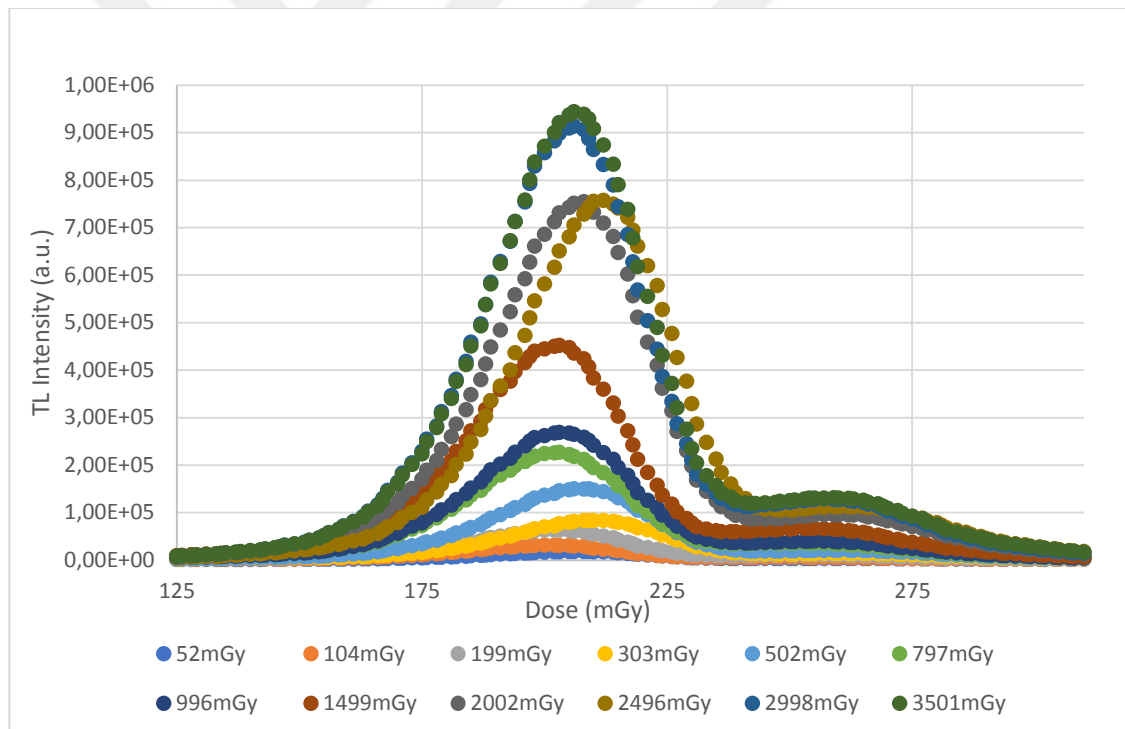


Figure 4.1 TL glow curves of $\text{Li}_2\text{B}_4\text{O}_7:\text{Cu}$, In obtained after various doses within the range 50 mGy – 3500 mGy at a dose rate of 2 Gy/h. Each TL glow curve is the average of two individual measurements. Reheats (background) has been subtracted

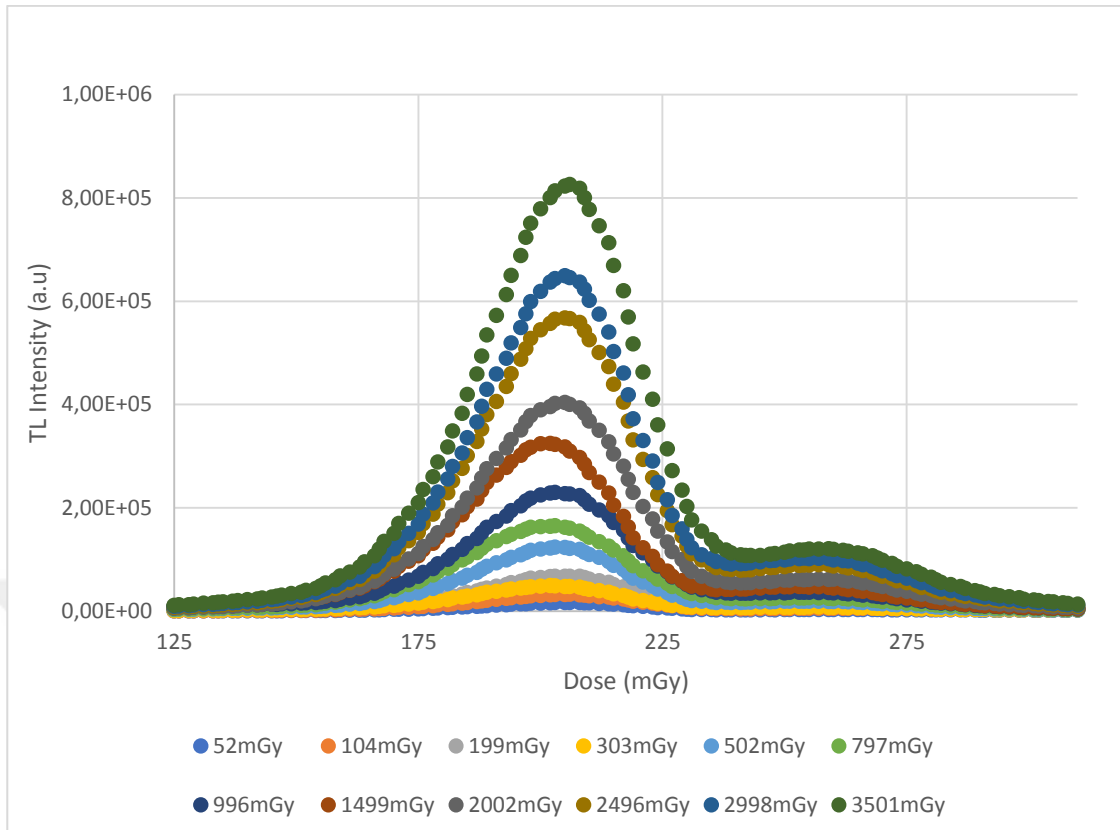


Figure 4.2 TL glow curves of $\text{Li}_2\text{B}_4\text{O}_7: \text{Cu,In}$ obtained after various doses within the range 50 mGy – 3500 mGy at a dose rate of 30 Gy/h. Each TL glow curve is the average of two individual measurements. Reheats (background) has been subtracted

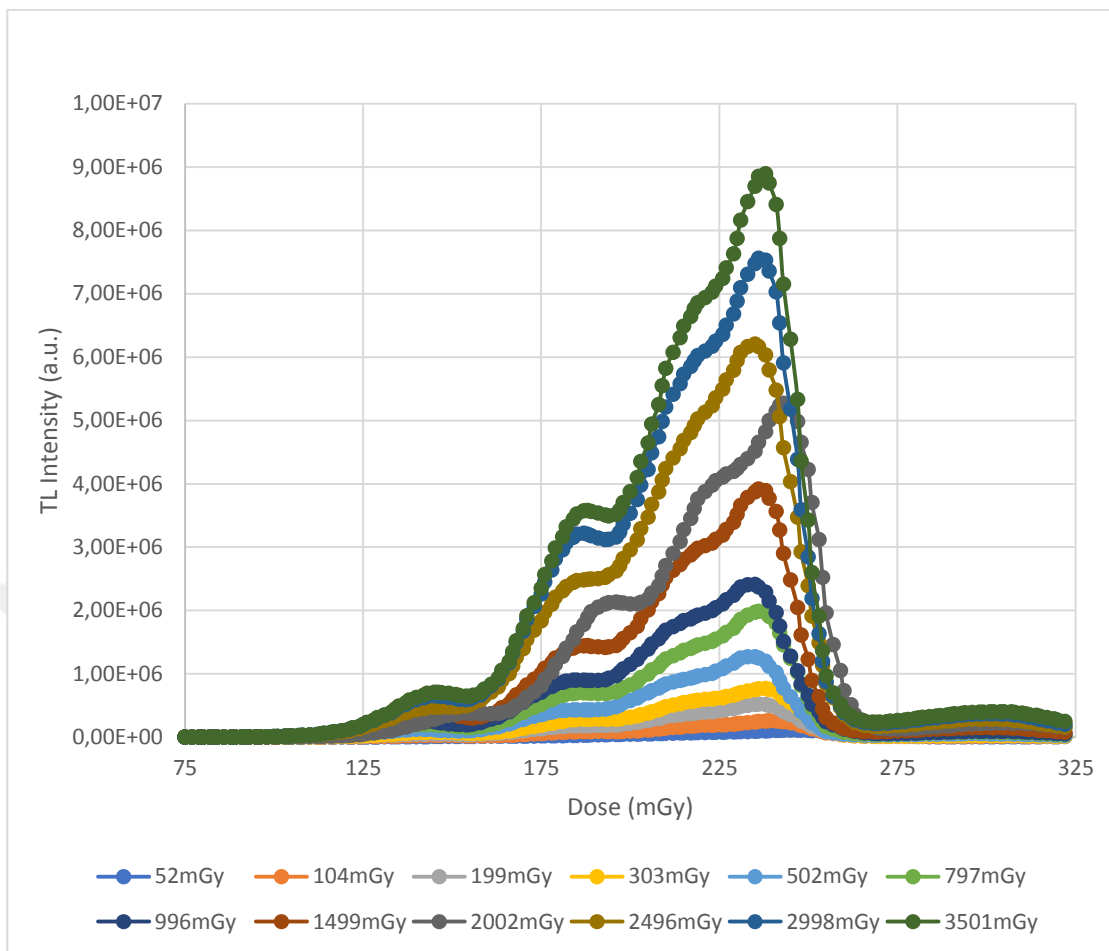


Figure 4.3 TL glow curves of LiF: Mg,Ti (TLD 100) obtained after various doses within the range 50 mGy – 3500 mGy at a dose rate of 2 Gy/h. Each TL glow curve is the average of two individual measurements. Reheats (background) has been subtracted

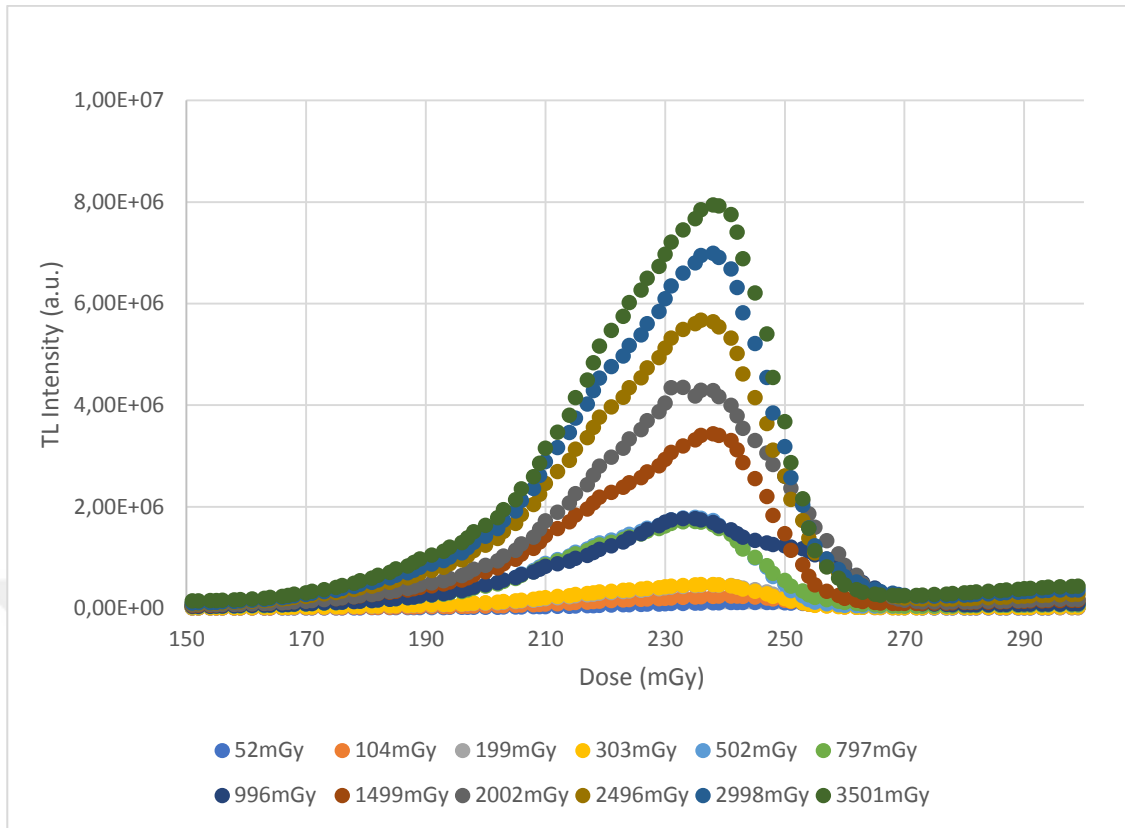


Figure 4.4 TL glow curves of LiF: Mg,Ti (TLD 100) obtained after various doses within the range 50 mGy – 3500 mGy at a dose rate of 30 Gy/h. Each TL glow curve is the average of two individual measurements. Reheats (background) has been subtracted

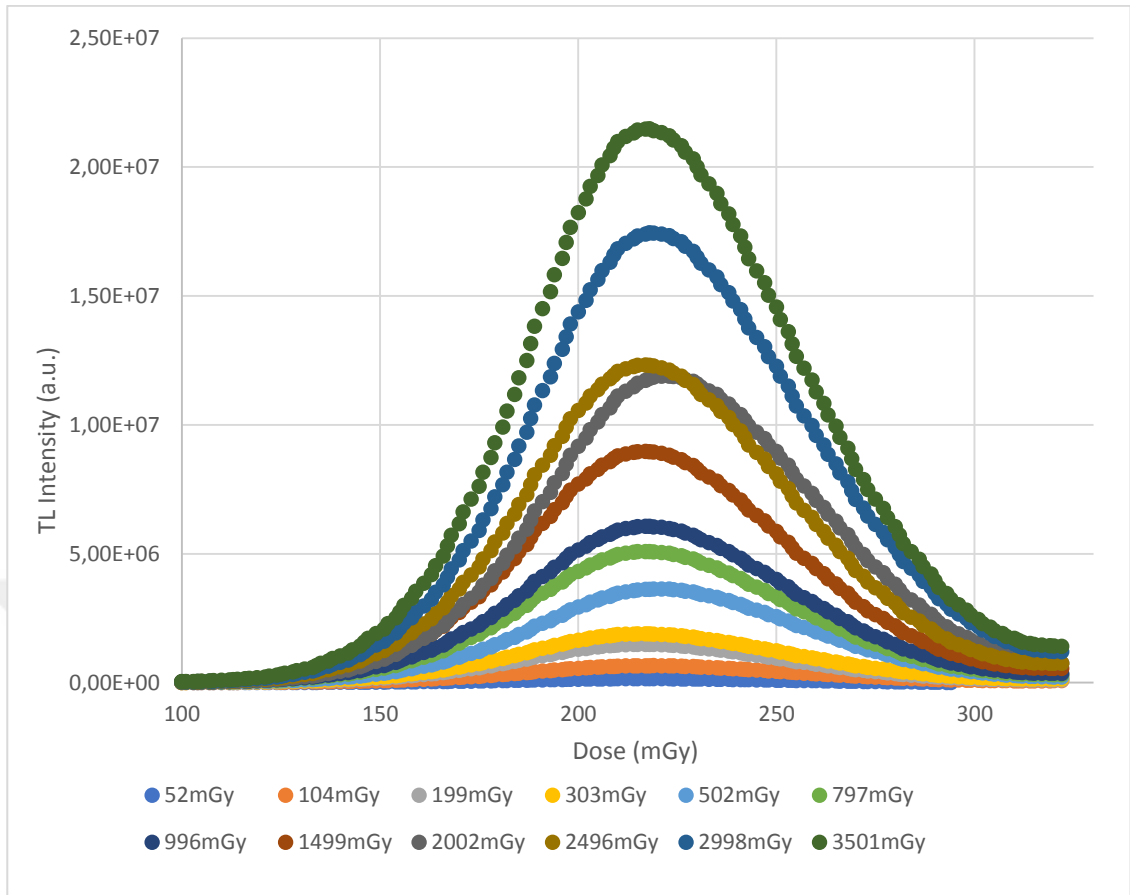


Figure 4.5 TL glow curves of $\text{MgB}_4\text{O}_7:\text{Dy, Na}$ obtained after various doses within the range 50 mGy – 3500 mGy at a dose rate of 2 Gy/h. Each TL glow curve is the average of two individual measurements. Reheats (background) has been subtracted

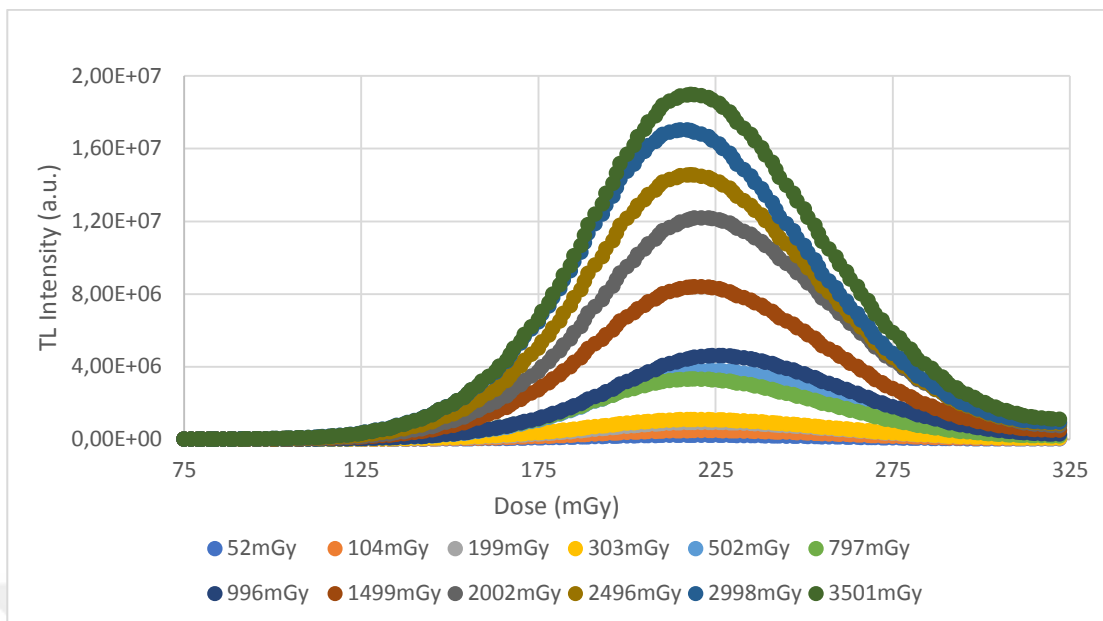


Figure 4.6 TL glow curves of MgB_4O_7 : Dy, Na obtained after various doses within the range 50 mGy – 3500 mGy at a dose rate of 30 Gy/h. Each TL glow curve is the average of two individual measurements. Reheats (background) has been subtracted

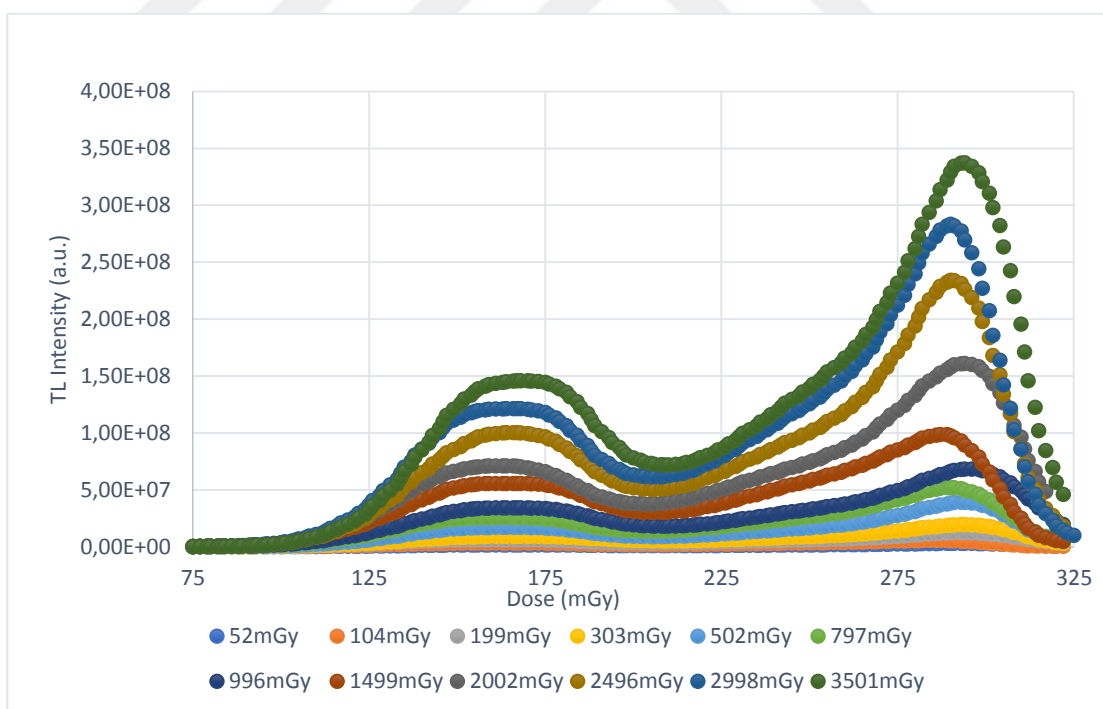


Figure 4.7 TL glow curves of CaF_2 : Dy (TLD 200) obtained after various doses within the range 50 mGy – 3500 mGy at a dose rate of 2 Gy/h. Each TL glow curve is the average of two measurements. Reheats (individual background) has been subtracted

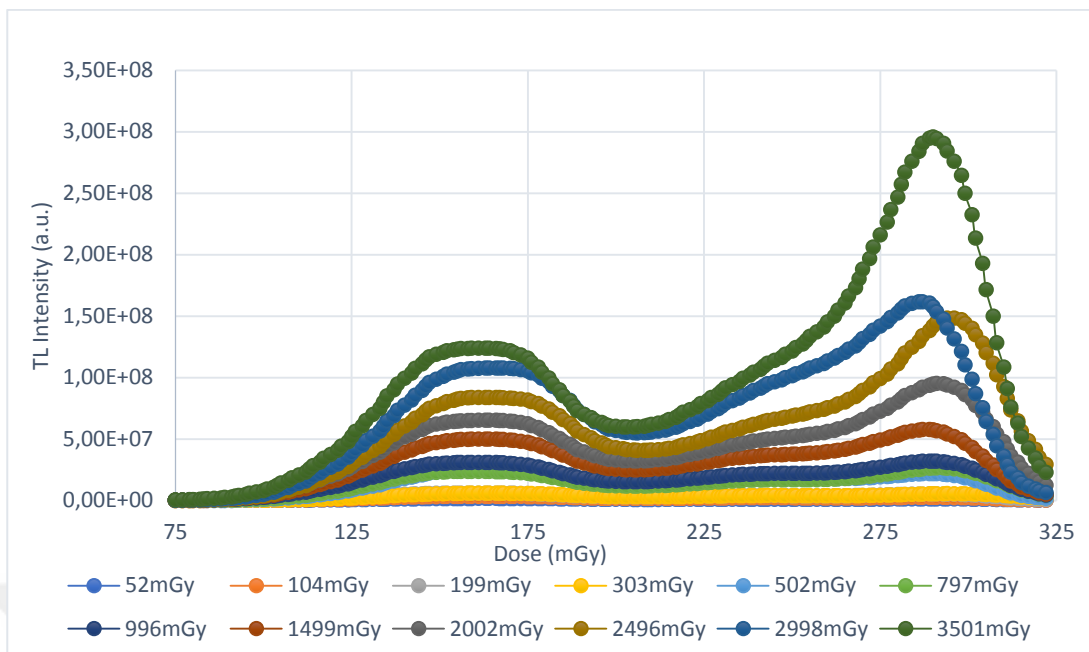


Figure 4.8 TL glow curves of $\text{CaF}_2:\text{Dy}$ (TLD 200) obtained after various doses within the range 50 mGy – 3500 mGy at a dose rate of 30 Gy/h. Each TL glow curve is the average of two individual measurements. Reheats (background) has been subtracted

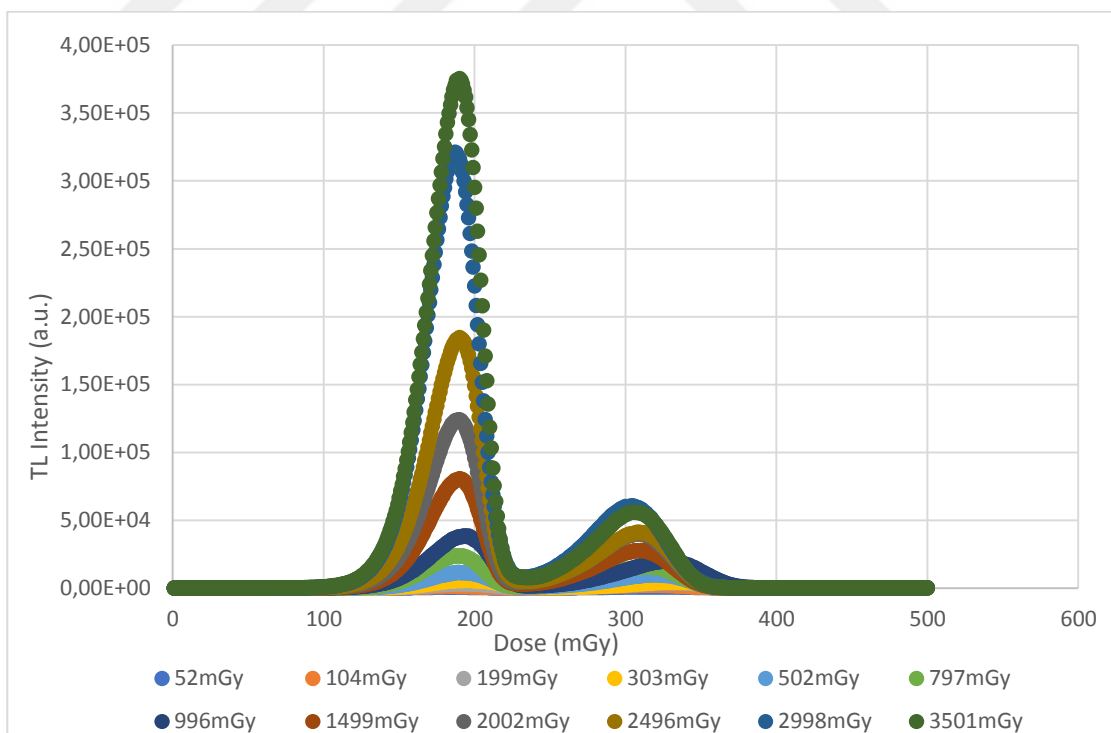


Figure 4.9 TL glow curves of BeO obtained after various doses within the range 50 mGy – 3500 mGy at a dose rate of 2 Gy/h. Each TL glow curve is the average of two individual measurements. Reheats (background) has been subtracted

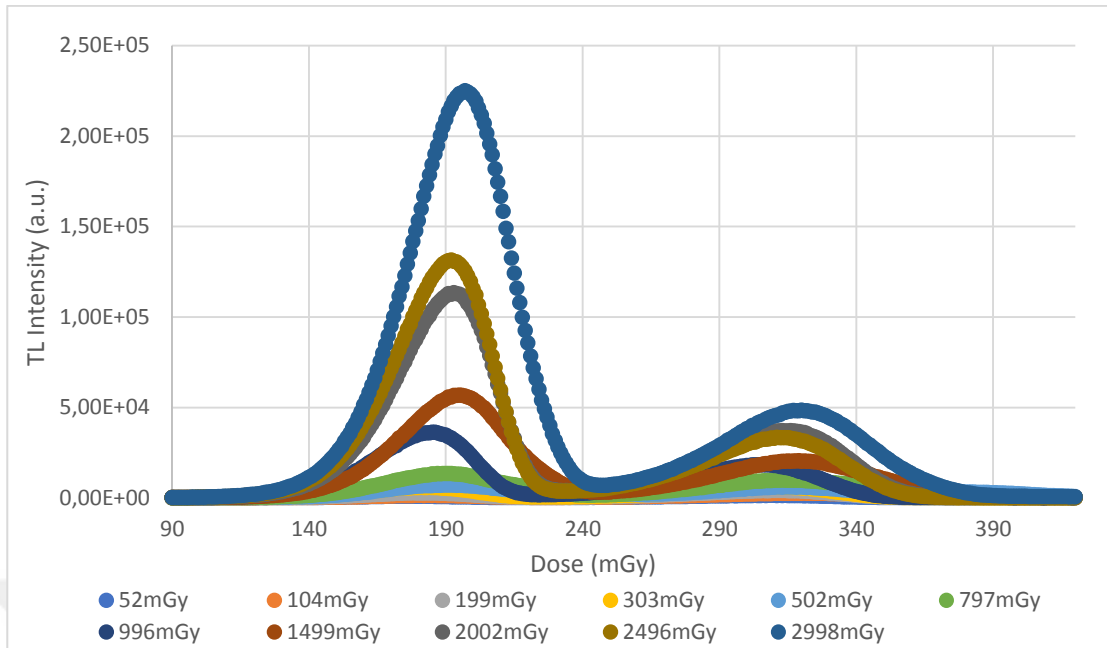


Figure 4.10 TL glow curves of BeO obtained after various doses within the range 50 mGy – 3500 mGy at a dose rate of 30 Gy/h. Each TL glow curve is the average of two individual measurements. Reheats (background) has been subtracted

Figures 4.11 and 4.12 present the BeO OSL decay curves (OSL intensity versus dose), for both dose rates of 2 Gy/h and 30 Gy/h, respectively. Like TL measurements at each dose rate and each dose step two individual measurements were performed. The average of these two individual measurements were calculated and used in the graphs. Curves' y axis are logarithmic.

Figure 4.13, Figure 4.14, Figure 4.15 are the Quartz OSL decay curves (OSL intensity versus dose), for both dose rates of 27 Gy/h, 311 Gy/h and 1305 Gy/h, respectively. Like TL measurements at each dose rate and each dose step two individual measurements were performed. The average of these two individual measurements were calculated and used in the graphs. Curves' y axis are logarithmic

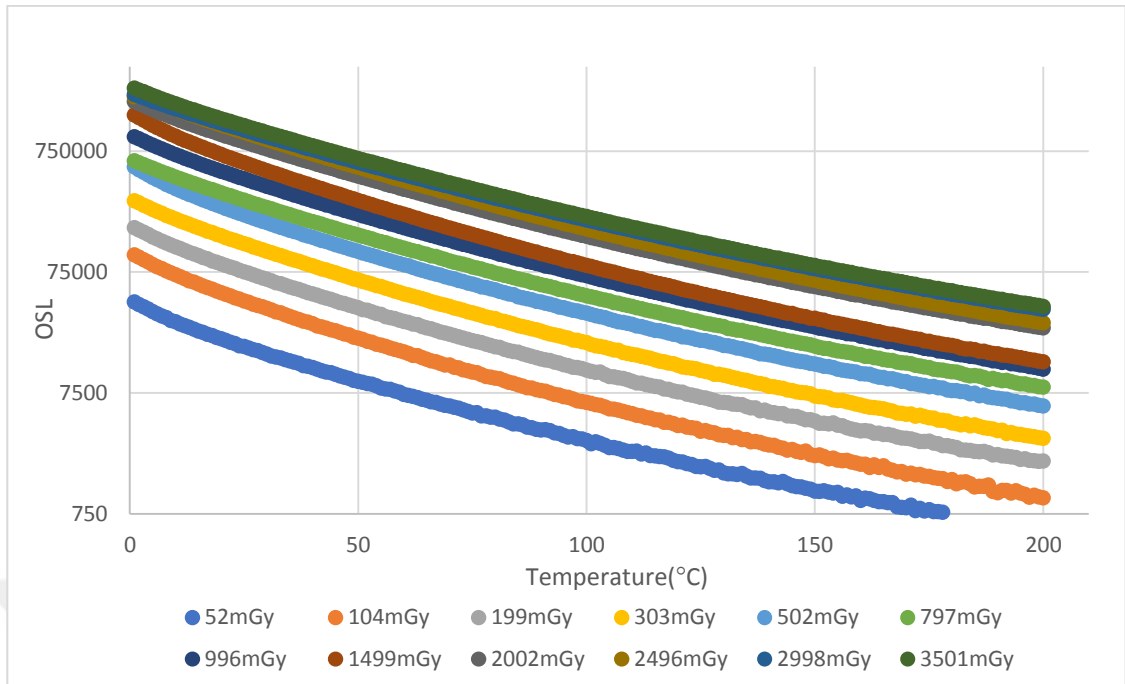


Figure 4.11 OSL decay curves of BeO obtained after various doses within the range 50 mGy – 3500 mGy at a dose rate of 2 Gy/h. Each OSL curve is the average of two individual measurements (y axis is logarithmic)

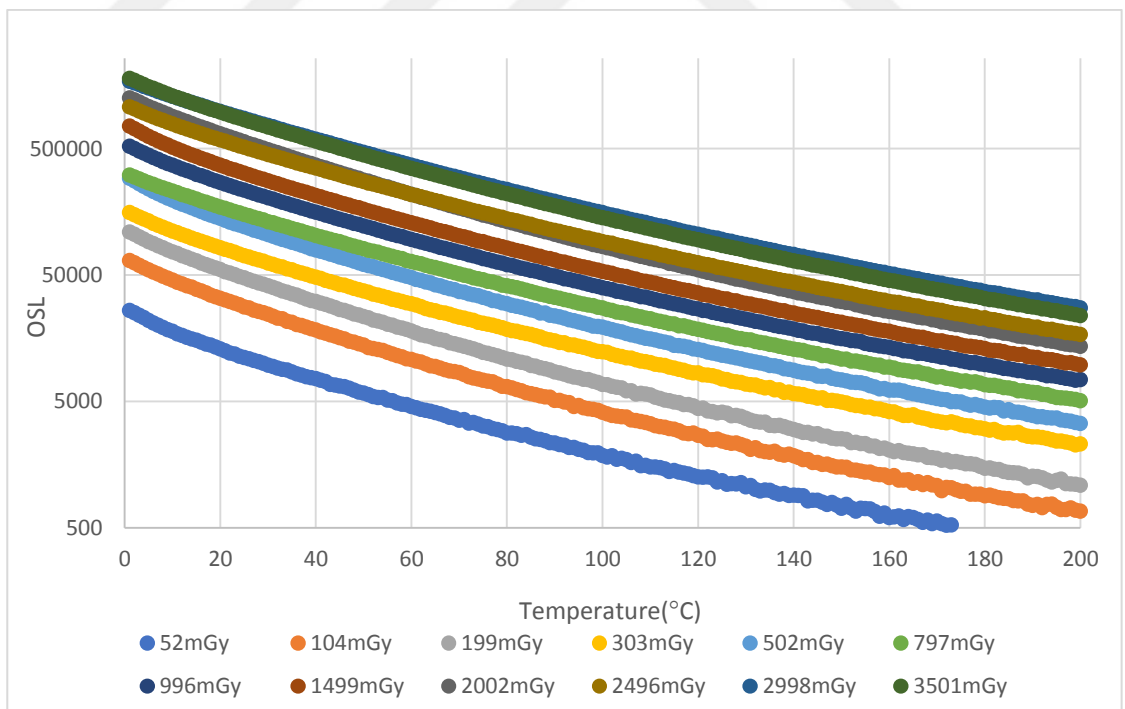


Figure 4.12 OSL decay curves of BeO obtained after various doses within the range 50 mGy – 3500 mGy at a dose rate of 30 Gy/h. Each OSL curve is the average of two individual measurements (y axis is logarithmic)

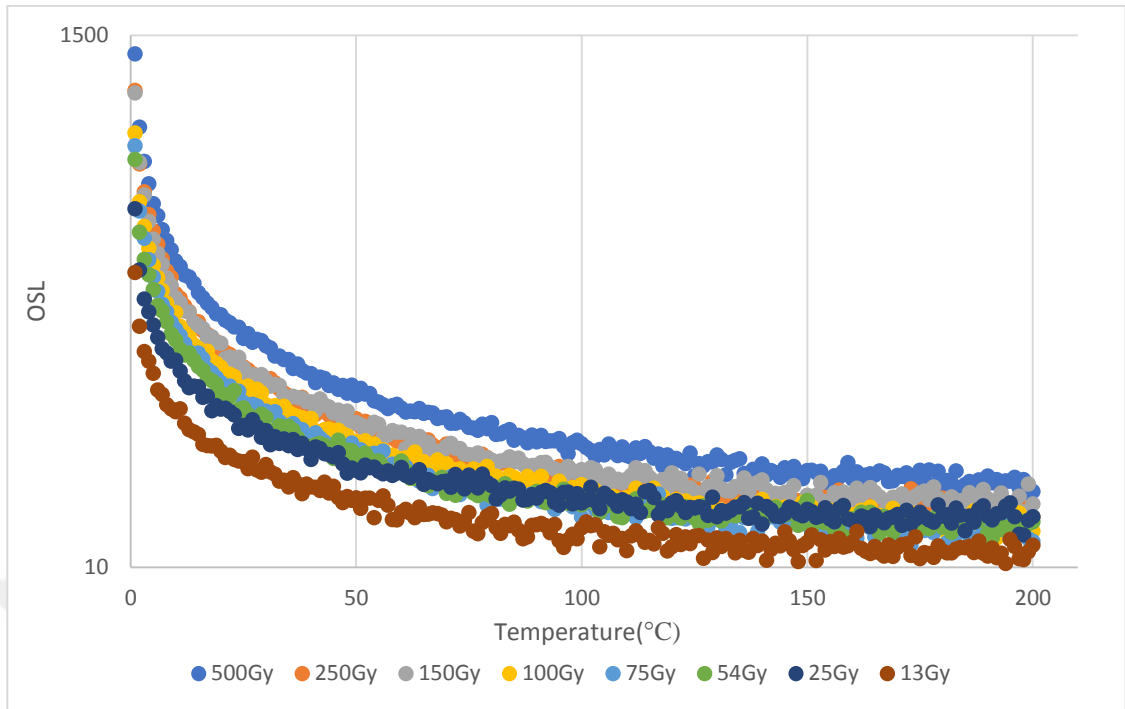


Figure 4.13 OSL decay curves of Quartz obtained after various doses within the range 13 Gy – 500 Gy at a dose rate of 27 Gy/h. Each OSL curve is the average of two individual measurements (y axis is logarithmic)

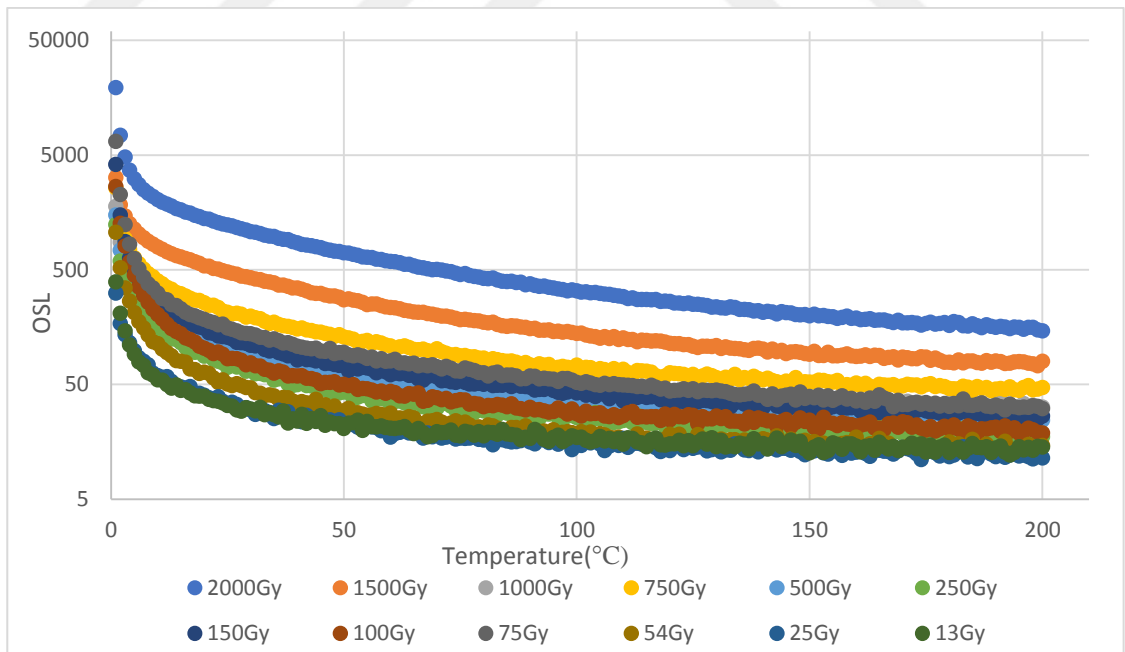


Figure 4.14 OSL decay curves of Quartz obtained after various doses within the range 13 Gy – 2000 Gy at a dose rate of 311 Gy/h. Each OSL curve is the average of two individual measurements (y axis is logarithmic)

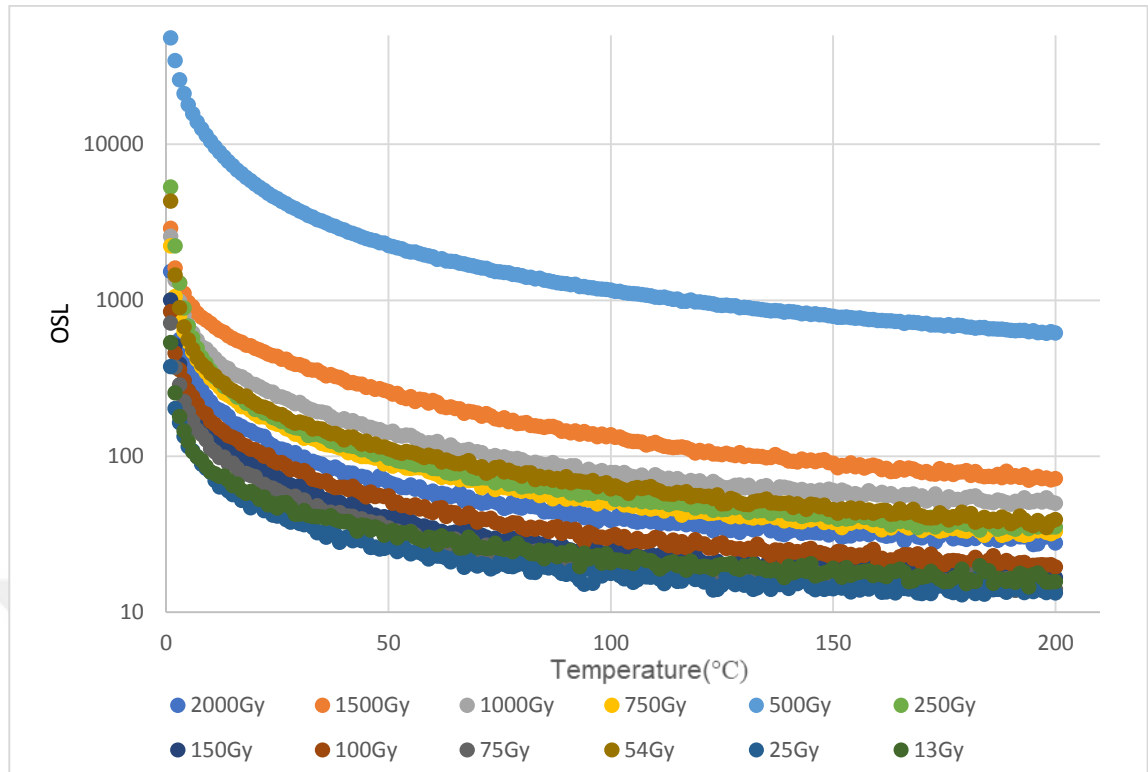


Figure 4.15 OSL decay curves of Quartz obtained after various doses within the range 13 Gy – 2000 Gy at a dose rate of 1305 Gy/h. Each OSL curve is the average of two individual measurements (y axis is logarithmic)

4.2 TL and OSL Deconvolution

To determine the kinetic parameters of TL glow curves, deconvolution analysis was used in this study. The deconvolution analysis of the TL signals was based on the experience gained on each material upon previous related studies; similar studies could be found at the book of McKeever et al., (1997), as well as to more recent related papers (Kitis et al., 2015; 2016; Sadek et al., 2017; Aşlar et al., 2017a,b; Şahiner, 2017; Karsu Asal et al., 2018). The TL glow curve of magnesium borate was not deconvolved as (a) it consists of one single broad peak and (b) the general order kinetics model could not be applied for this material, as the TL signal is attributed to tunneling recombination (Kitis et al., 2016).

A typical, characteristic deconvolution graph for each material and each luminescence signal, at each dose rate was selected; these are shown in Figs 4.16 up to 4.23 just for the TL signals. For $\text{Li}_2\text{B}_4\text{O}_7 : \text{Cu, In}$ at 2 Gy/h, the dose was 2002 mGy and for 30 Gy/h

the dose was 2496 mGy. For CaF:Dy (TLD 200) for 2 Gy/h and 30 Gy/h, the doses were 2998 mGy. For LiF: Mg,Ti for 2 Gy/h the dose was 2496 mGy and for 30 Gy/h the dose was 2998 mGy. For BeO for 2 Gy/h, the dose was 2496 mGy and for 30 Gy/h the dose was 2496 mGy. Except BeO, only peak 4 and peak 5 was shown because the other peaks (a) were very small in intensity and (b) are unstable for dosimetric applications. Therefore, as these did not contribute while determining the kinetic parameters, they were neglected. As for BeO, both peaks 1 and peak 2 were examined to determine the kinetic parameters, other peaks were neglected due to the very low intensity. FOM values are between 0.580 and 5.147. MgB₄O₇ :Dy, Na has only one peak so deconvolution was not performed.

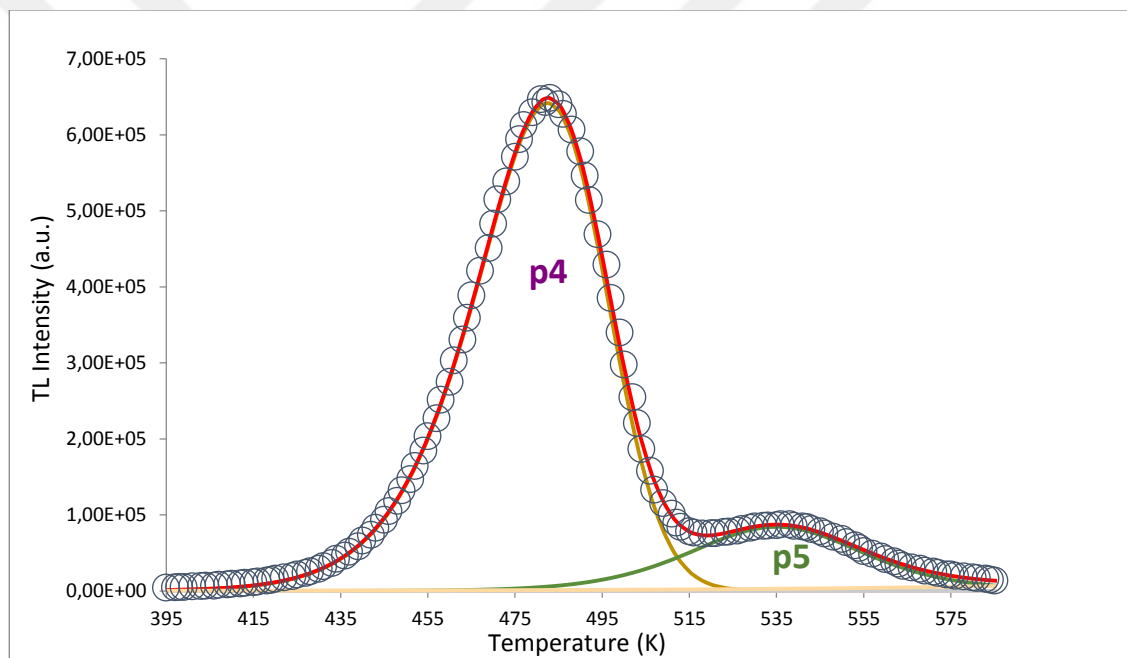


Figure 4.16 Deconvolution example for the TL glow curve of Li₂B₄O₇ : Cu, In. The curve corresponds to a dose of 2002 mGy at a dose rate of 2 Gy/h. Open dots correspond to experimentally obtained data points, while lines correspond to the individual TL peaks as well as the theoretical (fitted) line. Two TL peaks were used for fitting of high quality. FOM value was 1.990

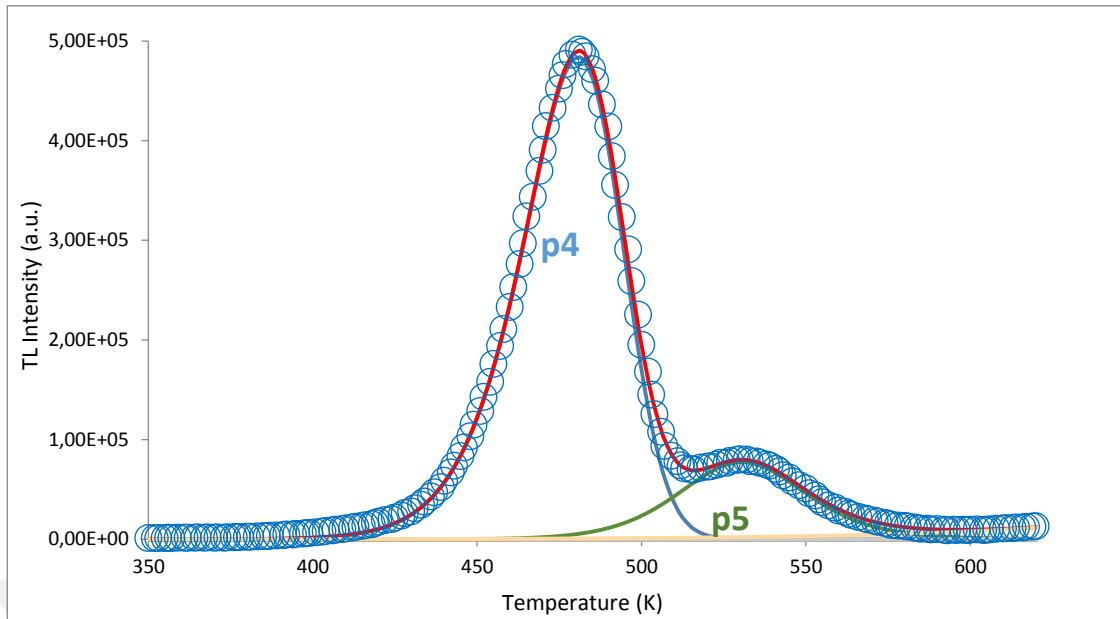


Figure 4.17 Deconvolution example for the TL glow curve of $\text{Li}_2\text{B}_4\text{O}_7 : \text{Cu, In}$. The curve corresponds to a dose of 2496 mGy at a dose rate of 30 Gy/h. Open dots correspond to experimentally obtained data points, while lines correspond to the individual TL peaks as well as the theoretical (fitted) line. Two TL peaks were used for fitting of high quality. FOM value was 2.622

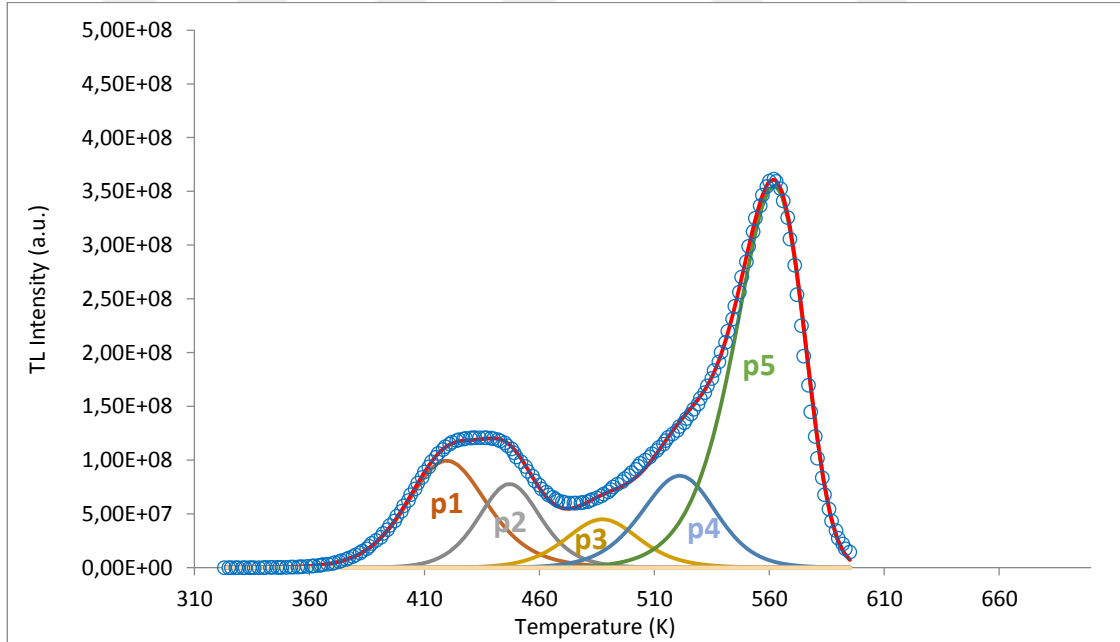


Figure 4.18 Deconvolution example for the TL glow curve of CaF:Dy (TLD 200). The curve corresponds to a dose of 2998 mGy at a dose rate of 2 Gy/h. Open dots correspond to experimentally obtained data points, while lines correspond to the individual TL peaks as well as the theoretical (fitted) line. Two TL peaks were used for fitting of high quality. FOM value was 2.74

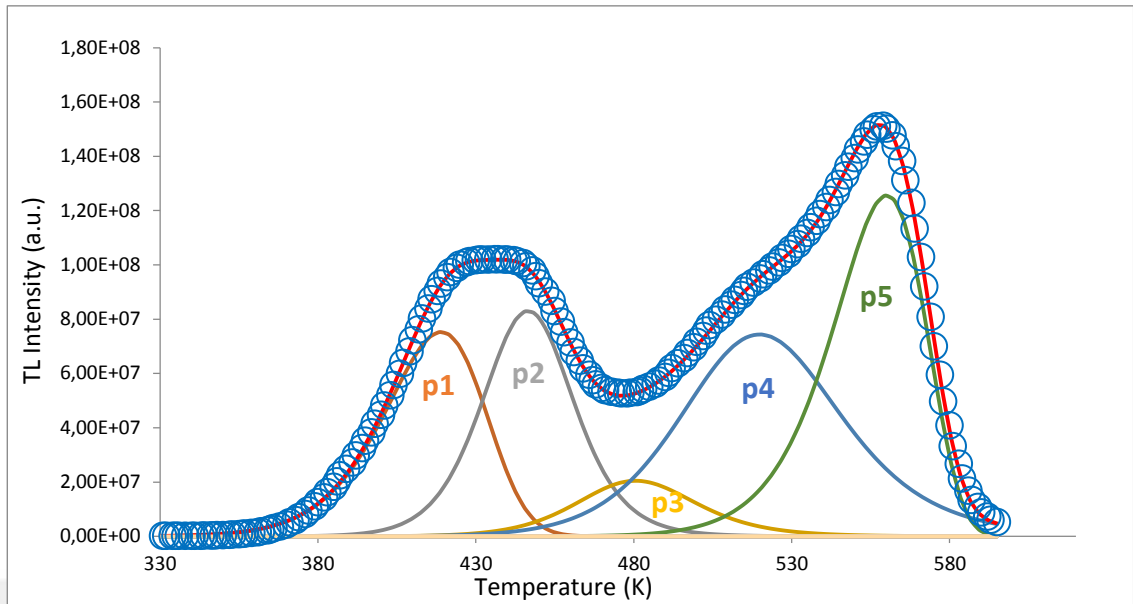


Figure 4.19 Deconvolution example for the TL glow curve of CaF:Dy (TLD 200). The curve corresponds to a dose of 2998 mGy at a dose rate of 30 Gy/h. Open dots correspond to experimentally obtained data points, while lines correspond to the individual TL peaks as well as the theoretical (fitted) line. Two TL peaks were used for fitting of high quality. FOM value was 1.085

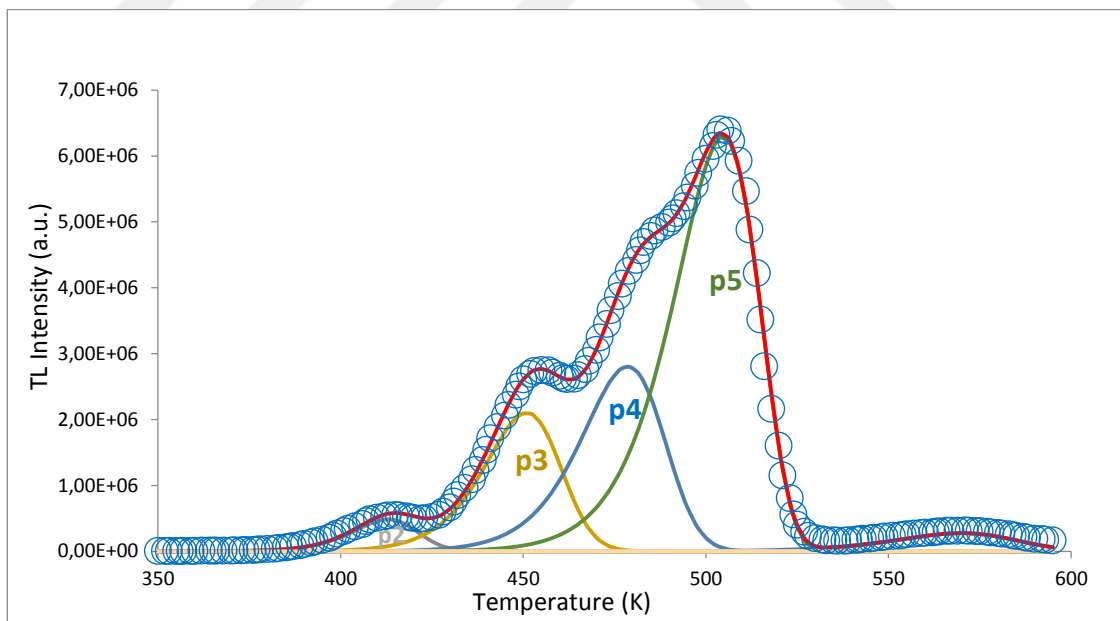


Figure 4.20 Deconvolution example for the TL glow curve of LiF: Mg,Ti (TLD 100). The curve corresponds to a dose of 2496 mGy at a dose rate of 2 Gy/h. Open dots correspond to experimentally obtained data points, while lines correspond to the individual TL peaks as well as the theoretical (fitted) line. Two TL peaks were used for fitting of high quality. FOM value was 3.117

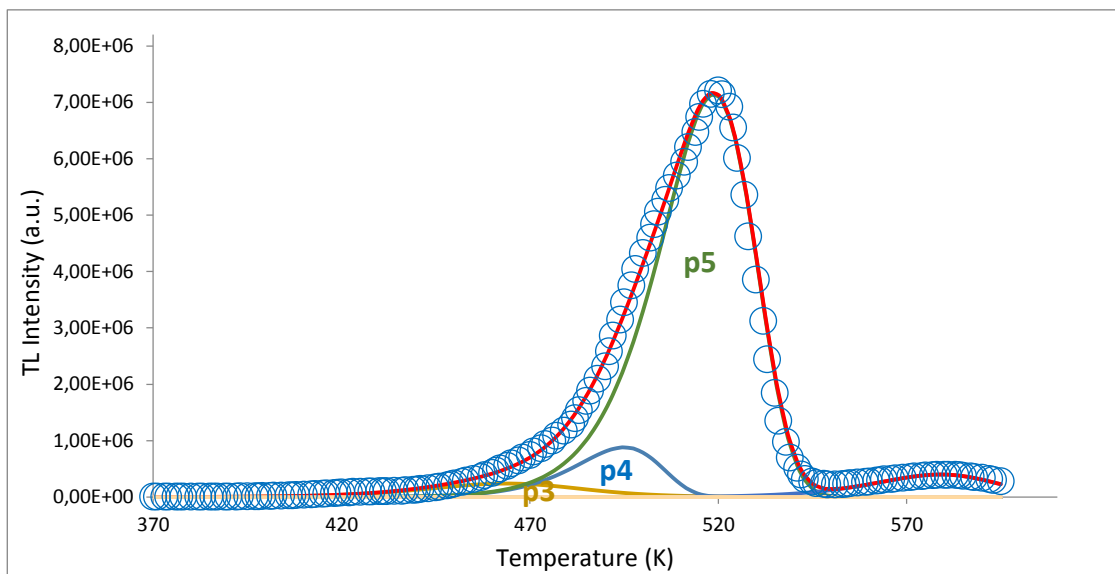


Figure 4.21 Deconvolution example for the TL glow curve of LiF : Mg,Ti (TLD 100). The curve corresponds to a dose of 2998 mGy at a dose rate of 30 Gy/h. Open dots correspond to experimentally obtained data points, while lines correspond to the individual TL peaks as well as the theoretical (fitted) line. Two TL peaks were used for fitting of high quality. FOM value was 5.147

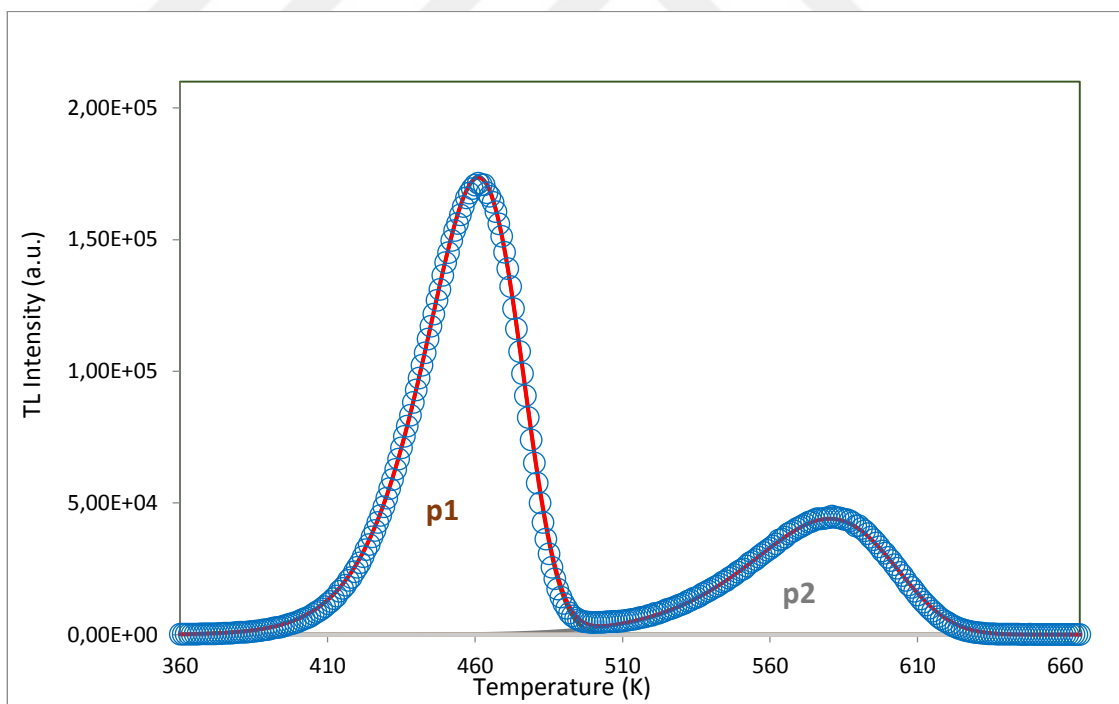


Figure 4.22 Deconvolution example for the TL glow curve of BeO. The curve corresponds to a dose of 2496 mGy at a dose rate of 2 Gy/h. Open dots correspond to experimentally obtained data points, while lines correspond to the individual TL peaks as well as the theoretical (fitted) line. Two TL peaks were used for fitting of high quality. FOM value was 0.580

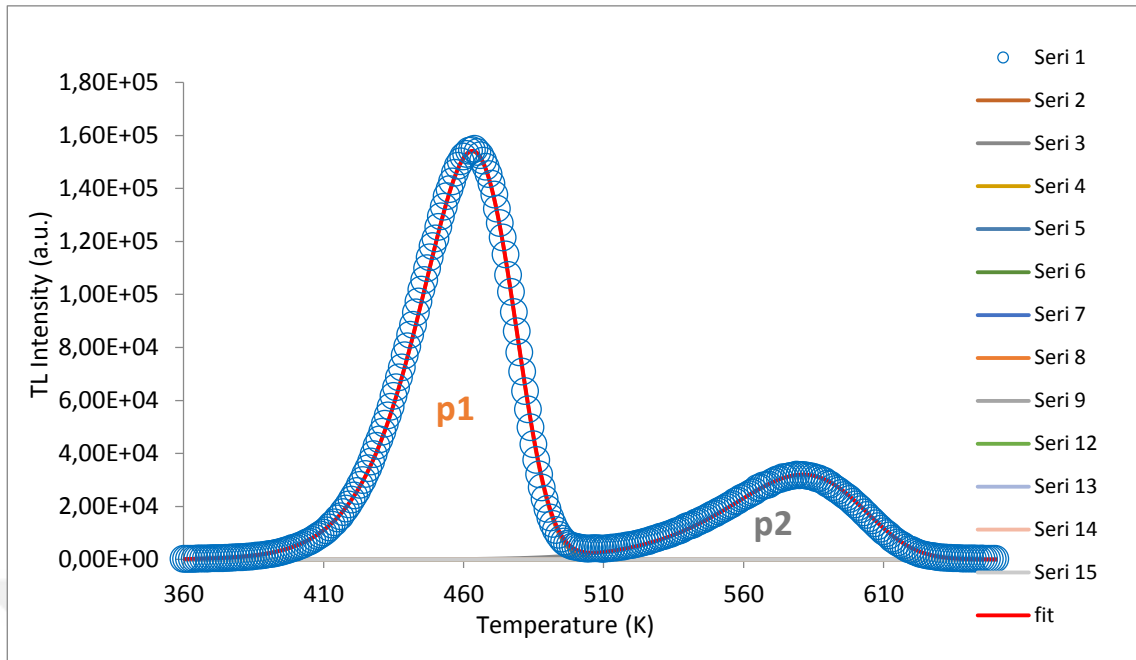


Figure 4.23 Deconvolution example for the TL glow curve of BeO. The curve corresponds to a dose of 2496 mGy at a dose rate of 30 Gy/h. Open dots correspond to experimentally obtained data points, while lines correspond to the individual TL peaks as well as the theoretical (fitted) line. Two TL peaks were used for fitting of high quality. FOM value was 0.762

Figures, between Figure 4.24 and 4.28 show typical deconvolution examples of OSL decay curves of BeO and quartz samples.

Figs 4.24 and 4.25 shows BeO deconvolution examples and the FOM values are 0.39 and 0.80 at 2Gy/h and 30 Gy/h dose rates, respectively. Two components were examined in BeO deco-OSL decay curves, one is fast, the other is medium. Fast component means trap lifetime is lowest, medium component's lifetime is higher than the fast one.

Figures 4.26, 4.27 and 4.28 show characteristic deconvolution examples of OSL decay curves of Quartz. FOM values are 5.15, 5.78 and 4.15 at 27Gy/h, 311 Gy/h and 1305 Gy/h dose rates, respectively. Three components were examined in Quartz deco-OSL decay curves, fast, medium and slow. Fast means trap lifetime is the smallest. Slow component's lifetime is the biggest, while medium component's lifetime lies between the corresponding values for the fast and slow components.

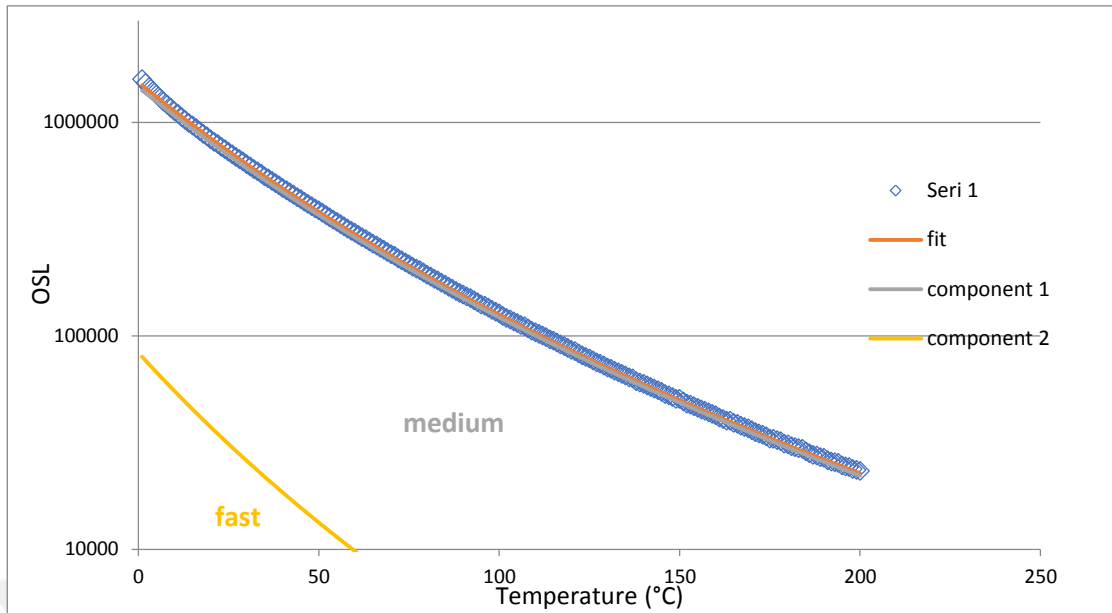


Figure 4.24 Deconvolution example for the OSL decay curve of BeO. The curve corresponds to a dose of 2496 mGy at a dose rate of 2 Gy/h. Open dots correspond to experimentally obtained data points, while lines correspond to the individual OSL components as well as the theoretical (fitted) line. Two OSL components were used for fitting of high quality. FOM value was 0.39

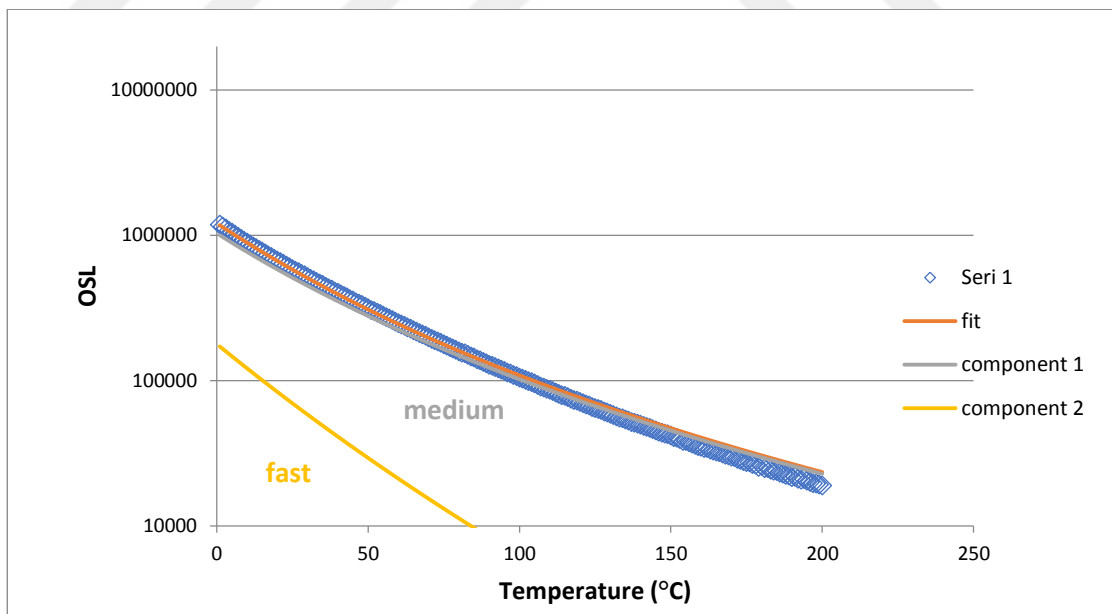


Figure 4.25 Deconvolution example for the OSL decay curve of BeO. The curve corresponds to a dose of 2496 mGy at a dose rate of 30 Gy/h. Open dots correspond to experimentally obtained data points, while lines correspond to the individual OSL components as well as the theoretical (fitted) line.

Two OSL components were used for fitting of high quality. FOM value was 0.80

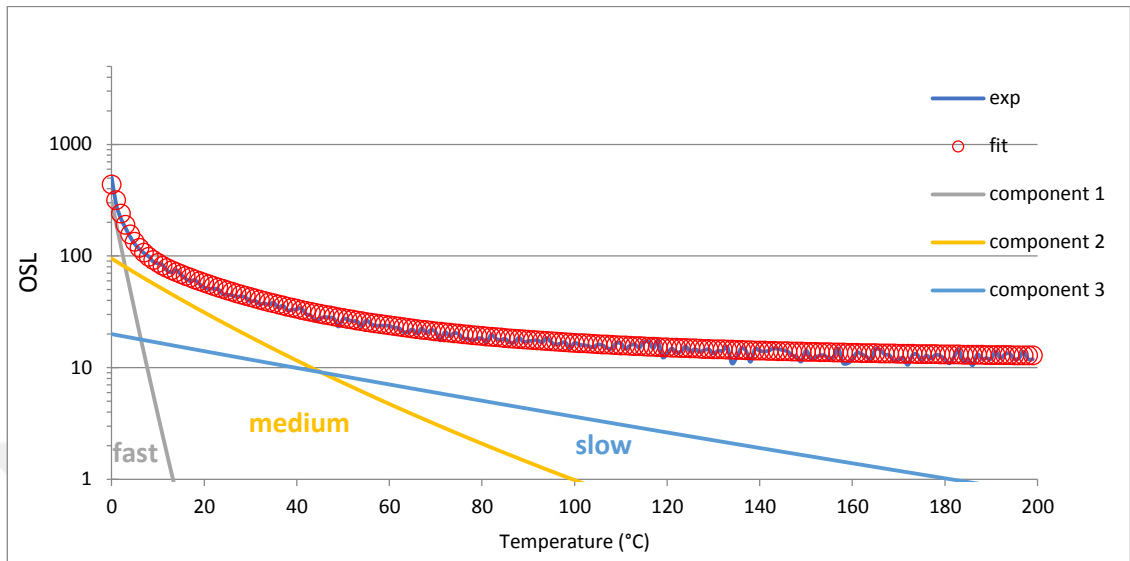


Figure 4.26 Deconvolution example for the OSL decay curve of Quartz. The curve corresponds to a dose of 75 Gy at a dose rate of 27 Gy/h. Open dots correspond to experimentally obtained data points, while lines correspond to the individual OSL components as well as the theoretical (fitted) line. Three OSL components were used for fitting of high quality. FOM value was 5.15

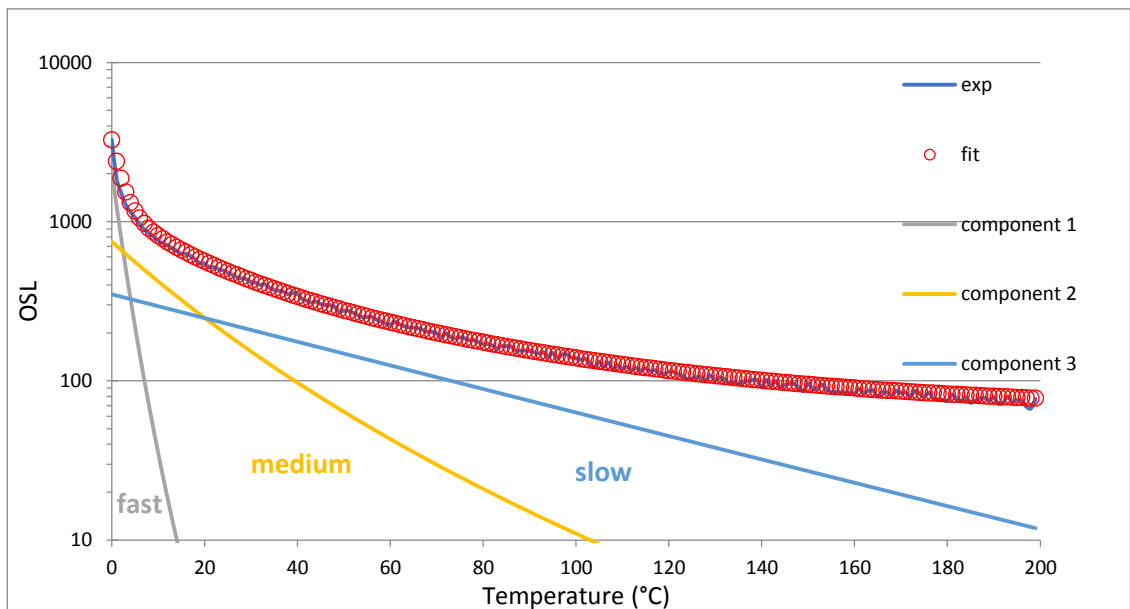


Figure 4.27 Deconvolution example for the OSL decay curve of Quartz. The curve corresponds to a dose of 1500 Gy at a dose rate of 311 Gy/h. Open dots correspond to experimentally obtained data points, while lines correspond

to the individual OSL components as well as the theoretical (fitted) line. Three OSL components were used for fitting of high quality. FOM value was 5.78

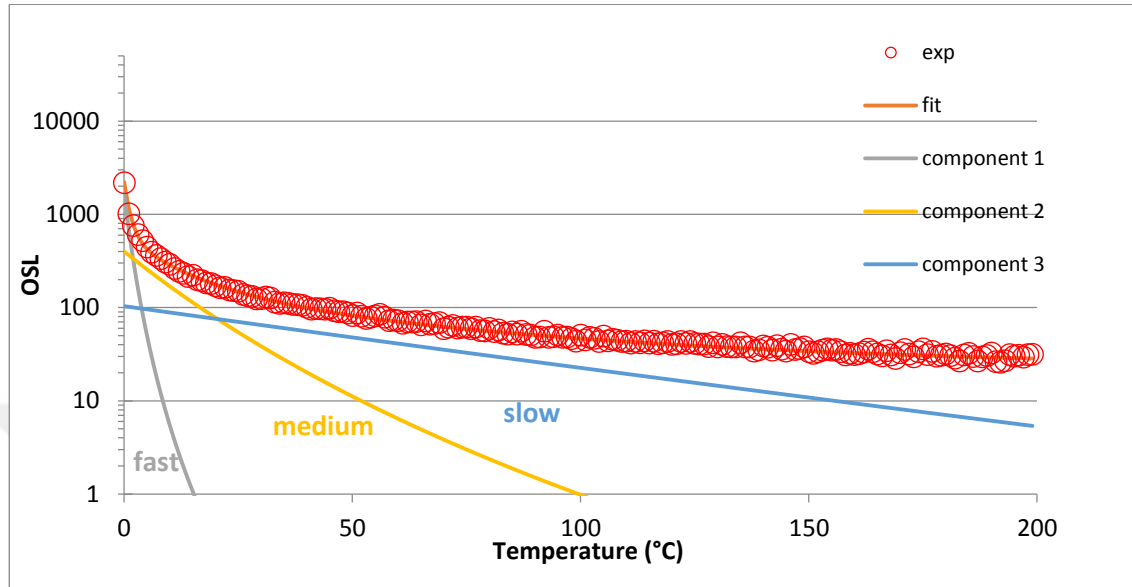


Figure 4.28 Deconvolution example for the OSL decay curve of Quartz. The curve corresponds to a dose of 750 Gy at a dose rate of 1305 Gy/h. Open dots correspond to experimentally obtained data points, while lines correspond to the individual OSL components as well as the theoretical (fitted) line. Three OSL components were used for fitting of high quality. FOM value was 4.15

4.3 Dose Response Curves For TL Peaks Following Deconvolution Of TL Glow Curves

Figs 4.29 – 4.37 present the TL dose response for each one of the stable TL traps of the materials subjected to the present study. The dose responses corresponding to both dose rates (2 Gy/h and 30 Gy/h) are presented in the same Fig. for each TL peak for the sake of comparison. Specifically:

Fig. 4.29 presents the dose response of TL single peak of $MgB_4O_7 :Dy, Na$ for both dose rates.

Fig. 4.30 presents the dose response of TL peak 4 of $Li_2B_4O_7 :Cu, In$ for both dose rates.

Fig. 4.31 presents the dose response of TL peak 5 of $Li_2B_4O_7 :Cu, In$ for both dose rates.

Fig. 4.32 presents the dose response of TL peak 4 of CaF₂:Dy (TLD200) for both dose rates.

Fig. 4.33 presents the dose response of TL peak 5 of CaF₂:Dy (TLD 200) for both dose rates.

Fig. 4.34 presents the dose response of TL peak 4 of LiF: Mg,Ti (TLD 100) for both dose rates.

Fig. 4.35 presents the dose response of TL peak 5 of LiF: Mg,Ti TLD 100 for both dose rates.

Figure 4.36 and 4.37 shows the BeO dose response curves which were obtained like the previous ones but for BeO examined peaks are peak 1 and peak 2. Errors were calculated for each plots.

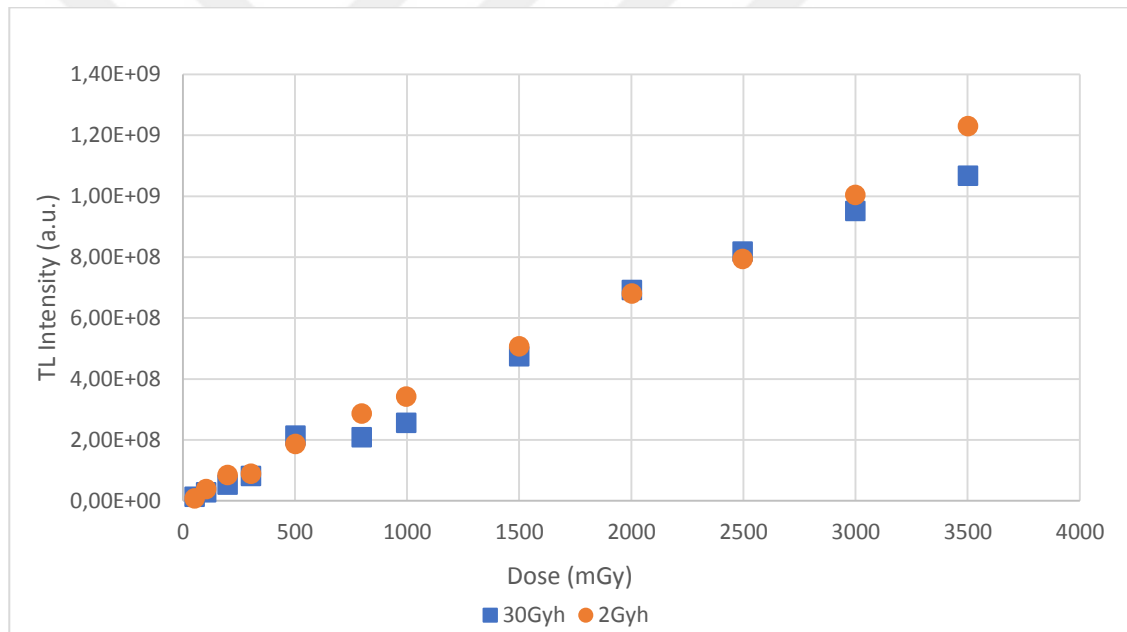


Figure 4.29 Component resolved TL dose response curves obtained for TL single peak of MgB₄O₇:Dy:Na. Dots correspond to 2 Gy/h and squares correspond to 30 Gy/h. Each data point corresponds to an average of two individually measured values. Error bars correspond to 1 σ (Errors are very small)

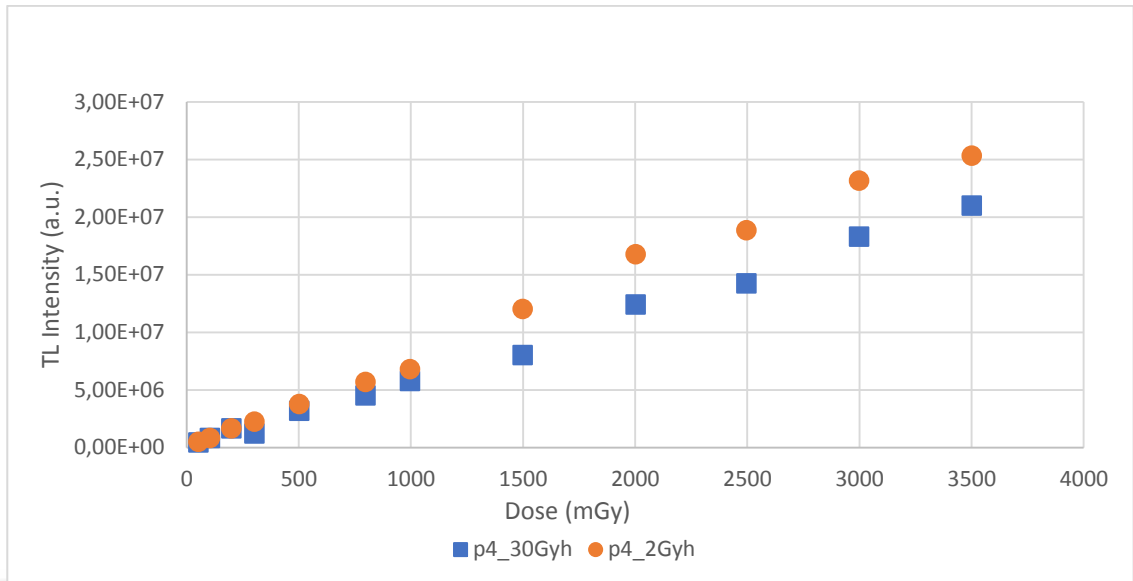


Figure 4.30 Component resolved TL dose response curves obtained for TL peak 4 of $\text{Li}_2\text{B}_4\text{O}_7 \cdot \text{Cu}$, In. Dots correspond to 2 Gy/h and squares correspond to 30 Gy/h. Each data point corresponds to an average of two individually measured values. Error bars correspond to 1σ (Errors are very small)

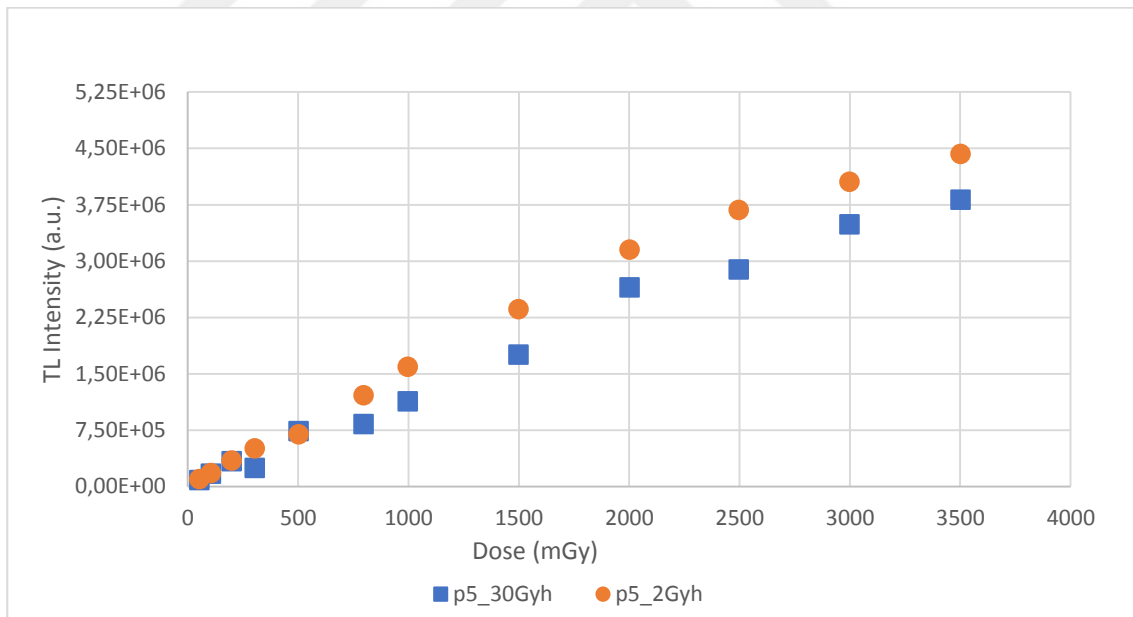


Figure 4.31 Component resolved TL dose response curves obtained for TL peak 5 of $\text{Li}_2\text{B}_4\text{O}_7 \cdot \text{Cu}$, In. Dots correspond to 2 Gy/h and squares correspond to 30 Gy/h. Each data point corresponds to an average of two individually measured values. Error bars correspond to 1σ (Errors are very small)

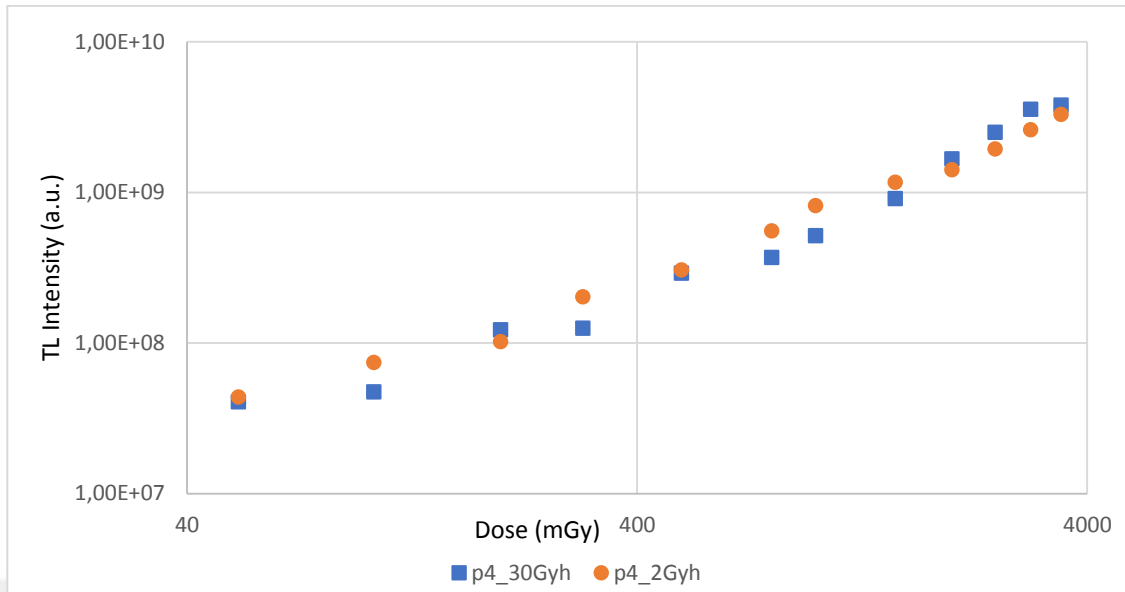


Figure 4.32 Component resolved TL dose response curves obtained for TL peak 4 of CaF₂: Dy (TLD 200). Dots correspond to 2 Gy/h and squares correspond to 30 Gy/h. Each data point corresponds to an average of two individually measured values. Error bars correspond to 1 σ (Errors are very small) (TL&dose axis are logarithmic)

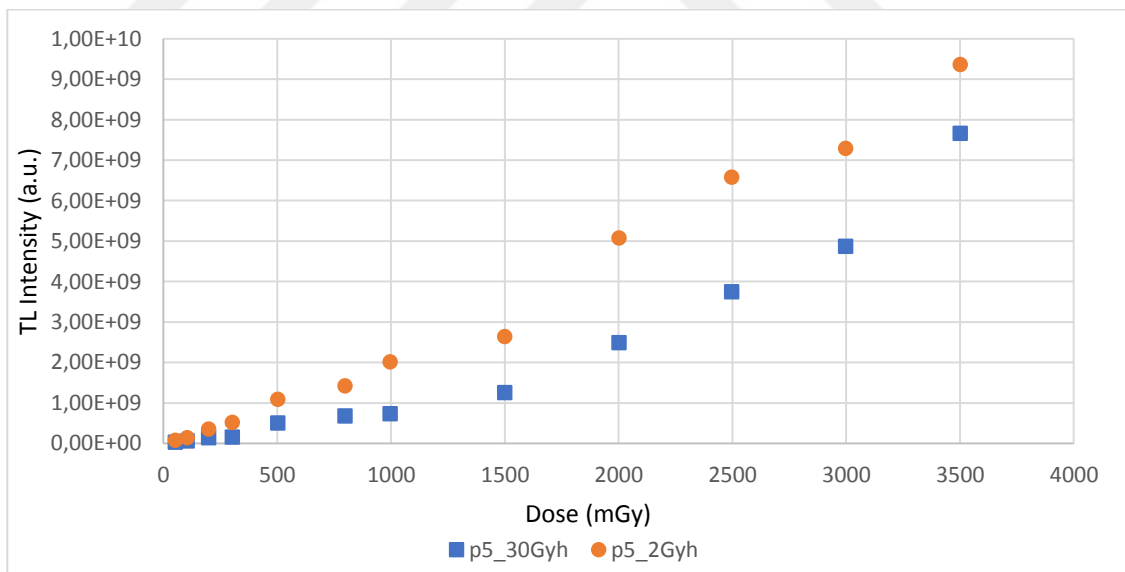


Figure 4.33 Component resolved TL dose response curves obtained for TL peak 5 of CaF₂: Dy (TLD 200). Dots correspond to 2 Gy/h and squares correspond to 30 Gy/h. Each data point corresponds to an average of two individually measured values. Error bars correspond to 1 σ (Errors are very small)

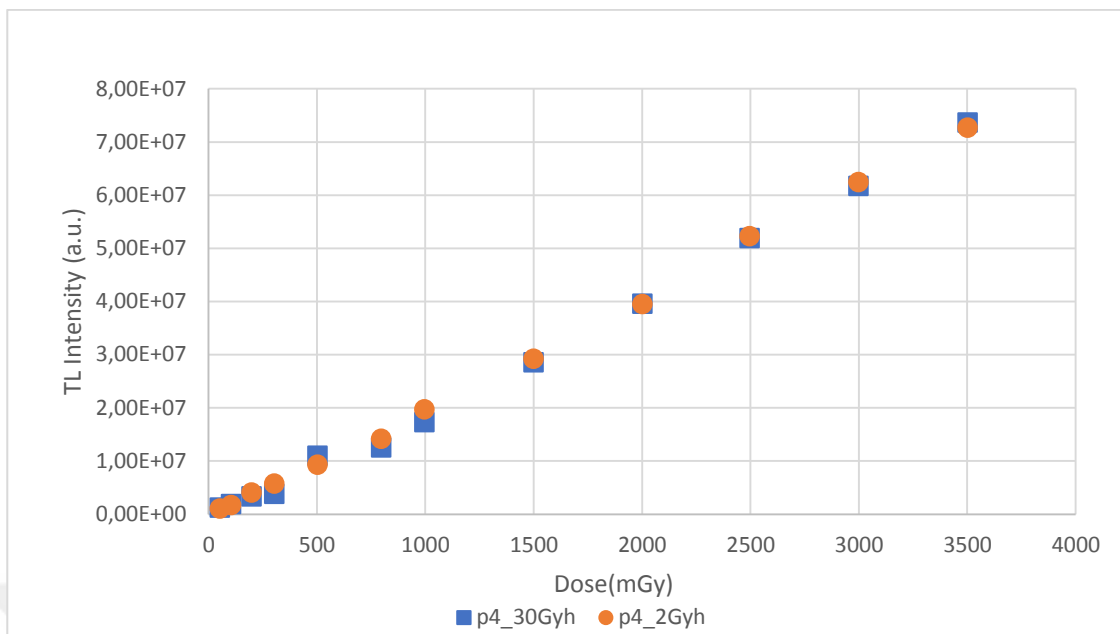


Figure 4.34 Component resolved TL dose response curves obtained for TL peak 4 of LiF: Mg, Ti (TLD 100). Dots correspond to 2 Gy/h and squares correspond to 30 Gy/h. Each data point corresponds to an average of two individually measured values. Error bars correspond to 1σ (Errors are very small)

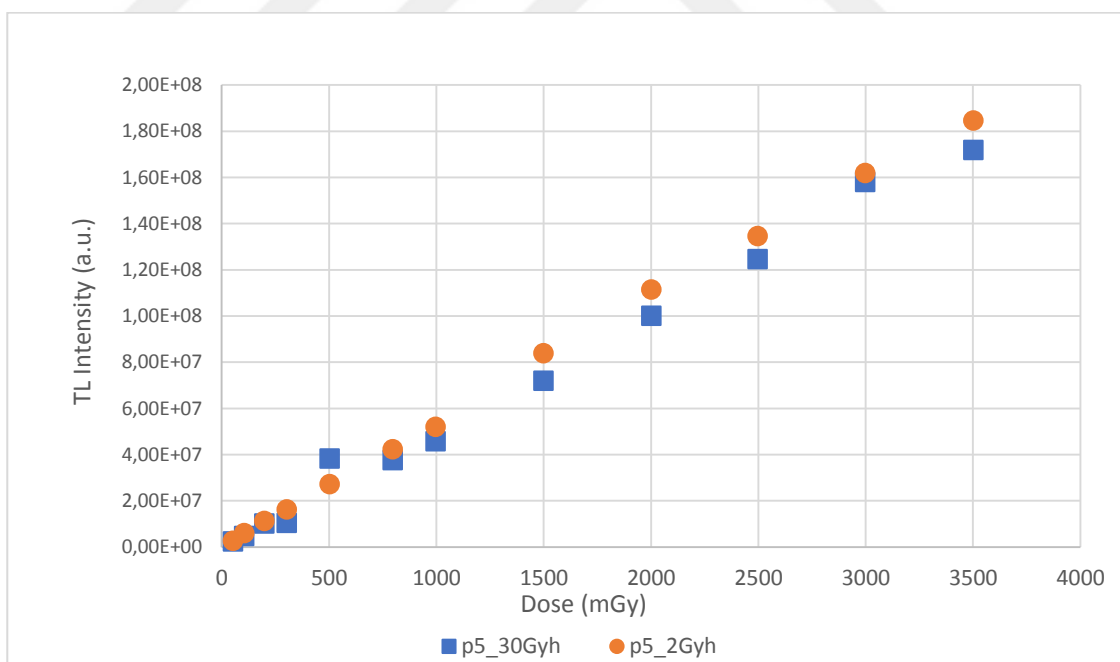


Figure 4.35 Component resolved TL dose response curves obtained for TL peak 5 of LiF : Mg,Ti (TLD 100). Dots correspond to 2 Gy/h and squares correspond to 30 Gy/h. Each data point corresponds to an average of two individually measured values. Error bars correspond to 1σ (Errors are very small)

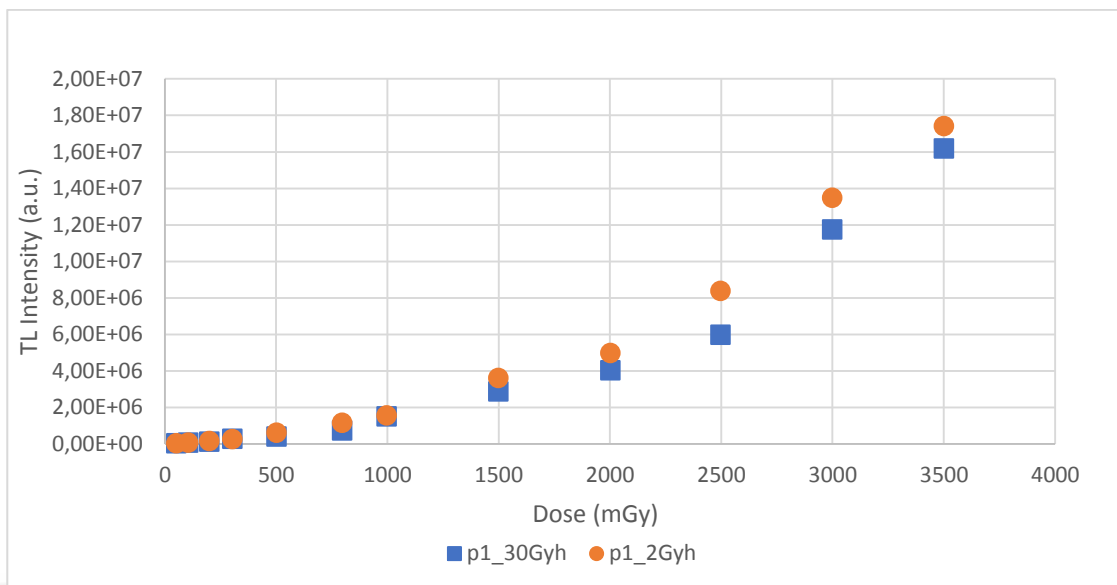


Figure 4.36 Component resolved TL dose response curves obtained for TL peak 1 of BeO. Dots correspond to 2 Gy/h and squares correspond to 30 Gy/h. Each data point corresponds to an average of two individually measured values. Error bars correspond to 1σ (Errors are very small)

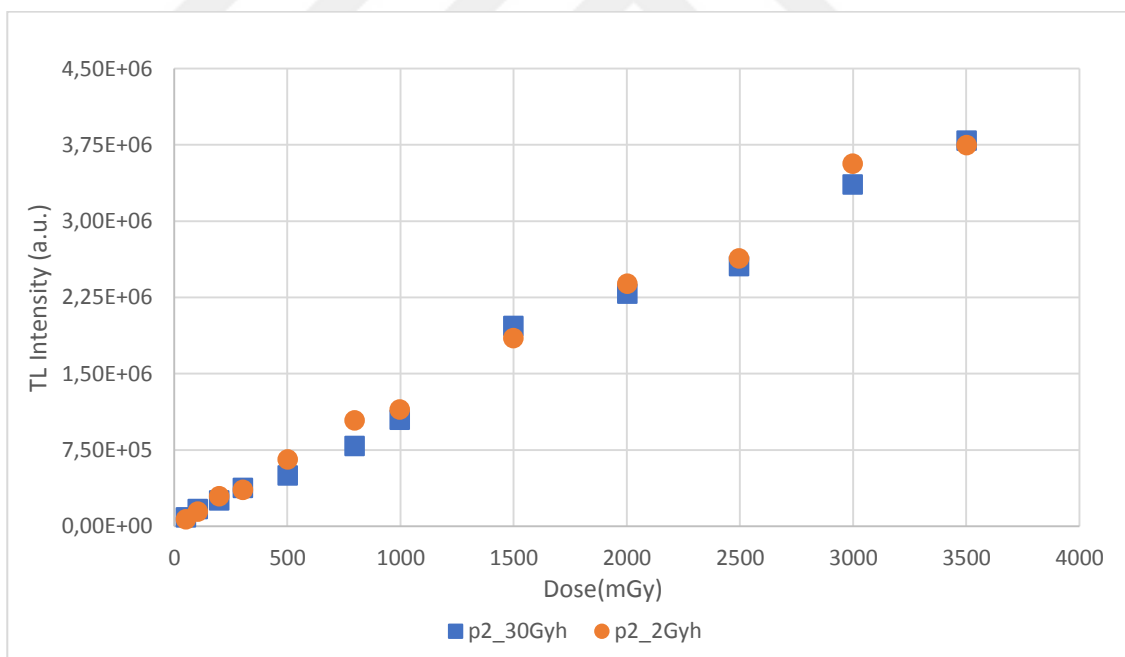


Figure 4.37 Component resolved TL dose response curves obtained for TL peak 2 of BeO. Dots correspond to 2 Gy/h and squares correspond to 30 Gy/h. Each data point corresponds to an average of two individually measured values. Error bars correspond to 1σ (Errors are very small)

4.4 Kinetic Parameters For TL Peaks Following Deconvolution Of TL Glow Curves

After deconvolution analyses, of all artificial materials/dosimeters the order of kinetic, b values were determined for each peak. The next step is to plot the b values versus dose for all dose rates applied. Figures between the Figure 4.38 and 4.43 present these plots.

Figure 4.44 and 4.45 shows the BeO b versus dose curves which were obtained like the previous ones but for BeO, examined peaks are peak 1 and peak 2.

Errors were calculated for each plots.

Similar plots were also presented for the case of activation energies. Plots lies between 4.45 and 4.52 are related to activation energy.

Fig. 4.46 presents the dose response of TL peak 4 of $\text{Li}_2\text{B}_4\text{O}_7$:Cu, In for both dose rates.

Fig. 4.47 presents the dose response of TL peak 5 of $\text{Li}_2\text{B}_4\text{O}_7$:Cu, In for both dose rates.

Fig. 4.48 presents the dose response of TL peak 4 of CaF_2 :Dy (TLD 200) for both dose rates.

Fig. 4.49 presents the dose response of TL peak 5 of CaF_2 :Dy (TLD 200) for both dose rates.

Fig. 4.50 presents the dose response of TL peak 4 of LiF: Mg,Ti (TLD 100) for both dose rates.

Fig. 4.51 presents the dose response of TL peak 5 of LiF: Mg,Ti (TLD 100) for both dose rates.

Figure 4.52 and 4.53 shows the BeO E versus dose curves which were obtained like the previous ones but for BeO examined peaks are peak 1 and peak 2.

Errors were calculated for each plots.

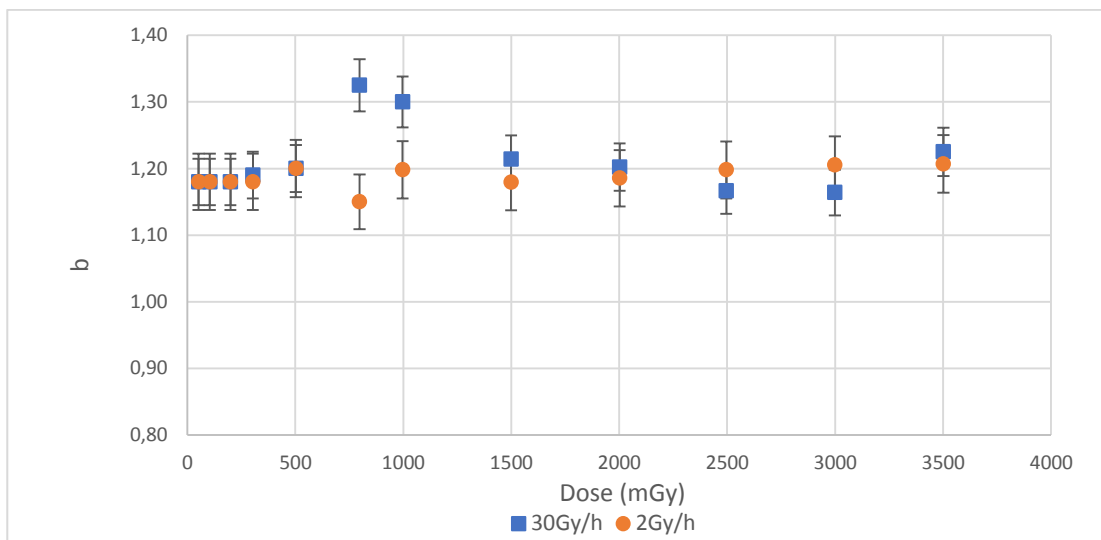


Figure 4.38 Order of kinetic, b , versus dose curves obtained for TL peak 4 of $\text{Li}_2\text{B}_4\text{O}_7$: Cu, In; the values were yielded after deconvolution analysis. Dots correspond to 2 Gy/h and squares correspond to 30 Gy/h. Each data point corresponds to an average of two individually measured values. Error bars correspond to 1σ

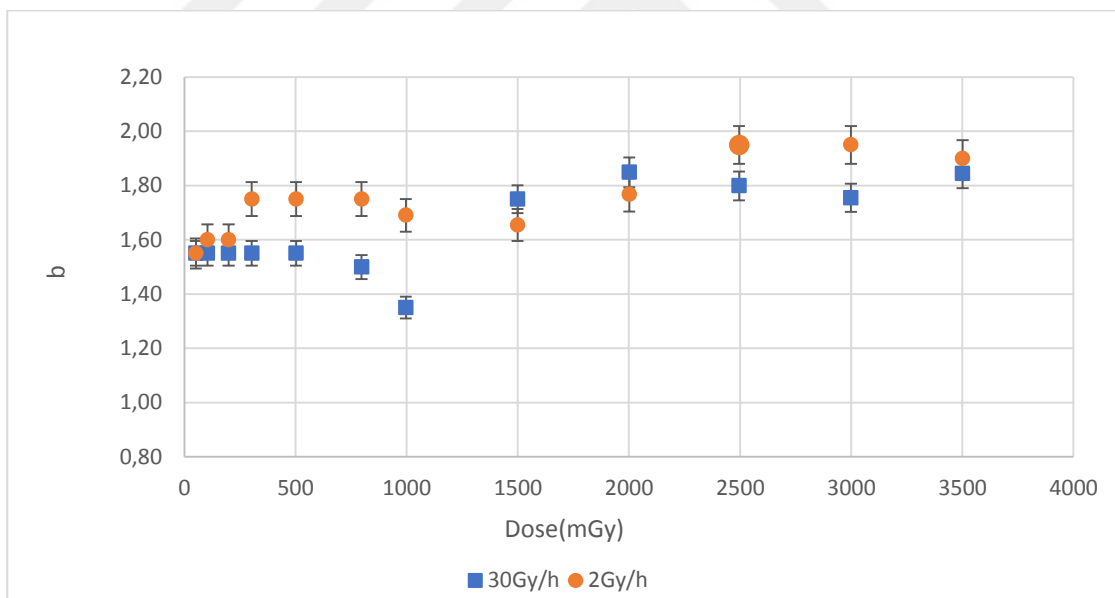


Figure 4.39 Order of kinetic, b , versus dose curves obtained for TL peak 5 of $\text{Li}_2\text{B}_4\text{O}_7$: Cu, In; the values were yielded after deconvolution analysis. Dots correspond to 2 Gy/h and squares correspond to 30 Gy/h. Each data point corresponds to an average of two individually measured values. Error bars correspond to 1σ

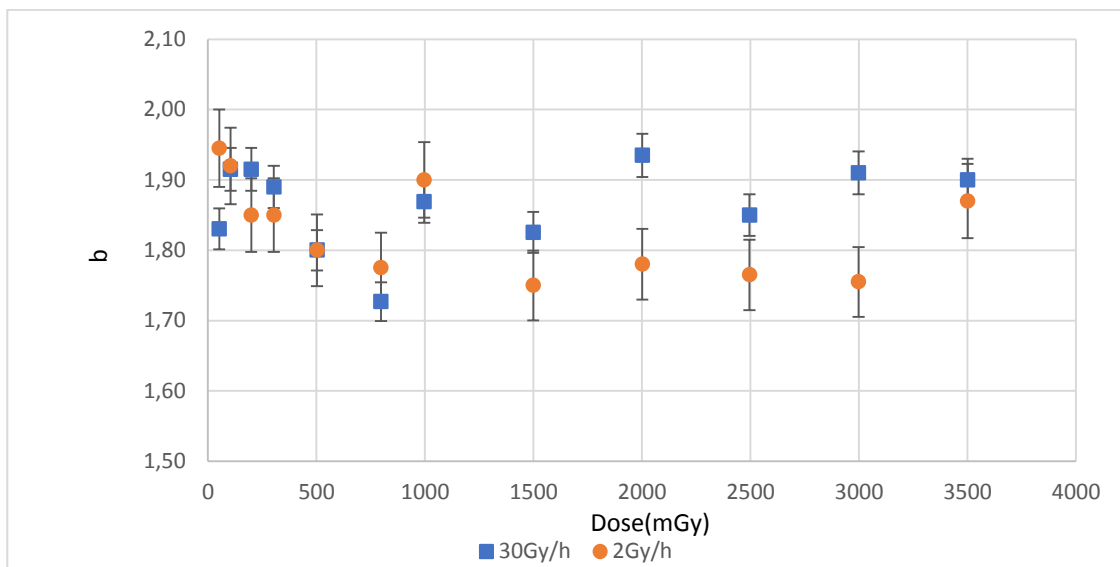


Figure 4.40 Order of kinetic, b , versus dose curves obtained for TL peak 4 of $\text{CaF}_2:\text{Dy}$ (TLD 200); the values were yielded after deconvolution analysis. Dots correspond to 2 Gy/h and squares correspond to 30 Gy/h. Each data point corresponds to an average of two individually measured values. Error bars correspond to 1σ (Errors are very small)

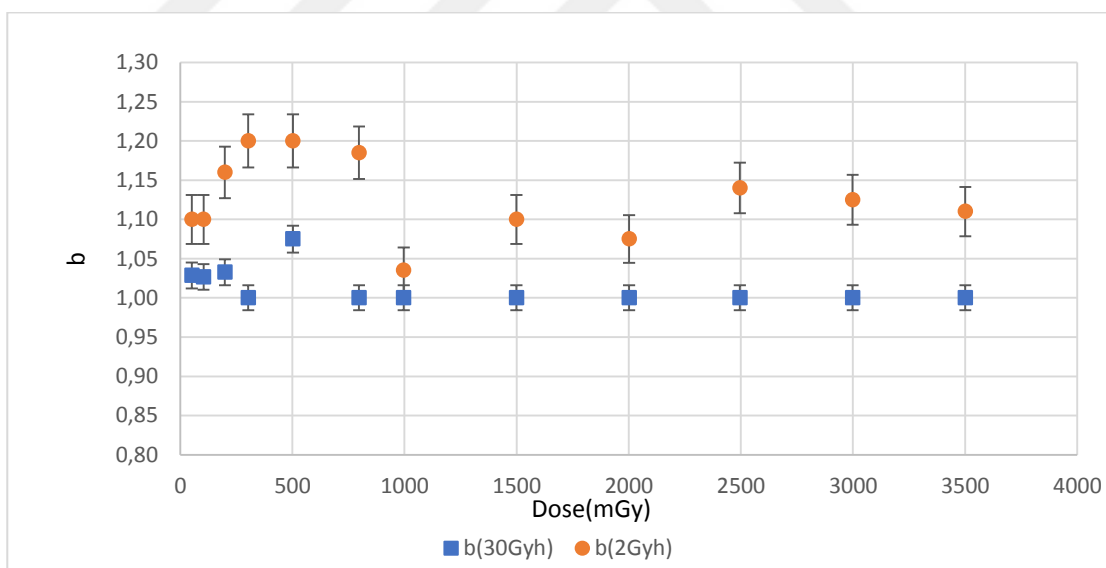


Figure 4.41 Order of kinetic, b , versus dose curves obtained for TL peak 5 of $\text{CaF}_2:\text{Dy}$ (TLD 200); the values were yielded after deconvolution analysis. Dots correspond to 2 Gy/h and squares correspond to 30 Gy/h. Each data point corresponds to an average of two individually measured values. Error bars correspond to 1σ

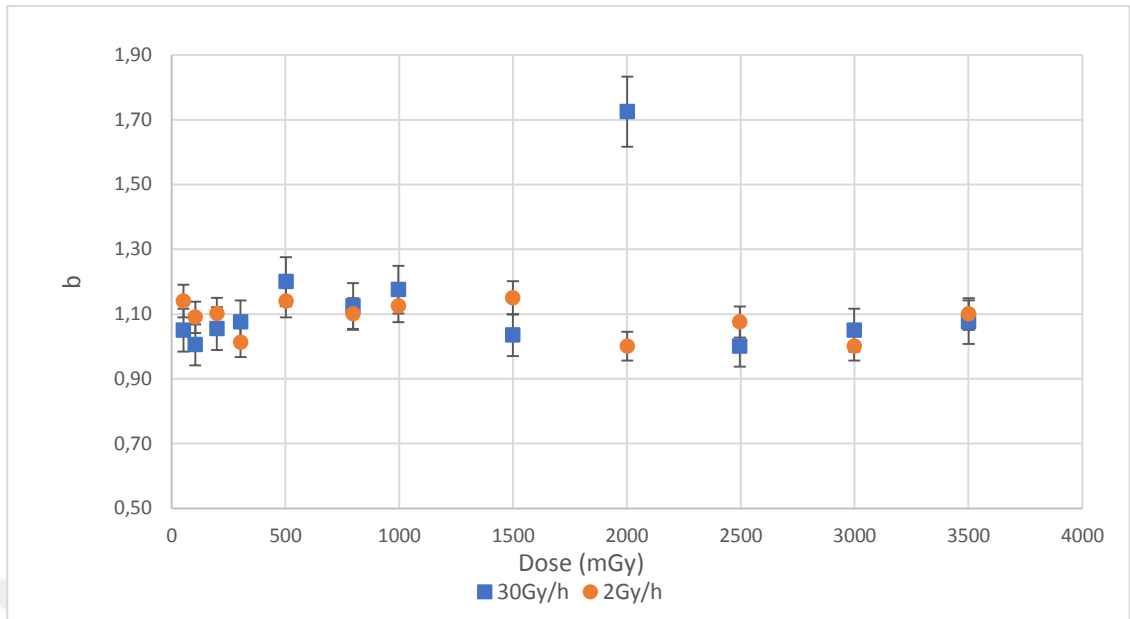


Figure 4.42 Order of kinetic, b , versus dose curves obtained for TL peak 4 of LiF: Mg,Ti (TLD 100); the values were yielded after deconvolution analysis. Dots correspond to 2 Gy/h and squares correspond to 30 Gy/h. Each data point corresponds to an average of two individually measured values. Error bars correspond to 1σ

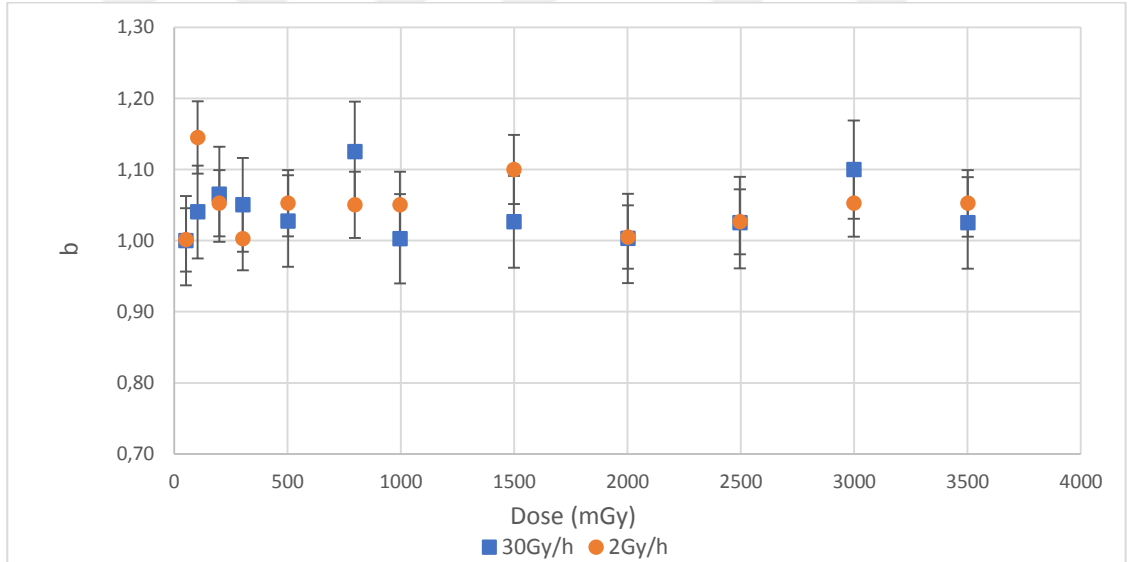


Figure 4.43 Order of kinetic, b , versus dose curves obtained for TL peak 5 of LiF : Mg,Ti (TLD 100); the values were yielded after deconvolution analysis. Dots correspond to 2 Gy/h and squares correspond to 30 Gy/h. Each data point corresponds to an average of two individually measured values. Error bars correspond to 1σ

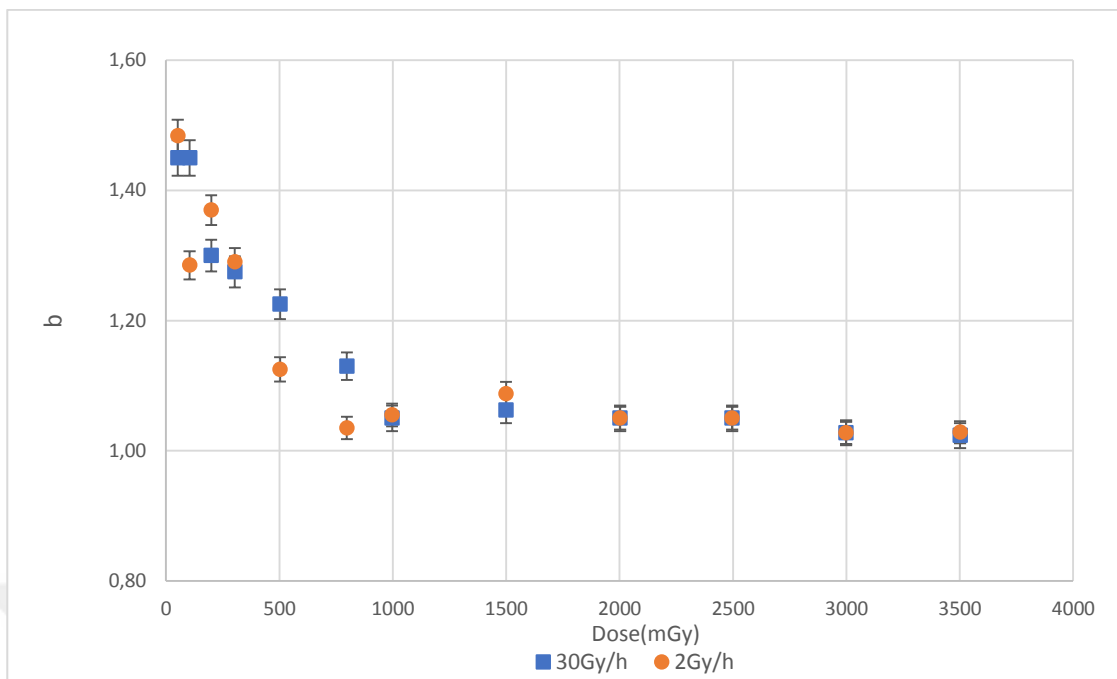


Figure 4.44 Order of kinetic, b , versus dose curves obtained for TL peak 1 of BeO; the values were yielded after deconvolution analysis. Dots correspond to 2 Gy/h and squares correspond to 30 Gy/h. Each data point corresponds to an average of two individually measured values. Error bars correspond to 1σ

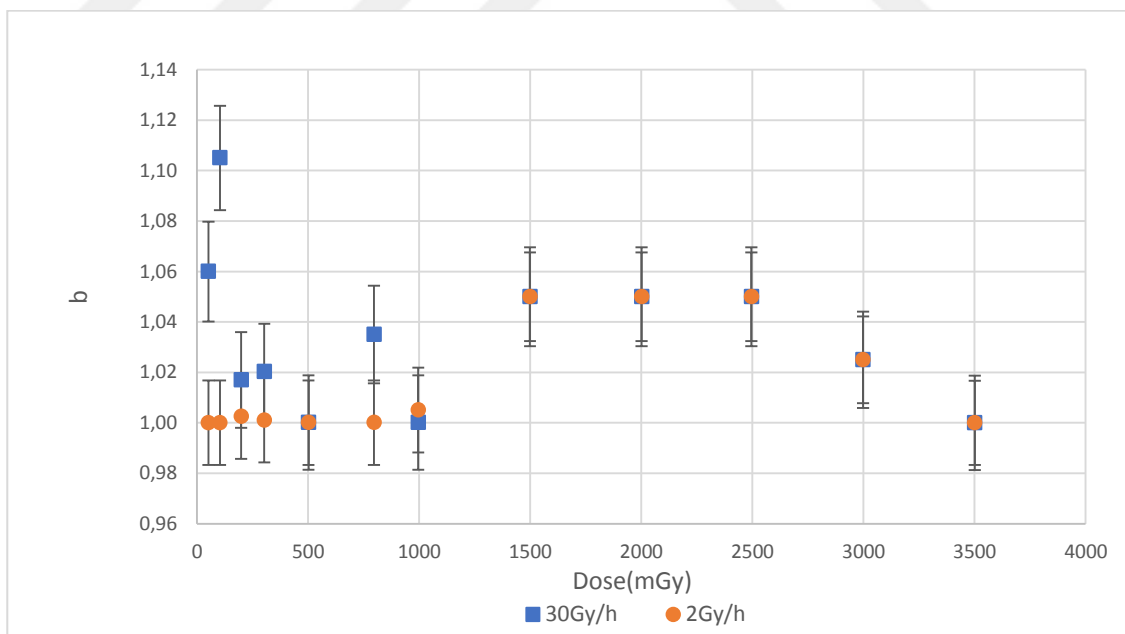


Figure 4.45 Order of kinetic, b , versus dose curves obtained for TL peak 2 of BeO; the values were yielded after deconvolution analysis. Dots correspond to 2 Gy/h and squares correspond to 30 Gy/h. Each data point corresponds to an average of two individually measured values. Error bars correspond to 1σ

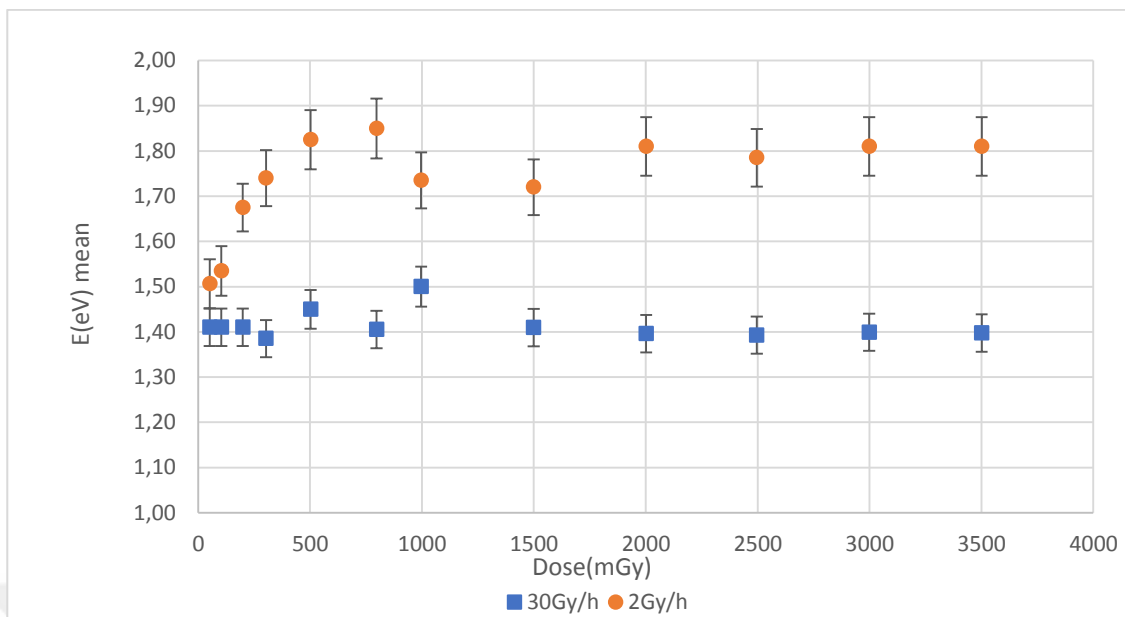


Figure 4.46 Activation energy, E, versus dose curves obtained for TL peak 4 of $\text{Li}_2\text{B}_4\text{O}_7$:Cu, In; the E values were yielded after deconvolution analysis. Dots correspond to 2 Gy/h and squares correspond to 30 Gy/h. Each data point corresponds to an average of two individually measured values. Error bars correspond to 1σ .

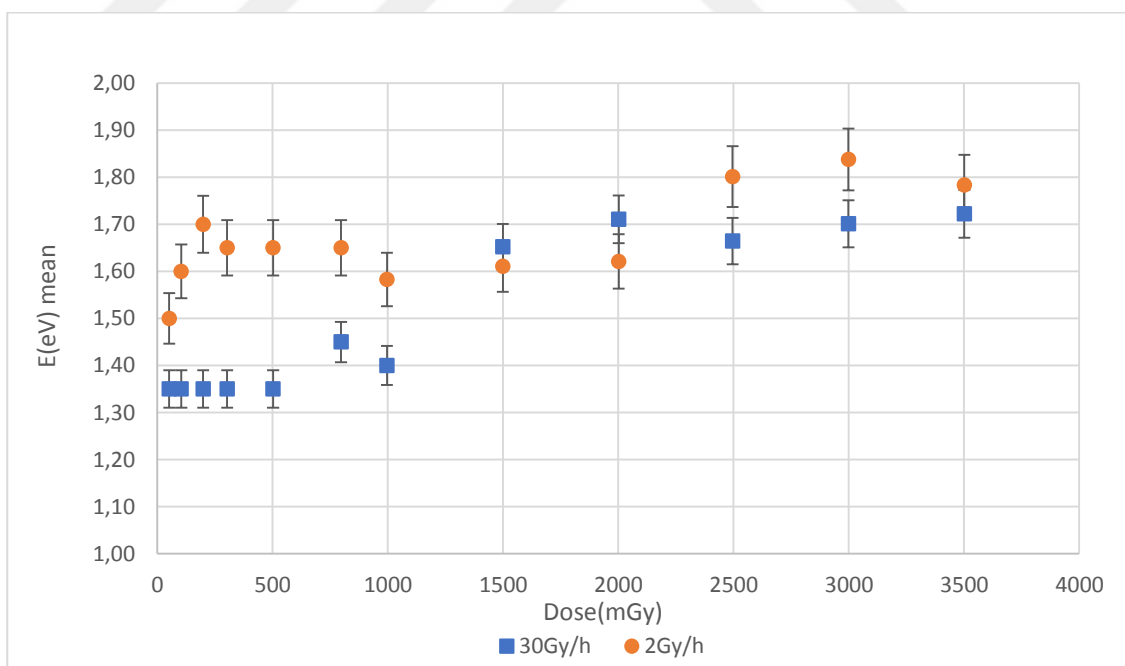


Figure 4.47 Activation energy, E, versus dose curves obtained for TL peak 5 of $\text{Li}_2\text{B}_4\text{O}_7$:Cu, In; the E values were yielded after deconvolution analysis. Dots correspond to 2 Gy/h and squares correspond to 30 Gy/h. Each data point corresponds to an average of two individually measured values. Error bars correspond to 1σ .

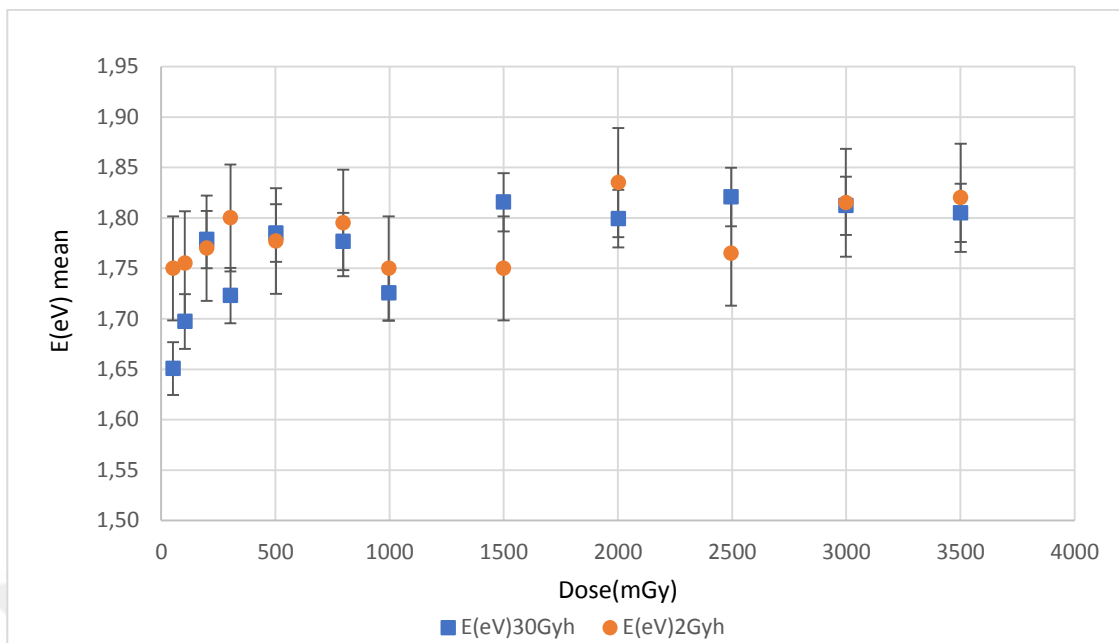


Figure 4.48 Activation energy, E , versus dose curves obtained for TL peak 4 of CaF_2 :Dy (TLD 200); the E values were yielded after deconvolution analysis. Dots correspond to 2 Gy/h and squares correspond to 30 Gy/h. Each data point corresponds to an average of two individually measured values. Error bars correspond to 1σ (Errors are very small)

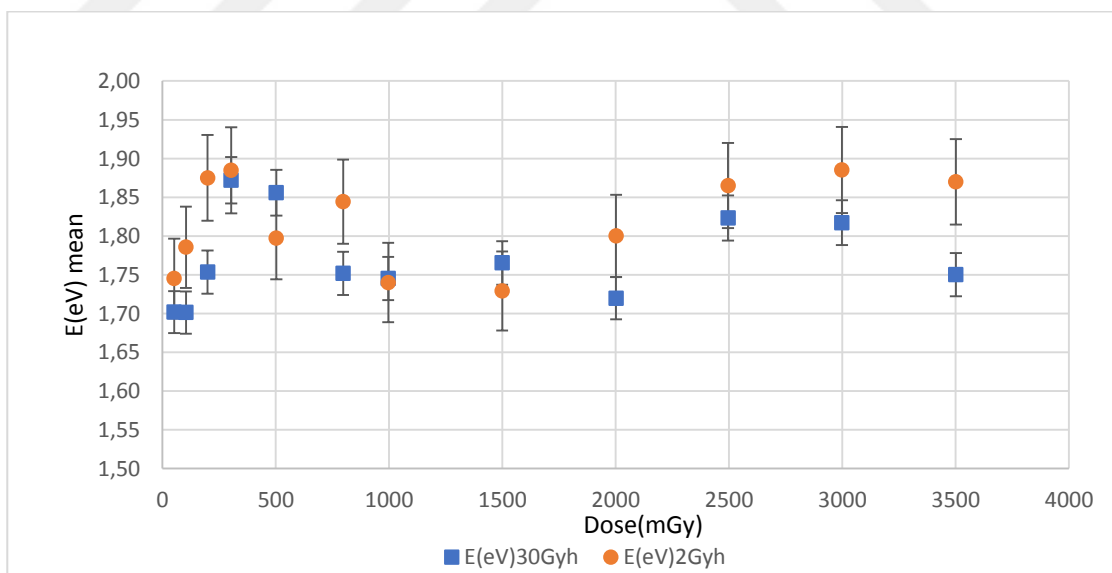


Figure 4.49 Activation energy, E , versus dose curves obtained for TL peak 5 of CaF_2 :Dy (TLD 200); the E values were yielded after deconvolution analysis. Dots correspond to 2 Gy/h and squares correspond to 30 Gy/h. Each data point corresponds to an average of two individually measured values. Error bars correspond to 1σ (Errors are very small)

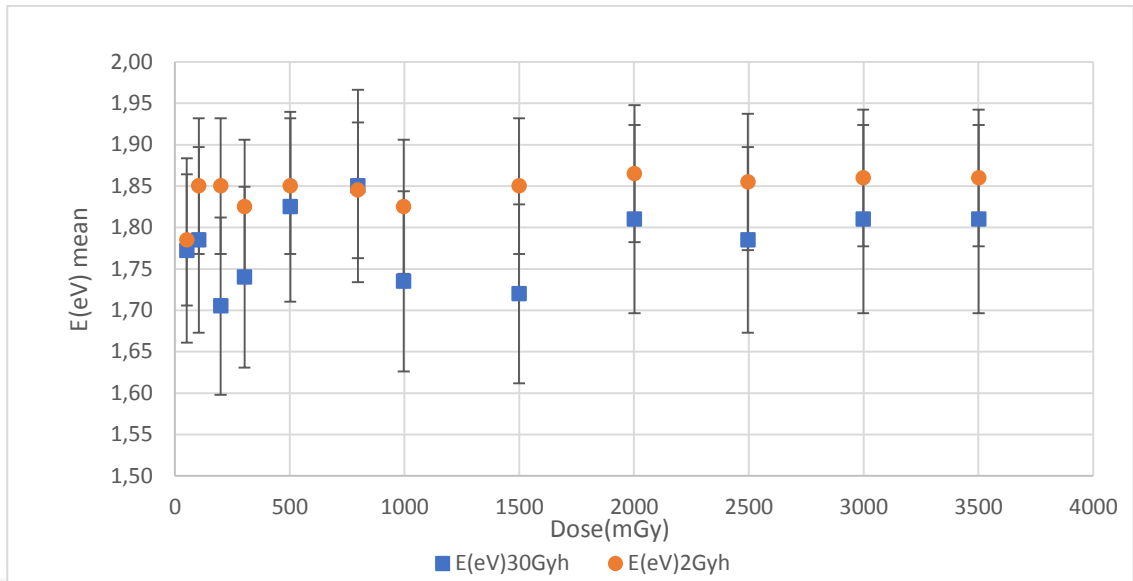


Figure 4.50 Activation energy, E , versus dose curves obtained for TL peak 4 of LiF: Mg,Ti (TLD 100); the E values were yielded after deconvolution analysis. Dots correspond to 2 Gy/h and squares correspond to 30 Gy/h. Each data point corresponds to an average of two individually measured values. Error bars correspond to 1σ

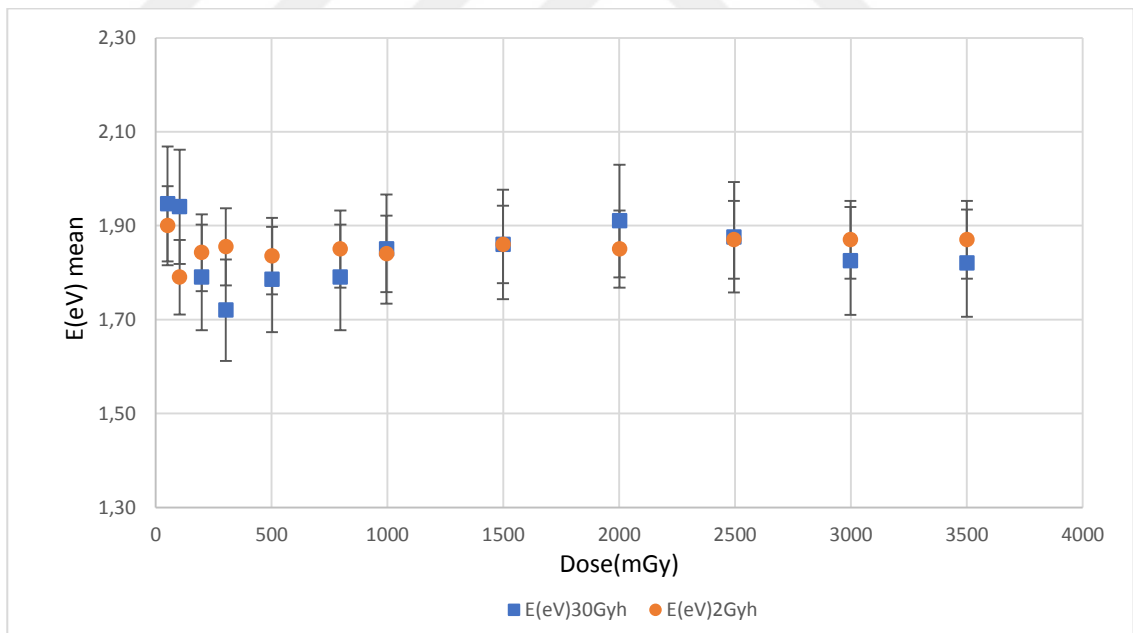


Figure 4.51 Activation energy, E , versus dose curves obtained for TL peak 5 of LiF: Mg,Ti (TLD 100); the E values were yielded after deconvolution analysis. Dots correspond to 2 Gy/h and squares correspond to 30 Gy/h. Each data point corresponds to an average of two individually measured values. Error bars correspond to 1σ

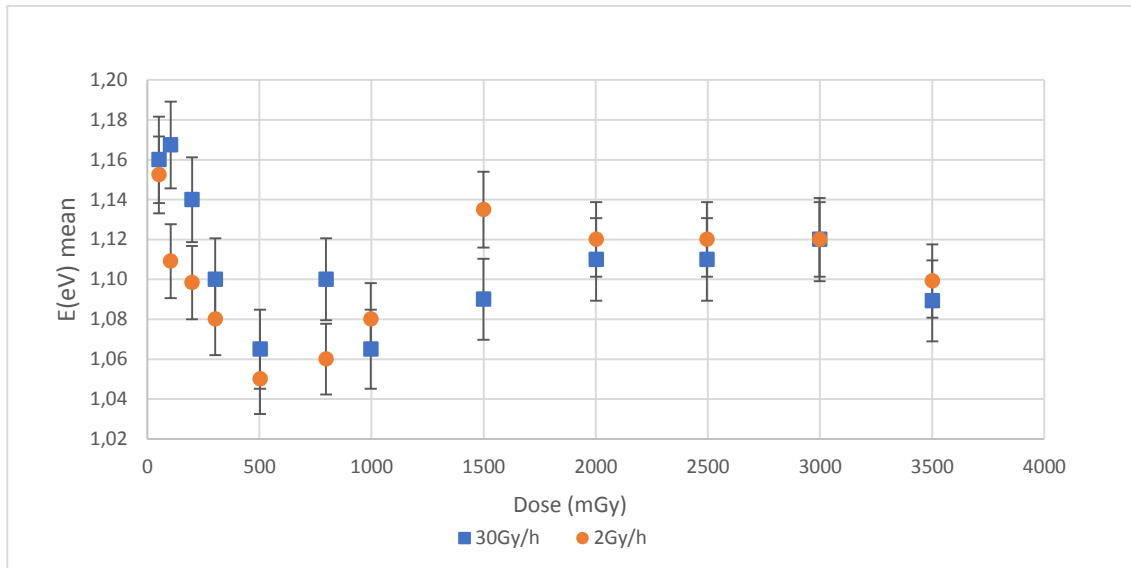


Figure 4.52 Activation energy, E , versus dose curves obtained for TL peak 1 of BeO; the E values were yielded after deconvolution analysis. Dots correspond to 2 Gy/h and squares correspond to 30 Gy/h. Each data point corresponds to an average of two individually measured values. Error bars correspond to 1σ

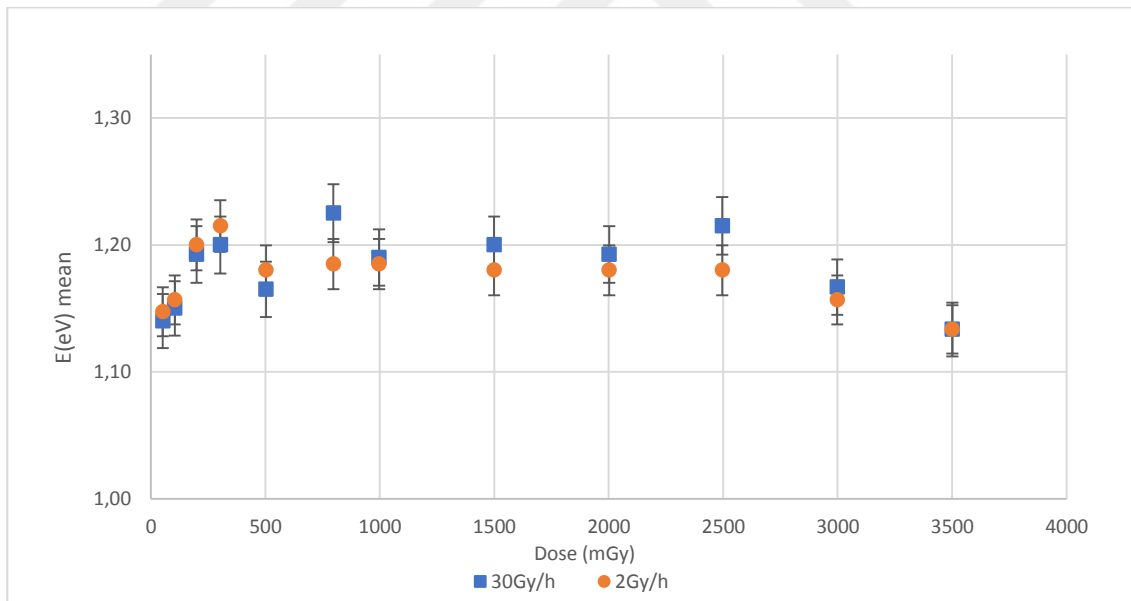


Figure 4.53 Activation energy, E , versus dose curves obtained for TL peak 2 of BeO; the E values were yielded after deconvolution analysis. Dots correspond to 2 Gy/h and squares correspond to 30 Gy/h. Each data point corresponds to an average of two individually measured values. Error bars correspond to 1σ

4.5 Dose Response Curves for OSL Components Following Deconvolution of OSL Decay Curves

For the case of OSL of BeO, the presence of two components of first order of kinetics was recently established by both Aşlar et al. (2019) as well as by Bulur et al. (2010; 2013). Finally, for the case of the OSL signal from quartz, the presence of three components was initially suggested by Bailey et al. (1997); this is the case throughout the voluminous quartz OSL literature (Bøtter-Jensen et al., 2003). Also the same terminology, namely fast, medium and slow components, was also adopted. It is important to note that the shape of the TL glow curves is not affected at all from the various dose rates. This is the case for all materials of the present study.

After deconvolution analyses of OSL decay curves of BeO and Quartz materials, c_i components were obtained from resolved OSL dose response curves. Figure 4.54 and 4.55 shows c_1 and c_2 components of BeO in two different dose rates at 12 dose steps. For BeO, c_1 is fast and c_2 is medium component. Each dose steps average of two individually measured values calculated and mean values used. Figure 4.56, 4.57 and 4.58 shows the Quartz' c_1 , c_2 and c_3 corresponding to fast, medium and slow components respectively values versus dose. Plots included, Quartz' c_1 , c_2 and c_3 components in three different dose rates and at different dose steps. Each dose steps average of two individually measured values calculated and mean values used. Axis are logarithmic and Errors are calculated at each dose steps.

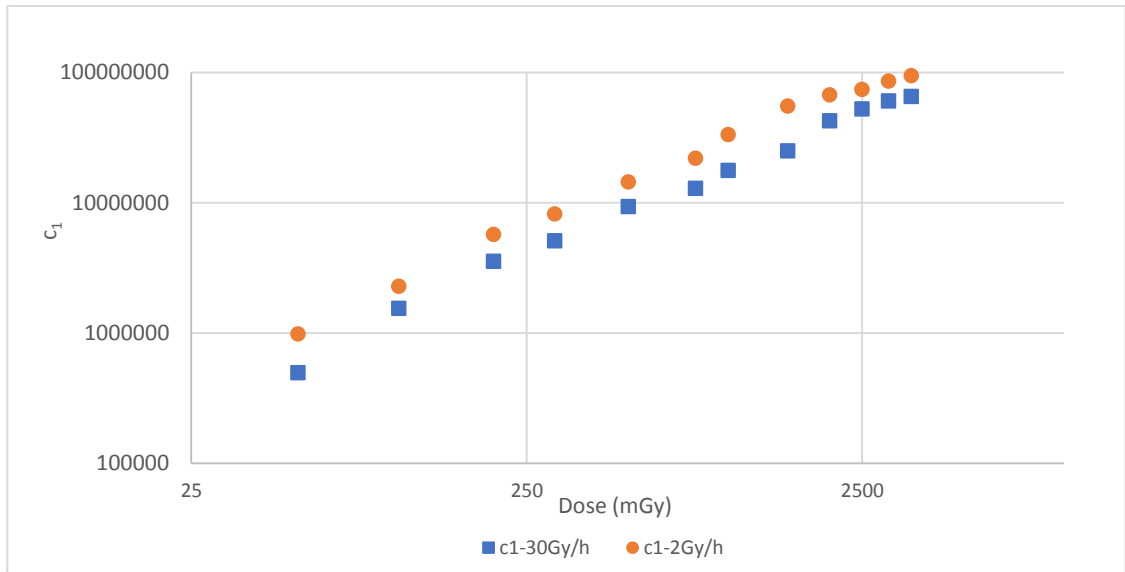


Figure 4.54 Component resolved OSL dose response curves obtained for OSL component c_1 of BeO. Dots correspond to 2 Gy/h and squares correspond to 30 Gy/h. Each data point corresponds to an average of two individually measured values. Error bars correspond to 1σ . (Errors are very small)(axis are logarithmic)

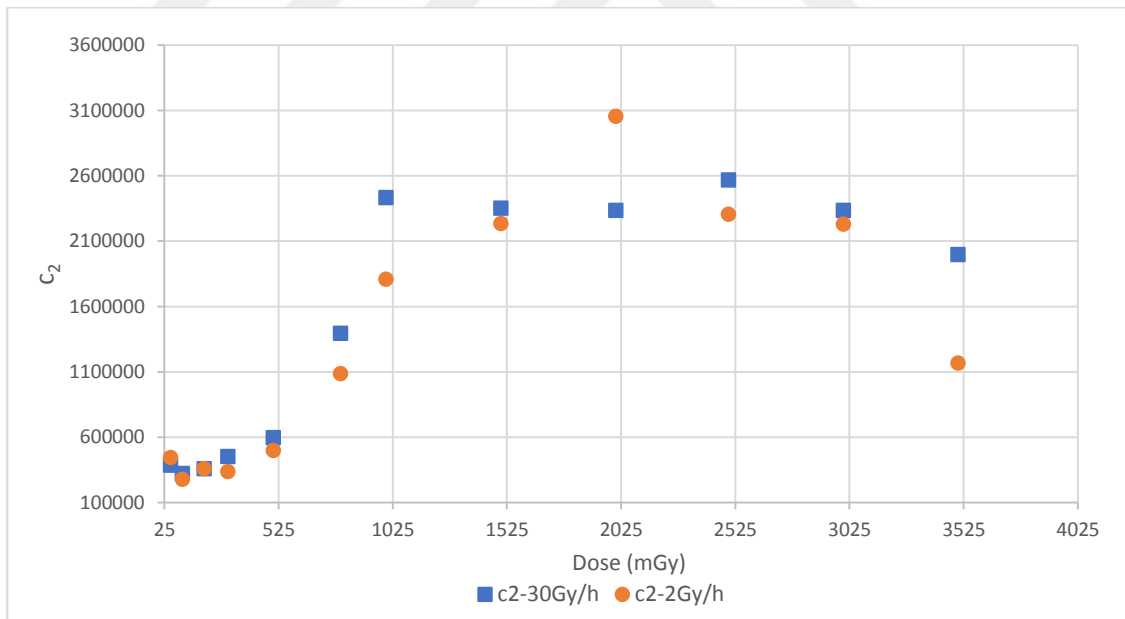


Figure 4.55 Component resolved OSL dose response curves obtained for OSL component c_2 of BeO. Dots correspond to 2 Gy/h and squares correspond to 30 Gy/h. Each data point corresponds to an average of two individually measured values. Error bars correspond to 1σ . (Errors are very small)(axis are logarithmic)

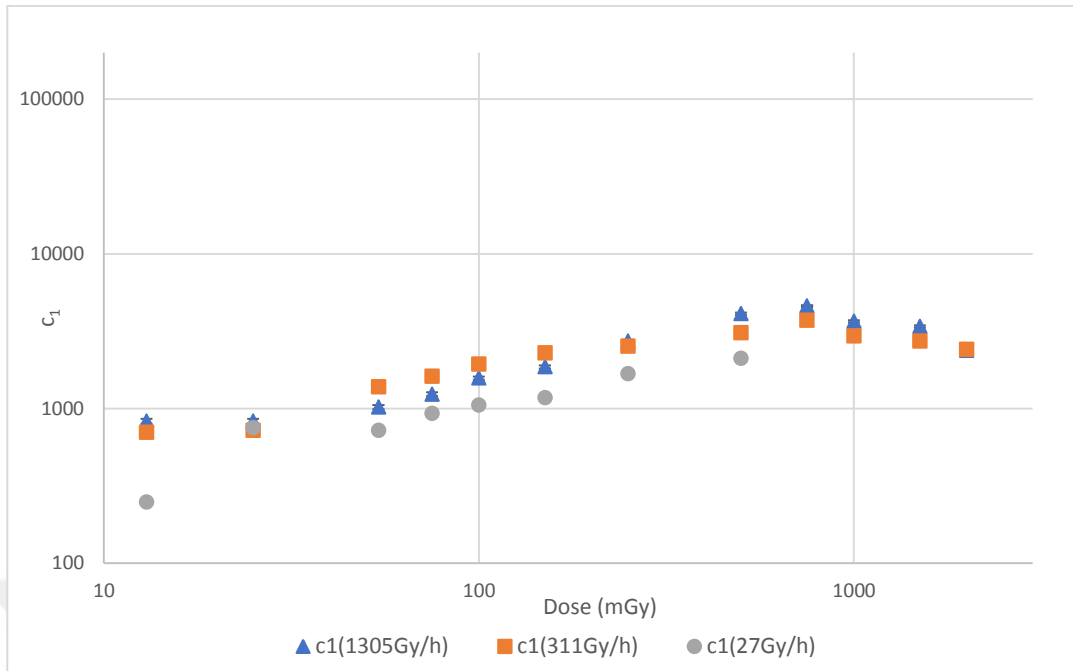


Figure 4.56 Component resolved OSL dose response curves obtained for OSL component c_1 of Quartz. Dots correspond to 27 Gy/h, squares correspond to 311 Gy/h and triangles correspond to 1305Gy/h. Each data point corresponds to an average of two individually measured values. Error bars correspond to 1σ . (Errors are very small)(axis are logarithmic)

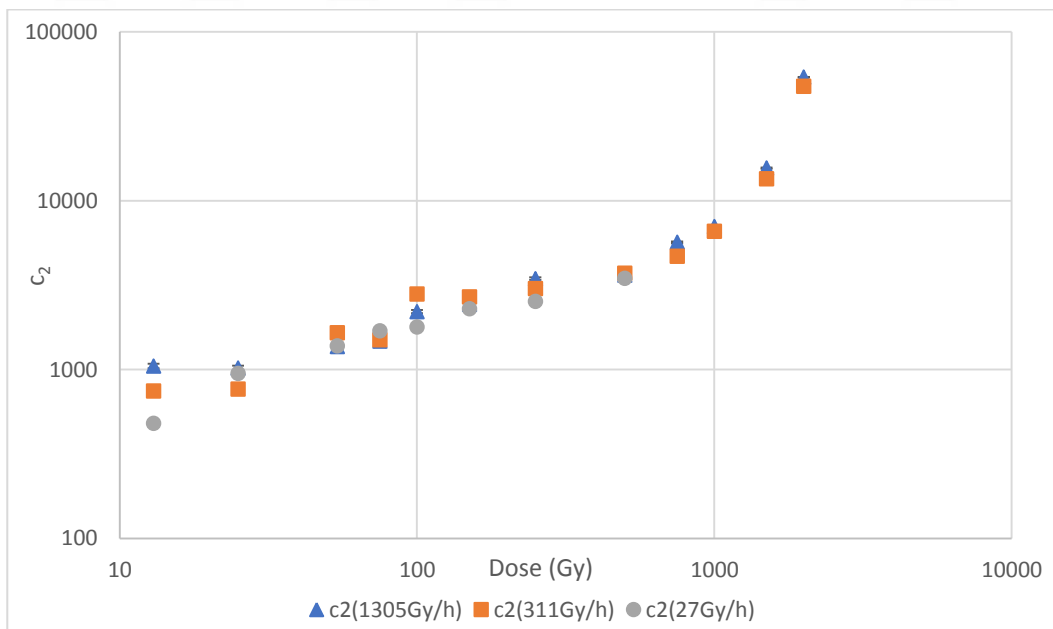


Figure 4.57 Component resolved OSL dose response curves obtained for OSL component c_2 of Quartz. Dots correspond to 27 Gy/h, squares correspond to 311 Gy/h and triangles correspond to 1305 Gy/h. Each data point corresponds to an average of two individually measured values. Error bars correspond to 1σ . (Errors are very small)(axis are logarithmic)

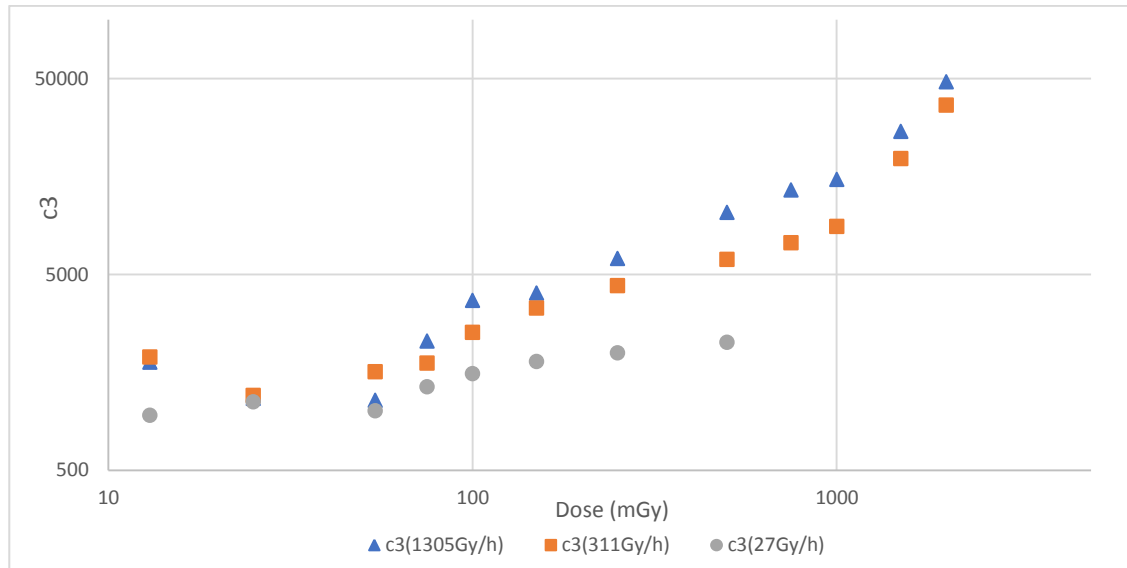


Figure 4.58 Component resolved OSL dose response curves obtained for OSL component c_3 of Quartz. Dots correspond to 27 Gy/h, squares correspond to 311 Gy/h and triangles correspond to 1305 Gy/h. Each data point corresponds to an average of two individually measured values. Error bars correspond to 1σ . (Errors are very small)(axis are logarithmic)

4.6 Kinetic Parameters of OSL Components Following Deconvolution of OSL Decay Curves

After deconvolution analyses of OSL decay curves of BeO and Quartz materials, another fitting parameter, namely the decay lifetime, τ , was obtained from resolved OSL dose response curves. This decay lifetime is directly related to the photo-ionization cross section of the corresponding OSL component. Figures 4.59 and 4.60 show lifetime components of BeO τ_1 and τ_2 in two different dose rates at 12 dose steps. For BeO, τ_1 is fast and τ_2 is medium lifetime components. Each dose steps average of two individually measured values calculated and mean values used. Figure 4.61, 4.62 and 4.63 show the Quartz' τ_1 , τ_2 , τ_3 values versus dose corresponding to fast, medium and slow components respectively values versus dose. Plots included, Quartz' τ_1 , τ_2 , τ_3 lifetime components in three different dose rates and at different dose steps. Each dose steps average of two individually measured values calculated and mean values used. Axis are logarithmic and errors are calculated at each dose steps.

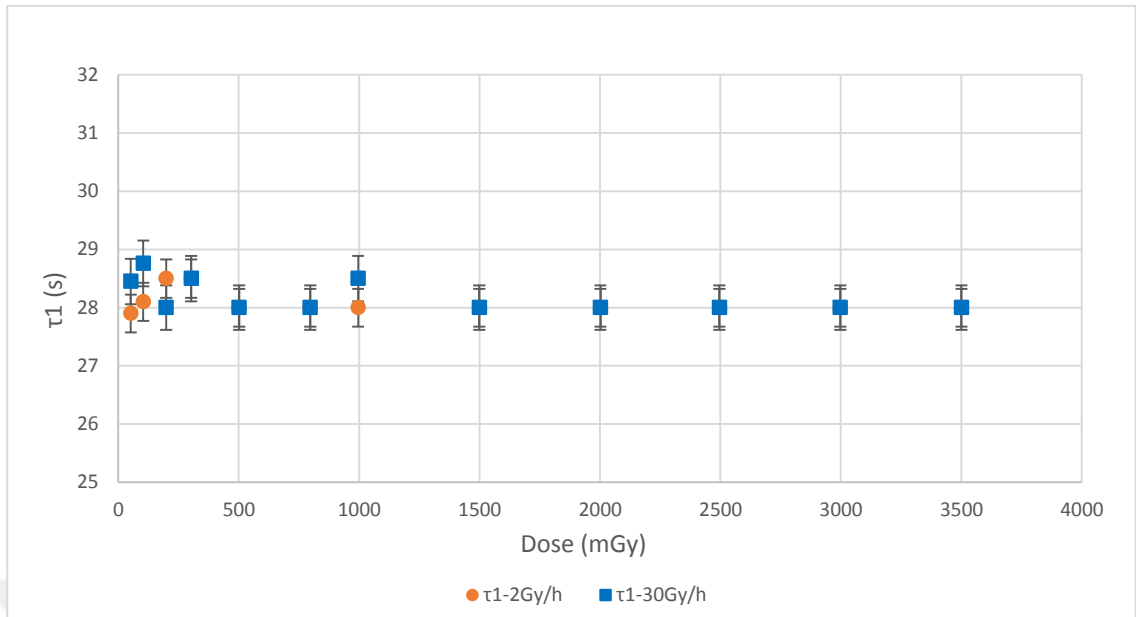


Figure 4.59 OSL component lifetime, τ , versus dose curves obtained for OSL component τ_1 of BeO; these τ values were yielded after deconvolution analysis. Dots correspond to 2 Gy/h and squares correspond to 30 Gy/h. Each data point corresponds to an average of two individually measured values. Error bars correspond to 1σ .

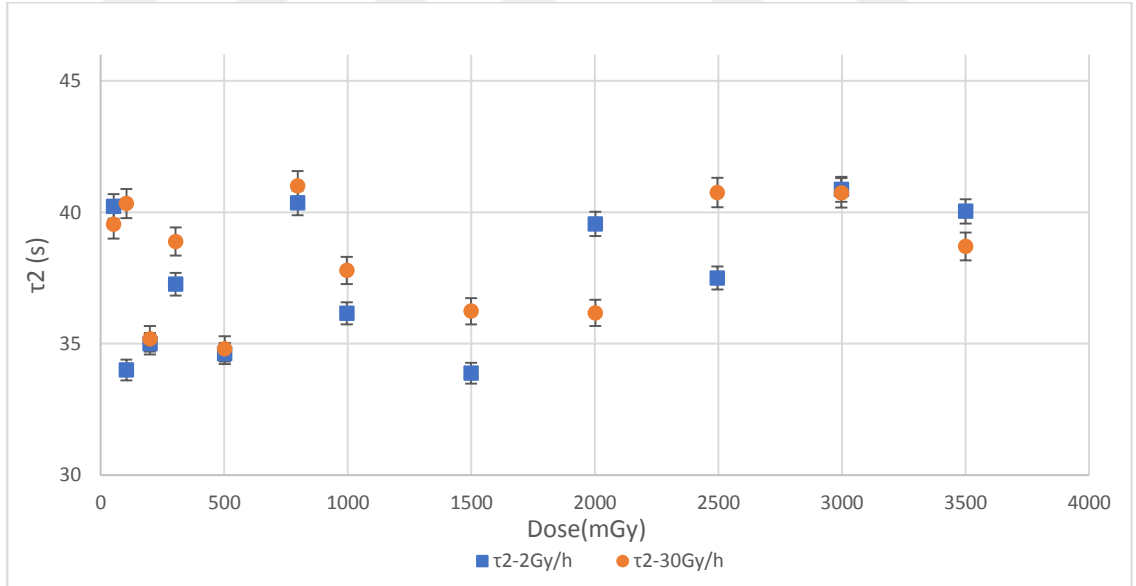


Figure 4.60 OSL component lifetime, τ , versus dose curves obtained for OSL component τ_2 of BeO; these τ values were yielded after deconvolution analysis. Dots correspond to 30 Gy/h and squares correspond to 2 Gy/h. Each data point corresponds to an average of two individually measured values. Error bars correspond to 1σ .

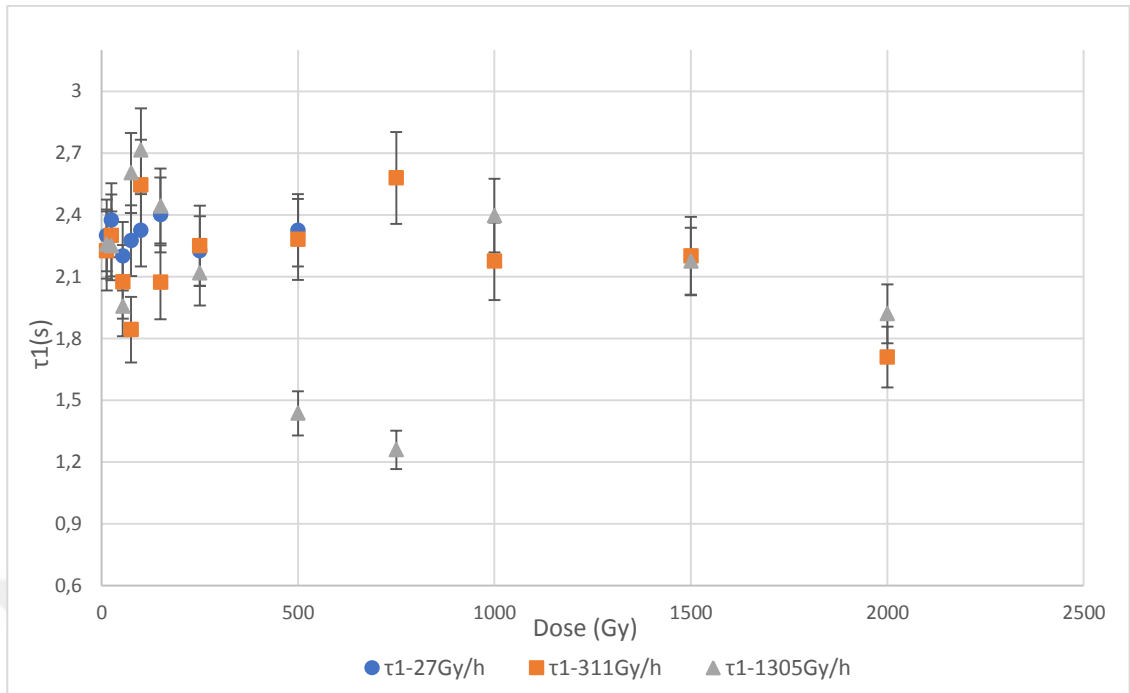


Figure 4.61 OSL component lifetime, τ , versus dose curves obtained for OSL component τ_1 of Quartz; these τ values were yielded after deconvolution analysis. Dots correspond to 27 Gy/h, squares correspond to 311 Gy/h and triangles correspond to 1305 Gy/h. Each data point corresponds to an average of two individually measured values. Error bars correspond to 1σ

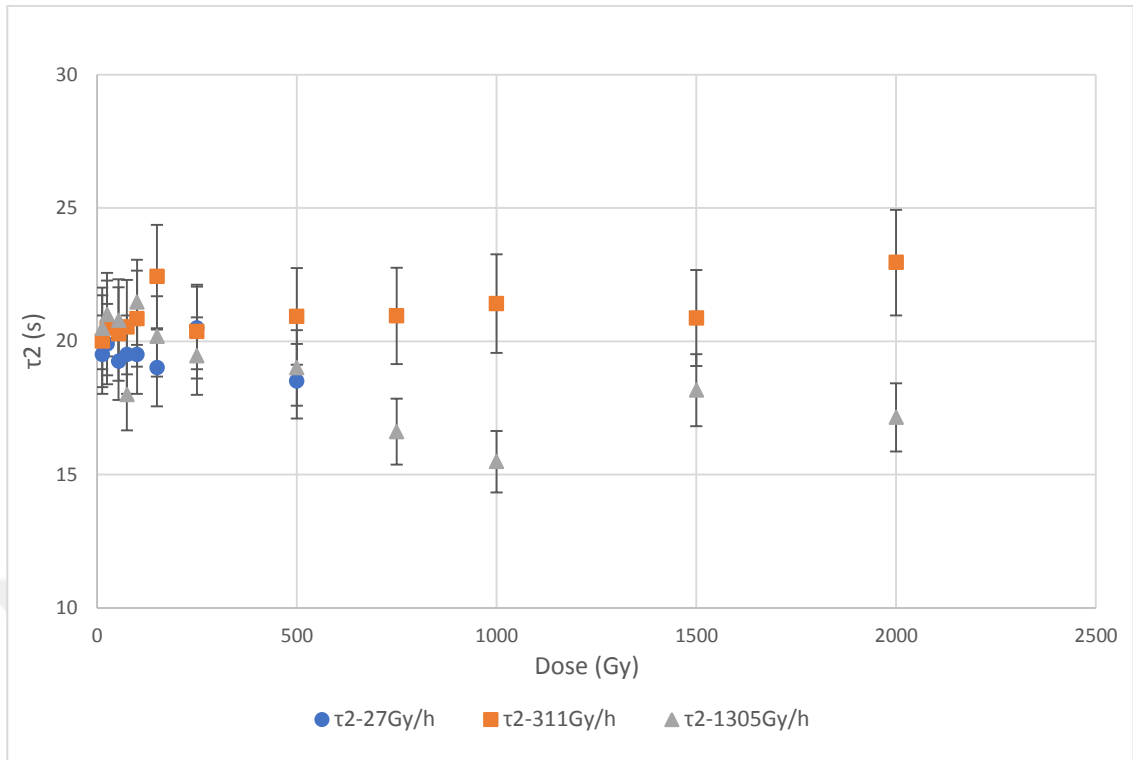


Figure 4.62 OSL component lifetime, τ , versus dose curves obtained for OSL component τ_2 of Quartz; these τ values were yielded after deconvolution analysis. Dots correspond to 27 Gy/h, squares correspond to 311 Gy/h and triangles correspond to 1305 Gy/h. Each data point corresponds to an average of two individually measured values. Error bars correspond to 1σ

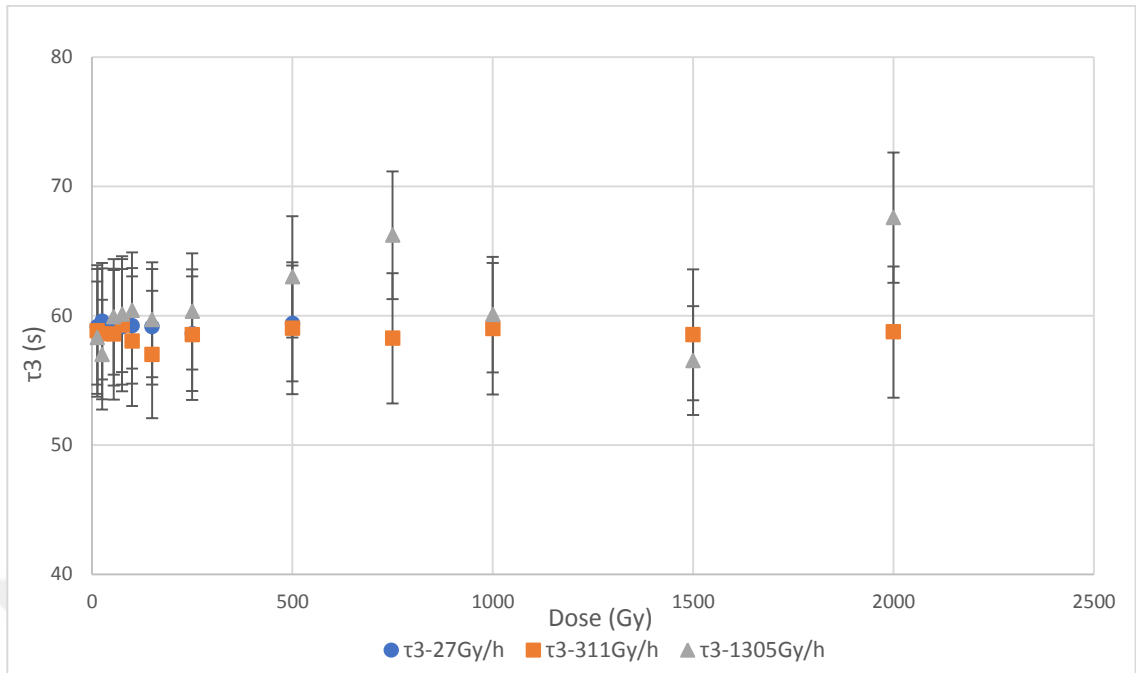


Figure 4.63 OSL component lifetime, τ , versus dose curves obtained for OSL component τ_3 of Quartz; these τ values were yielded after deconvolution analysis. Dots correspond to 27 Gy/h, squares correspond to 311 Gy/h and triangles correspond to 1305 Gy/h. Each data point corresponds to an average of two individually measured values. Error bars correspond to 1σ .

5. DISCUSSION

At first, it is important to note that for each dose of each dose rate, two different measurements were performed. Therefore, as the measurement procedure includes multiple discs/aliquots, reproducibility is quite an important issue in the framework of the present study. Reproducibility was achieved using: (a) a normalization factor based on a measurement following the same test dose for all artificial materials-dosimeters and (b) mass measurement for the case of naturally occurring quartz. For both cases, reproducibility was excellent, further supporting thus the trustworthy results. Deconvolution analysis of both OSL and TL signals was mandatory, as both signals are composed of multi components. It is the appropriate time to point out that between the irradiation and the TL/OSL measurements, specific time intervals have been elapsed. However, these time intervals do not exceed 1 week. Therefore, the stable dosimetric signals are not influenced at all by this waiting. For the case of TL, only the dose response of the stable TL peaks has been studied. This stability has been established based on the deconvolution results. For the case of the OSL signals from either BeO or quartz, a preheat has been used in order to specifically elapse any unstable remaining signal.

Table 5.1 presents the dose response features for all materials of the present study, namely the linearity index k as well as the lowest detectable dose limit (LDDL) for each peak/component of each signal (TL or OSL). These features were calculated according to the methodology presented by Kaya-Keles et al. (2019). In dosimetric studies, when the dose response curve is examined, there is a dose value where the corresponding signal intensity starts increasing is called lowest detectable dose limit. LDDL is observed after a certain dose level is exceeded. When the LDDL value is exceeded, the dose response curve begins to rise to saturation, indicating that traps are full. The region where is in the dose response curve between the LDDL and the saturation value is very important for dosimetric studies. According to Halperin and Chen (1966) the dose dependence with TL method can be described by the equation 5.1.

$$I \sim \alpha D^k \tag{5.1}$$

where α is a proportionality coefficient and k is a constant which indicates the linearity of the curve (Nikiforov et al 2017). k is an expression from the region between LDDL and saturation level. k gives information about dose linearity features of the material. The ideal case of $k = 1$ is observed in linear dose responses of the material. $k > 1$ shows that the increase is supra-linear and $k < 1$, means that the dose response curve behavior is sub-linear. For the linear dose response of the material if $k = 1$ this is the ideal case. (Halperin and Chen 1966, Chen and Leung 2001). Ideal case is the most wanted situation of the dosimetric materials, but most of the dosimetric materials, especially in natural occurring, dose response curve behavior different from linearity (Nikiforov et al 2017). To determine the dose response curve behaviors and to compare them each other, the k values, calculated in Microsoft Excel software package using with the solver utility, is used for to compare the dose response curve behaviors of the de-convolved TL peaks and OSL components, these values were presented in Table 5.1

Table 5.1 Dose response curve behaviours of the de-convolved TL peaks and OSL components

Dosimeter	TL/OSL	Peak/component	Dose rate (Gy/h)	k	k-range (mGy)	LDDL (mGy)	D _E according to 5.2 (mGy)	D ₀ according to 5.2 (mGy)
LiF: Mg,Ti	TL	Peak 4	2	1.085	50 - 3500	15.00	-	-
LiF: Mg,Ti	TL	Peak 4	31	1.098	50 - 3500	18.50	-	-
LiF: Mg,Ti	TL	Peak 5	2	1.011	50 - 3500	0.091	-	-
LiF: Mg,Ti	TL	Peak 5	31	1.098	50 - 3500	0.072	-	-
Li ₂ B ₄ O ₇ :Cu,In	TL	Peak 4	2	0.985	50 - 3500	10.50	-	-
Li ₂ B ₄ O ₇ :Cu,In	TL	Peak 4	31	0.956	50 - 3500	33.70	-	-
Li ₂ B ₄ O ₇ :Cu,In	TL	Peak 5	2	0.969	50 - 2500	0.015	0.255	35000
Li ₂ B ₄ O ₇ :Cu,In	TL	Peak 5	31	1.052	50 - 3000	0.172	0.320	49000
MgB ₄ O ₇ :Dy, Na	TL	Entire TL signal	2	0.995	50 - 3500	2.50	-	-
MgB ₄ O ₇ :Dy, Na	TL	Entire TL signal	31	0.973	50 - 3500	14.70	-	-
CaF ₂ :Dy	TL	Peak 4	2	1.042	50 - 3500	0.150	-	-
CaF ₂ :Dy	TL	Peak 4	31	1.102	50 - 3500	0.225	-	-
CaF ₂ :Dy	TL	Peak 5	2	1.056	50 - 3500	0.095	-	-

Table 5.1 Dose response curve behaviours of the de-convolved TL peaks and OSL components (continued)

Dosimeter	TL/OSL	Peak/component	Dose rate (Gy/hr)	k	k-range (mGy)	LDDL (mGy)	D _E according to 5.2 (mGy)	D ₀ according to 5.2 (mGy)
CaF ₂ :Dy	TL	Peak 5	31	0.859	50 - 3500	88.55	-	-
BeO	TL	Peak 1	2	1.681	50 - 3500	1.70	-	-
BeO	TL	Peak 1	31	1.762	50 - 3500	4.30	-	-
BeO	TL	Peak 2	2	0.987	50 - 3500	12.50	-	-
BeO	TL	Peak 2	31	0.978	50 - 3500	17.80	-	-
BeO	OSL	Component 1	2	1.312	50 - 3500	0.73	-	-
BeO	OSL	Component 1	31	1.443	50 - 3500	1.05	-	-
BeO	OSL	Component 2	2	1.088	200 - 1500	38	58	1370
BeO	OSL	Component 2	31	1.198	200 - 1500	65	67	1295
Quartz	OSL	Component 1 (fast)	27	-	13 - 2000	-	13.50	184.70
Quartz	OSL	Component 1 (fast)	311	-	13 - 2000	-	12.80	208.90
Quartz	OSL	Component 1 (fast)	1305	-	13 - 2000	-	13.20	195.75
Quartz	OSL	Component 2 (medium)	27	0.499	75-2000	45	-	-
Quartz	OSL	Component 2 (medium)	311	0.543	75-2000	50	-	-
Quartz	OSL	Component 2 (medium)	1305	0.569	75-2000	53	-	-
Quartz	OSL	Component 3 (slow)	27	-	13 - 2000	-	28.20	325.50
Quartz	OSL	Component 3 (slow)	311	-	13 - 2000	-	51.20	525.50
Quartz	OSL	Component 3 (slow)	1305	-	13 - 2000	-	39.50	595.50

Figures, between Figure 5.1 and 5.9 shows the difference between the τ_1, τ_2, τ_3 lifetime $\Delta\tau_i$ component values of Quartz at different dose rates. Each figure included different dose rate combination and τ_i component. Figure 5.10 shows $\Delta\tau_1$ differences between 2Gy/h and 30 Gy/h, Figure 5.11 shows $\Delta\tau_2$ differences between 2Gy/h and 30 Gy/h

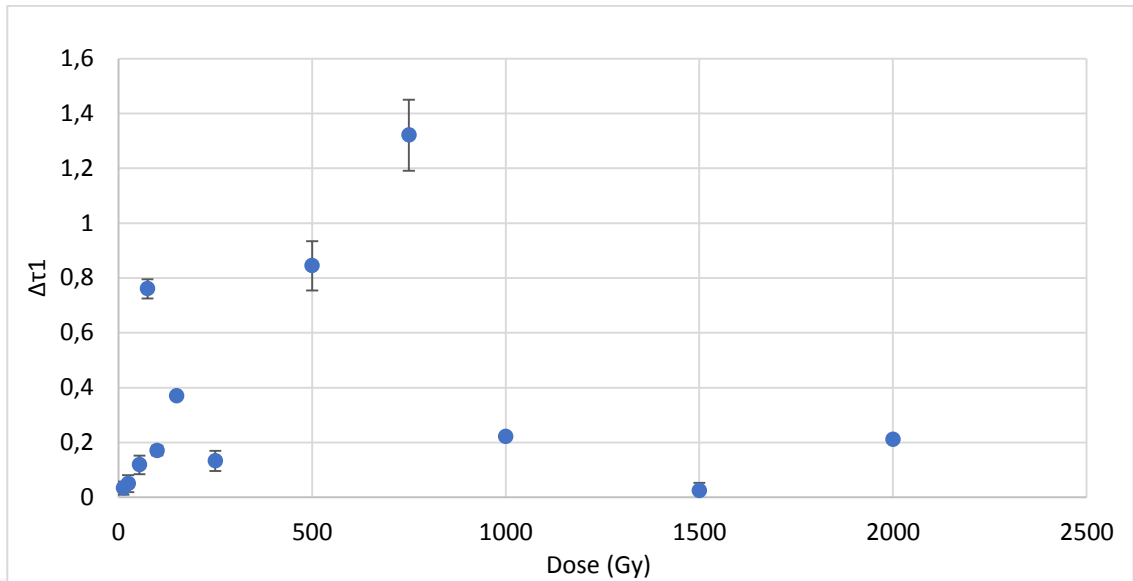


Figure 5.1 OSL component lifetime differences, $\Delta\tau$, versus dose curves obtained for OSL component τ_1 of Quartz. The differences were calculated for the dose rates 1305 Gy/h and 311 Gy/h Error bars correspond to 1σ . (Errors are small)

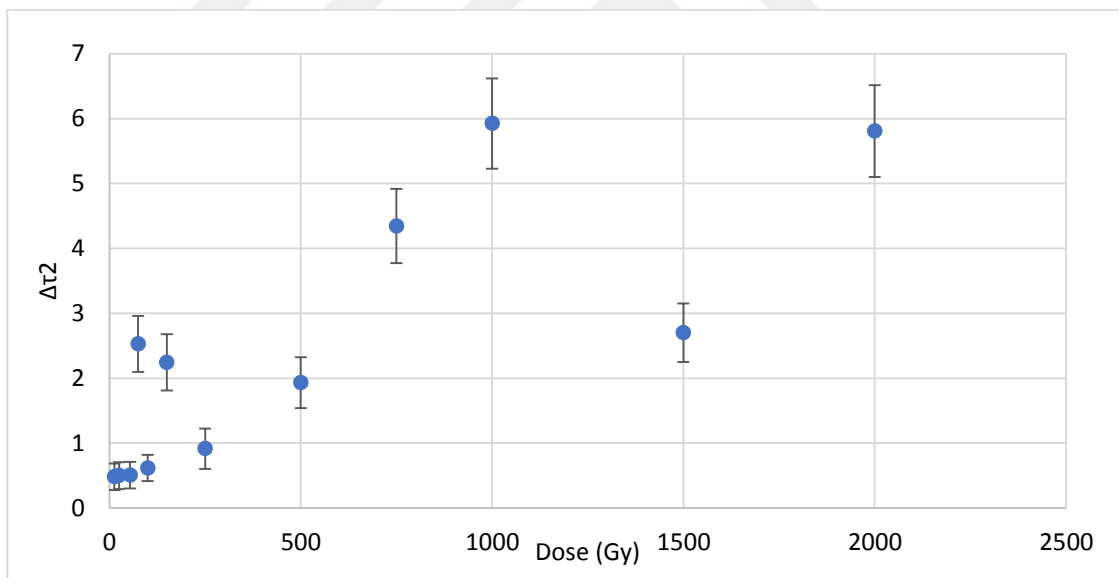


Figure 5.2 OSL component lifetime differences, $\Delta\tau$, versus dose curves obtained for OSL component τ_2 of Quartz. The differences were calculated for the dose rates 1305Gy/h and 311 Gy/h. Error bars correspond to 1σ .

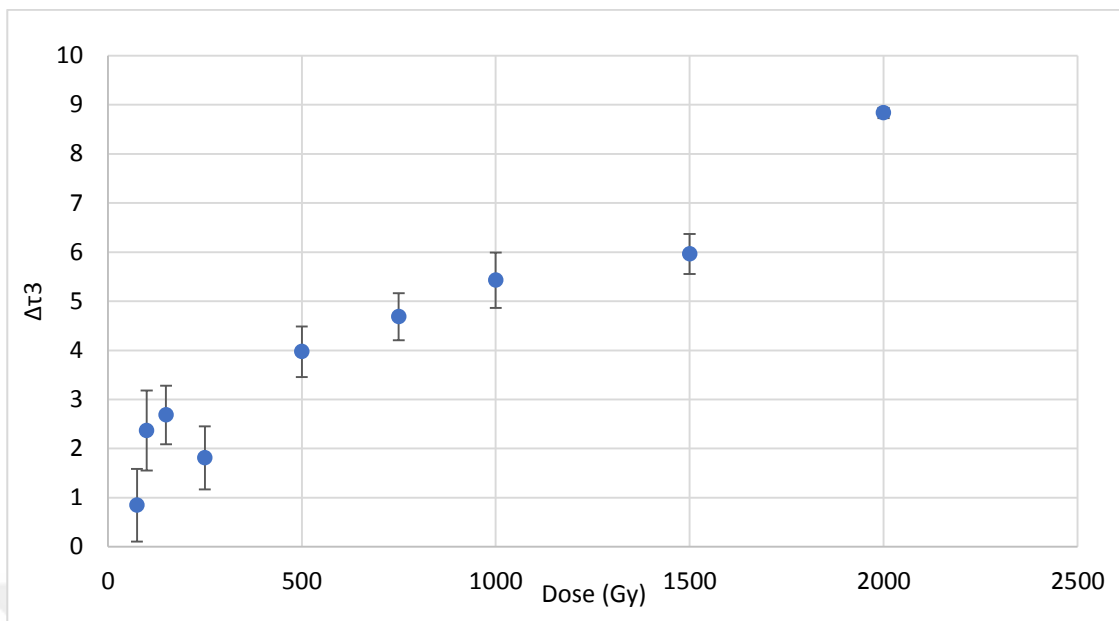


Figure 5.3 OSL component lifetime differences, $\Delta\tau$, versus dose curves obtained for OSL component τ_3 of Quartz. The differences were calculated for the dose rates 1305Gy/h and 311 Gy/h. Error bars correspond to 1σ .

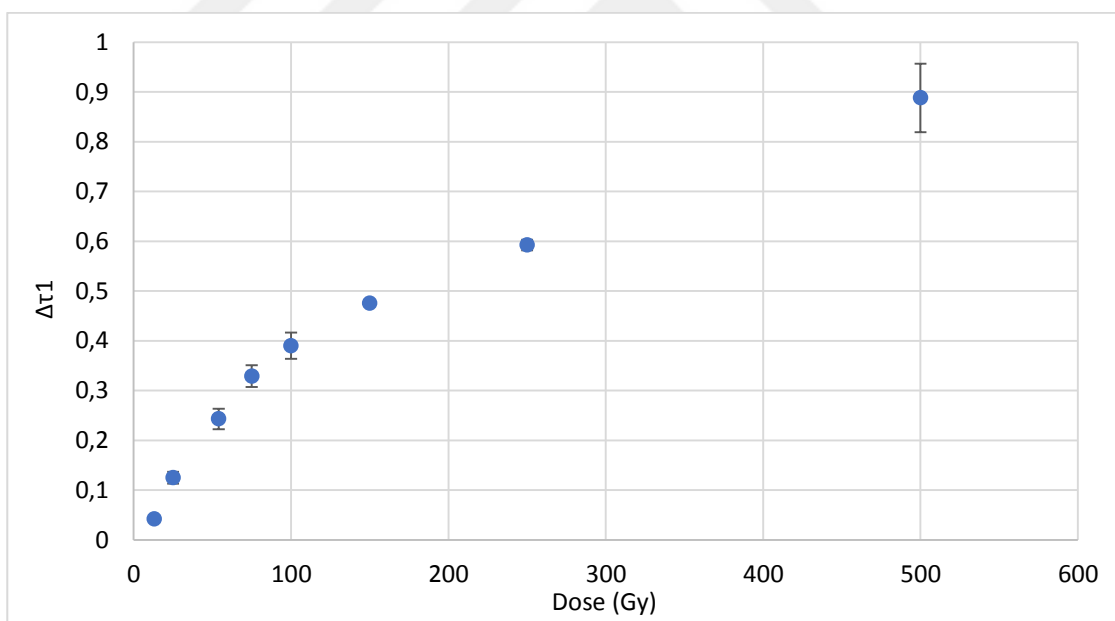


Figure 5.4 OSL component lifetime differences, $\Delta\tau$, versus dose curves obtained for OSL component τ_1 of Quartz. The differences were calculated for the dose rates 1305 Gy/h and 27 Gy/h. Error bars correspond to 1σ . (Errors are small)

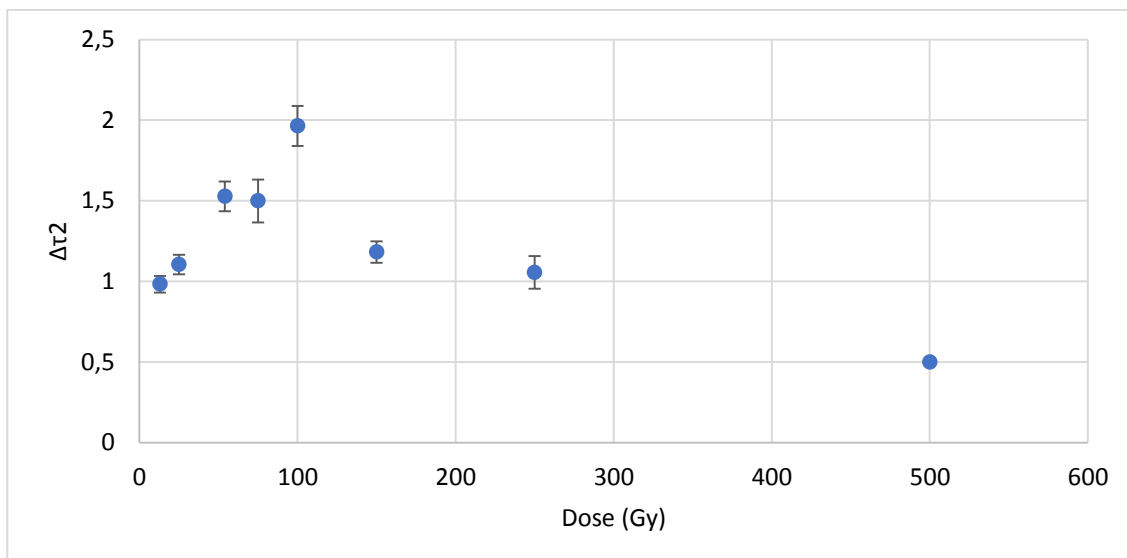


Figure 5.5 OSL component lifetime differences, $\Delta\tau$, versus dose curves obtained for OSL component τ_2 of Quartz. The differences were calculated for the dose rates 1305 Gy/h and 27 Gy/h. Error bars correspond to 1σ .

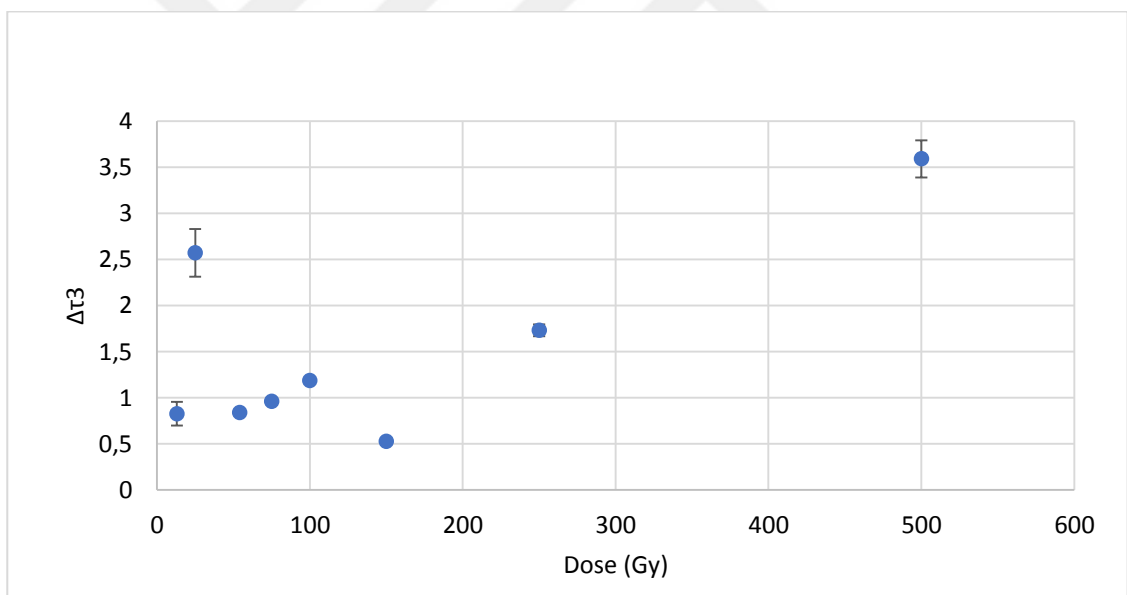


Figure 5.6 OSL component lifetime differences, $\Delta\tau$, versus dose curves obtained for OSL component τ_3 of Quartz. The differences were calculated for the dose rates 1305 Gy/h and 27 Gy/h. Error bars correspond to 1σ . (Errors are small)

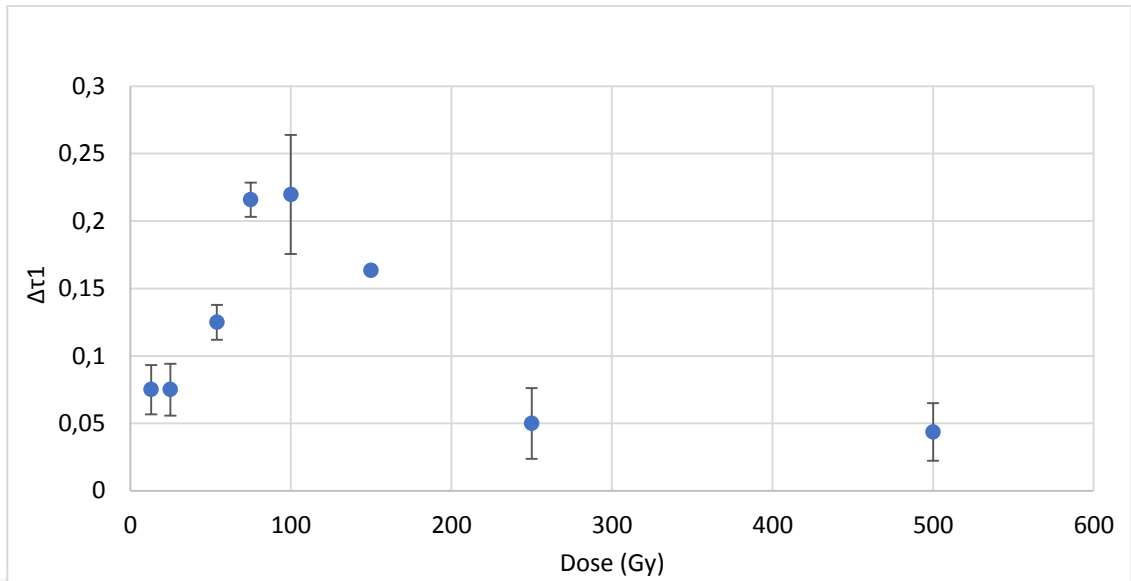


Figure 5.7 OSL component lifetime differences, $\Delta\tau$, versus dose curves obtained for OSL component τ_1 of Quartz. The differences were calculated for the dose rates 311 Gy/h and 27 Gy/h. Error bars correspond to 1σ .

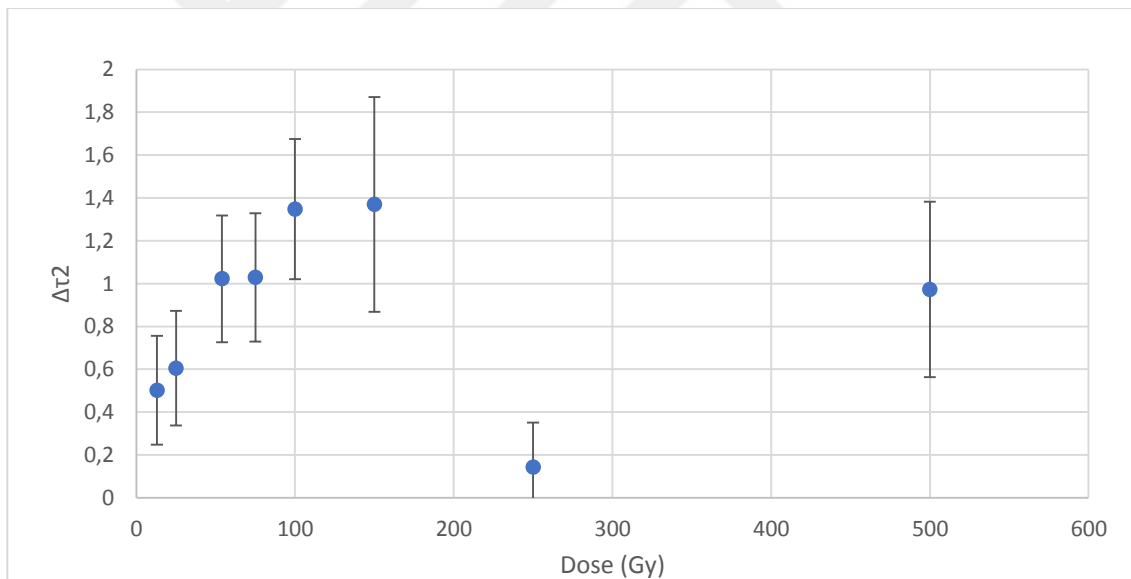


Figure 5.8 OSL component lifetime differences, $\Delta\tau$, versus dose curves obtained for OSL component τ_2 of Quartz. The differences were calculated for the dose rates 311 Gy/h and 27 Gy/h. Error bars correspond to 1σ .

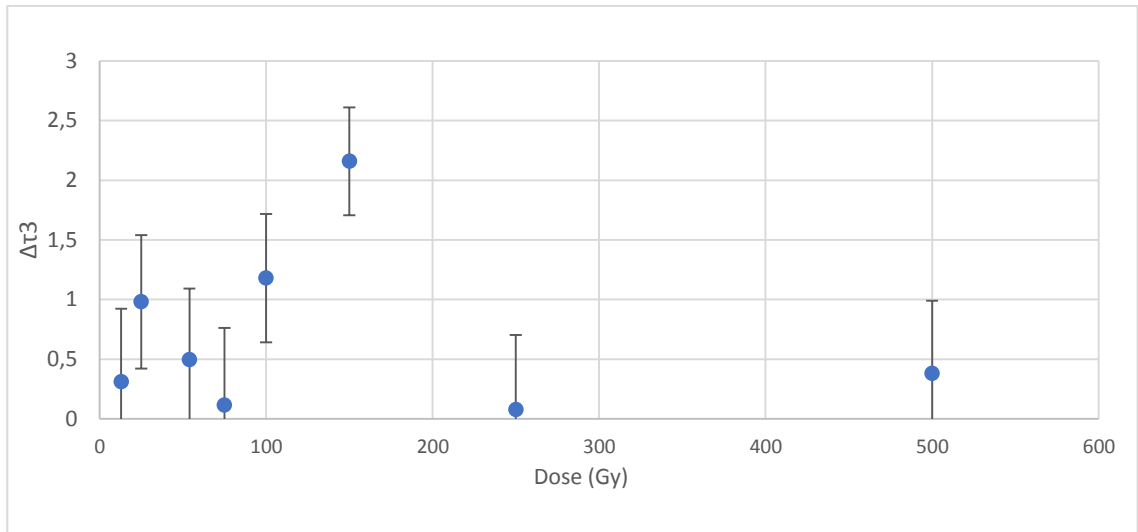


Figure 5.9 OSL component lifetime differences, $\Delta\tau$, versus dose curves obtained for OSL component τ_3 of Quartz. The differences were calculated for the dose rates 311 Gy/h and 27 Gy/h. Error bars correspond to 1σ .

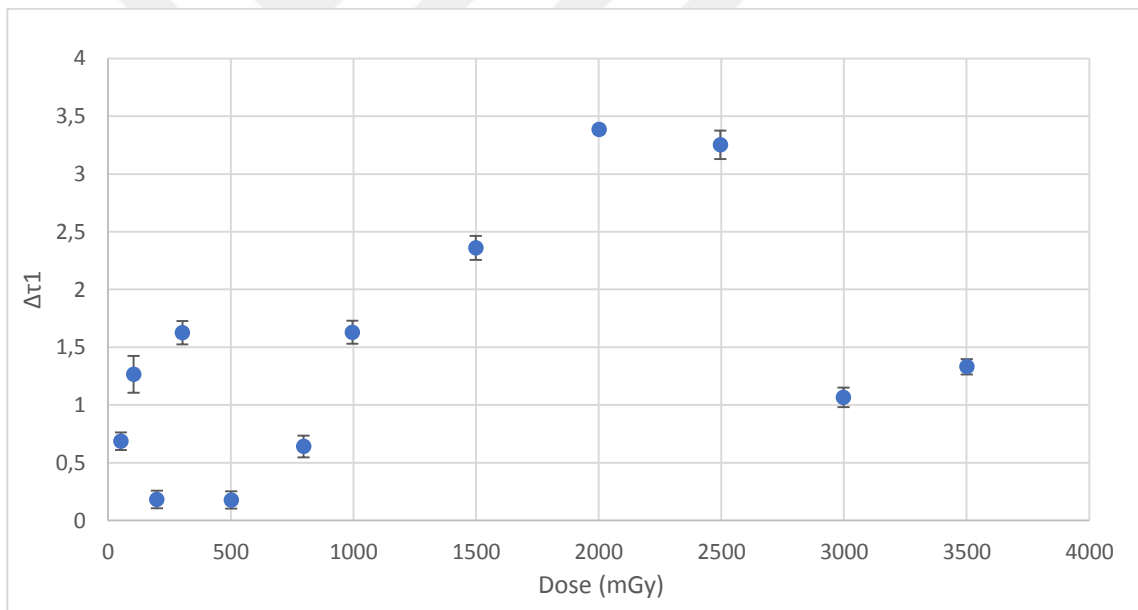


Figure 5.10 OSL component lifetime differences, $\Delta\tau$, versus dose curves obtained for OSL component τ_1 of BeO. The differences were calculated for the dose rates 30 Gy/h and 2 Gy/h. Error bars correspond to 1σ .

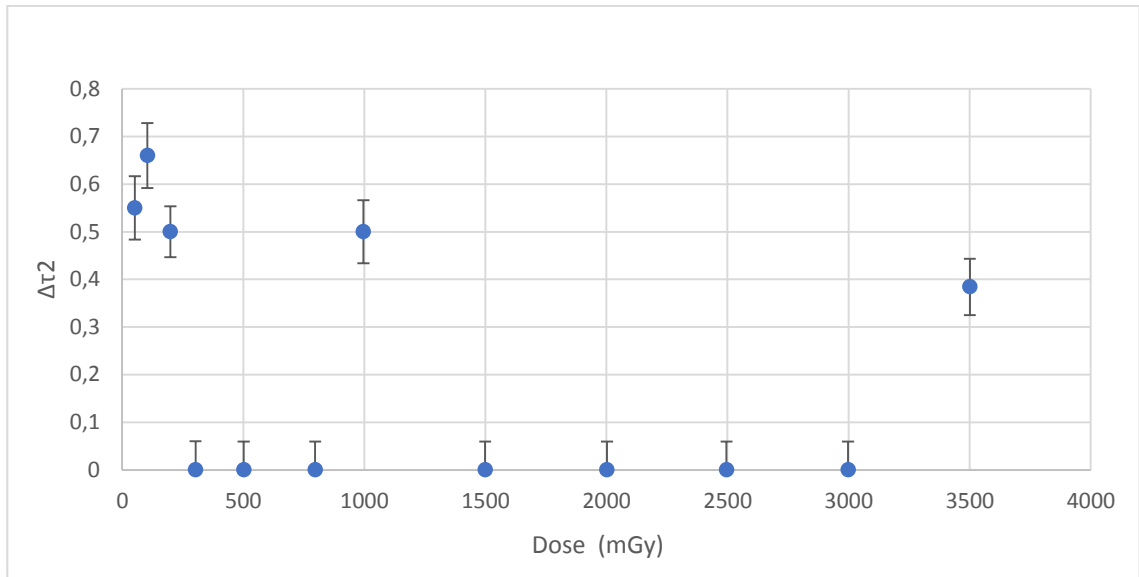


Figure 5.11 OSL component lifetime differences, $\Delta\tau$, versus dose curves obtained for OSL component τ_2 of BeO. The differences were calculated for the dose rates 30 Gy/h and 2 Gy/h. Error bars correspond to 1σ .

Figures, between Figure 5.12 and 5.20 shows the OSL component integrated intensity differences, ΔI_{ci} , versus dose curves obtained for OSL component c_1, c_2 and c_3 of values of Quartz at different dose rates. Each figure included different dose rate combination and c_i component. Figure 5.21 shows c_1 differences between 2Gy/h and 30 Gy/h, Figure 5.11 shows c_2 differences between 2Gy/h and 30 Gy/h.

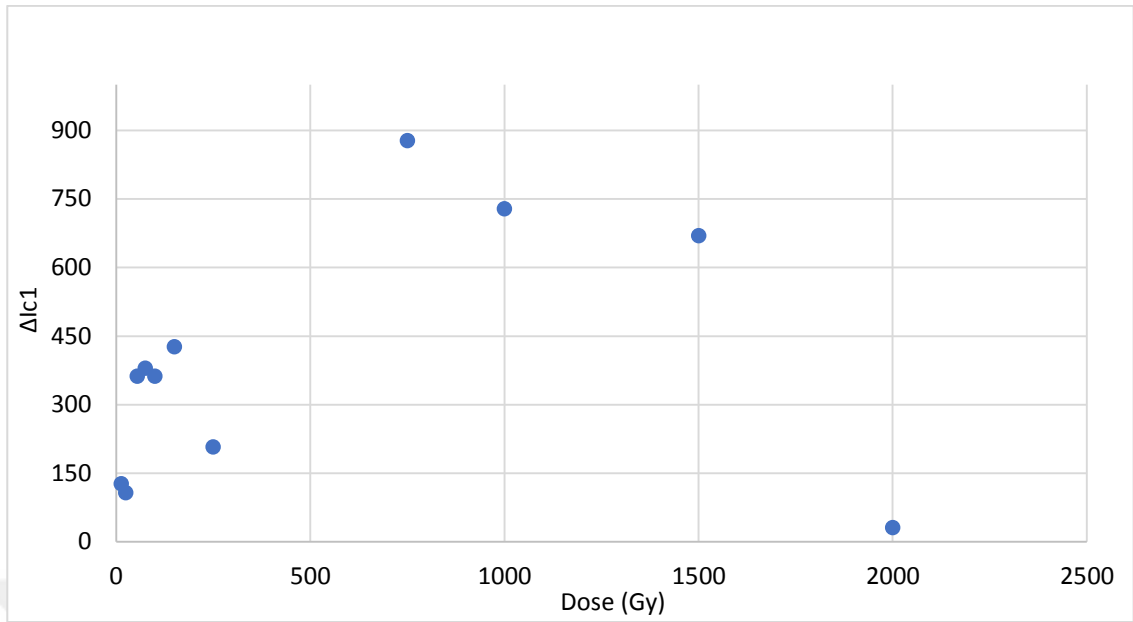


Figure 5.12 OSL component integrated intensity differences, ΔI_{c1} , versus dose curves obtained for OSL component c_1 of Quartz. The differences were calculated for the dose rates 1305 Gy/h and 311 Gy/h. Error bars correspond to 1σ . (Errors are very small)

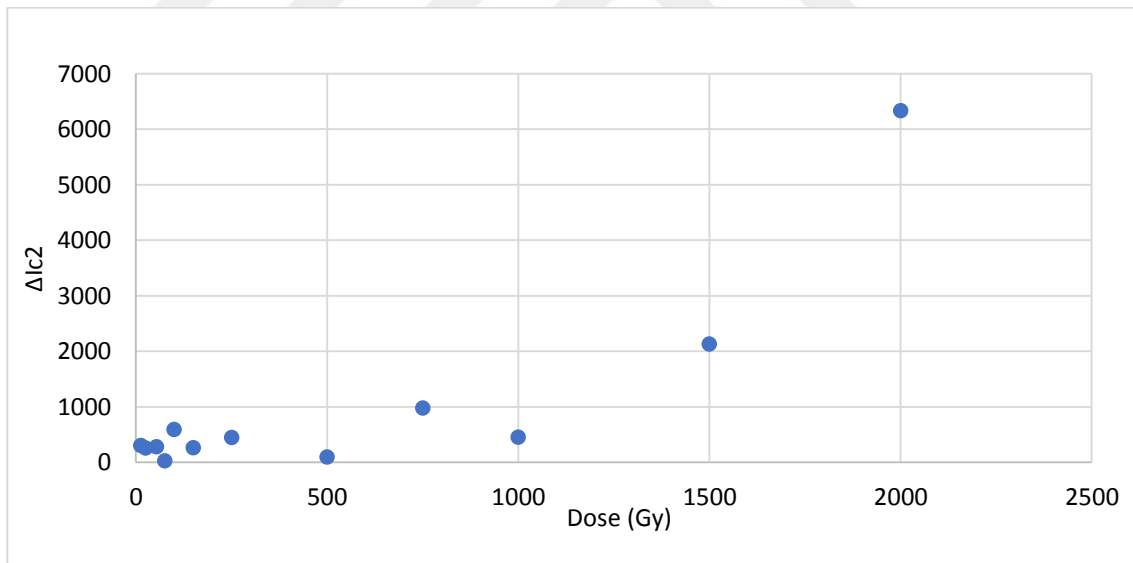


Figure 5.13 OSL component integrated intensity differences, ΔI_{c2} , versus dose curves obtained for OSL component c_2 of Quartz. The differences were calculated for the dose rates 1305 Gy/h and 311 Gy/h. Error bars correspond to 1σ . (Errors are very small)

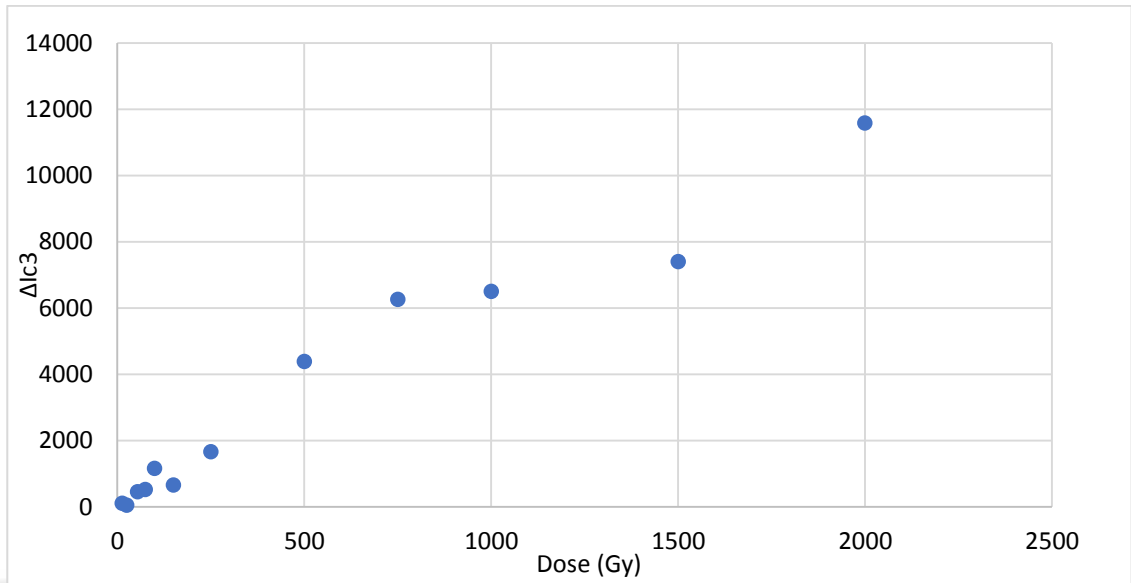


Figure 5.14 OSL component integrated intensity differences, ΔI_{c_i} , versus dose curves obtained for OSL component c_3 of Quartz. The differences were calculated for the dose rates 1305 Gy/h and 311 Gy/h. Error bars correspond to 1σ . (Errors are very small)

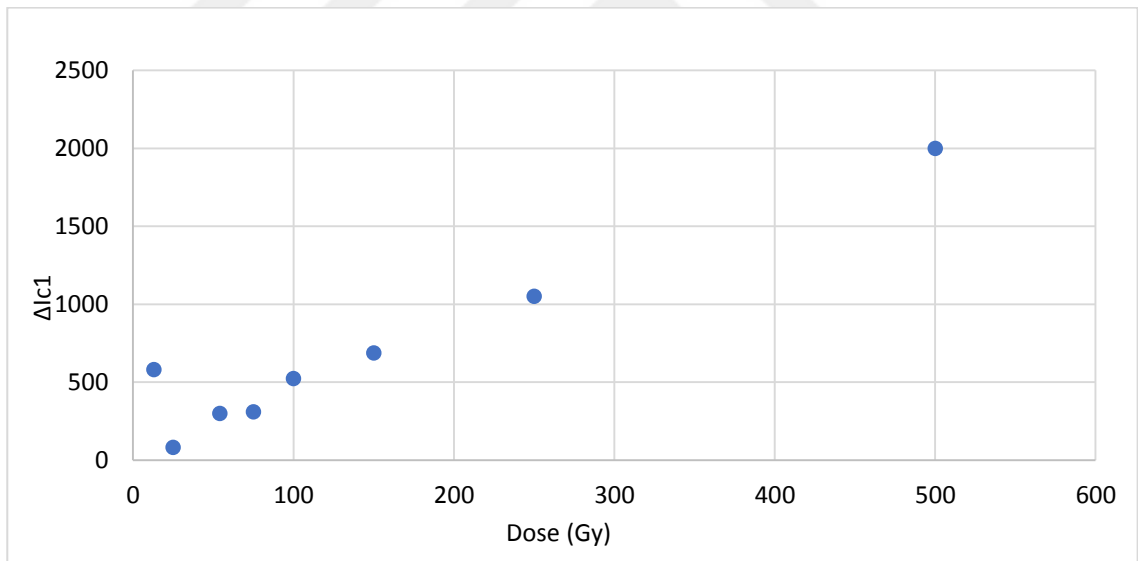


Figure 5.15 OSL component integrated intensity differences, ΔI_{c_i} , versus dose curves obtained for OSL component c_1 of Quartz. The differences were calculated for the dose rates 1305 Gy/h and 27 Gy/h. Error bars correspond to 1σ . (Errors are very small)

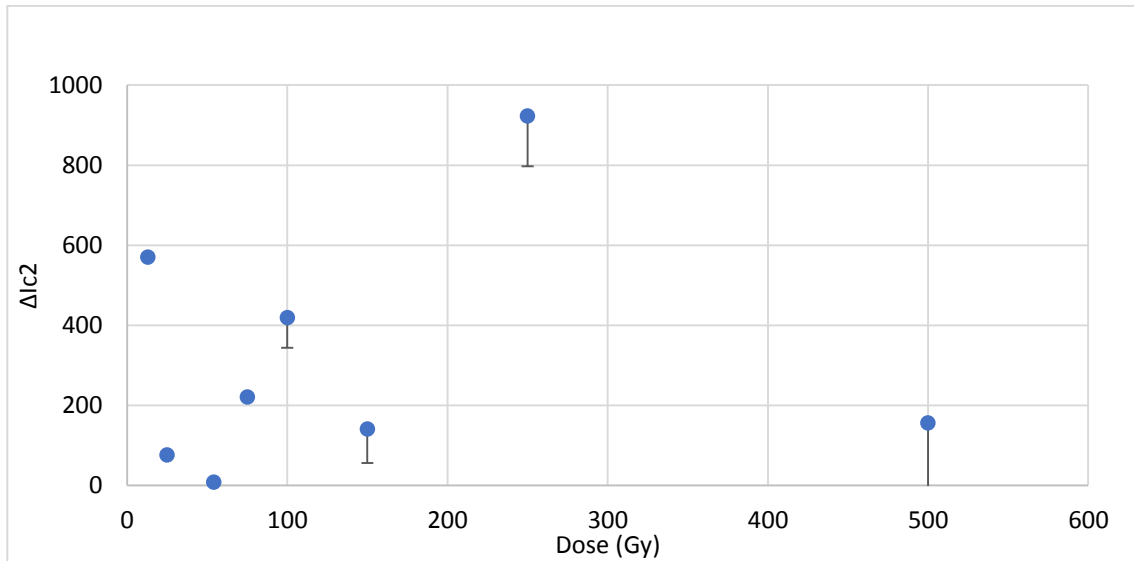


Figure 5.16 OSL component integrated intensity differences, ΔI_{c_i} , versus dose curves obtained for OSL component c_2 of Quartz. The differences were calculated for the dose rates 1305 Gy/h and 27 Gy/h. Error bars correspond to 1σ

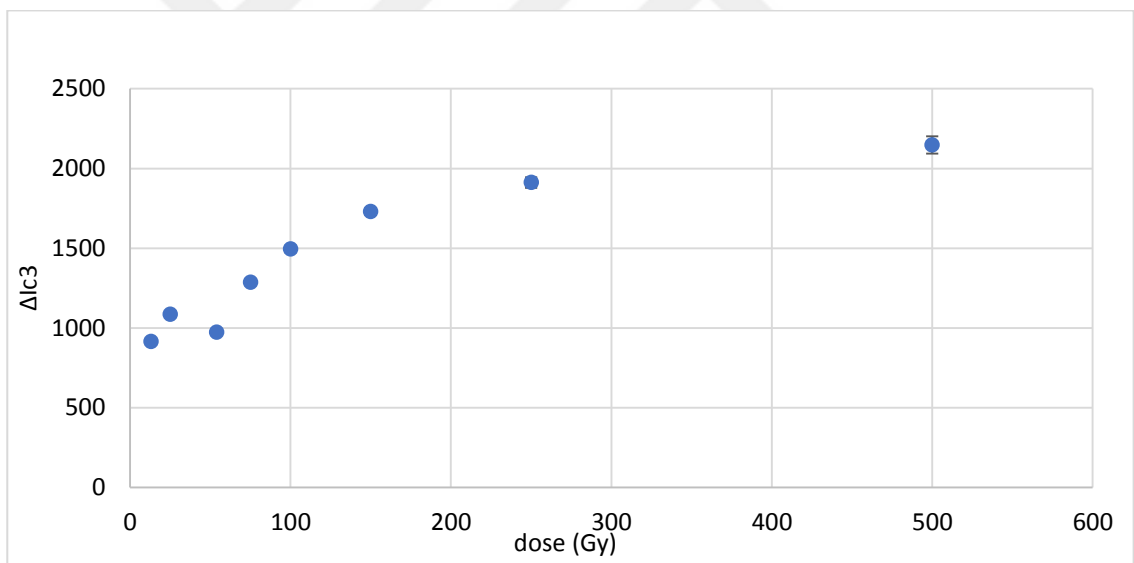


Figure 5.17 OSL component integrated intensity differences, ΔI_{c_i} , versus dose curves obtained for OSL component c_3 of Quartz. The differences were calculated for the dose rates 1305 Gy/h and 27 Gy/h. Error bars correspond to 1σ (Errors are very small)

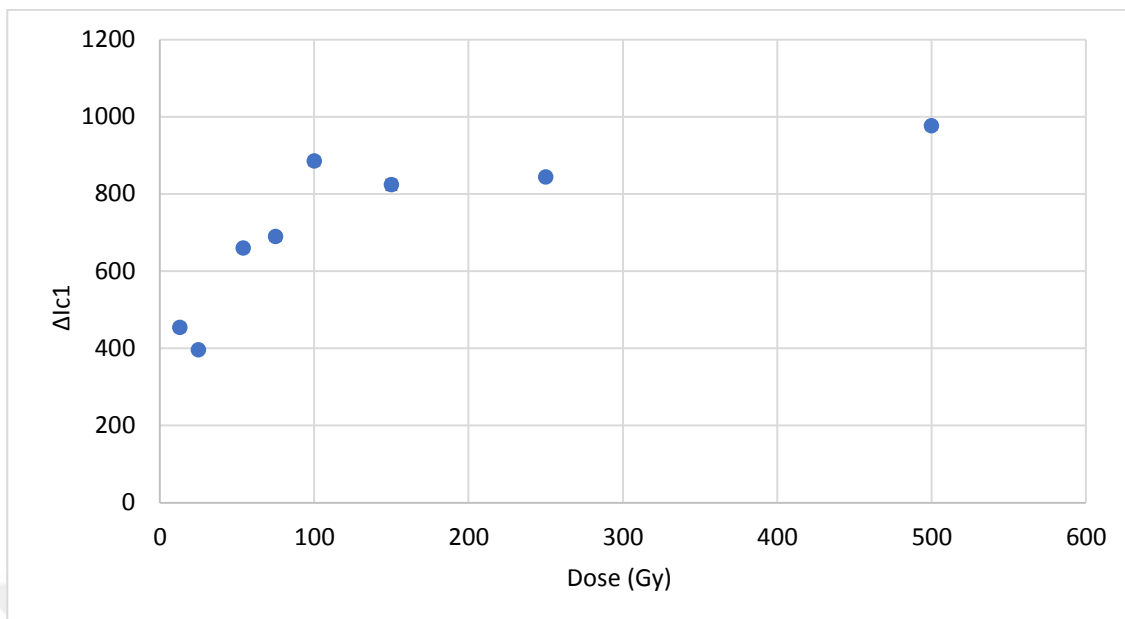


Figure 5.18 OSL component integrated intensity differences, ΔI_{c1} , versus dose curves obtained for OSL component c_1 of Quartz. The differences were calculated for the dose rates 311 Gy/h and 27 Gy/h. Error bars correspond to 1σ (Errors are very small)

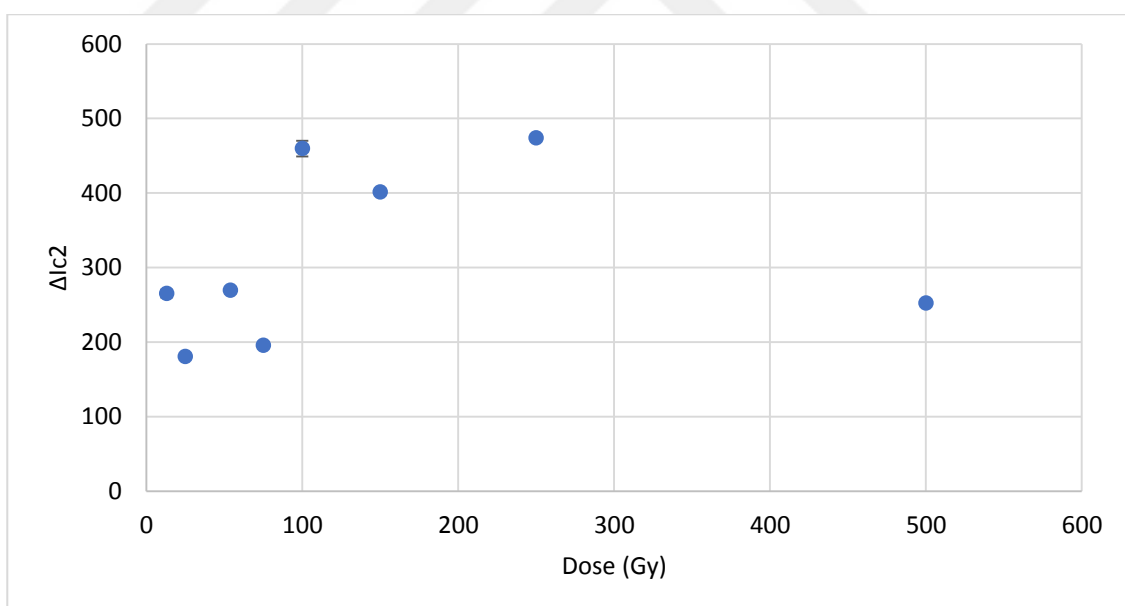


Figure 5.19 OSL component integrated intensity differences, ΔI_{c2} , versus dose curves obtained for OSL component c_2 of Quartz. The differences were calculated for the dose rates 311 Gy/h and 27 Gy/h. Error bars correspond to 1σ (Errors are very small)

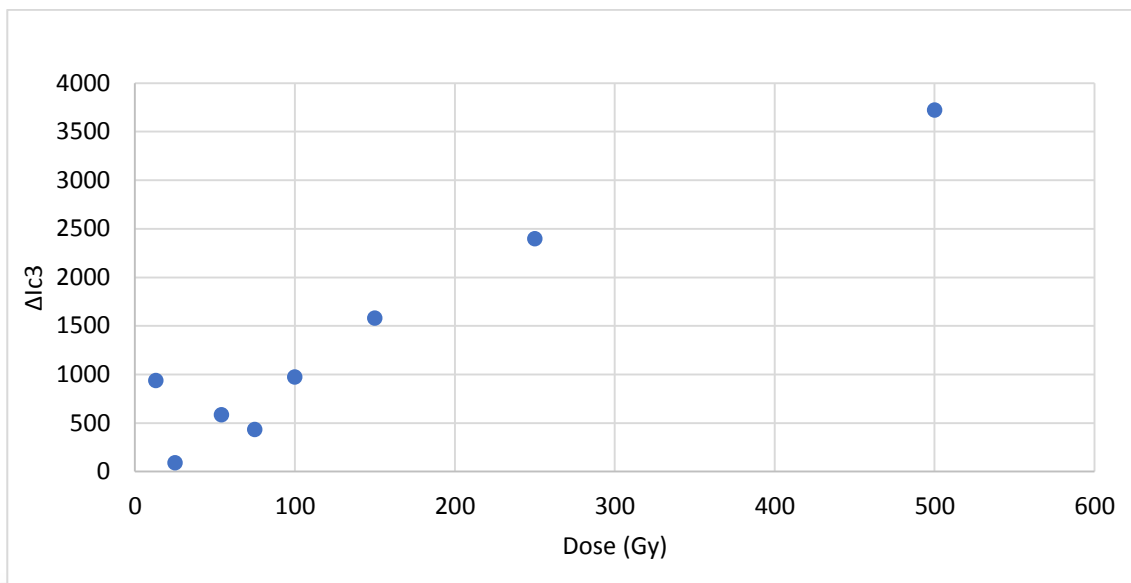


Figure 5.20 OSL component integrated intensity differences, ΔI_{c_i} , versus dose curves obtained for OSL component c_3 of Quartz. The differences were calculated for the dose rates 311 Gy/h and 27 Gy/h. Error bars correspond to 1σ (Errors are very small)

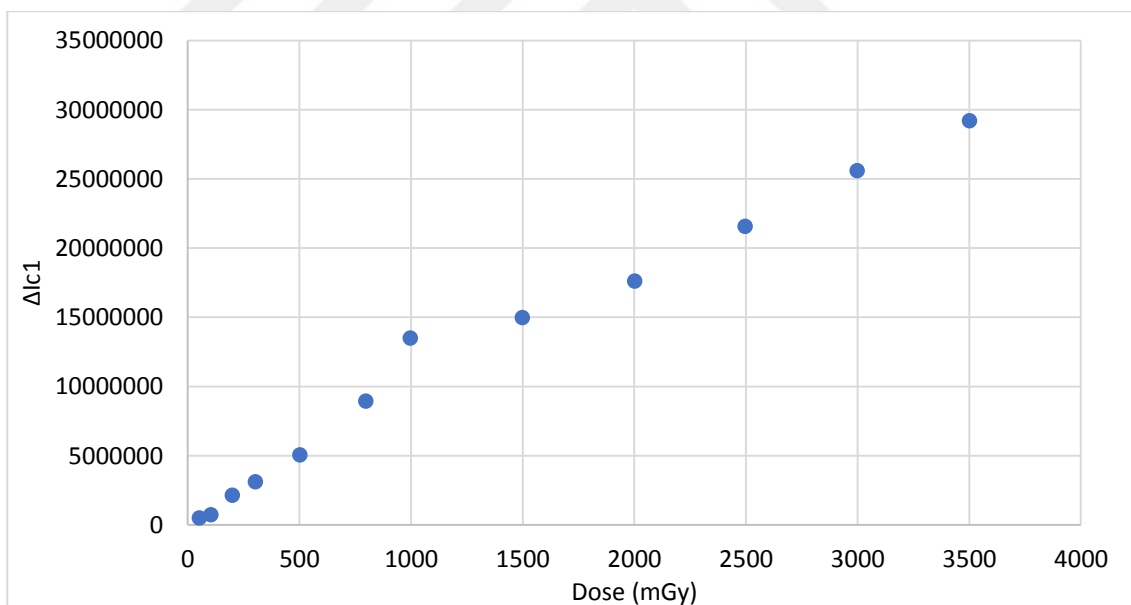


Figure 5.21 OSL component integrated intensity differences, ΔI_{c_i} , versus dose curves obtained for OSL component c_1 of BeO. The differences were calculated for the dose rates 30 Gy/h and 2 Gy/h. Error bars correspond to 1σ (Errors are very small)

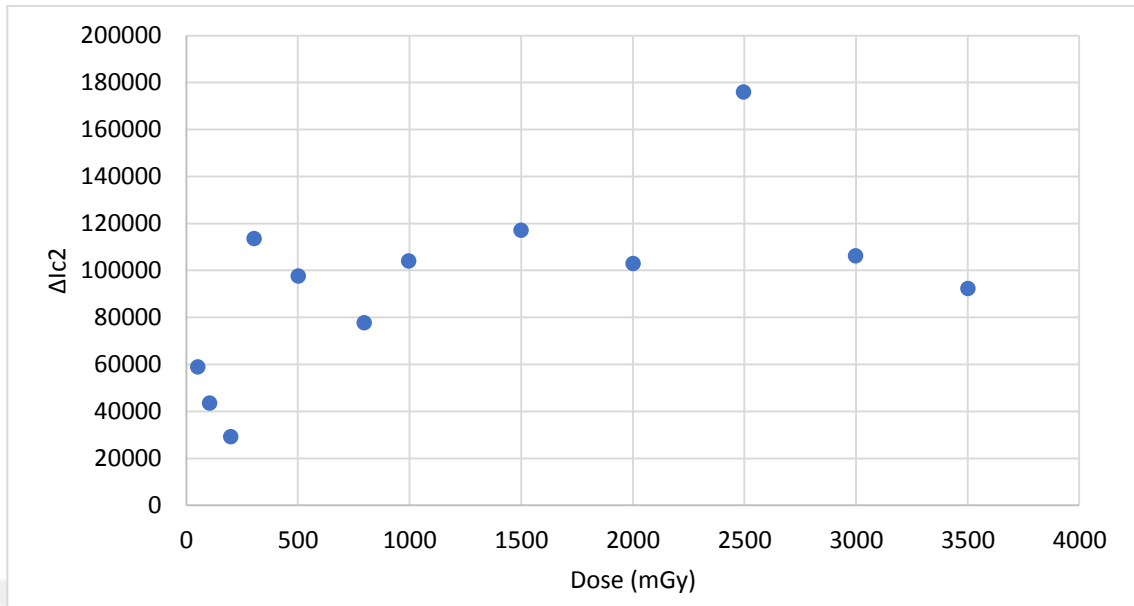


Figure 5.22 OSL component integrated intensity differences, ΔI_{c_i} , versus dose curves obtained for OSL component c_2 of BeO. The differences were calculated for the dose rates 30 Gy/h and 2 Gy/h. Error bars correspond to 1σ (Errors are very small)

After deconvolution analyses, for $\text{Li}_2\text{B}_4\text{O}_7 : \text{Cu, In, CaF}_2 : \text{Dy}$ (TLD200) , LiF: Mg, Ti (TLD 100), TL peak integrated intensity differences, ΔI_{p_i} , versus dose curves obtained for TL peak 4 and peak 5, respectively. The difference between peak 4 values at 2 Gy/h and 30 Gy/h and also the same for peak 5 are shown between the Figure 5.23 and 5.28.

Figure 5.29 shows the $\Delta I_{\text{singlepeak}}$ of $\text{MgB}_4\text{O}_7 : \text{Dy, Na}$ at 2 Gy/h.

Figure 5.30 and 5.31 shows the BeO TL peak integrated intensity differences, ΔI_{p_i} , versus dose curves obtained for TL peak 1 and peak 2, respectively at 2 Gy/h and 30 Gy/h.

Errors are calculated each of the measurements.

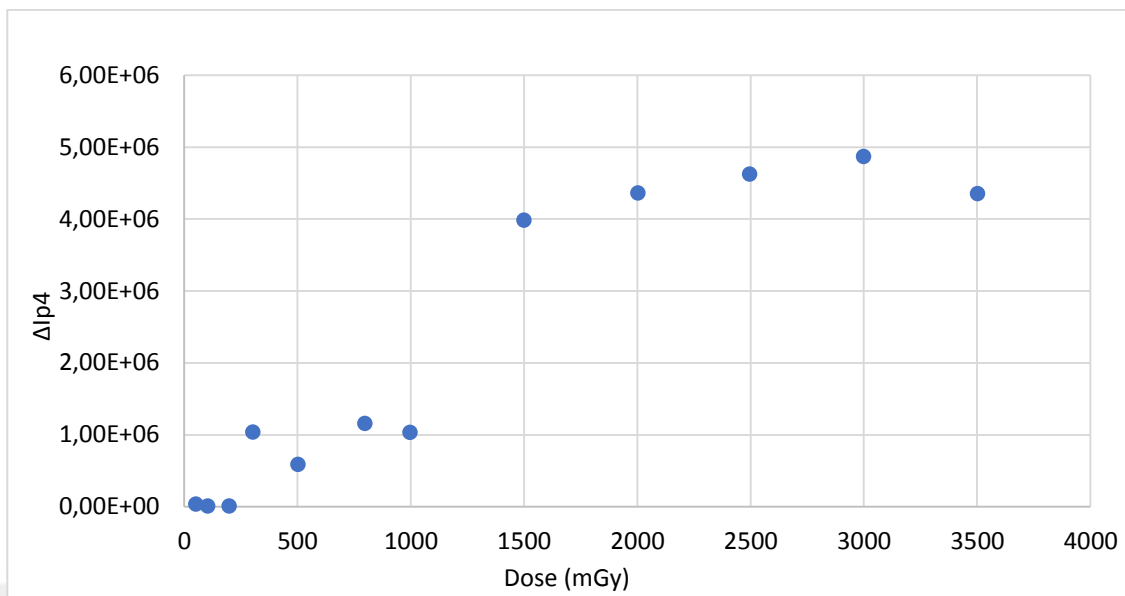


Figure 5.23 TL peak integrated intensity differences, ΔI_{pi} , versus dose curves obtained for TL peak 4 of $\text{Li}_2\text{B}_4\text{O}_7:\text{Cu}$, In. The differences were calculated for the dose rates 30 Gy/h and 2 Gy/h. Error bars correspond to 1σ (Errors are very small)

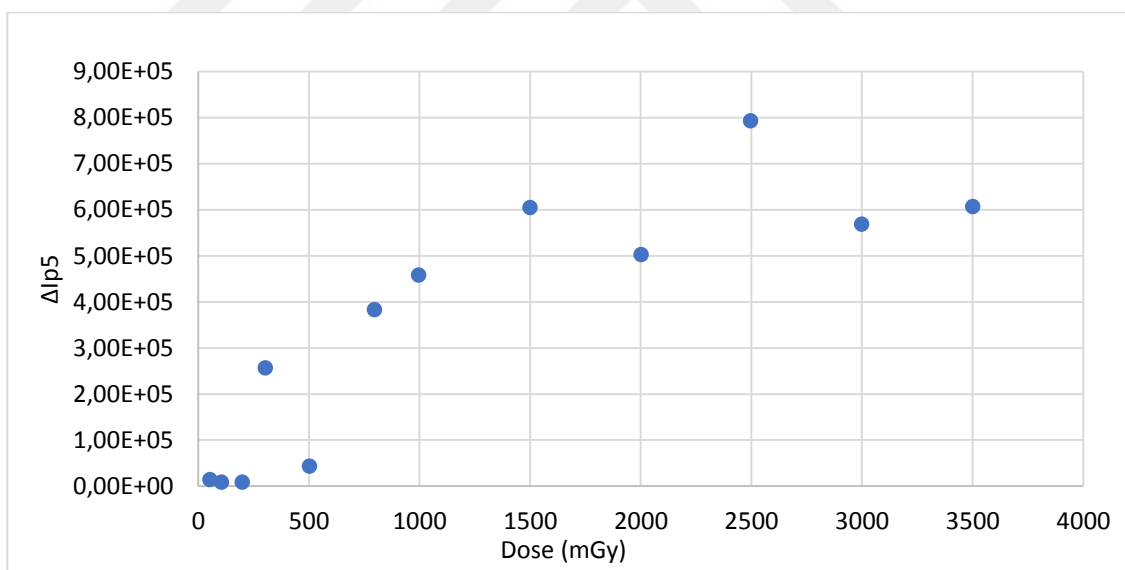


Figure 5.24 TL peak integrated intensity differences, ΔI_{pi} , versus dose curves obtained for TL peak 5 of $\text{Li}_2\text{B}_4\text{O}_7:\text{Cu}$, In. The differences were calculated for the dose rates 30 Gy/h and 2 Gy/h. Error bars correspond to 1σ (Errors are very small)

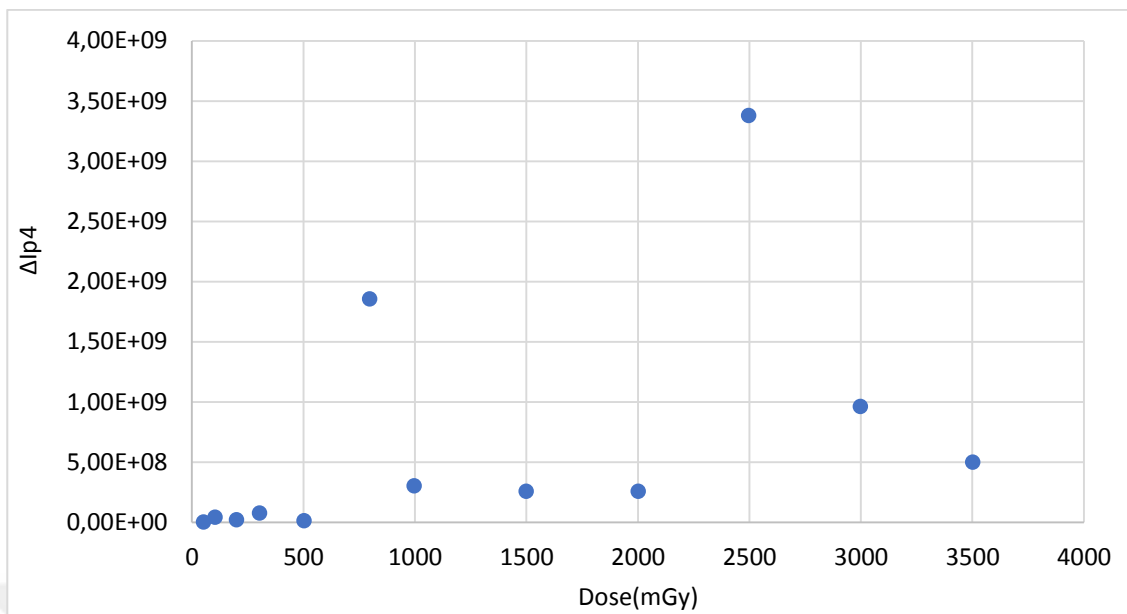


Figure 5.25 TL peak integrated intensity differences, ΔI_{pi} , versus dose curves obtained for TL peak 4 of $\text{CaF}_2:\text{Dy}$ (TLD 200). The differences were calculated for the dose rates 30 Gy/h and 2 Gy/h. Error bars correspond to 1σ (Errors are very small)

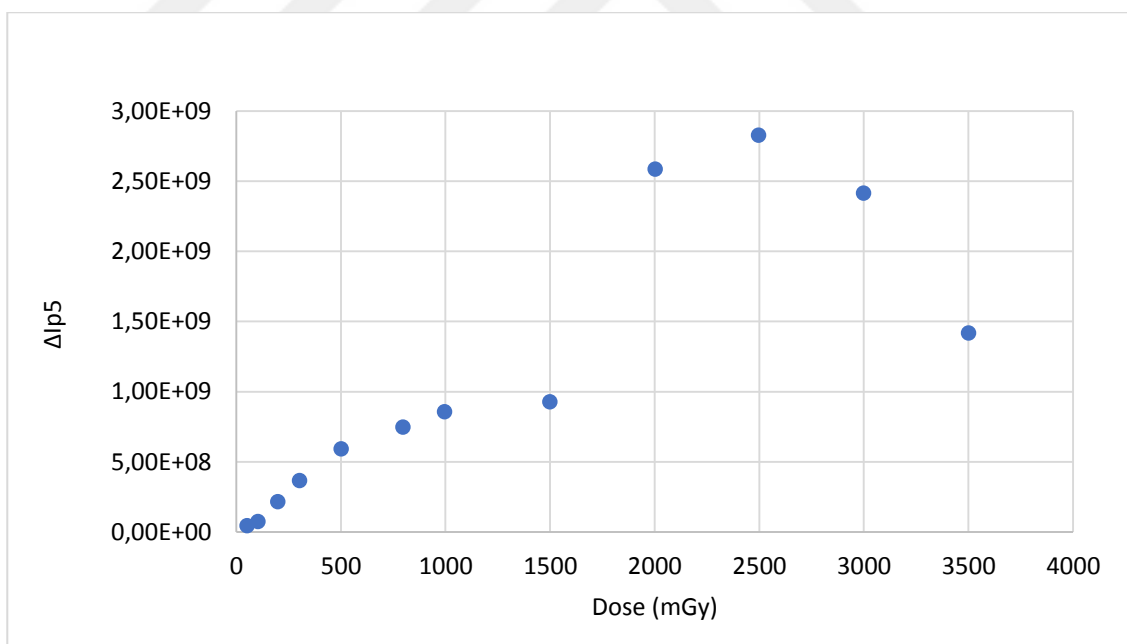


Figure 5.26 TL peak integrated intensity differences, ΔI_{pi} , versus dose curves obtained for TL peak 5 of $\text{CaF}_2:\text{Dy}$ (TLD 200). The differences were calculated for the dose rates 30 Gy/h and 2 Gy/h. Error bars correspond to 1σ (Errors are very small)

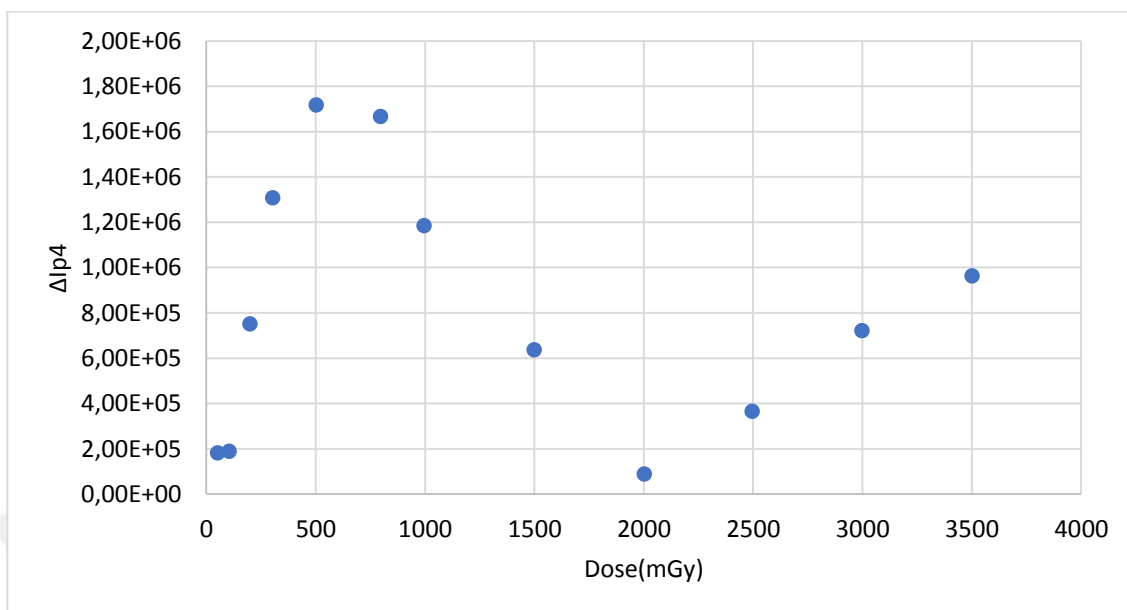


Figure 5.27 TL peak integrated intensity differences, ΔI_{pi} , versus dose curves obtained for TL peak 4 of LiF: Mg,Ti (TLD 100). The differences were calculated for the dose rates 30 Gy/h and 2 Gy/h. Error bars correspond to 1σ (Errors are very small)

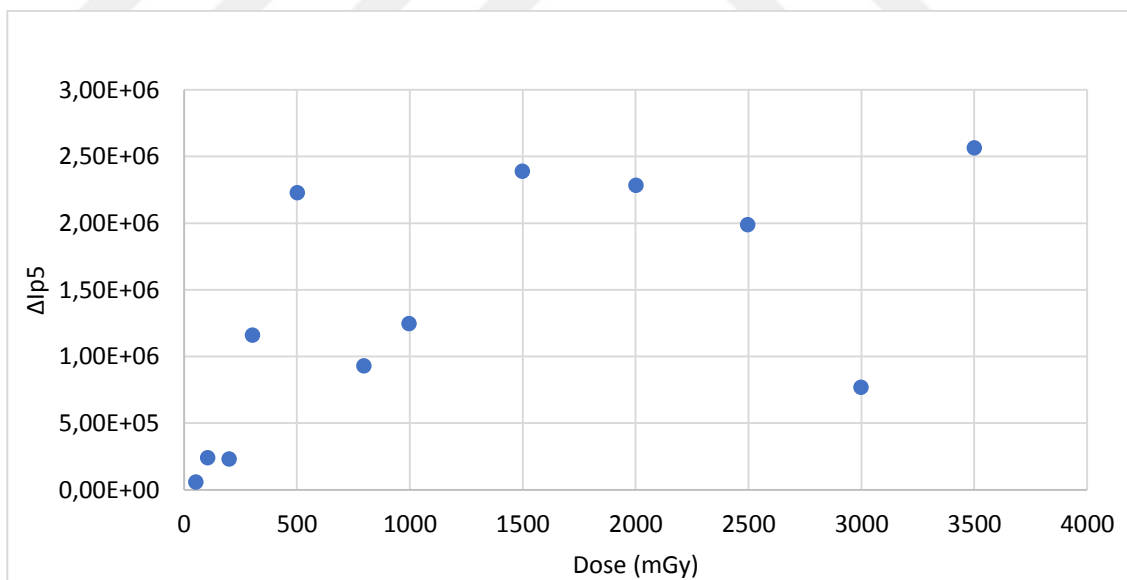


Figure 5.28 TL peak integrated intensity differences, ΔI_{pi} , versus dose curves obtained for TL peak 5 of LiF: Mg,Ti (TLD 100). The differences were calculated for the dose rates 30 Gy/h and 2 Gy/h. Error bars correspond to 1σ (Errors are very small)

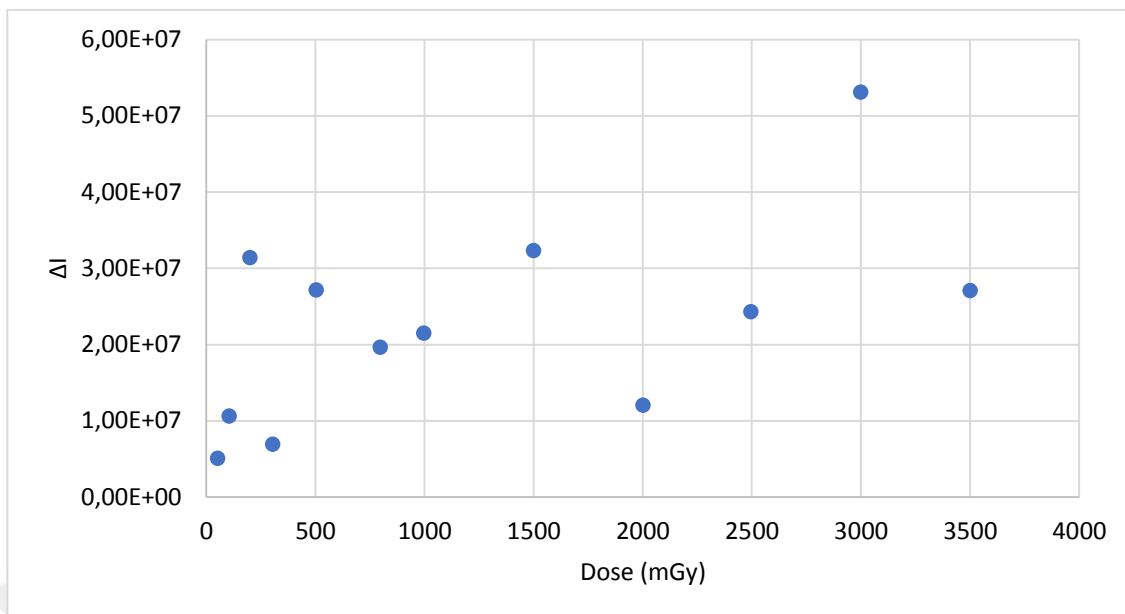


Figure 5.29 TL peak integrated intensity differences, ΔI_{pi} , versus dose curves obtained for TL single peak of $MgB_4O_7: Dy,Na$. The differences were calculated for the dose rates 30 Gy/h and 2 Gy/h. Error bars correspond to 1σ (Errors are very small)

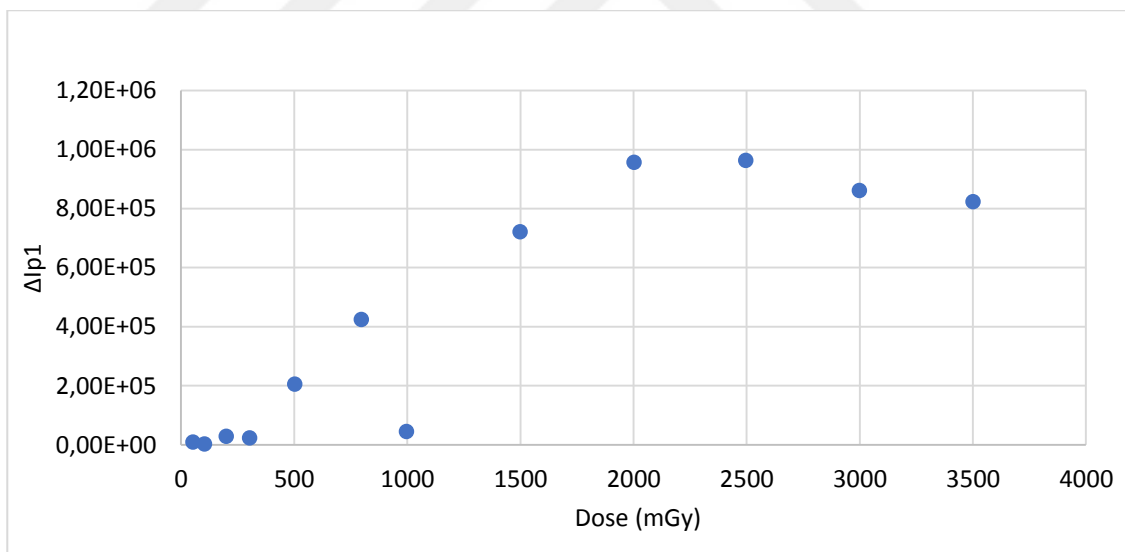


Figure 5.30 TL peak integrated intensity differences, ΔI_{p1} , versus dose curves obtained for TL peak 1 of BeO . The differences were calculated for the dose rates 30 Gy/h and 2 Gy/h. Error bars correspond to 1σ (Errors are very small)

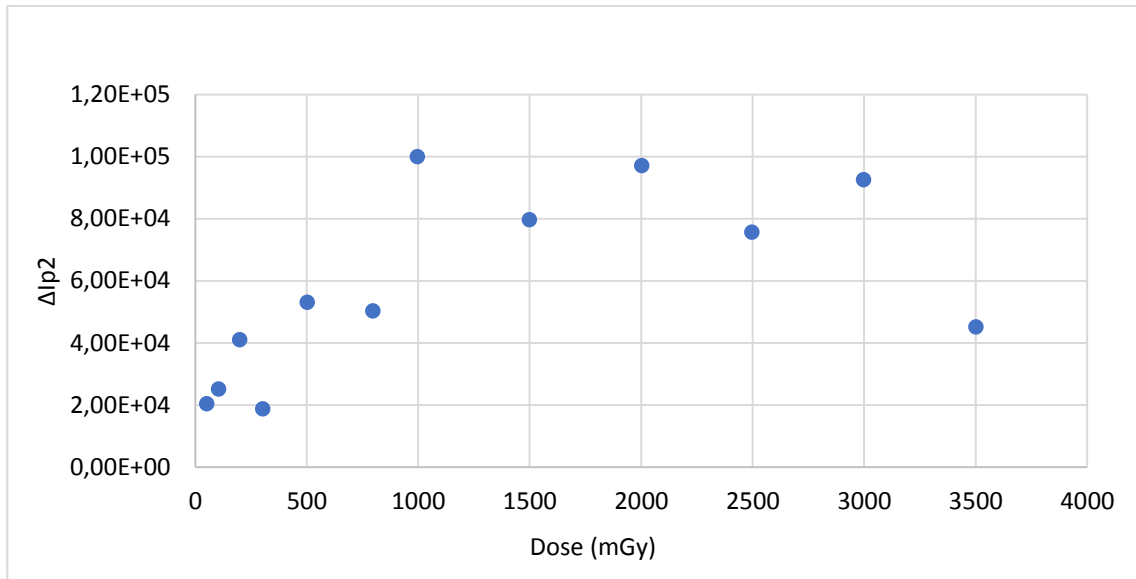


Figure 5.31 TL peak integrated intensity differences, ΔI_{p_i} , versus dose curves obtained for TL peak 2 of BeO. The differences were calculated for the dose rates 30 Gy/h and 2 Gy/h. Error bars correspond to 1σ (Errors are very small)

After deconvolution analyses, for $\text{Li}_2\text{B}_4\text{O}_7:\text{Cu}$, In, $\text{CaF}_2:\text{Dy}$ (TLD200), $\text{LiF}:\text{Mg,Ti}$ (TLD 100), activation energy differences, ΔE , versus dose curves obtained for TL peak 4 and peak 5, respectively. The difference between peak 4 values at 2 Gy/h and 30 Gy/h and also the same for peak 5 are shown between the Figure 5.32 and 5.37.

Figure 5.38 and 5.39 shows the BeO activation energy differences, ΔE , versus dose curves obtained for TL peak 1 and peak 2, respectively

Errors are calculated each of the measurements.

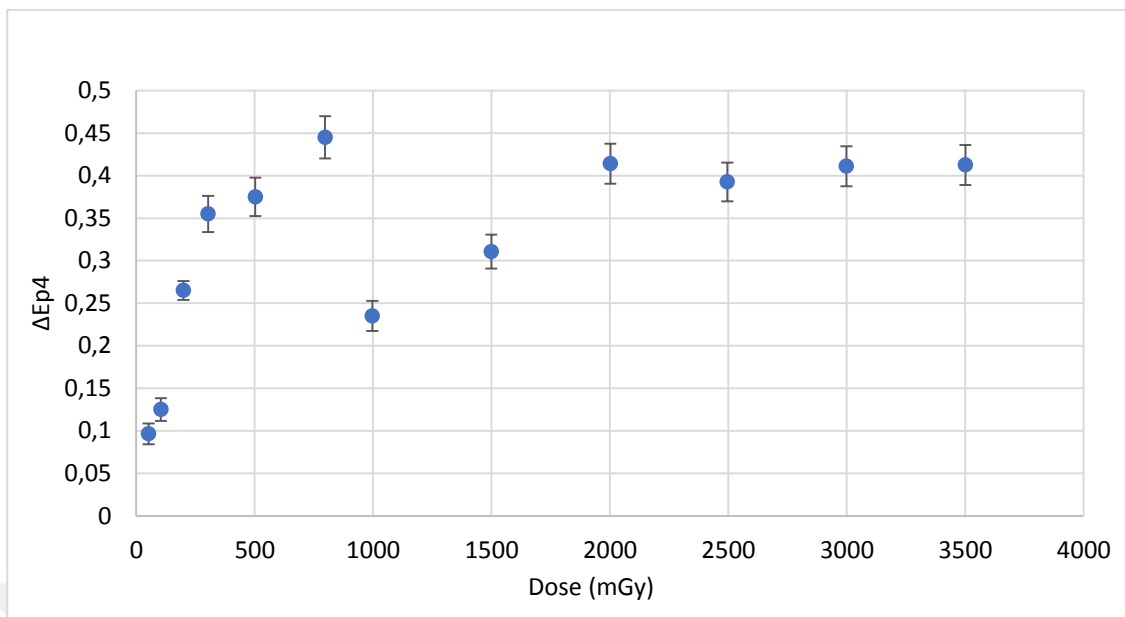


Figure 5.32 Activation energy differences, ΔE , versus dose curves obtained for TL peak 4 of $\text{Li}_2\text{B}_4\text{O}_7:\text{Cu}$, In. The differences were calculated for the dose rates 30 Gy/h and 2 Gy/h. Error bars correspond to 1σ

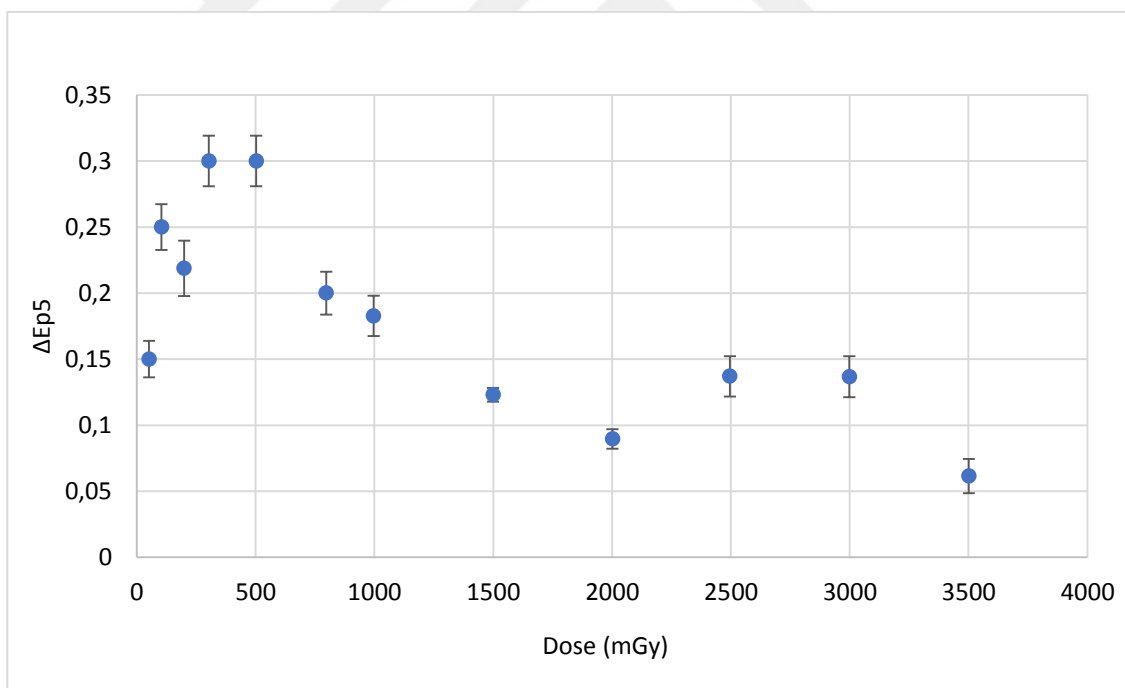


Figure 5.33 Activation energy differences, ΔE , versus dose curves obtained for TL peak 5 of $\text{Li}_2\text{B}_4\text{O}_7:\text{Cu}$, In. The differences were calculated for the dose rates 30 Gy/h and 2 Gy/h. Error bars correspond to 1σ

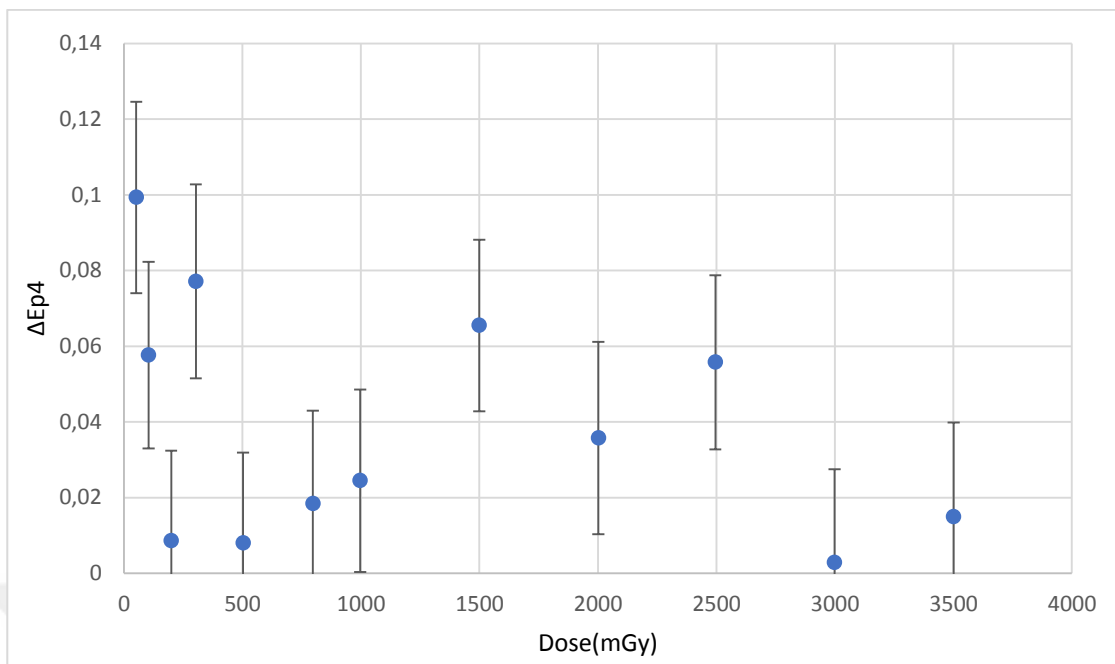


Figure 5.34 Activation energy differences, ΔE , versus dose curves obtained for TL peak 4 of $\text{CaF}_2:\text{Dy}$ (TLD 200). The differences were calculated for the dose rates 30 Gy/h and 2 Gy/h. Error bars correspond to 1σ

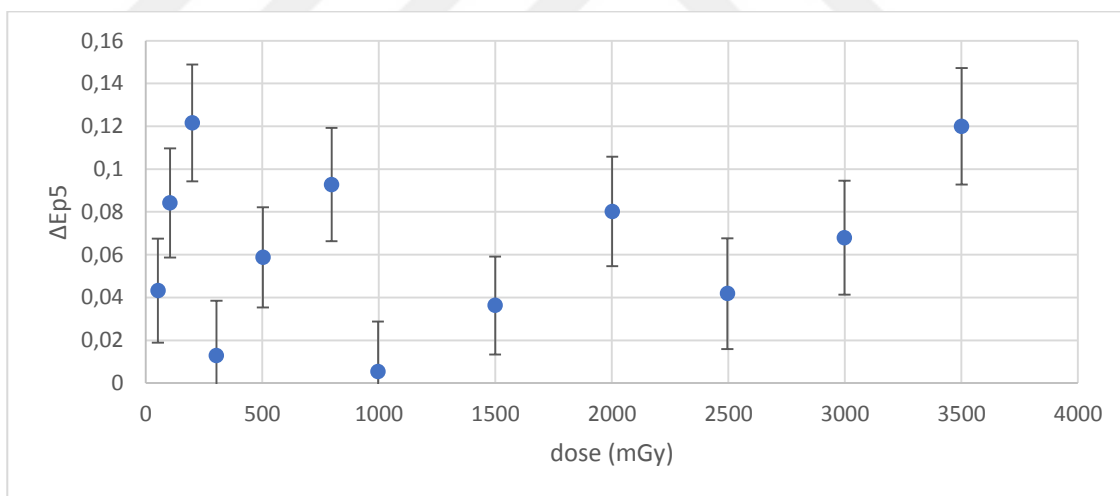


Figure 5.35 Activation energy differences, ΔE , versus dose curves obtained for TL peak 5 of $\text{CaF}_2:\text{Dy}$ (TLD 200). The differences were calculated for the dose rates 30 Gy/h and 2 Gy/h. Error bars correspond to 1σ

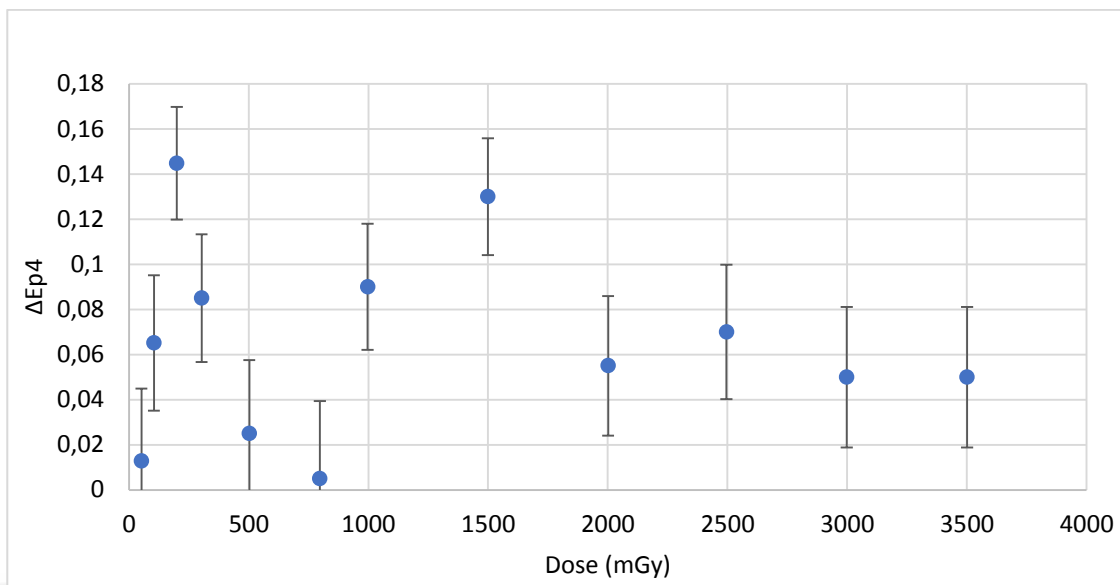


Figure 5.36 Activation energy differences, ΔE , versus dose curves obtained for TL peak 4 of LiF: Mg, Ti (TLD 100). The differences were calculated for the dose rates 30 Gy/h and 2 Gy/h. Error bars correspond to 1σ

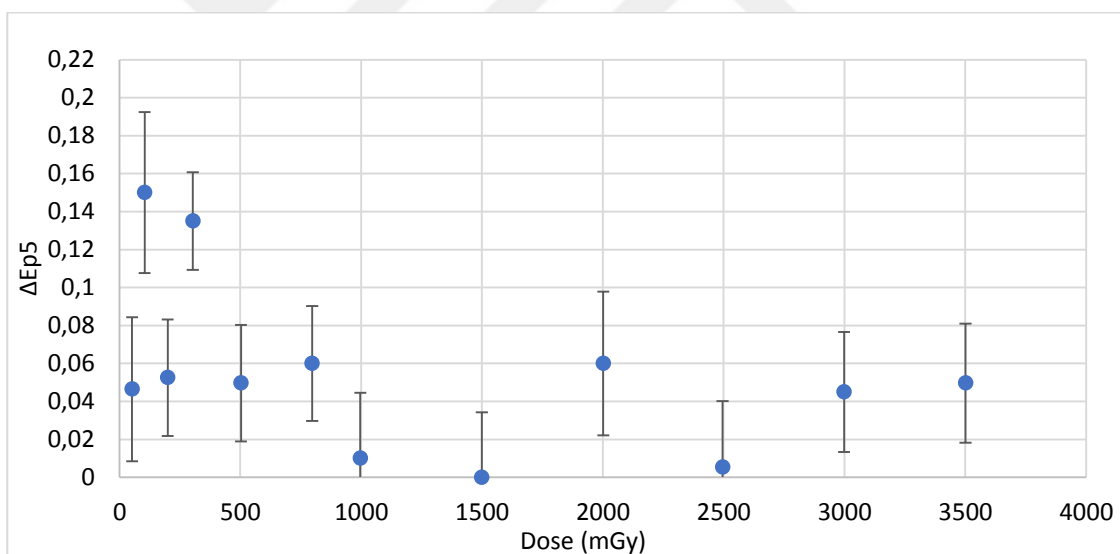


Figure 5.37 Activation energy differences, ΔE , versus dose curves obtained for TL peak 5 of LiF: Mg, Ti (TLD 100). The differences were calculated for the dose rates 30 Gy/h and 2 Gy/h. Error bars correspond to 1σ

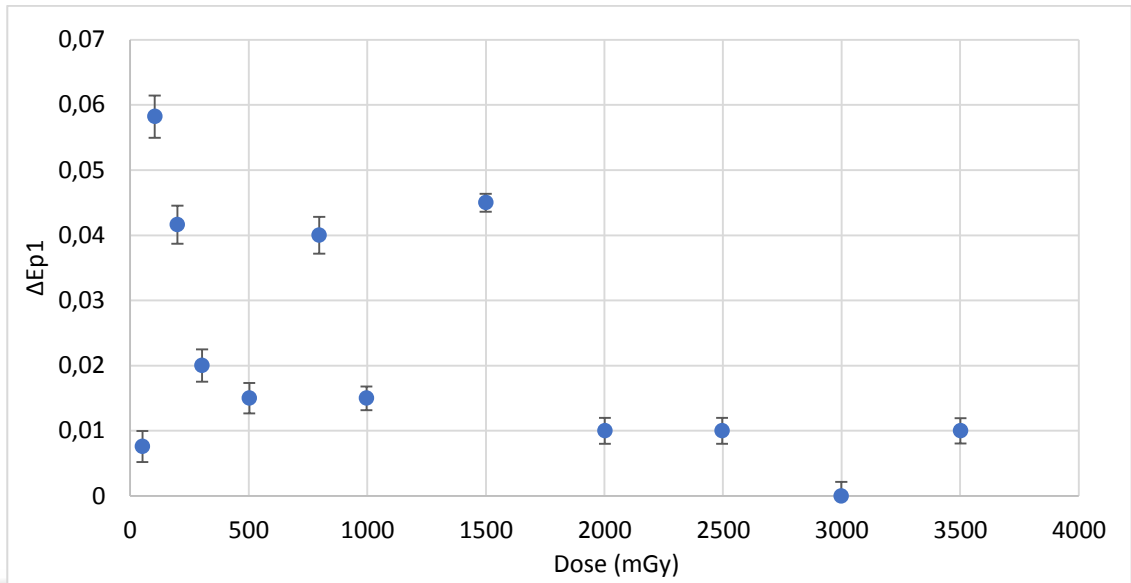


Figure 5.38 Activation energy differences, ΔE , versus dose curves obtained for TL peak 1 of BeO. The differences were calculated for the dose rates 30 Gy/h and 2 Gy/h. Error bars correspond to 1σ

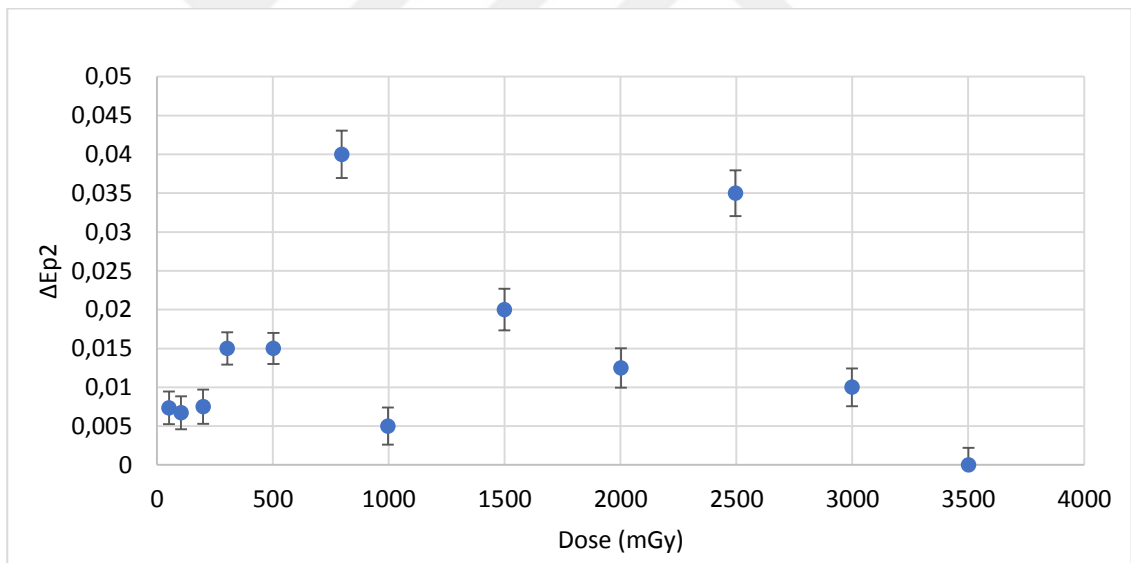


Figure 5.39 Activation energy differences, ΔE , versus dose curves obtained for TL peak 2 of BeO. The differences were calculated for the dose rates 30 Gy/h and 2 Gy/h. Error bars correspond to 1σ

5.1 Case of LiF:Mg,Ti

Figs. 4.3, 4.4, 4.20, 4.21, 4.34, 4.35, 4.42, 4.43, 4.50 and 4.51 present the case of LiF:Mg,Ti material. According to the related literature (McKeever et al., 1997 and references therein) the dose rate effects of this specific material have been studied in the past over a vast dose rate region, covering the range between $10^{-6} - 10^2$ Gy/h. Throughout this dose range region, the dose response properties have been reported not to change at all. This is also the case of the present study. Figs 5.27 and 5.28 present the difference ΔTLp_4 and ΔTLp_5 for both peaks 4 and 5. According to these later figures, the absolute intensities yielded for the two applied dose rates indicate minor changes. However, based on Figs 4.34 and 4.35, the ΔTLp_i indicate just a minor fraction of the integrated signal of each peak, $<0.7\%$. This is an insignificant level of difference, supporting the results of previous studies as well. Moreover, according to Table 5.1, the dose response parameters of both TL peaks 4 and 5 of LiF: Mg,Ti are almost similar. Noteworthy that the dose response of both peaks for both dose rates is linear throughout the entire dose region of the present study.

However, so far in the literature, the dose dependence of the kinetic parameters b and E has not been previously studied. Deconvolution analysis yielded that for both dose rates, each one of the TL peaks 4 and 5 are described by first order of kinetics (Figs 4.42 and 4.43). Moreover, the values of the b parameter are independent on both dose as well as dose rate. Figs 4.50 and 4.51 present the dependence of the activation energy of each peak on both dose and dose rate. Figs 5.36 and 5.37 present the ΔEp_4 and ΔEp_5 variations versus dose. Insignificant variations are monitored, as these values do not exceed 0.11 eV.

5.2 Case of Li₂B₄O₇:Cu:In

Figs. 4.1, 4.2, 4.16, 4.17, 4.30, 4.31, 4.38, 4.39, 4.46 and 4.47 correspond to the case of Li₂B₄O₇:Cu:In material. According to the related literature (McKeever et al., 1997 and references therein) the dose rate effects of this specific material have not been studied extensively in the past. According to the deconvolution results of Figs 4.16 and 4.17, the main dosimetric peak is TL peak 4. According to Figs 4.30 and 4.31, as well as to

Table 5.1, the dose response is linear throughout the entire dose region. However, this is not the case for TL peak 5; according to Table 5.1 the dose response is linear for doses up to 2500-3000 mGy, while beyond, saturation features are monitored. Therefore, the dose response of TL peak 5 was studied using two different approaches: (a) using the usual equation for the linear dose response within the linearity dose region and (b) using the following equation 5.2 (Grün, 1996 and Şahiner et al. 2017):

$$I = I_{max} \cdot \left(1 - \exp\left(-\frac{D - D_E}{D_0}\right) \right) \quad (5.2)$$

where I is the luminescence signal at dose D and I_{max} express the maximum dose response intensity at the level of saturation. Nevertheless, the explanation of the two parameters D_0 and D_E is quite important. D_0 stands for the dose at which the luminescence signal is saturated. The physical meaning of the D_E parameter value deals with the lowest detectable limit achievable (LDDL, Şahiner et al. 2017). A least-square fit of the experimental data provides for each luminescence signal and each material the values for the parameters D_0 and D_E in units of Gy. Error values on these parameters were derived according to the fitting errors. These values are presented in Table 5.1

Moreover, as Figs 4.30 and 4.31 further reveal, there is a dependence of the absolute intensity of each TL peak on the dose rate. Figs 5.23 and 5.24 present the variations ΔTLp_4 and ΔTLp_5 for both peaks 4 and 5 for the two different dose rates. According to these later figures, the absolute intensities yielded for the two applied dose rates indicate major changes. Based on Figs 4.30 and 4.31, the ΔTLp_4 and ΔTLp_5 indicate just a fraction of the integrated signal of each peak around 10-15%, which increases with increasing dose. Surprisingly, the b (order of kinetics) parameters of both $Li_2B_4O_7:Cu:In$ peaks do not indicate significant variations with test dose. Nevertheless, according to Figs 4.46, 4.47, 5.32 and 5.33, strong dependence on the dose rate is yielded for the activation energies E of each peak. For the higher dose rate of 30 Gy/h, the activation energies indicate values almost 0.3 – 0.4 eV higher. For TL peak 5, these major differences could be attributed to the low deconvolution resolution, as this TL

peak is of much lower intensity. However the absolute differences on TL peak 4 are not an analysis artefact.

5.3 Case of MgB₄O₇:Dy

Figs. 4.5, 4.6, and 4.29, correspond to the case of MgB₄O₇: Dy material. According to the related literature (McKeever et al. 1997 and references therein) the dose rate effects of this specific material have not been studied extensively in the past. Deconvolution was not performed for the reasons that were reported previously; therefore plots for trap's activation energy and order of kinetic parameter are not presented. The dose response of both peaks for both dose rates is linear throughout the entire dose region of the present study. Fig 5.29 presents the difference $\Delta TL_{\text{singlepeak}}$ for the integrated TL signal. According to these later figures, the absolute intensities yielded for the two applied dose rates indicate minor changes. However, based on Fig. 4.29, the ΔTL indicates just a minor fraction of the integrated signal of each peak, <0.4%. This is an insignificant level of difference, supporting the results of previous studies as well. Moreover, according to Table 5.1, the dose response parameters of both TL signals are almost similar. One exception is monitored for the LDDL; this latter parameter is 5 times higher for the dose rate of 30 Gy/h

5.4 Case of CaF₂:Dy

Figs. 4.7, 4.8, 4.18, 4.19, 4.32, 4.33, 4.40, 4.41, 4.48 and 4.49 correspond to the case of CaF₂: Dy material. According to the related literature (McKeever et al.1997 and references therein) the dose rate effects of this specific material have not been studied extensively in the past. According to the deconvolution results of Figs 4.18 and 4.19, the main dosimetric peaks are TL peaks 4 and 5.

5.5 Case of BeO TL

Figs. 4.9, 4.10, 4.22, 4.23, 4.36, 4.37, 4.44, 4.45, 4.52 and 4.53 present the TL glow curves, deconvolution analysis, dose response, b and E parameters for the TL signal of BeO dosimeter. According to Figs 4.22 and 4.23, the dose response of TL peak 1 is

supralinear, while the corresponding dose response of TL peak 2 is linear. Both behaviours are monitored throughout the entire dose region of the present study. This supralinearity is also verified by the k-values presented in Table 5.1. For this reason, the TL dose response of TL peak 1 is also presented below in log-log scales as well.

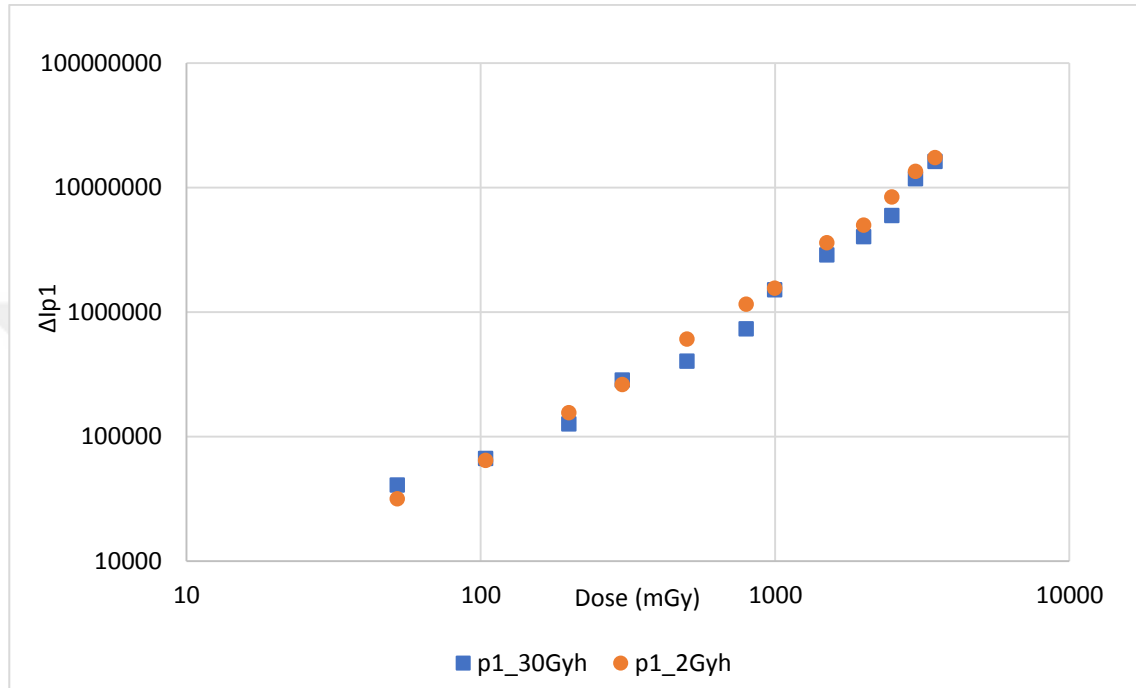


Figure 5.40 Component resolved TL dose response curves obtained for TL peak 1 of BeO. Dots correspond to 2 Gy/h and squares correspond to 30 Gy/h. Each data point corresponds to an average of two individually measured values. Error bars correspond to 1σ (Errors are very small)(Axis are logarithmic)

The LDDL of TL peak 1 is less than 10 mGy for both dose rates, while the corresponding value for the TL peak 2 gets values around 15 mGy for both dose rates, without any significant variation for the two applied dose rates. The results regarding the deconvolution parameters are in excellent agreement with previous studies (Aşlar et al. 2017a,b and Sahiner 2017). The activation energies for these two peaks were calculated at 1.08 eV and 1.21 eV for TL peaks 1 and 2 respectively (Figs 4.52 and 4.53 respectively) with insignificant variations for the two dose rates (Figs 5.38 and 5.39 respectively). Finally, Figs 4.44 and 4.45 verify that both TL glow peaks are described by first order of kinetics, without significant variations for the two dose rates used. Figs 5.30 and 5.31 present the difference ΔTLp_1 and ΔTLp_2 for both peaks 1 and 2 for the two dose rates. According to these later figures, similarly to the case of LiF: Mg,Ti, the

absolute intensities yielded for the two applied dose rates indicate minor changes. However, based on Figs 4.36 and 4.37, the ΔTLp_i indicate just a minor fraction of the integrated signal of each peak, $<0.1\%$. This is an insignificant level of difference, supporting the results of previous studies as well.

5.6 Case of BeO OSL

Figs. 4.11, 4.12, 4.24, 4.25, 4.54, 4.55, 4.59, and 4.60 present the OSL decay curves, deconvolution analysis, dose response and lifetime τ parameters for the OSL signal of BeO dosimeter. For both dose rates, the dose response of the fast OSL component C_1 is slightly supralinear, similar to the case of BeO TL peak 1. Even though the LDDL values are quite similar, Fig. 4.54 indicates a large difference in the absolute intensity of each component for the two dose rates applied. Similar results are also revealed by Fig. 5.21 for component C_1 . On the contrary, the variations in component C_2 are quite insignificant in both terms of integrated intensity as well as decay lifetime τ . It should be emphasized that for OSL component C_2 , two different fitting approaches were adopted for the fitting analysis: one using equation 5.1 as well as one using equation 5.2. The corresponding results are presented in Table 5.1.

5.7 Case of Quartz OSL

Quartz stands as the second most abundant mineral in the Earth's crust. Only the OSL of quartz was studied. TL was not studied because the TL glow curves did not yield sufficient reproducibility, as the quartz sample is not annealed. Figs. 4.13 – 4.15, 4.26 – 4.28, 4.56 – 4.58 and 4.61 – 4.63 present the OSL decay curves, deconvolution analysis, dose responses and lifetime τ parameters for the case of quartz's OSL. According to the dose response features, only the medium component (C_2) yields dose response that could be fitted using the equation 5.1; the corresponding results are presented in Table 5.1. For all three dose rates, the dose response is sublinear, with quite high LDDL limits. However, both k and LDDL parameters are independent on the dose rate.

For the two other components, namely fast C_1 and slow C_3 , a successful dose response analysis includes fitting using equation 5.1 solely. An example of the fitting is presented in Fig. 5.41. Saturation exponential behavior is monitored for both

components. For the fast component, the various fitting parameters are quite stable and independent on the dose rate. Similar results are also yielded for the decay lifetimes of each component, according to Figs 4.61 – 4.63 as well as Figs 5.1 – 5.11.

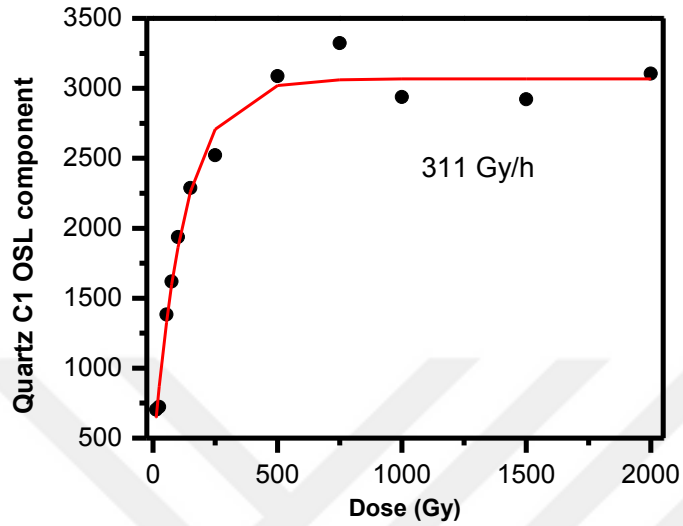


Figure 5.41 An example of dose response fitting using equation 5.1 for the fast (c_1) component of quartz. The fitting parameters are presented in Table 5.1

6. CONCLUSION

Before working on the thesis due to the lack of study in the literature, the results were unpredictable. Only for the cases of LiF: Mg, Ti and quartz there were results on the gamma dose rate effects in TL measurements in the literature. In TL measurements, all of the artificial materials except MgB₄O₇:Dy, Na include deconvolution analyses and each of the peaks yield the corresponding kinetic parameters. These kinetic parameters are obtained and compared at two different dose rates. Except MgB₄O₇: Dy, each material's main peaks are found. The observed differences of each material are explained in the below part.

LiF: Mg, Ti (TLD 100), the dose rate effects of this specific material have been studied before in the literature. The dose response of both peaks for both dose rates is linear throughout the entire dose region of the present study and this is supported from the results of the previous studies. Kinetic parameters were not studied before so the results could not be compared. Order of kinetic, b and activation energy, E are independent on both dose as well as dose rates.

For the Li₂B₄O₇ : Cu, In, the dose rate effects of this specific material have not been studied vastly in the past. The dose response is linear throughout the entire dose region for peak 4 but as for peak 5, saturation occurs at 3000 mGy. There is a dependence of the absolute intensity of each TL peak on the dose rate. When the dose gets higher the difference between TLP₄ and TLP₅ gets higher. Observed variations related to b (order of kinetic) parameters of both Li₂B₄O₇:Cu, In peaks are not important to evaluate. For activation energies, especially peak 5 there is dependency on dose rate but not so much due to the low TL intensity.

For the MgB₄O₇: Dy the dose response of both peaks for both dose rates is linear throughout the entire dose region. This is an insignificant level of difference on TL intensity, activation energy E and order of kinetic b for single peak at two different dose rates. The LDDL parameter is 5 times higher for the dose rate of 30 Gy/h.

For CaF₂: Dy, the dose response of both peaks for both dose rates is linear throughout the entire dose region but there are slight differences on dose response curves at two different dose rates. E and b parameters are independent on both dose as well as dose rate.

As for the TL of BeO, the dose response of TL peak 1 is supralinear, while the corresponding dose response of TL peak 2 is linear. LDDL values are different between peak 1 and peak 2. The absolute intensities yielded for the two applied dose rates show minor changes so TL intensity has no dependency on dose rates. b and E parameters are independent on both dose as well as dose rate. Deconvolution parameters are in coherent with the previous studies.

Regarding the OSL of the same material, the dose response of the fast OSL component c_1 is slightly supralinear, similar to the case of BeO TL peak 1. LDDL values are quite similar. As for component c_2 saturation occurs and LDDL values are different at two dose rates, 2 Gy/h and 30 Gy/h. The variations in component c_1 are significant. Decay lifetime τ is independent on both dose as well as dose rate. τ values are similar at two dose rates.

Quartz holds totally different properties. Due to the lack of annealing procedure on quartz materials, insufficient reproducibility were obtained so TL measurement could not be done. When the dose response features were evaluated, the dose response of the medium component (c_2) for all three dose rates is sublinear, with quite high LDDL limits. However, both k and LDDL parameters are independent on the dose rate. Fast and slow components, c_1 and c_3 respectively, indicate a successful dose response analysis. Decay lifetime τ is independent on both dose as well as dose rate. Slow component c_3 has some changes according to different dose rates. Having higher dose rates caused higher c_3 values and attaining higher evacuation times for the traps.

As a brief of conclusion, For materials like LiF: Mg, Ti (TLD 100), BeO and MgB₄O₇: Dy, Na, no differences are monitored for the two dose rates using all aforementioned criteria in TL.

There are differences in specific TL peaks (peak 5) on Li₂B₄O₇: Cu, In and CaF₂: Dy (TLD 200) for the two dose rates applied.

There are differences in certain OSL components in both BeO (c_1) and Quartz (c_3) b , kinetic order parameter is not sensitive in discriminating dose rate effects.

The most sensitive criteria include signal intensity, LDDL, k linearity index and E activation energy in decreasing order.

REFERENCES

- Aitken, M.J. 1985. Thermoluminescence Dating., Academic Press, p.118; London.
- Aşlar, E., Meriç, N., Şahiner, E., Erdem, O., Kitis, G., Polymeris, G.S. 2019. A correlation study on the TL, OSL and ESR signals in commercial BeO dosimeters yielding intense transfer effects. *Journal of Luminescence*, 214; 116533.
- Aşlar, E., Meriç, N., Şahiner, E., Kitis, G., Polymeris, G.S. 2017b. Calculation of thermal quenching parameters in BeO ceramics using solely TL measurements. *Radiation Measurements*, 103; 13-25.
- Aşlar, E., Şahiner, E., Polymeris, G.S., Meriç, N. 2017a. Determination of trapping parameters in BeO ceramics in both quenched as well as reconstructed thermoluminescence glow curves using various analysis methods. *Applied Radiation and Isotopes*, 129; 142–151.
- Azorin J. 2014. Preparation methods of thermoluminescent materials for dosimetric applications: An overview. *Applied Radiation and Isotopes*, 83; 187–191.
- Bailey, R. M. 2001. Towards a general kinetic model for optically and thermally stimulated luminescence of quartz. *Radiation Measurements*, 33(1); 17-45.
- Bailey, R.M., Smith, B.W., Rhodes, E.J. 1997. Partial bleaching and the decay from characteristics of quartz OSL. *Radiation Measurements*, 27; 123–136.
- Balian, H. G., Eddy, N. W. 1977. Figure-of-merit (FOM), an improved criterion over the normalized chi-squared test for assessing goodness-of-fit of gamma-ray spectral peaks. *Nuclear Instruments and Methods*, 145(2); 389-395.
- Becker, K. 1973. *Solid State Dosimetry*. CRC Press.
- Bos, J.A.A. 2007. *Theory of Thermoluminescence*. *Radiation Measurements* 4; 45-56.
- BøtterJensen, L., McKeever, S.W.S. and Wintle, A.G. 2003. *Optically stimulated luminescence dosimetry*. Elsevier Science B.V., 355 p.; Netherlands
- Bulur, E., Saraç, B.E. 2013. Time-resolved OSL studies on BeO ceramics, *Radiation Measurements*, 59; 129–138.
- Bulur, E., Yeltik, A. 2010. Optically stimulated luminescence from BeO ceramics: an LM-OSL study, *Radiation Measurements*, 45; 29–34.
- Busuoli, G., Lembo, L., Nanni, R., Sermenghi, I. 1984. Use of BeO in Routine Personnel Dosimetry, *Radiation Protection Dosimetry*, 6; 317-320.

- Chen, R., McKeever, S.W.S. and Durrani, A.S. 1981. Solution of the kinetic equations governing trap filling. Consequences concerning dose dependence and dose-rate effects. *Physical Review B.*, Volume 24; number 9.
- Chen, R., Kirsh, Y. 1981. *Internat. Ser. Sci. Solid State. Analysis of Thermally Stimulated Processes*; 15.
- Chen, R., McKeever, S.W.S. 1997. *Theory of Thermoluminescence and Related Phenomena* World Scientific; London.
- De Lima, F.J., Navarro, S.M., Valerio G.E.M. 2002. Effects of thermal treatment on the TL emission of natural quartz, *Radiation Measurements* Volume 35; 155–159.
- Fleming, S. J. 1979. *Thermoluminescence Techniques in Archaeology*. New York: Oxford University Press.
- Garlic, G.F.J., Gibson, A.F. 1948. The Electron Trap Mechanism of Luminescence in Sulphide and Silicate Phosphors. *Proc. Phys. Soc.*, 60; 574-590.
- Geoscience News and Information Geology.com web site, 2019. <https://geology.com/minerals/quartz.shtml> A ubiquitous mineral with an enormous number of uses Article by: Hobart M. King, Ph.D., RPG. Last Accessed: 01.06.2019.
- Grün, R. 1996. Errors in dose assessment introduced by the use of the linear part of a saturating dose–response curve. *Radiation Measurements*, 26; 297–305.
- Güneşdoğdu S. 1998. Determining of the Quartz Kinetic Parameters with TL Method, Master of Science Thesis , Kocaeli University Physics Department, 84 p., Kocaeli
- Hashimoto, T., Yasuda, K., Sato, K., Sakaue, H. and Katayama, H. 1998. Radiation-induced luminescence images and TL-property change with thermal annealing treatment on Japanese twin quartz. *Radiation Measurements*, 29(5); 493-502.
- <http://www.taek.gov.tr> 2019. Last Accessed: 05.06.2019.
- Horowitz, Y. 1984. *Thermoluminescence and Thermoluminescent Dosimetry*. C.R.C. Press; Florida.
- Huntley, D. J.; Berger, G. W.; Bowman, S. G. E. 1988: Thermoluminescence responses to alpha and beta irradiations, and age determination when the high dose response is nonlinear. *Radiation Effects*, 105; 279-284.
- Huntley, D.J, Godfrey-Smith, D.I. and Thewalt, M.L.W. 1985. Optical dating of sediments. *Nature*, 313; 105 – 107.

- Karagöz A. 2011. Investigation Of Dosimetric Properties And Luminescence Sensitivity Of Graphite Dopped Pencils, Master of science Thesis, Ankara University Graduate School of Natural and Applied Sciences Department of Engineering Physics, 91p., Ankara.
- Karsu Asal, E., Polymeris, G.S., Kitis, G. 2018. Thermoluminescence response of $\text{CaF}_2:\text{Dy}$ as a function of irradiation temperature between room temperature and 270 °C. *Radiation Measurements*, 118; 14-19.
- Kaya-Keles, S., Polymeris, G.S., Meriç, N. 2019. A component-resolved study on the stable signal of Merck a-quartz: tentative correlation among TL peaks, OSL components and EPR signals. Accepted for publication to *Nuclear Instruments and Methods in Physics Research B*.
- Khairi M.S.A. 2014. *Fundamentals In Nuclear Physics*, University of Duhok Publishing, Iraq.
- Khan, F. M. 2014. *The Physics of Radiation Therapy* fifth edition. Lippincott Williams & Wilkins; 121-445, Philadelphia
- Kitis, G., Gomez-Ros, J. M., & Tuyn, J. W. N. 1998. Thermoluminescence glow curve deconvolution functions for first, second and general orders of kinetics. *Journal of Physics D: Applied Physics*, 31(19); 2636.
- Kitis, G., Kiyak, N.G., Polymeris, G.S. 2015. Temperature lags of luminescence measurements in a commercial luminescence reader. *Nuclear Instruments and Methods in Physics Research B*, 359; 60–63.
- Kitis, G., Polymeris, G.S., Sfampa, I.K., Prokic, M., Meriç, N., Pagonis, V. 2016. Prompt isothermal decay of thermoluminescence in $\text{MgB}_4\text{O}_7:\text{Dy,Na}$ and $\text{LiB}_4\text{O}_7:\text{Cu}$, in dosimeters. *Radiation Measurements*, 84; 15-25.
- Larsen, N. A. 1999. Dosimetry based on thermally and optically stimulated luminescence. PhD. thesis, Risø-R-1090(EN), Niels Bohr Institute, University of Copenhagen, Denmark.
- Levy, P. W. 1985. Thermoluminescence kinetics in materials exposed to the low doses applicable to dating and dosimetry. *Nuclear Tracks Radiation Measurements*, 10; 547- 556.
- Li, S. H., & Chen, G. 2001. Studies of thermal stability of trapped charges associated with OSL from quartz. *Journal of Physics D: Applied Physics*, 34(4); 493.
- Lima, J.F., Snavarro, M., Gvalerio, E.M. 2002. Effects of thermal treatment on the TL emission of natural quartz. *Radiation Measurements* Volume 35, Issue 2; 155-159

- Martini, M., Fasoli, M., & Villa, I. 2014. Defect studies in quartz: Composite nature of the blue and UV emissions. *Nuclear Instruments and Methods in Physics Research Section B: Beam Interactions with Materials and Atoms*, 327; 15-21.
- McKeever 1991. Mechanisms of thermoluminescence production: Some problems and a few answers. *International Journal of Radiation Applications and Instrumentation. Part D. Nuclear Tracks and Radiation Measurements Volume 18, Issues 1–2*; 5-12.
- McKeever, S.W.S. 1985. *Thermoluminescence of solids*, Cambridge University Press, 376 p., New York.
- McKeever, S.W.S., Moscovitch, M., Townsend, D.P. 1995. *Thermoluminescence Dosimetry Materials: Properties and Uses*, Nuclear Technology Publishing, 202 p., England.
- McKeever, S.W.S., Moscovitch, M., Townsend, P.D., 1997. *Thermoluminescence Dosimetry Materials: properties and uses*. Nuclear Technology Publishing, 212 p, England.
- Oniya, E. O., Polymeris, G. S., Tsirliganis, N. C., & Kitis, G. 2012. Radiation dose response correlation between thermoluminescence and optically stimulated luminescence in quartz. *Journal of Luminescence*, 132(7); 1720-1728.
- Pagonis V., Kitis, G. and Furetta, C. 2006. *Numerical and Practical Exercises in Thermoluminescence*. Springer Publishing, 207 p., USA.
- Petrov, S. A., Bailiff, I. K. 1995. The '110 C' TL peak in synthetic quartz. *Radiation Measurements*, 24(4); 519-523.
- Poolton, N. R. J., Smith, G. M., Riedi, P. C., Bulur, E., Bøtter-Jensen, L., Murray, A. S., Adrian, M. 2000. Luminescence sensitivity changes in natural quartz induced by high temperature annealing: a high frequency EPR and OSL study. *Journal of Physics D: Applied Physics*, 33(8); 1007-1017.
- Preusser, F., Degering, D., Fuchs, M., Hilgers, A., Kadereit, A., Klasen, N., Krbetschek, M., Richter, D. and Spencer, J. Q. G. 2008. Luminescence dating: basics, methods and applications. *Eiszeitalter & Gegenwart Quaternary Science Journal*, 57(1/2); 95-149.
- Preusser, F., Chithambo, M. L., Götte, T., Martini, M., Ramseyer, K., Sendezera, E. J. & Wintle, A. G. 2009. Quartz as a natural luminescence dosimeter. *Earth-Science Reviews*, 97(1-4); 184-214

- Protherm Furnaces web site 2019. <http://www.prothermfurnaces.com/chamber-furnaces/plf-series110-130>. Last Accessed: 18.07.2019.
- PTW Freiburg Oven Typ 1321, Instruction manual. Freiburg, Germany. <http://www.ptw.de/assets/Uploads/2011-2012-Solutions.pdf>. Last Accessed: 15.06.19.
- PTW Manuel 2016. Detectors Including Codes of Practice for ionizing radiation.
- RADAT Dozimetri Laboratuvar Hizmetleri A.Ş. 2019. Web Site. <https://www.radat.com.tr/documents/tld-oven.pdf> Last Accessed: 15.07.2019
- Randall, J.T. ve Wilkins, M.H.F. 1945. Phosphorescence and Electron Traps I. The Study of Trap Distributions. Proc. R. Soc. A, 184; 365-389.
- Risø DTU, Guide to the Risø TL/OSL Reader, February 2008. Risø National Laboratory, Roskilde, Denmark.
- Sadek, A.M., Khamis, F., Polymeris, G.S., Carinou, E., Kitis, G. 2017. Similarities and differences between two different types of the thermoluminescence dosimeters belonging to the LiF family. Phys. Status Solidi C 14, No. 1–2, 1600220.
- Santos J.A.A., de Lima F.J., Valerio G.E.M. 2001. Phototransferred thermoluminescence of quartz. Radiation Measurements Volume 33, Issue 4, Pages 427-430.
- Subedi, B., Polymeris, G. S., Tsirliganis, N. C., Pagonis, V., Kitis, G. 2012. Reconstruction of thermally quenched glow curves in quartz. Radiation Measurements, 47(4); 250-257.
- Şahiner, E. 2017. Deconvolution analysis of thermoluminescent glow curves in various commercial dosimeters using two different approaches in the framework of the one-trap, one-recombination model. Turk. J. Physics, 41; 477 - 490.
- Şahiner, E., Meriç, N., Polymeris, G.S. 2017. Thermally assisted OSL application for equivalent dose estimation; comparison of multiple equivalent dose values as well as saturation levels determined by luminescence and ESR techniques for a sedimentary sample collected from a fault gouge. Nuclear Instruments and Methods in Physics Research B, 392; 21–30.
- Thermo Fisher Scientific Web site, 2019. (<https://www.thermofisher.com/order/catalog/product/SNO10106>, 2017. Last Accessed: 01.07.2019
- Thermo Fisher Scientific Web Site 2019. <https://www.thermofisher.com/order/catalog/product/3500TLDDS3>. Last Accessed: 10.07.2019

- Thomsen, J.K. 2004. Optically Stimulated Luminescence Techniques in Retrospective Dosimetry using Single Grains of Quartz extracted from Unheated Materials, PhD Thesis, Risø National Laboratory Roskilde, 176 p., Denmark.
- Topaksu, M., Yüksel, M., Dogan, T., Nur, N., Akkaya, R., Yegingil, Z., Topak, Y. 2013. Investigation of the characteristics of thermoluminescence glow curves of natural hydrothermal quartz from Hakkari area in Turkey. *Physica B: Condensed Matter*, 424; 27-31.
- Tsukamoto, S., Murray, A. S., Huot, S., Watanuki, T., Denby, P. M., Bøtter-Jensen, L. 2007. Luminescence property of volcanic quartz and the use of red isothermal TL for dating tephra. *Radiation Measurements*, 42(2); 190-197.
- Vandenbergh, D. 2004. Investigation of the optically stimulated luminescence dating method for application to young geological sediments. PhD. Thesis. Universiteit gent, 298 p., Holland.
- Watanuki T. and Tsukamoto S. 2001. A comparison of GLSL, IRSL and TL dating methods using loess deposits from Japan and China. *Quaternary Science Reviews Volume 20, Issues 5–9*; 847-851.
- Watanuki, T. , Murray, S.A., Tsukamoto, S. 2005. Quartz and polymineral luminescence dating of Japanese loess over the last 0.6 Ma: Comparison with an independent chronology. *Earth and Planetary Science Letters Volume 240, Issues 3–4*; 774-789
- Wintle, A. G. 1975. Thermal quenching of thermoluminescence in quartz. *Geophysical Journal International*, 41(1); 107-113.
- Wintle, A. G., Murray, A. S. 1997. The relationship between quartz thermoluminescence, photo-transferred thermoluminescence, and optically stimulated luminescence. *Radiation Measurements*, 27(4); 611
- Wintle, A. G., Adamiec, G. 2017. Optically stimulated luminescence signals from quartz: A review. *Radiation Measurements*, 98; 10-33.
- Yamashita T., Yasuno Y., Ikeda M., 1974. *Health Physics*, 27; 201.

CURRICULUM VITAE

Name Surname : Miray BAŞDOĞAN

Birth Place : Adana

Birth Date : 22. 05. 1983

Marital Status : Married

Languages : Turkish, English

Educational Information:

High School : Adana Anatolian High School 2001

Bachelors Degree : Ankara University Physics Engineering 2005

Master of Science : Ankara University Institute of Nuclear Sciences Medical Physics
Department, Health Physics Program 2019